KfK 4968
Februar 1992

Transient Evaporation and Stratification of Two Immiscible Liquids for LMFBR Transition Phase Analysis

D. Wilhelm, A. Roth
Institut für Neutronenphysik und Reaktortechnik
Projekt Nukleare Sicherheitsforschung

Kernforschungszentrum Karlsruhe

KERNFORSCHUNGSZENTRUM KARLSRUHE

Institut für Neutronenphysik und Reaktortechnik

Projekt Nukleare Sicherheitsforschung

KfK 4968

Transient Evaporation and Stratification of Two Immiscible Liquids for LMFBR Transition Phase Analysis

D. Wilhelm, A. Roth

Kernforschungszentrum Karlsruhe GmbH, Karlsruhe

Kernforschungszentrum Karlsruhe GmbH
Postfach 3640, 7500 Karlsruhe 1

ISSN 0303-4003

Transient Evaporation and Stratification of Two Immiscible Liquids for LMFBR Transition Phase Analysis

Abstract

Two immiscible liquids at different temperatures are suddenly brought together inside a rectangular box. The colder liquid evaporates upon contact of the hotter, less volatile liquid. Fast thermal equilibrium is achieved by vapor-generated mixing of the fluids. The denser, less volatile liquid finally stratifies below the remaining liquid phase of the more volatile fluid. This report describes the experimental apparatus of the Multiphase Multicomponent Box (MMB) experiment, and presents the experimental results of seven tests. The results may shed some light on the fundamental thermal hydraulics of the transition phase during beyond-design accidents in liquid metal fast breeder reactors (LMFBR).

Transiente Verdampfung und Stratifikation von zwei nicht mischbaren Flüssigkeiten für die Analyse der LMFBR Transition Phase

Zusammenfassung

Zwei nicht mischbare Flüssigkeiten von unterschiedlichen Temperaturen werden in einem rechteckigen Behälter plötzlich zusammengebracht. Beim Kontakt mit der heißen, weniger flüchtigen Flüssigkeit verdampft die kältere Flüssigkeit. Von Dampfblasen getriebene Mischungsvorgänge der beiden Flüssigkeiten fördern das schnell eintretende thermische Gleichgewicht. Die dichtere, weniger flüchtige Flüssigkeit stratifiziert schließlich unterhalb der flüssigen Phase der flüchtigen Flüssigkeit. Dieser Bericht beschreibt den experimentellen Aufbau des Mehrphasen-Mehrkomponenten-Behälter (MMB) Experimentes und geht auf die Ergebnisse von sieben Experimenten ein. Die Ergebnisse eröffnen Einblicke in die grundlegende Thermohydraulik der Transition-Phase während eines hypothetischen Unfalls in einem Flüssigmetall-gekühlten Schnellen Brutreaktor (LMFBR).

Contents

Introduction

In liquid metal fast reactors, beyond-design accidents may lead to local configurations where liquid fuel and liquid steel are close enough to interact like two liquids at different temperatures. Computer codes /1, 2/ are used to analyze this interaction of increased mobility of the reactor components in the so-called transition phase. A good estimate of the complicated thermal hydraulics is necessary to describe the accident sequence and the neutronics feedback. Disregarding the neutronics, the physics inside the fluid volume is characterized by rapid heat transfer, evaporation, condensation, and stratification. Assuming that liquid fuel and liquid steel are immiscible, it is of advantage to find a similar pair of liquids to study the fundamental thermal hydraulics at moderate pressures and temperatures. As new models and methods for the assessment of beyond-design accidents are under investigation /2/, the transient behavior of the two simulant fluids represents a first test on the ability to recalculate the complex transient process.

Simulant Fluids

The main condition for finding appropriate simulant fluids was to lower saturation and fusion temperatures. Additionally, both liquids were to be immiscible, a condition that greatly restricted the choices. For modelling the rapid heat transfer at liquid-liquid contact, the thermal diffusivity of the fuel simulant had to be lower than that of the steel simulant. For the stratification, the fuel simulant had to be denser than the steel simulant. There were a number of additional conditions which could not be met simultaneously, as there are: the vapor pressure curve of the more volatile steel simulant should meet similarity laws; upon boil-up in a two-component pool, the vapor pressures of the steel simulant should correspond to the hydrostatic head of the pool; as droplet were to be levitated at phase transition, the Kutateladze numbers should be similar; for natural convection in single-phase two component liquid systems, the Grashof numbers should be similar.

First, ammonia was selected as the steel simulant because its saturation temperature and density met similarity laws with a number of liquid hydrocarbons. Then, there were two choices for the fuel simulant, cyclohexane, C_6H_{12}, and tetralin, $C_{10}H_{12}$, which

is equivalent to 1.2.3.4-tetrahydronaphthaline. Cyclohexane has a fusion temperature of 280 K. Approaching this temperature from the liquid phase, the liquid viscosity increases rapidly which poses major problems in running and analyzing the experiments. Concentrating on the hydrodynamics rather than on the freezing phenomena, tetralin was used throughout the experiments presented in this report.

Table I shows representative average properties of the prototype system, stainless steel/mixed (U-Pu) oxide, and the simulant system, ammonia/tetralin. The simulant system meets the condition to lower characteristic temperatures. The dominant temperature is the saturation temperature of the volatile component at prevailing pressures, i.e. atmospheric pressure in the experiment (because of safety requirements in the vented apparatus). The less volatile component is better characterized by the fusion temperature being closer to the prevailing transient conditions. The ratio of prototype to simulant characteristic temperatures are the same in both cases, see Table II. The liquid Prandtl number, governing the liquid-liquid heat exchange, is

$$Pr = \frac{\eta \; c}{\lambda}$$

where η is the viscosity, c is the specific heat, and λ is the thermal conductivity. The Prandtl numbers of steel and its simulant are consistently lower than of oxide and its simulant. However, the values for the simulants are above unity, which is apparent from the Prandtl number ratio of Table II. Therefore, temperature and velocity profiles of the simulant system are bound to behave differently than in the prototype system. This is a substantial difference. The length scale, L, is derived directly from the dimensionless momentum equation. Its inverse value is

$$\frac{1}{L} = \frac{g}{c \; T}$$

where g is the gravitational acceleration, and T is the characteristic liquid temperature. The values are listed in Table II. Consequently, the simulant length scale is about a third of the prototypic length scale. The normalized density difference, R, is

$$R = \frac{\rho_{oxide} - \rho_{steel}}{\rho_{steel}}$$

where ρ is the liquid density. Both prototypic and simulant systems yield positive values of R. The density difference of the simulant system is more pronounced. This leads to the ratio of 0.61 for prototypic over simulant normalized density difference

in Table II. Consequently, the simulant system shows a stronger stratification potential. The pressure scale, P, is derived from the dimensionless momentum equation, like the length scale. The inverse pressure scale is

$$\frac{1}{P} = \frac{1}{\rho\, c\, T}$$

The ratio of the prototypic to simulant pressure scales are listed in Table II. They indicate that, in order to be consistent with the temperature scaling, the characteristic system pressure should be much lower than the prototypic pressure. With the present experimental apparatus, however, atmospheric pressure was set as reference, which then leads back to chosing the characteristic temperatures. Additionally, the inverse pressure scale values indicate that the vapor pressure curves of steel and ammonia, normalized with the characteristic temperature previously chosen, do not meet similarity criteria. The normalized ammonia vapor pressures are 30 to 50 times higher than the normalized steel pressures for the same normalized temperatures. It suggests that the vapor pressure plays a more dominant role in the simulant system compared to prototypic conditions.

Finally, we come back to the last three similarity conditions mentioned at the beginning of this chapter. The comparison of vapor pressures to hydrostatic head has been proposed by /3/ to be defined by

$$\frac{dp}{dz} = \rho\, g$$

where z is the vertical height of the boiled-up pool. Expanding the left hand side

$$\frac{dp}{dz} = \frac{dp}{dT}\,\frac{dT}{dz}$$

and using a two-parameter-approximation for the vapor pressure

$$p = p^{\star}\, exp\left(-\frac{T^{\star}}{T}\right)$$

where $p^{\star}$ and $T^{\star}$ are material-dependent constants, combining the above equations, and solving for the vertical temperature gradient yields

$$\frac{dT}{dz} = -\frac{\rho\, g\, T^2}{p\, T^{\star}}$$

This gradient which depends on the ambient pressure and temperature and the material properties represents the conditions necessary for a steady-state boil-up. In the prototypic system, steel contributes to the vapor pressure most. T^* of steel is 43370 K. Again, atmospheric pressure is assumed, and the liquid density varies between pure steel and pure fuel, so that dT/dz varies between -147 and -184K/m The simulant system, with $T^* = 2868$ K for ammonia, yields between -1.3 and -1.9K/m. The values are listed in Table III. The values for the simulant system suggest that boiled-up conditions in the pool are achieved at relatively low heat fluxes. Therefore, the latent heat terms in the energy equation are likely to dominate terms of temperature gradients. Similarity conditions with respect to the prototypic system are not maintained.

The Kutateladze number is defined with the latent heat rather than with the velocity of the steel vapor. It characterizes the levitation of droplets in a steel vapor stream that are subject to break-up by dynamic forces. The definition used here yields

$$Ku = \frac{(h_v \rho)^{1/2}}{(\sigma g \Delta\rho)^{1/4}}$$

where ρ is the steel vapor density, and $\Delta\rho$ the density difference between the vapor and the liquid that forms the droplets. There is a choice of two droplets, either fuel or steel. Therefore, the values of $\Delta\rho$ and σ have to cover this range, as given in Table III. The values of the prototypic and simulant systems differ by about a factor 5 indicating a moderate difference in levitation criteria.

Finally, the Grashof-number is defined using the characteristic length, L, of 0.3 m for the prototypic system and 0.1 m for the simulant system according to the length scaling previously mentioned.

$$Gr = \frac{g \rho \Delta\rho L^3}{\eta^2}$$

Unlike in a single component system, the density difference is defined between the two liquid components, and the lighter component (steel) is supposed to be the continuous phase, setting the values for ρ and η. The two Grashof-numbers are shown in Table III. They are defined by the ratio of buoyancy forces over viscous forces. The values of prototypic and simulant systems are close together. For turbulent flow, for example, the heat transfer to a rigid wall in a single-component system is pro-

portional to $Gr^{0.333}$ indicating that differences in the Grashof numbers are less effective.

Experimental Apparatus

Fig. 1 shows side and front views of the main reaction box. A rectangular box with double pane front and side windows houses plastic inserts which form an exhaust volume at the upper rear, and a test volume close to the front window. A stainless steel hollow cylinder can be moved right up to the front window. A plastic washer between the cylinder and the window provides a leak-tight connection. At the rear end of the stainless steel cylinder, a plastic insert with a concentric duct closes the void volume in front. Prior to the test, the apparatus is cooled down to 340 K and below, with a liquid coolant flowing through the space between the double pane windows. Liquid ammonia is introduced into the volume next to the front window outside the stainless steel cylinder. The inside of the cylinder is still void. Tetralin, the liquid hydrocarbon, is heated in an outside container.

Shortly before the test, the tetralin is injected through the duct of the stainless steel cylinder insert into the voided cylinder. After the filling has been completed, the movie camera and the frequency modulated (FM) tape recorder are started. The pressure and temperature signals are recorded on the tape. With the ignition of an electronic flash, a motor is started that drives the stainless steel cylinder to the rear. As the cylinder disappears into the plastic displacement inserts, both liquids, ammonia and tetralin, interact inside the volume next to the front window. There are seven thermocouples visible through this window, from number 2 to 8, the numbers shown in Fig. 1 inside solid line circles.

Fig. 2 shows a photo taken of the front window. The plastic hoses provide the box with the coolant liquid. The stainless steel cylinder is clearly visible with the concentric hydrocarbon inlet duct, and three thermocouples extending from the inlet. The plastic inserts house several photo diodes to identify photographic distortions while taking movie pictures. The photodiodes are 15 mm apart, see Fig. 1. Fig. 3 shows, from the same angle, the front window, the movie camera, and the spotlight on the right hand side. A 10 mm wide and 200 mm high sheet of light is projected into the box through the right side window. The beam is directed into the box only after the

start of the transient. Prior to it, a metal shield between the main lamp and the box is closed to prevent the box from being heated.

Fig. 4 shows a downward view of the experimental apparatus with the movie camera in front, and the spotlight on the right side. To the left, a rack houses the data acquisition for the temperatures and the pressure, behind it is an extended time line plotter to monitor the temperatures in the external containers and in the test section. In the right rear, the photo shows the thermostat control of the tetralin heater, and the programmable controller. Fig. 5 shows the whole area photographed from the left front. On the left hand side stands the liquid nitrogen dewar. The liquid nitrogen was used to condense ammonia and to keep the cooling liquid at constantly low temperatures.

Data Acquisition

Fig. 6 shows a block diagram to identify the data acquisition and the controls. The programmable controller starts the FM tape recorder, the camera, the electronic flash, and the cylinder drive motor. While the analogue tape records seven temperatures and the pressure inside the box, the camera takes about 500 frames per second through the front window. The tetralin is colored by a red dye, Sudan red for microscopy. While recording, the analogue tape was run at 3¾ inches per second. The same speed was used to read the data, convert to 12-bit digital data, and read it into the memory of a PDP-11/23 microcomputer. Typically, a set of data was sampled each 20 ms. The pressure transducer was located at the end of a long tube filled with liquid ammonia. It was not possible to prevent the liquid from evaporating inside the tube. Therefore, the pressures recorded do not represent the transient inside the box sufficiently well. The pictures, recorded on the high-speed movie, were rear-projected on a screen with cartesian co-ordinates. Points on the picture hat to be hand-picked by moving graphic arms. The co-ordinates of these points were read as analogue data, digitized to 8-bit values, and read into the memory of a Commodore 4032 microcomputer

While the absolute steady-state temperature was measured with an accuracy of ± 0.5 K, the transient temperature is a function of the time constant the thermocouple lags behind the continuous fluid temperature. The time constant is

$$\tau = \frac{V \rho c}{A h}$$

where V, ρ, and c are the volume, density, and specific heat of the sensitive tip of the thermocouple, and A, and h are the surface area and heat transfer coefficient to the adjacent flow. If we simply take the geometry of a sphere with the diameter of $d = 0.3$ mm, then

$$\tau = \frac{d \rho c}{6 h}$$

A rough estimate of the heat transfer coefficient is used for low Reynolds-number (Re≈700), and a Nusselt-number defined by $Nu = 0.4\, Re^{0.6}\, Pr^{0.3}$. Ammonia is supposed to be the adjacent fluid, and τ yields values of 0.01 s and below. Therefore, with a transient of about 3 s, the error in time scale is below 1%. Frequencies above 10 Hz are not observed so that there is no influence on the amplitude. The threshold frequency for $\tau = 0.01$ s is about 40 Hz. For frequencies higher than 40 Hz, there is a substantial reduction in the recorded amplitude.

Time dependant data, while being compared to calculations, depend on the accuracy of measuring the start of the transient. It took about 150 ms to withdraw the separating stainless steel cylinder from the reaction chamber next to the front window. However, the error recorded over 10 experiments was of the order of 10%, so that the uncertainties with respect to the time scale are of the order of 10 ms, or 5 frames. The errors for the digitized co-ordinates of the movie frames depend more on the optics than on the method of digitization. The optical error is at least ± 1 mm. While looking at a sharp interface between liquid and vapor through the front window, the error increases to ± 2 mm. If the box was filled to a liquid level of 90 mm, the error at defining the cross section area of the liquid was therefore 4%. However, during the transient, poorly defined fluid topologies had to be analyzed. Judging by repeated digitizations of one and the same frame with two phases churned up, the error in defining the hold-up turned out to be a few ten percent. Only qualitative data of the topologies can hence be extracted using the present technology.

Test Matrix

A total of seven experiments will be described in this report. Table IV gives an overview over major initial conditions and experimental parameters.

The table lists the ammonia level measured from the bottom of the pool, the area that the liquid component projects on a plane parallel to the front window, and the total initial volume of the liquid component. In all cases, the tetralin injected into the hollow stainless steel cylinder filled the whole inside volume available. The cross section area of the stainless steel cylinder has not been taken into account, see MMB-07 for details. The plastic inserts inside the box were changed during the course of refining the apparatus. In test MMB-07, the depth of the reaction chamber (perpendicular to the front window) inside the box was still 5.23 cm (see Fig. 1) which led to considerable three-dimensional effects especially during the withdrawal of the stainless steel cylinder. Furtheron, the time for total withdrawal was too long. The sheet lighting from the side illuminated almost the total volume. By moving the sheet of light closer to the front window, three dimensional effects in the rear were still visible. It was decided to decrease the depth, to 3.23 cm for test MMB-19, and to 2.07 cm for the remainder of the tests. By doing so, the three-dimensional effects were reduced, and the boundary layer effects of the main walls, i.e. the front window and the back plane, were increased. The boundary layer effects were judged to be still of little effect on the main pool flow. In Table IV, liquid level, cross section areas parallel to the front window, and liquid volumes are given as effective values. This was done because structures in the corners of the rectangular reaction chamber had to be taken into account. As the apparatus was refined, the associated volumes of structures were reduced, and an unobstructed view through the front window was obtained.

In Table IV, the temperatures are estimated averages for each component. In the ammonia, the very top layer was usually at saturation, and the bottom layer at a slightly lower temperature than average. The two isothermal experiments, MMB-07 and MMB-21 were performed near the saturation temperature of ammonia. The slight differences between the two bulk temperatures observed in these experiments are neglected. For all experiments, the temperature of the box walls and plastic inserts can be assumed to be very close to the value of the initial ammonia pool. Due

to the large mass involved, the wall temperatures can be assumed constant during the transient.

Individual Test Description

Each of the seven tests will be described in this chapter. After the definition of the test set-up and initial conditions, the basic transient data are shown in graphs. These are the temperatures, and the hold-up. The hold-up, H , is defined by

$$H = \frac{V}{V_0} - 1$$

Where V is the total volume of the multiphase pool extending up to the open pool surface. V_0 is the total volume before the transient starts. We refer to MMB-07 for the definition of the idealized initial value.

All times are recorded from the start of the withdrawal of the stainless steel cylinder. The start of the movement was recorded on the analogue type and on the movie film. At this point, the time is set to zero.

MMB-07

This isothermal test will be described predominantly to quantity differences to the second isothermal experiment, MMB-21. While the MMB-07 box depth was still 5.23 cm, the MMB-21 box depth had the final value of 2.07 cm. The initial ammonia temperature was high enough to maintain a rather constant pool boiling at a void fraction of approximately 10%. This was due to heat fluxes from the adjacent walls and the tetralin which were slightly warmer than ammonia. Fig. 7 shows handpicked interfaces drawn from the frames shot by the high-speed movie camera through the front window. The time = 0-frame shows idealized interfaces. This is done to help specify initial conditions for computer codes. Therefore, the area occupied by the stainless steel cylinder wall has been neglected. Prior to the withdrawal of the stainless steel cylinder, tetralin filled the whole inner cross section with a radius of 32.5 mm. Assuming the steel cylinder would not be there, tetralin is supposed to fill the

area defined by the outer radius of the steel cylinder (35 mm). To maintain the original cross section area, a horizontal line is drawn to cut off a segment at the top end. This is done according to observations of the tetralin level decreasing inside the steel cylinder immediately after the start of the cylinder withdrawal. The upper level of the ammonia has to be reduced by the area of the steel cylinder wall, as well. In MMB-07, the center of the cylinder is at an elevation of 56 mm. In all other experiments, this elevation is 45.5 mm. The remainder of the ten frames show solid lines of interfaces where these were clearly visible, and dashed lines where the view through the front windows was obstructed or a clear-cut interface could not be identified.

Compared to MMB-21, the transient of MMB-07 is slower because of the presence of the vapor bubbles and the longer period the stainless steel cylinder needed to move back. At about 0.15 s, the coherent MMB-07 tetralin mass is still 15 mm higher than in MMB-21. At about 0.21 s, this difference has increased to 20 mm, mainly because of the longer time the MMB-07 steel cylinder needs to cross the 5.23 cm box depth. Additionally, three-dimensional effects change the transient, too. When the steel cylinder is partly withdrawn, tetralin pours out near the front windows and displaces ammonia to the back. Therefore, the apparent tetralin cross section is increased, and the ammonia cross section decreased. At 0.3 s and later, tetralin has reached the bottom of the box, moves horizontally to the left and right corners, and then upwards along the side windows. While the beginning of the upward slosh looks similar in both experiments, the MMB-07 tetralin reaches its highest elevation later at around 0.6 s. The upper parts of the tetralin area are not coherent, they are filled with tetralin droplets rather than with continuous tetralin, which is indicated by dashed lines. Beyond 0.7 s, tetralin moves downwards. This movement is slowed down by the presence of ammonia vapor bubbles. Bubble sizes of 1 to 5 mm can be identified. Most bubbles have a diameter of 1 to 2 mm, but at later times, bubbles of up to 5 mm diameter may appear close to the interface between tetralin and ammonia. At around 1.0 s, MMB-21 tetralin is stratified, but MMB-07 tetralin is still at its final downward slosh. It takes about 1.2 s in MMB-07 for tetralin to stratify below the ammonia pool.

MMB-19

For this test, the box depth was reduced to 3.2 cm which was found to be still too large. The effective ammonia level is very low, indeed below the top of the tetralin. During the withdrawal of the stainless steel cylinder, the tetralin discharged near the front window until its level reached that of the ammonia. The center of the cylinder is at an elevation of 45.5 mm. The initial temperature difference is the highest of this test series. It is therefore appropriate to check whether the instantaneous contact temperature exceeds the homogeneous nucleation temperature of ammonia. The instantaneous contact temperature, T_I is

$$T_I = \frac{(\lambda\, c\, \rho)_A^{1/2}\ T_A + (\lambda\, c\, \rho)_T^{1/2}\ T_T}{(\lambda\, c\, \rho)_A^{1/2} + (\lambda\, c\, \rho)_T^{1/2}}$$

where the subscripts A and T stand for ammonia, and tetralin, respectively. ρ is the liquid density, c the liquid specific heat, and λ the liquid thermal conductivity. The homogeneous nucleation temperature, T_H, for ammonia is calculated using the approximation for non-metals

$$T_H = \frac{27}{32}\ T_{crit}$$

where T_{crit} is the critical temperature. For MMB-19, the contact temperature is $T_I = 265K$. This is well below $T_H = 342K$ so that homogeneous nucleation can be ruled out. The minimum film boiling temperature of ammonia on contact with a horizontal surface has been assessed using correlations of /4/ and /5/. At this temperature, a film of ammonia vapor may be stable. However, the correlations yielded temperatures close to the homogeneous nucleation temperature. Consequently, T_H = 342 K may equally well represent the threshold for a stable ammonia vapor film. This stable film can hence be ruled out for all MMB experiments, including MMB-19.

Fig. 8 shows the idealized initial configuration of MMB-19. The tetralin area is surrounded by a dashed line. Its shape has been obtained the same way as that of MMB-07. There are seven thermocouples in MMB-19 registering the transient temperatures. The thermocouple locations are given in Fig. 8. The assigned channel numbers are listed on the right hand side of the frame. The location of thermocouple 2 which is inside the tetralin moves into the region outside the effective tetralin area

when using the idealized interface shape, see also MMB-07. However, its location should be moved to 2a, indicated by a square just below the original location. Thermocouple 8 touches the stainless steel cylinder before withdrawal. At time = 0, the steel temperature is close to the ammonia temperature. Thermocouples 6 and 7 are inside the liquid ammonia. The ammonia interface to the vapor volume is represented by a solid line. As the stainless steel cylinder is withdrawn, tetralin pours out at the front end. A three dimensional mixing process is started during which a considerable amount of vapor is produced locally. Prior to 0.15 s, the pool height is about 6 cm, corresponding to an average void fraction of a few percent. The void fraction increases rapidly. Between 0.15 s and 0.39 s, the average pool height is about 9 cm, corresponding to an average void fraction of 36%.

Figs. 9 and 10 show the temperatures measured during the transient of MMB-19. Channels 2, 3, 4, and 5 start inside the hot tetralin. Around 0.3 s, rapid equilibration of temperatures indicates the violent mixing process. Channels 6 and 7 start inside the liquid ammonia, and channel 8 inside the nitrogen plenum. At the bottom, channel 6 starts from the coldest temperature but contacts the hot bulk of tetralin falling down first. At the time of contact (0.2 s), the liquids are still forming coherent masses, only the fringes are being dispersed. After the violent mixing, the thermocouples register frequent redistributions of the liquids, and a final stratification of ammonia above the tetralin. Channels 5 and 6 lie well within the tetralin layer. There is a residual temperature difference between tetralin and ammonia of 10 to 20 K.

Fig. 11 shows the reading of the pressure transducer compared to that of thermocouple channel 5. As mentioned before, the absolute values of pressures are unreliable, however, the pressure peak at 0.43 s coincides with visual observations of a rapid increase of fluid velocity directing the bulk liquid into the upper plenum. The thermocouple which remains inside the bulk hot tetralin the longest (channel 5) reaches a fast temperature decrease at the same time because the rest of the coherent tetralin mass is rapidly dispersed. Judging from what can be seen in the movie pictures, the rapid dispersal starts at the lower right corner. A similar triggering event has not been observed in any other experiment. The increase in fluid velocity is rapidly progressing into the remainder of the multiphase pool. Velocities of up to 5 m/s are reached. A considerable amount of liquid is ejected beyond the top of the frame window. A part of the ejected fluid moves back between 0.55 s and 0.61 s. At 0.61 s, a second violent interaction takes place at the lower pool end. Another bulk of liquid is ejected into the upper part of the box. Again, the ejection is followed by fluid

sloshing back down around 0.8 s, with channel 5 reading an increase in temperature because of warm tetralin moving back.

The remainder of the transient is characterized by a churning pool with gradual equilibration of temperatures and a final stratification of tetralin below liquid ammonia. Around 0.98 s, the pool height is rather constant at 19 cm, corresponding to an average void fraction of about 70%. From the visual observation, the pool continuous phase is liquid. At the top end of the pool, a foamy flow regime can be identified. A clear interface between tetralin stratified below liquid ammonia is visible at 2.1 s. Stratification is completed shortly thereafter.

MMB-21

This isothermal test is the first of the series with refined box geometry. The box depth has been reduced to 2.07 cm, the width to 8.8 cm. Fig. 12 shows eight pictures taken from selected high speed movie frames. The ammonia pool is indicated by an "A" and has a white color, tetralin is dark with a label "T". At 0.15 s, during the withdrawal of the stainless steel cylinder, a gas bubble emerges from within the back-volume of the steel cylinder. The bubble has only a limited effect on the early tetralin movement. However, as it takes more than 0.15 s to withdraw the steel cylinder, this action has an influence, and data from the pictures have to be refined in order to compare them to model calculations. Fig. 13a shows a digitized picture taken from the time = 0-frame. The tetralin area, i.e. the inner diameter of the steel cylinder (65 mm) is marked by a dashed line. The center of the cylinder is at an elevation of 45.5 mm. The ammonia pool surface is at an elevation of 95 mm, however, the surface would be lower if the steel cylinder would not occupy any volume. For comparison with model calculations, the pool surface in Fig. 13b has been lowered to 84 mm, and the tetralin area is constructed as described for MMB-07. To place thermocouple 2 correctly into the bulk tetralin, location 2a is given by a square in the new geometry.

The same procedure produces Fig. 14b out of the original data of Fig. 14a, and Fig. 15b out of data from Fig. 15a. In all pictures, the total cross section area, and the tetralin area are listed. Figs. 16 through 21 need not be refined because the steel cylinder is fully withdrawn. Starting with Fig. 17, the tetralin becomes dispersed at its upper end. Therefore, there are two dashed lines, one for defining the area of very

high tetralin volume fractions, and the one above to identify the boundaries of a mixture of tetralin and ammonia to almost pure ammonia. The area of the mixture is given the name "2-COMP." After a transient similar to MMB-07, the heavier tetralin stratifies below the ammonia pool. Stratification is completed after about 1 s. While the measured total area stays constant during the transient, the Fig.21-tetralin area reads a deficit of 20% compared to the initial area. Tetralin leaks into gaps of the lower box and replaces ammonia, an effect that is visible in all following experiments.

MMB-26

MMB-26 is a thermal test with a relatively small temperature difference between tetralin and ammonia. The effective ammonia level is at an elevation of 8.6 cm. The initial tetralin temperature is 289 K, and ammonia is close to saturation. Fig. 22a shows the initial configuration of MMB-26 featuring the dashed line between tetralin and the steel cylinder as observed through the front window. Fig. 22b shows the idealized initial configuration of MMB-26 generated the same way as that of MMB-21. The channel numbers are marked at the position of the associated thermocouples. Instead of using the original thermocouple location 2, one should use location 2a in conjunction with idealized data. Figs. 23 through 29 show tetralin/ammonia interfaces (dashed) and ammonia/gas interfaces (solid lines) for MMB-26 at selected times. Figs. 30 and 31 show the transient temperatures of all thermocouples. Effective mixing of both liquids starts after 200 ms. Boil-up is less violent than for MMB-19, and it takes a longer time to achieve thermal equilibrium. Stratification starts after 1 s. A clear interface between the stratified liquids is visible after 2.9 s which completes the transient.

To quantify the information drawn from the movie pictures, the holdup, as defined previously, is plotted over the time. Figs. 32 and 33 show the holdup on two different time scales. The residual holdup for times greater than 4 s shows the magnitude of the error in defining the areas. The error is approximately 10%. Table V lists the areas and holups at given times.

MMB-27

MMB-27 is a thermal test with a maximum amount of ammonia and an average temperature difference. The effective ammonia level is 9.4 cm, the initial tetralin temperature is 300 K, and the initial ammonia temperature is 239 K. Fig. 34a shows the interfaces between tetralin and the steel cylinder (dashed line) and between ammonia and gas (solid line) as observed through the front window at time = 0. Fig. 34b shows the idealized configuration of MMB-27 generated like for the previous experiments. The channel numbers are given for the positions of the associated thermocouples. Number 2 is redirected to 2a the same way as for the previous experiments. Figs. 35 through 41 show the interfaces at selected times.

Stratification is first visible after 2.9 s, and completed at 3.9 s. Figs. 42 and 43 show the transient temperatures, except for channel 2 which failed. The transient is similar to that MMB-26, but the thermal equilibration takes a little bit longer. Figs. 44 and 45 show the holdups on two different time scales. The maximum visible holdup is 0.8. Therefore, between 0.36 s and 0.52 s, the holdup value is at a constant maximum. The curves are very similar to those of MMB-26. Table VI lists the areas and holdups at given times.

MMB-28

MMB-28 is a thermal test with a small amount of ammonia and a large temperature difference. The effective ammonia level is 6.9 cm, the initial tetralin temperature is 312 K, and the initial ammonia temperature is 240 K, indicating nucleate boiling at time = 0. Fig. 46a shows the interfaces between tetralin and the steel cylinder (dashed line), and between ammonia and gas or two-phase (solid line) as observed through the front windows at time = 0. The pool surface moves up and down and is, at an average, as low as the upper end of the steel cylinder which is covered by a layer of dense ammonia vapor bubbles. The uppermost thermocouple (number 8) is located within the layer of bubbles. Fig. 46b shows the idealized initial configuration of MMB-28. The liquid ammonia level is reduced by the cylinder wall cross section area. The effective tetralin area has a been modified slightly to make sure that the top ammonia surface and the tetralin surface are at the same elevation (69 mm). Thermocouple 8 is now well inside the cover gas indicating that its location is not con-

sistent with the idealized configuration. For consistency, thermocouple 2 has been redirected to 2a, as done in the previous experiments.

Figs. 47 through 53 show the interfaces of tetralin and ammonia at selected times. Stratification is first visible after 1.8 s which is much earlier than in the experiments described before, and completed at 2.9 s. Figs. 54 and 55 show the transient temperatures. Equilibration of temperatures takes a little bit longer than for MMB-28. Figs. 56 and 57 show the holdups on two different times scales. The maximum visible holdup is reached between 0.17 s and 0.31 s, its value is 1.68. The multiphase pool may extend well beyond the visible limit which is indicated by the steep upward and downward gradients at both sides of the maximum level. However, in the experiment, the top vessel head lies closely above the visible limit, and fluid hitting the head may be diverted into the backward safety volume which is voided, or back down into the pool. The slosh-back may partly be responsible for the fast collapse of the pool around 0.35 s. Table VII lists the areas and holdups at given times.

MMB-34

MMB-34 is a thermal test with a small amount of ammonia, and a high temperature difference. The effective ammonia level is 8.1 cm, the initial temperature difference is 82 K, and ammonia is subcooled by as much as 13 K. Fig. 58a shows the interfaces between tetralin and the steel cylinder (dashed line) and ammonia and gas (solid line) as observed through the front window at time = 0. Fig. 58b shows the idealized initial configuration, produced the same way as for the previous experiments. As in MMB-28, thermocouple 8 lies now within the cover gas region which is also not consistent with the experimental initial configuration. To achieve consistency, thermocouple 2 has been redirected to 2a the same way as before. A rather complete set of digitized frames is added. Figs. 59 through 108 show the interfaces of tetralin (dashed lines) and ammonia/gas (solid lines) at selected times. During the first 0.24 s, the coherent tetralin mass is diffused and moves down slightly, but not as fast as in the isothermal tests. Appreciable evaporation starts after 0.2 s.

Fig. 90 (1.339 s) shows a first reappearance of a tetralin interface, indicating that tetralin starts to form a coherent stratified layer below the churning pool. At 1.634 s (Fig. 95), a second solid line at 61 mm elevation separates an almost clear ammonia

pool below from a two-phase churning region above. There are only a few vapor bubbles emerging from the tetralin interface travelling upward through the clear ammonia pool, and tetralin droplets travelling downwards. As stratification continues, the tetralin layer grows, and the two phase region collapses. At 4.217 s (Fig. 106), the stratification is completed. Afterwards, more tetralin escapes through the backward gaps which is indicated by a decreasing elevation of the tetralin interface, similar to MMB-21.

Figs. 109 and 110 show the transient temperatures. During the first 0.5 s, the transient is similar to that of MMB-19. This is not surprising because the initial ammonia temperatures of both experiments are at a low 227 K. With respect to the other experiments, it takes about 0.1 s longer to increase ammonia temperatures to saturation so that vigorous evaporation can start. Except for thermocouple channel 8 which is inside the void after the collapse of the two-phase pool, all temperatures equilibrate quickly after 1.3 s. Again, a slosh-back may help to speed up equilibration, as the fluid may return quickly when it hits the vessel head.

Figs. 111 and 112 show the holdups on two different time scales. The maximum visible holdup is reached between 0.39 s and 0.58 s, its value is 1.28. The pool collapses slightly around 0.8 s, and rises to a second maximum at about 1.1 s. During the final collapse, larger vapor bubbles appear near the pool surface. The collapse is rather steady and takes more than 1 s. Whereas deviations in tetralin areas from time = 0 to time = 8 s exceed 40%, errors in total pool area are likely to be compensated by one liquid replacing the other liquid in the backward gaps. Therefore, the error of the final holdup value is about 10%. Tabel VIII lists the areas and holdups at given times.

Conclusion

To study the fluid dynamics and transient thermal hydraulics of two liquids in a rectangular pool, an experimental program has been carried out in the Multiphase Multicomponent Box (MMB) apparatus. Hydrodynamically, the pool of liquid ammonia and liquid tetralin is similar to what can be expected of a transition-phase liquid steel-liquid fuel pool without freezing. Major similarity laws are close to being obeyed for the stratification potential, the length scale, the temperature scale, the

levitation of droplets, and the liquid-liquid buoyancy. Similarity laws are not obeyed for two other important dimensionless groups. Particularly, the question whether a boiled-up pool can be maintained for a long time cannot directly be answered because the MMB system pressure was too high. Additionally, similarity for the vapor pressure of the steel simulant could not be achieved.

Isothermal test are characterized by a movement of a coherent tetralin mass downwards until it hits the bottom. Tetralin is directed into both corners of the rectangular box and upwards along the side walls. During the upward slosh, the tetralin front diffuses and tetralin droplets form. The droplets and the coherent tetralin mass ultimately fall back into a stratified layer of the heavier tetralin below the lighter ammonia. The whole transient is slightly delayed if vapor bubbles are present in the ammonia.

Thermal test are characterized by a premixing period in which the generated ammonia vapor drives the mixing process between tetralin and ammonia. Only in MMB-19, a triggering event was observed marking the initiation of a violent dispersal of the liquid pool into the cover gas volume. During all other transients, this period of integral pool movement began less violently, but was equally followed by a rapid thermal equilibration. As the boiled-up pool gradually collapsed, tetralin began to stratify below the remaining liquid ammonia. The time of stratification is difficult to define objectively. It takes between 1.5 s and 3.2 s for a clearly visible interface of the stratified tetralin to develop. The experiments with the highest initial temperature differences and the most violent dispersals have the shortest stratification times indicating that the fluid movement may be considerably influenced by the slosh-back after hitting the vessel head.

The pool fluid-dynamics is governed in large part by the geometry of the box. Extrapolation to prototypic conditions may only be possible by using computer codes verified on these experiments, and carefully adjusted to the geometry conditions of the prototypic configuration.

Acknowledgment

This report would not have been possible without the help of R. Eggmann, M. Kirstahler, J. Marek, L. Meyer, E. Wachter, and H. Zimmermann. The authors appreciate their collaboration and assistance.

Literature

/1/ W.R. Bohl, L. Luck, SIMMER-II: A Computer Program for LMFBR Disrupted Core Analysis, Los Alamos National Laboratory report LA-11415-MS, Los Alamos, June 1990

/2/ W.R. Bohl, D. Wilhelm, F.R. Parker, J. Berthier, L. Goutagny, H. Ninokata, AFDM: An Advanced Fluid-Dynamics Model, Vol. I: Scope, Approach, and Summary, Los Alamos National Laboratory Report, LA-11692-MS, Los Alamos, September 1990

/3/ W.R. Bohl, private communication

/4/ P.J. Berenson, Film-Boiling Heat Transfer From a Horizontal Surface, Trans. of the ASME Journal of Heat Transfer, August 1961, pp. 351 - 358

/5/ V.K. Dhir, G.P. Purohit, Subcooled Film-Boiling Heat Transfer From Spheres, Nucl. Engg. and Design, Vol. 47 (1978) pp. 49 - 66

Nomenclature

A	m^2	surface area
c	J/(kg K)	specific heat
d	m	diameter
g	m/s^2	gravitational acceleration
h	W/(m^2 K)	heat transfer coefficient
h_v	J/kg	latent heat of evaporation
H	-	holdup
L	m	length scale
p	Pa	pressure
P	Pa	pressure scale
R	-	normalized density difference
r	m	radius
T	K	temperature
V	m^3	volume
z	m	vertical length
η	kg/(m s)	dynamic viscosity
λ	W/(m K)	thermal conductivity
ρ	kg/m^3	density
σ	N/m	surface tension
τ	s	time constant

Gr	-	Grashof number
Ku	-	Kutateladze number
Nu	-	Nusselt number
Pr	-	Prandtl number
Re	-	Reynolds number

Tables and Figures

TABLE I Average Characteristic Properties of Prototypic and Simulant Components

	unit	prototypic		simulant	
component		stainless steel	mixed oxide	ammonia	tetralin
saturation temperature at atmospheric pressure	K	3070	3600	240	350
fusion temperature	K	1700	3050	195	235
molecular weight	mol/g	56	270	17	132
liquid density	kg/m^3	6900	8660	683	970
saturated vapor density at atmospheric pressure	kg/m^3	0.19		1.9	
liquid specific heat	$J/(kg\ K)$	785	504	4454	1690
latent heat of evaporation	J/kg	$6.5 \cdot 10^6$		$1.4 \cdot 10^6$	
liquid thermal conductivity	$W/(m\ K)$	20	5	0.5	0.2
liquid thermal diffusivity	m^2/s	$3.7 \cdot 10^{-6}$	$1.1 \cdot 10^{-6}$	$1.6 \cdot 10^{-7}$	$1.2 \cdot 10^{-7}$
liquid viscosity	$kg/(m\ s)$	0.004	0.005	0.0003	0.002
critical temperature	K	8000	10600	405	480
surface tension	N/m	0.2	0.47	0.023	0.04

TABLE II Ratio of Major Scaling Groups

ratio of prototypic to simulant group	steel	oxide
for the saturation temperature	13	--
for the fusion temperature	--	13
for the Prandtl number, Pr	0.06	0.03
for the inverse length scale, 1/L	0.44	0.26
for the normalized density difference	0.61	
for the inverse pressure scale	0.04	0.03

TABLE III Additional Scaling Groups

group	unit	prototype	simulant
vertical temperature gradient, -dT/dz	K/m	147 ... 184	1.3 ... 1.9
Kutateladse number, Ku	-	370 ... 460	80 ... 100
two-component Grashof number, Gr	-	$2.0 \cdot 10^{11}$	$2.1 \cdot 10^{10}$

TABLE IV MMB Testmatrix

TEST NUMBER	7	19	21	26	27	28	34
effective NH_3 level (cm)	9.9	4.2	8.4	8.6	9.4	6.9	8.1
effective NH_3 area (cm^2)	64.8	23.7	40.4	42.2	49.2	27.2	37.7
effective NH_3 volume (cm^3)	339	77.	84.	87.	102	56.	78.
effective $C_{10}H_{12}$ area (cm^2)	33.2	33.2	33.2	33.2	33.2	33.2	33.2
effective $C_{10}H_{12}$ volume (cm^3)	174	107	69.	69.	69.	69.	69.
initial NH_3 temperature (K)	240	227	237	239	239	240	227
initial $C_{10}H_{12}$ temperature (K)	240	319	237	289	300	312	309
initial temperature difference	0^+	94.	0^+	50.	61.	72.	82.

$^+$) There was a 2 to 4 K temperature difference between tetralin and the colder ammonia

TABLE V MMB-26 Area and Holdup Over Time

Time (s)	Area (mm^2)	Holdup
0.000	7540.	0.000
0.131	8412.	0.116
0.151	8372.	0.110
0.170	8693.	0.153
0.190	10154.	0.347
0.209	11820.	0.568
0.248	13757.	0.825
0.268	14373.	0.906
0.288	14368.	0.906
0.307	12785.	0.696
0.327	13252.	0.758
0.346	13875.	0.840
0.366	13831.	0.834
0.385	14373.	0.906
0.405	14465.	0.918
0.444	13705.	0.818
0.532	12464.	0.653
0.581	14078.	0.867
0.620	14462.	0.918
0.738	12591.	0.670
0.796	13108.	0.738
0.894	12189.	0.617
0.914	11660.	0.546
0.933	11800.	0.565
0.953	12546.	0.664
0.972	12102.	0.605
0.992	11857.	0.573
1.012	12263.	0.626
1.031	12161.	0.613
1.051	12077.	0.602
1.090	11360.	0.507
1.129	11881.	0.576
1.168	11593.	0.538
1.207	10873.	0.442
1.246	10669.	0.415
1.266	10636.	0.411
1.286	11037.	0.464
1.305	10816.	0.434
1.344	10924.	0.449
1.364	11259.	0.493
1.383	11054.	0.466
1.462	9799.	0.300
1.501	9655.	0.281
1.559	10125.	0.343
1.599	9616.	0.275
1.618	9865.	0.308
1.657	9930.	0.317
1.696	9346.	0.239
1.736	9374.	0.243
1.775	9078.	0.204
1.794	8956.	0.188
1.814	8941.	0.186
1.853	9091.	0.206
1.892	8747.	0.160
1.931	9030.	0.198
2.010	8989.	0.192
2.090	8589.	0.139
2.146	8596.	0.140
2.248	8470.	0.123
2.342	8433.	0.118
2.440	8244.	0.093
2.538	8163.	0.083
2.929	8147.	0.081
2.949	8262.	0.096
3.320	7917.	0.050
3.913	8158.	0.082
5.870	8000.	0.061
7.827	8061.	0.069
9.783	8180.	0.085

TABLE VI MMB-27 Area and Holdup Over Time

Time (s)	Area (mm^2)	Holdup
0.000	8240.	0.000
0.133	9827.	0.193
0.152	9970.	0.210
0.172	10709.	0.300
0.191	11555.	0.402
0.211	13083.	0.588
0.221	13759.	0.670
0.230	14615.	0.774
0.240	14904.	0.809
0.250	13974.	0.696
0.269	14449.	0.754
0.289	14896.	0.808
0.308	15400.	0.869
0.328	15900.	0.930
0.363	16192.	0.965
0.519	16192.	0.965
0.539	15250.	0.851
0.558	15090.	0.831
0.597	14350.	0.742
0.601	14150.	0.717
0.617	14510.	0.761
0.636	14570.	0.768
0.656	14500.	0.760
0.675	14660.	0.779
0.695	14750.	0.790
0.714	14800.	0.796
0.734	14160.	0.718
0.753	14100.	0.711
0.773	14400.	0.748
0.793	13900.	0.687
0.812	14000.	0.699
0.836	14161.	0.719
0.875	13333.	0.618
0.894	12856.	0.560
0.914	13518.	0.641
0.933	13225.	0.605
0.953	13230.	0.606
1.011	12912.	0.567
1.031	13987.	0.697
1.033	14143.	0.716
1.035	13659.	0.658
1.109	11393.	0.383
1.037	13480.	0.636
1.039	13322.	0.617
1.041	13359.	0.621
1.044	13420.	0.629
1.046	13472.	0.635
1.048	12339.	0.497
1.070	11498.	0.395
1.089	11369.	0.380
1.128	11545.	0.401
1.167	11828.	0.435
1.206	12163.	0.476
1.216	12572.	0.526
1.265	11364.	0.379
1.285	11774.	0.429
1.304	11361.	0.379
1.343	10988.	0.333
1.363	11032.	0.339
1.382	11551.	0.402
1.441	10246.	0.243
1.449	10577.	0.284
1.450	10137.	0.230
1.480	10657.	0.293
1.538	9762.	0.185
1.577	9655.	0.172
1.675	9436.	0.145
1.734	9787.	0.188
1.773	9625.	0.168
1.870	8985.	0.090
1.968	9166.	0.112
2.065	9073.	0.101
2.261	8956.	0.087
2.456	8388.	0.018
3.041	8500.	0.032
3.432	8358.	0.014
3.627	8350.	0.013
3.920	8349.	0.013
4.994	8513.	0.033
5.872	8687.	0.054
6.946	8467.	0.028

TABLE VII MMB-28 Area and Holdup Over Time

Time (s)	Area (mm^2)	Holdup	Time (s)	Area (mm^2)	Holdup
0.000	6040.	0.000	0.700	7538.	0.248
0.089	7298.	0.208	0.757	7487.	0.240
0.108	7482.	0.239	0.776	8124.	0.345
0.127	8164.	0.352	0.795	8126.	0.345
0.141	9729.	0.611	0.853	8336.	0.380
0.150	13331.	1.207	0.892	8153.	0.350
0.158	14683.	1.431	0.930	8112.	0.343
0.171	16192.	1.681	0.969	7447.	0.233
0.305	16192.	1.681	1.046	7380.	0.222
0.307	13500.	1.235	1.142	7579.	0.255
0.348	13000.	1.152	1.200	7264.	0.203
0.368	12500.	1.070	1.354	6043.	0.000
0.387	12000.	0.987	1.546	5635.	-0.067
0.407	10500.	0.738	1.739	5389.	-0.108
0.426	9800.	0.623	1.932	5416.	-0.103
0.446	8500.	0.407	2.124	5501.	-0.089
0.465	8100.	0.341	2.317	5621.	-0.069
0.504	8750.	0.449	2.509	5662.	-0.063
0.526	9061.	0.500	2.895	5766.	-0.045
0.584	8883.	0.471	3.280	5879.	-0.027
0.603	8061.	0.335	3.852	5878.	-0.027
0.622	7916.	0.311	5.777	6138.	0.016
0.641	7809.	0.293	7.703	6051.	0.002
0.661	7372.	0.221	9.629	6115.	0.012

TABLE VIII MMB-34 Area and Holdup Over Time

Time (s)	Area (mm^2)	Holdup
0.000	7090.	0.000
0.152	7418.	0.046
0.164	7325.	0.033
0.177	7419.	0.046
0.188	7885.	0.112
0.198	8590.	0.212
0.209	9137.	0.289
0.219	9590.	0.353
0.230	9946.	0.403
0.240	10290.	0.451
0.251	10542.	0.487
0.255	10881.	0.535
0.259	11703.	0.651
0.264	12851.	0.813
0.268	13646.	0.925
0.272	14246.	1.009
0.276	13750.	0.939
0.280	14000.	0.975
0.285	14100.	0.989
0.291	14300.	1.017
0.297	14400.	1.031
0.304	14600.	1.059
0.312	14900.	1.102
0.363	15100.	1.130
0.390	16192.	1.284
0.580	16192.	1.284
0.601	16000.	1.257
0.622	15800.	1.228
0.643	15500.	1.186
0.664	15089.	1.128
0.675	14334.	1.022
0.685	13626.	0.922
0.706	12949.	0.826
0.727	12686.	0.789
0.770	12288.	0.733
0.791	12322.	0.738
0.812	14482.	1.043
0.833	12831.	0.810
1.002	14265.	1.012
1.023	14442.	1.037
1.044	15017.	1.118
1.086	15371.	1.168
1.128	15471.	1.182
1.149	15309.	1.159
1.191	15033.	1.120
1.212	14420.	1.034
1.234	14195.	1.002
1.339	13232.	0.866
1.402	12620.	0.780
1.487	11787.	0.662
1.519	11355.	0.602
1.592	10973.	0.548
1.634	10588.	0.493
1.687	10170.	0.434
1.792	9184.	0.295
1.898	8508.	0.200
2.003	7837.	0.105
2.109	7299.	0.029
2.214	6814.	-0.039
2.319	6709.	-0.054
2.530	6651.	-0.062
2.741	6619.	-0.066
2.952	6717.	-0.053
4.217	6823.	-0.038
6.326	6824.	-0.038
8.434	6950.	-0.020

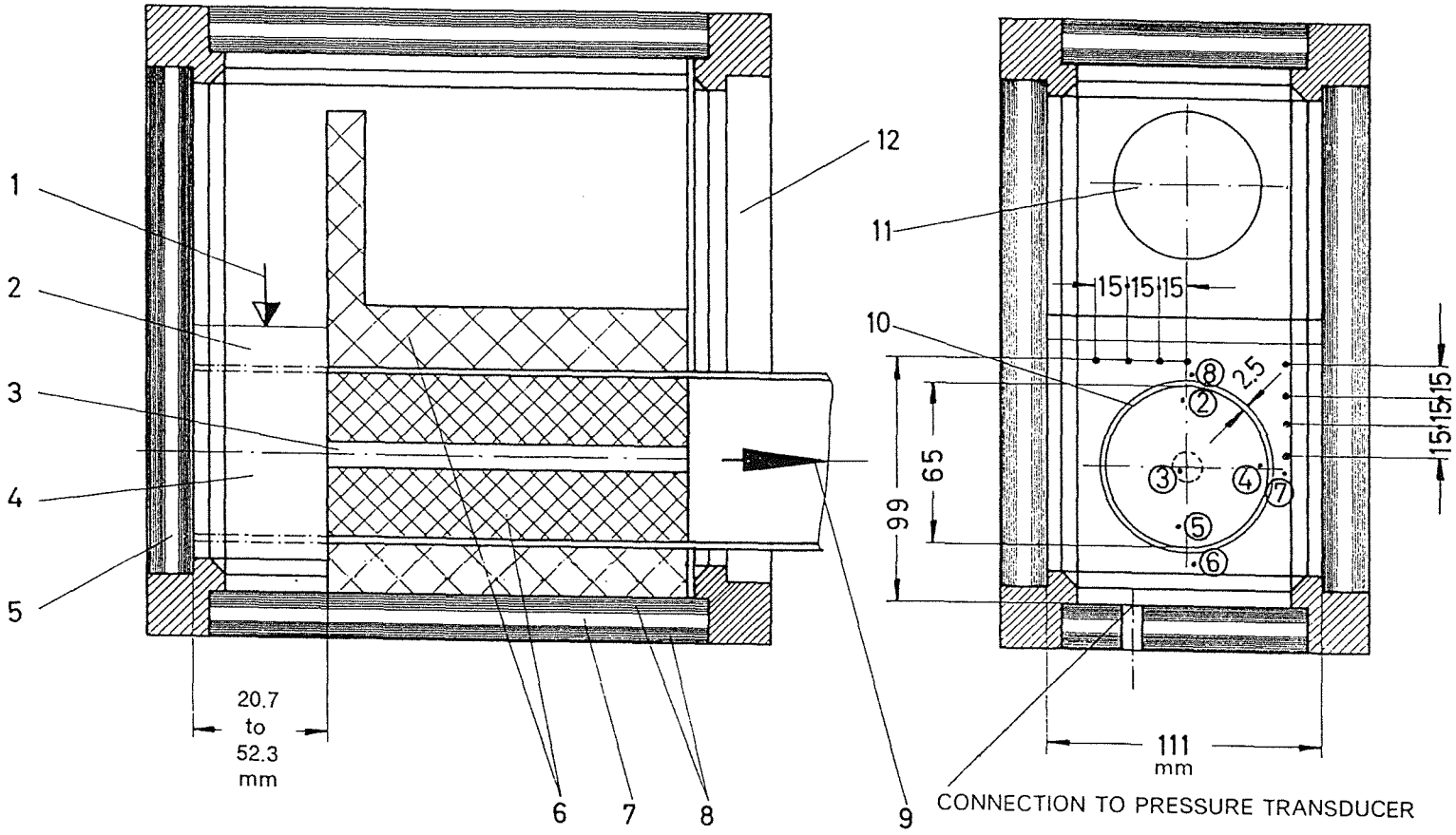

1 AMMONIA LIQUID LEVEL
2 LIQUID AMMONIA
3 HYDROCARBON INLET
4 LIQUID HYDROCARBON
5 DOUBLE PANE FRONT WINDOW
6 DISPLACEMENT INSERTS
7 CHANNEL FOR LIQUID COOLANT
8 DOUBLE PANE SIDE WINDOW
9 MOVEMENT OF SEPARATING CYLINDER
10 SEPARATING CYLINDER
11 EXHAUST
12 FITTING TO REAR AND MOTOR DRIVE

Fig.1 MMB Main Reaction Box, Side and Front View

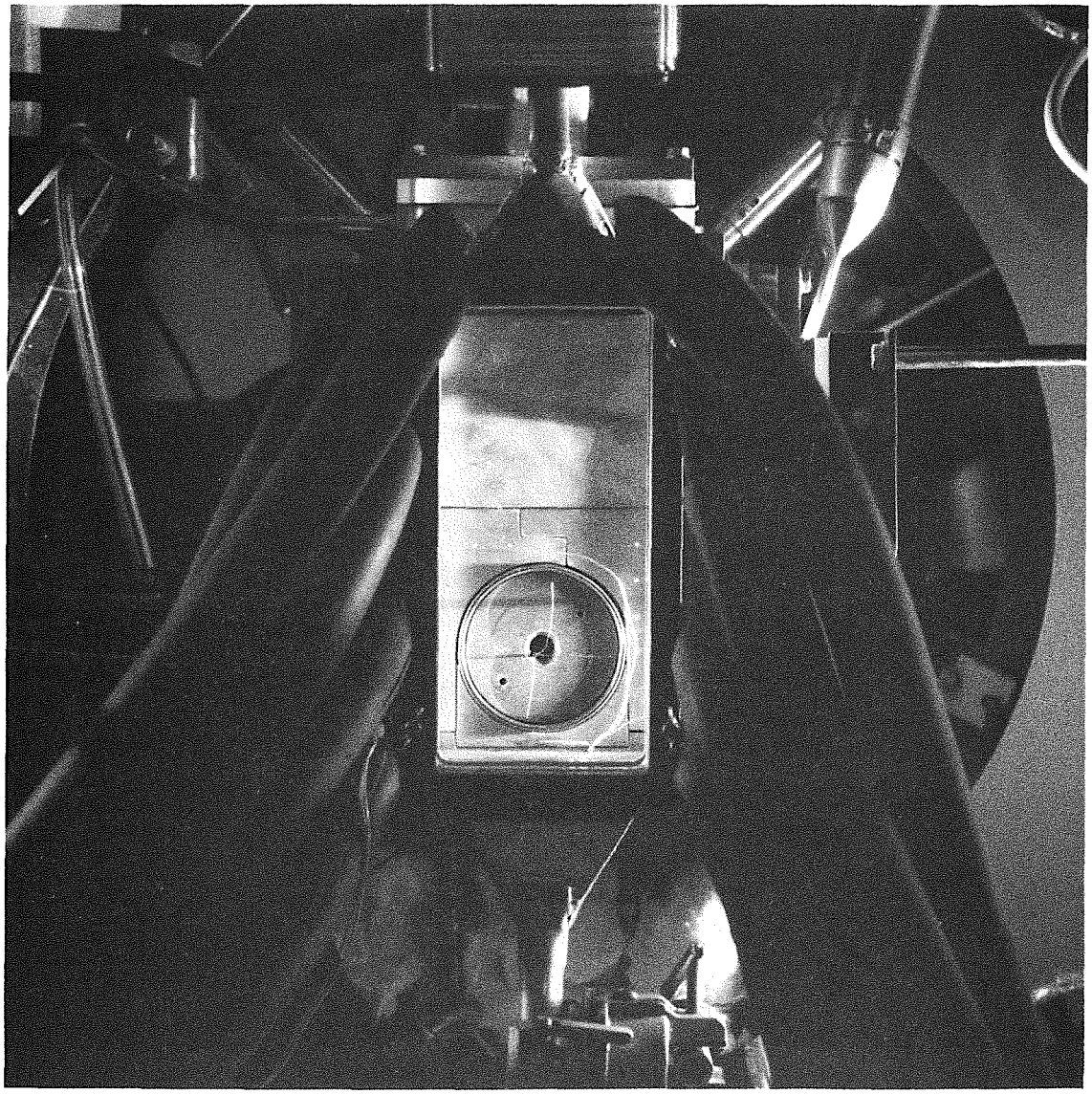

Fig.2 MMB Front Window

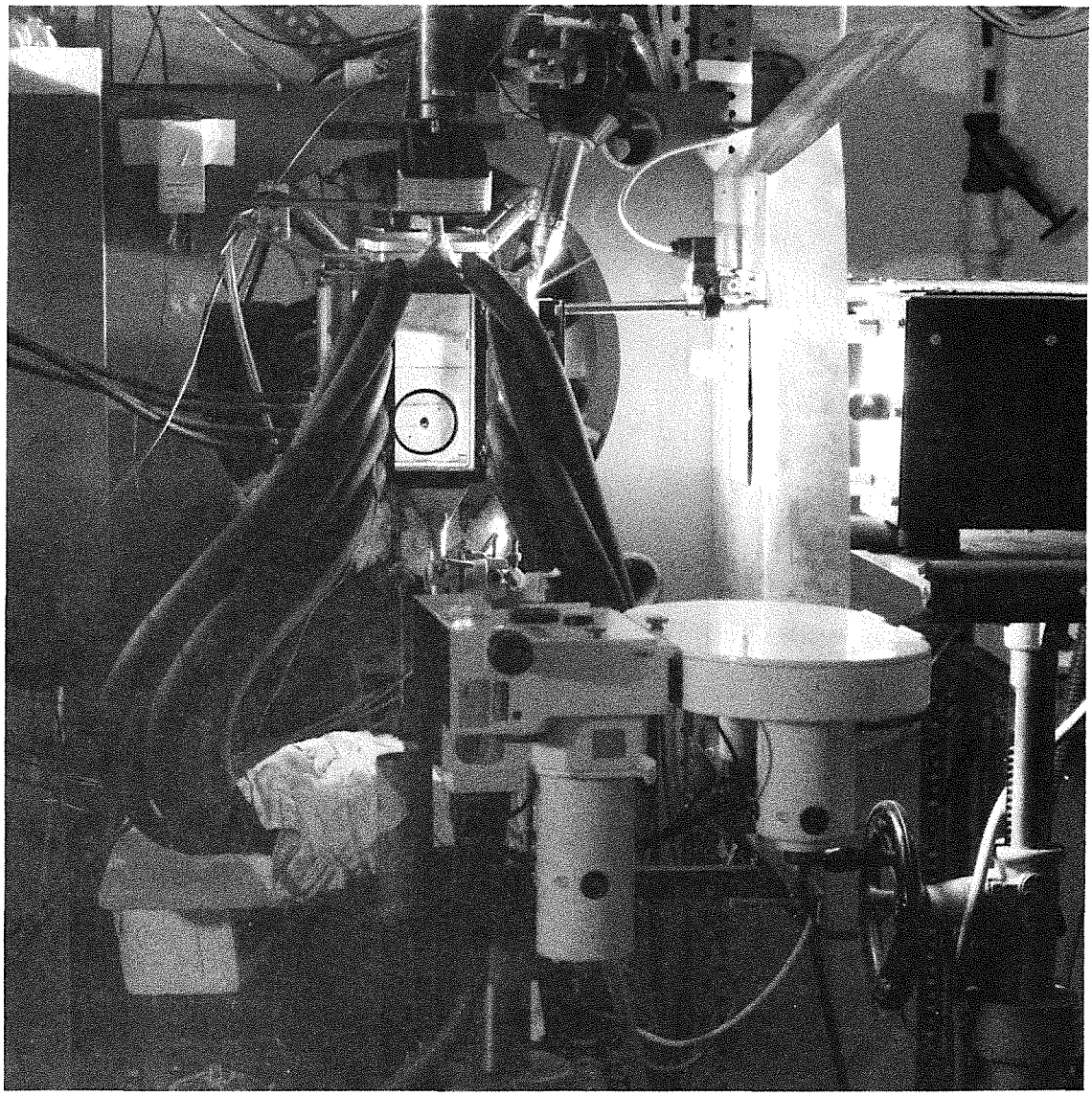

Fig.3 MMB Front View

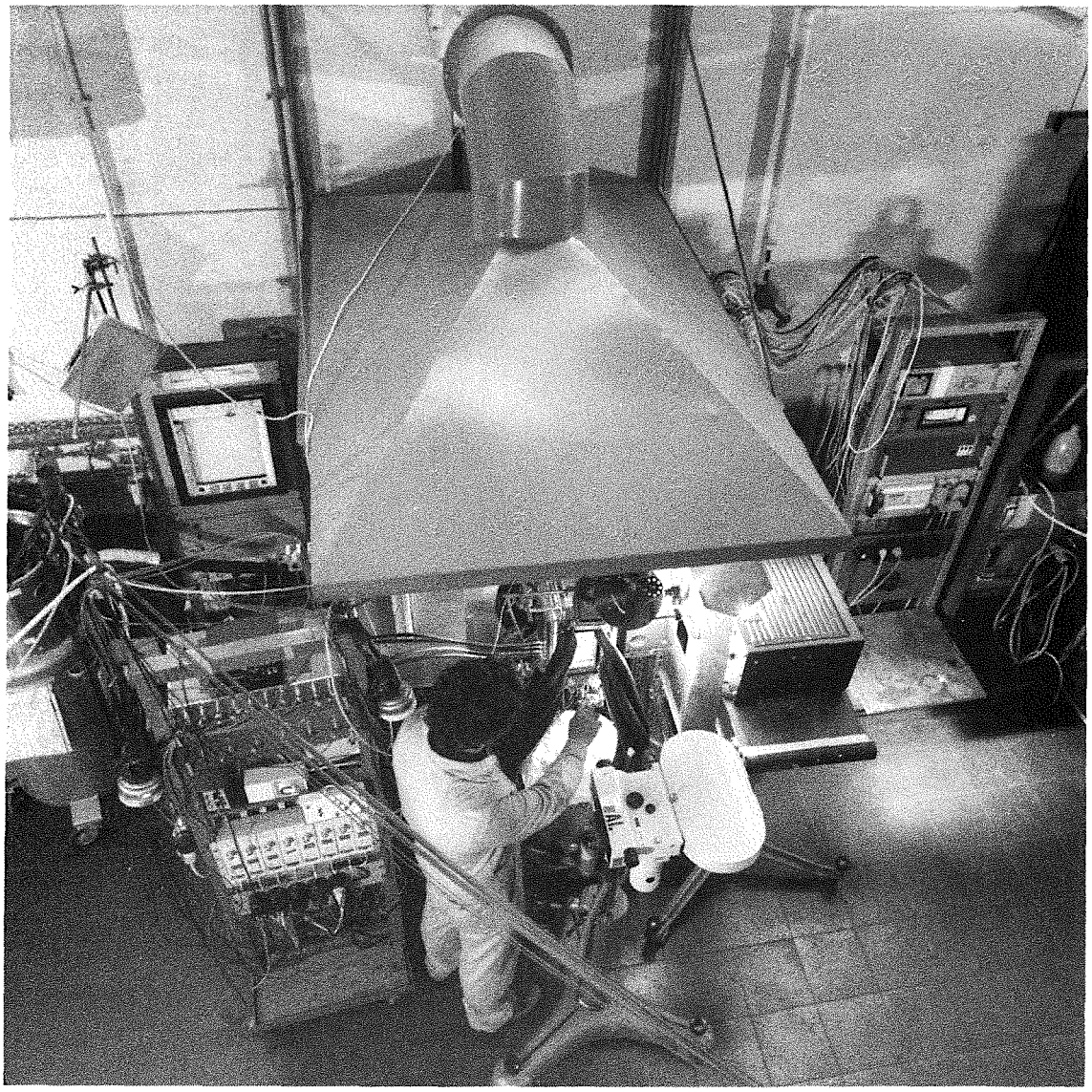

Fig.4 MMB Downward View

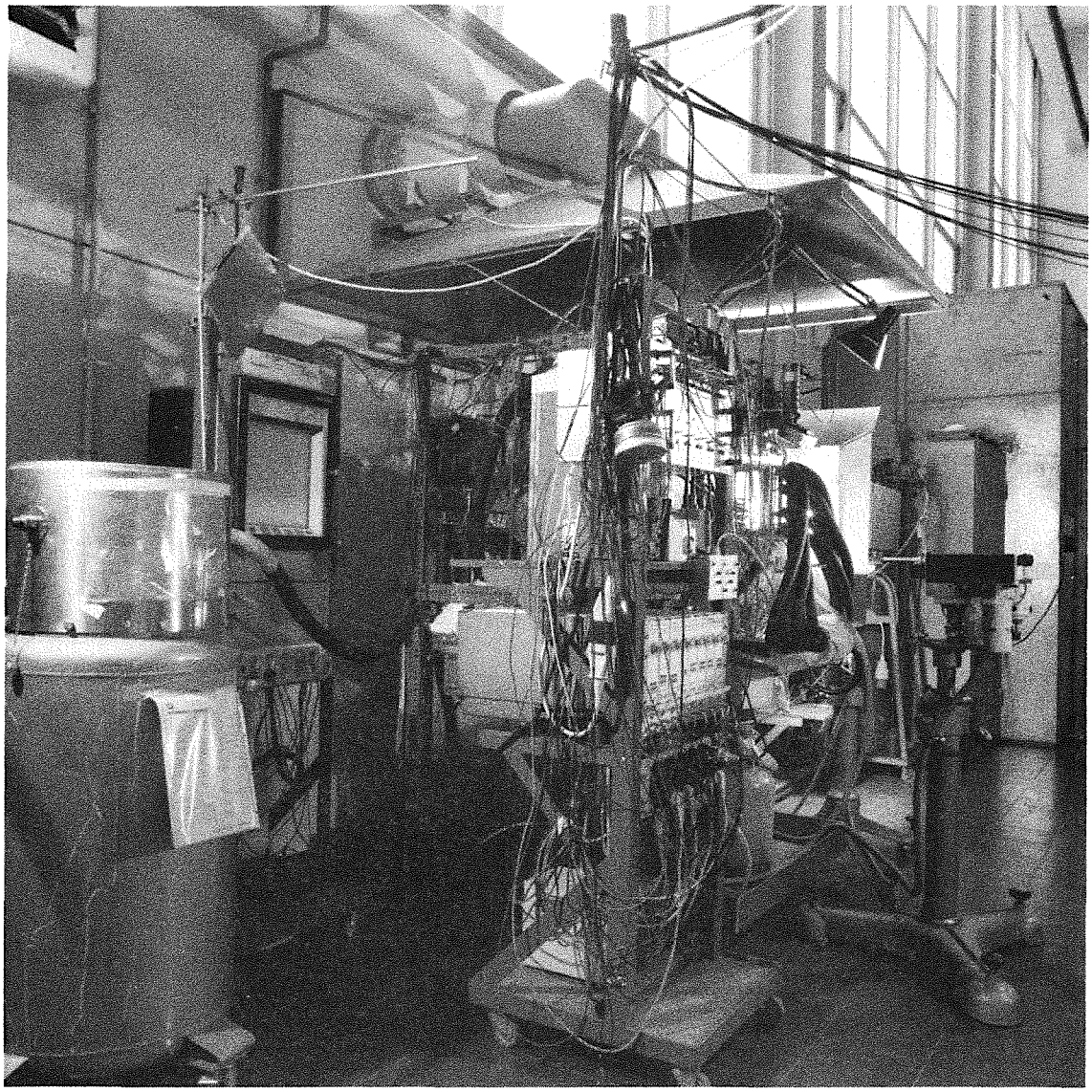

Fig.5 MMB Side View

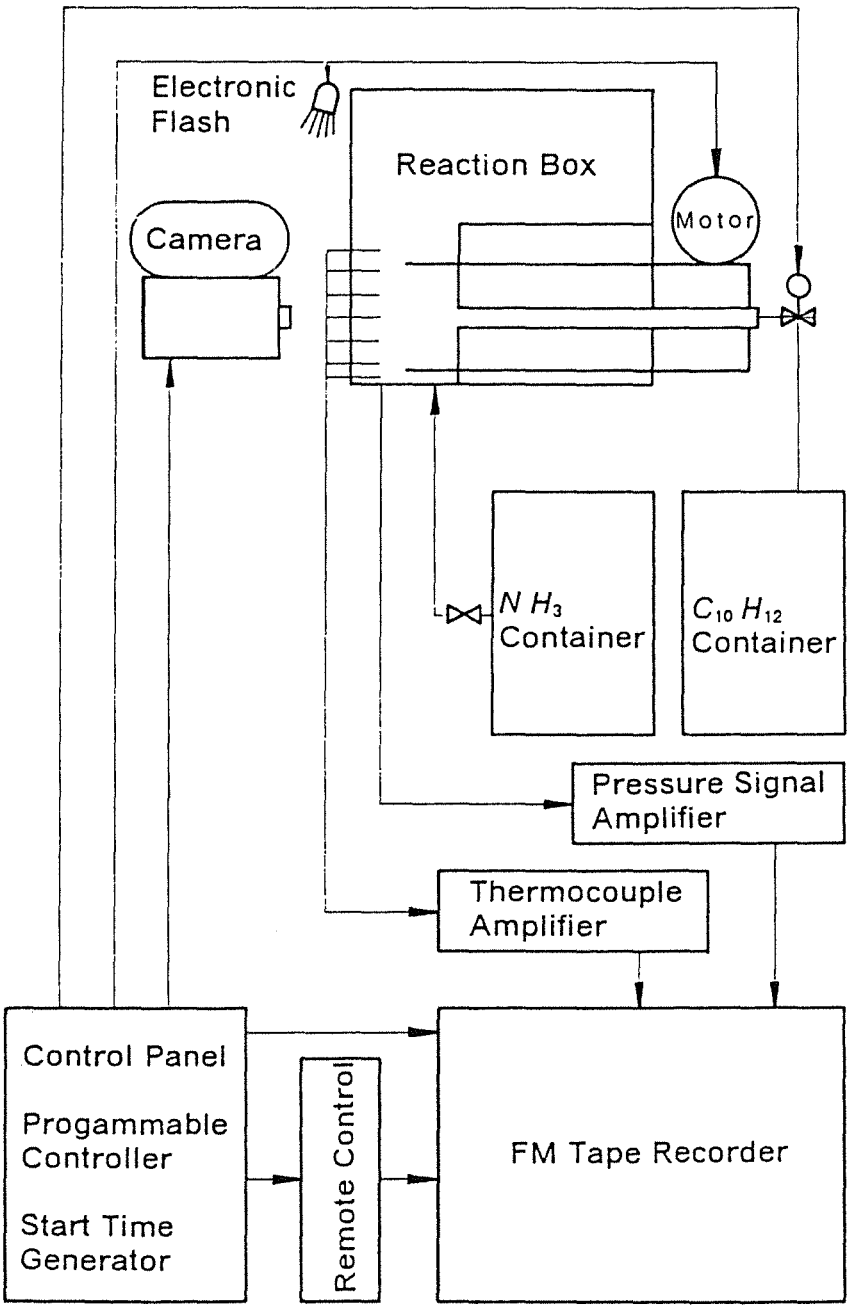

Fig.6 Control and Data Acquisition

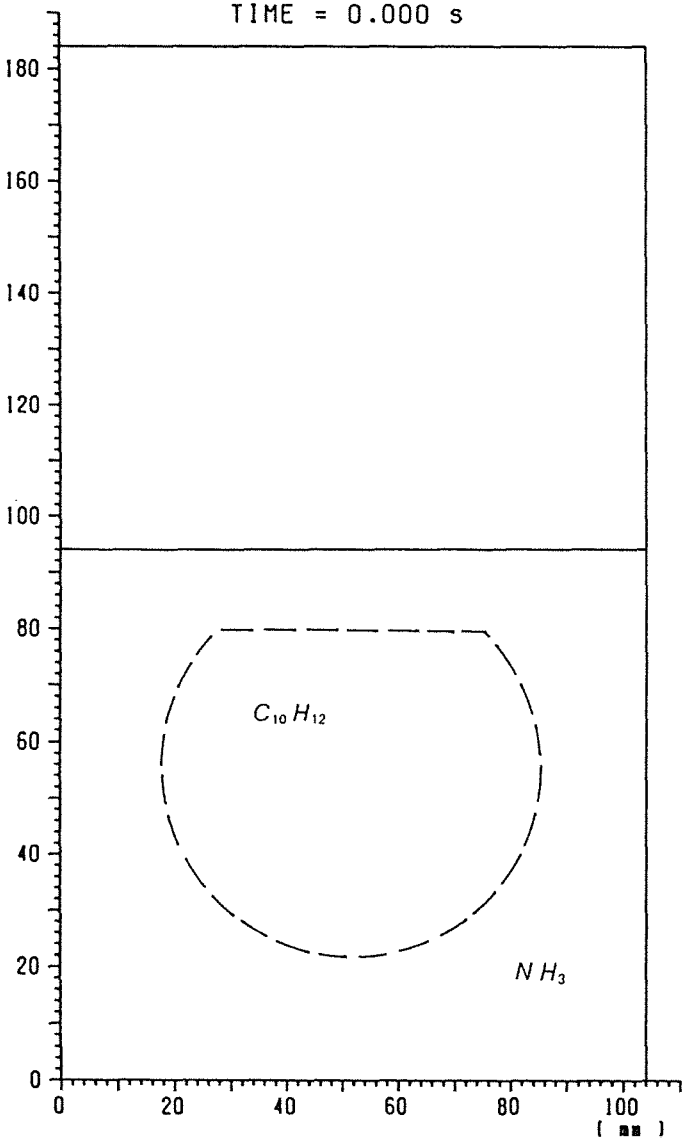

Fig.7a Isothermal Test Interfaces MMB-07

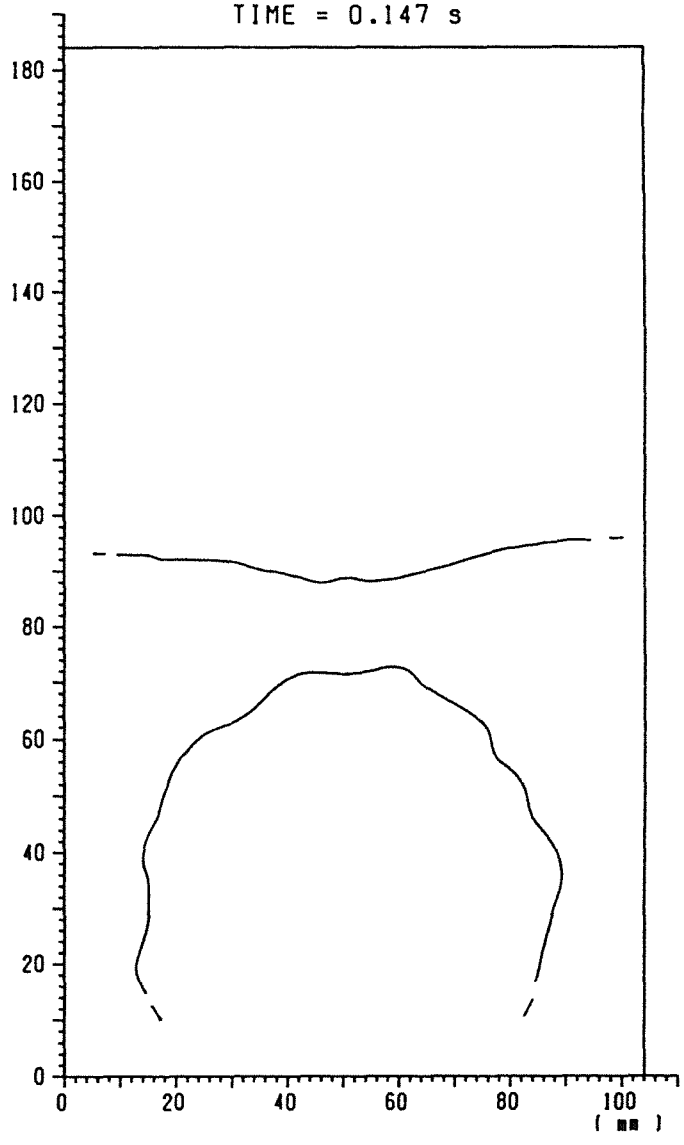

Fig.7b Isothermal Test Interfaces MMB-07

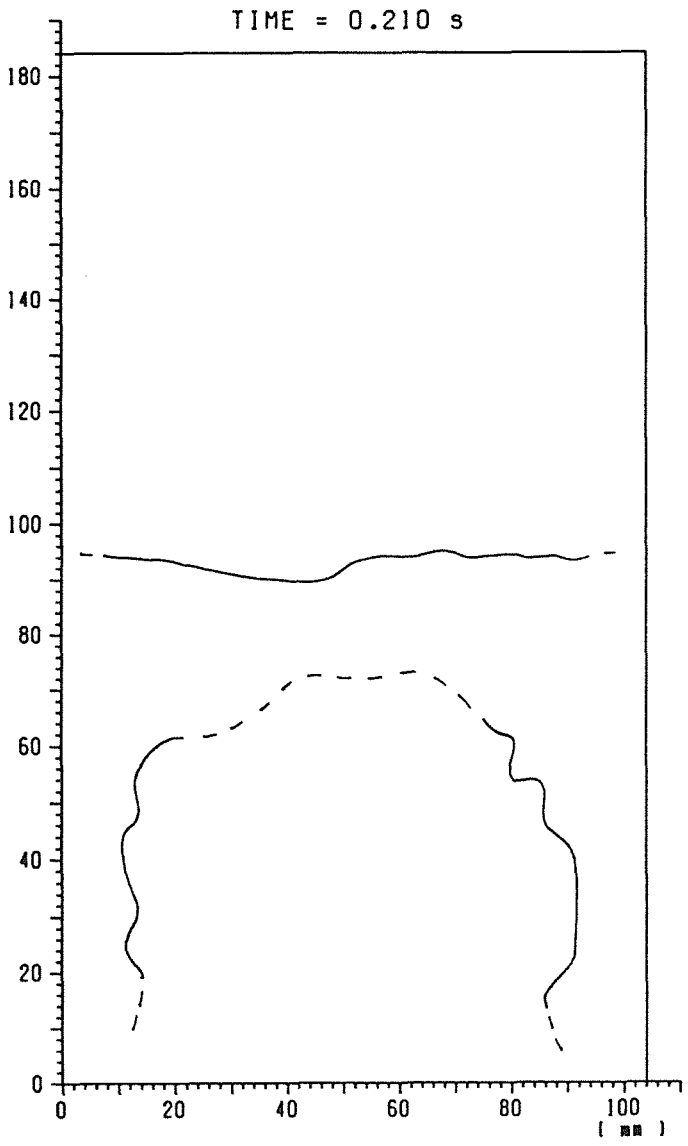

Fig.7c Isothermal Test Interfaces *MMB-07*

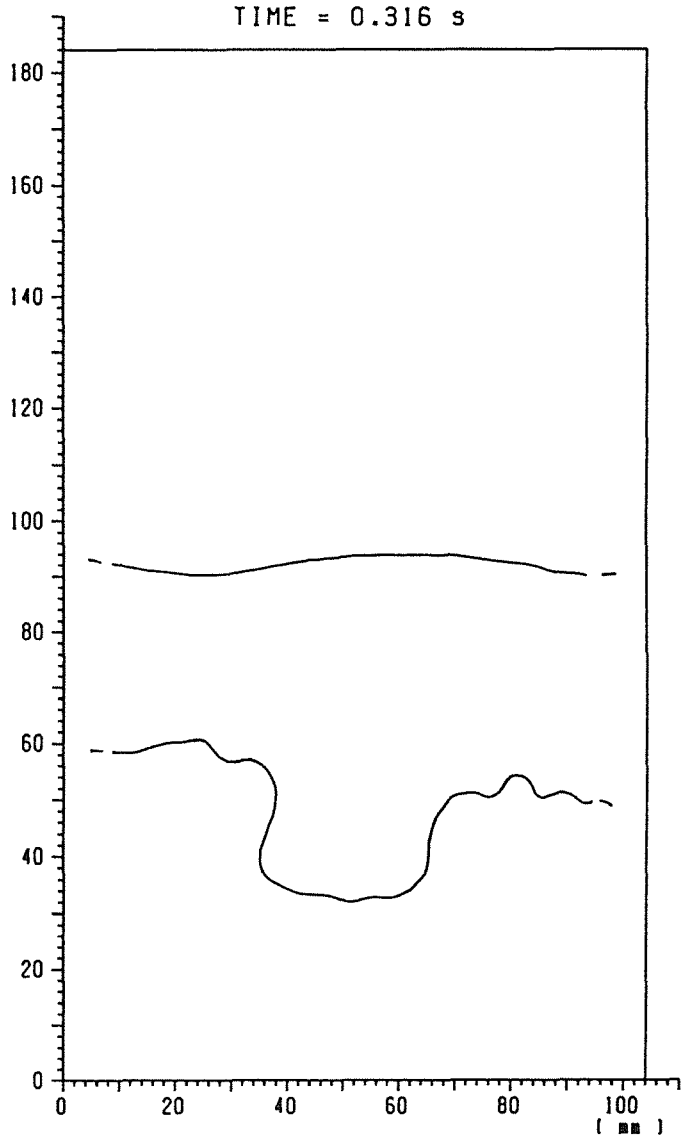

Fig.7d Isothermal Test Interfaces *MMB-07*

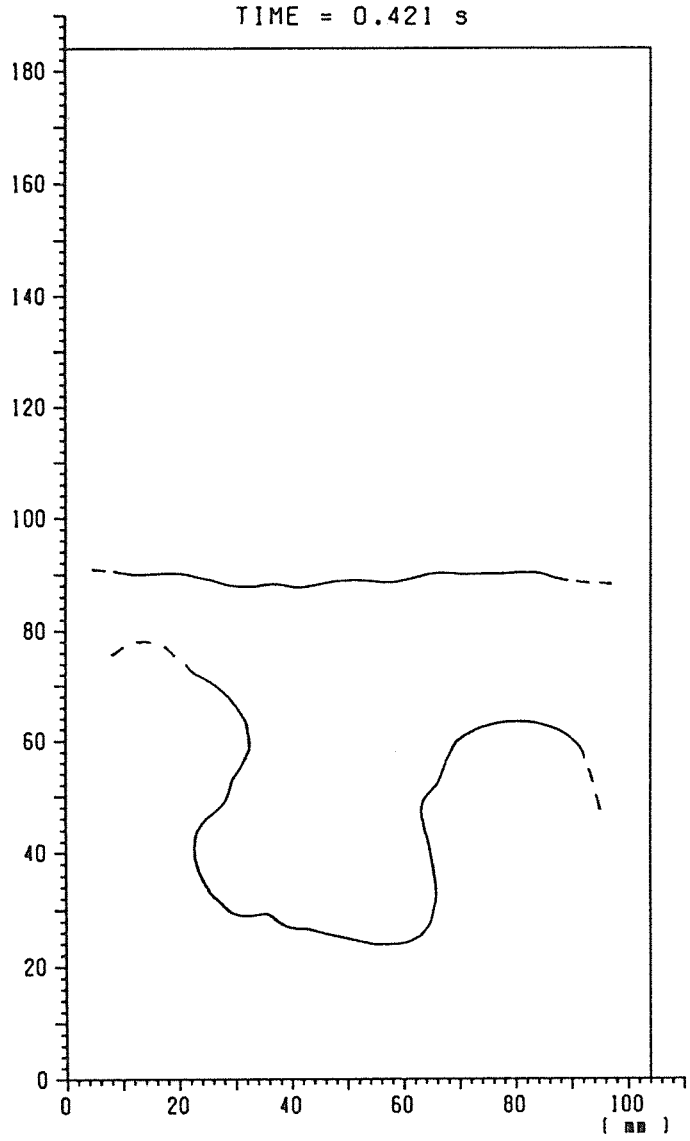

Fig.7e Isothermal Test Interfaces MMB-07

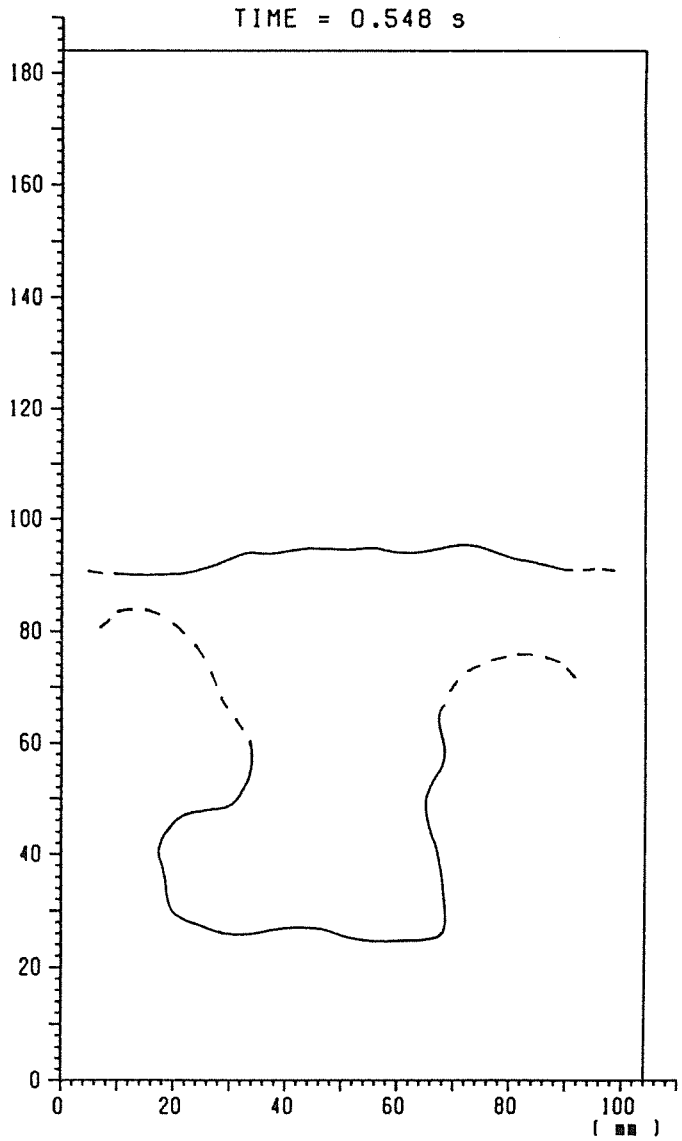

Fig.7f Isothermal Test Interfaces MMB-07

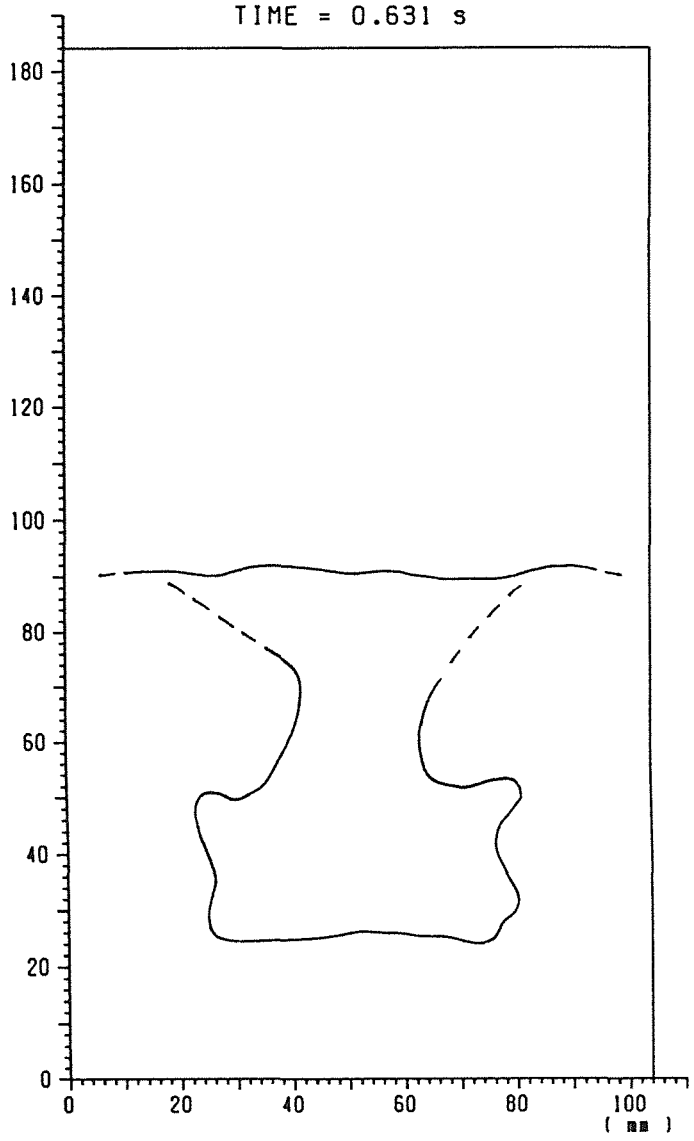

Fig.7g Isothermal Test Interfaces *MMB-07*

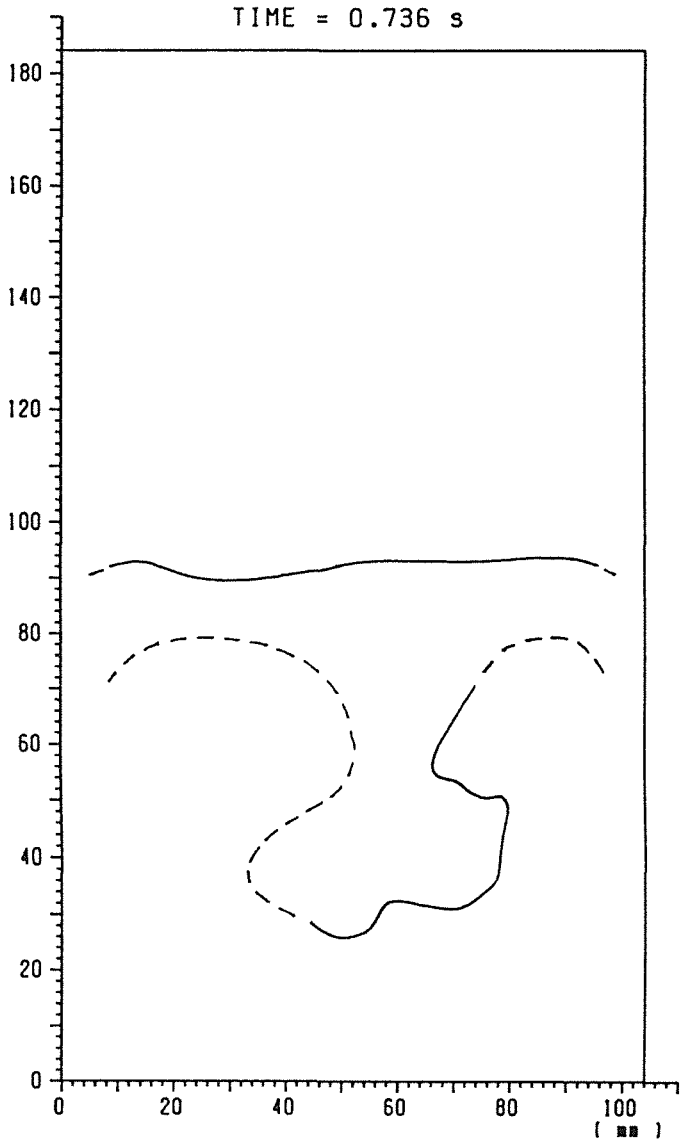

Fig.7h Isothermal Test Interfaces *MMB-07*

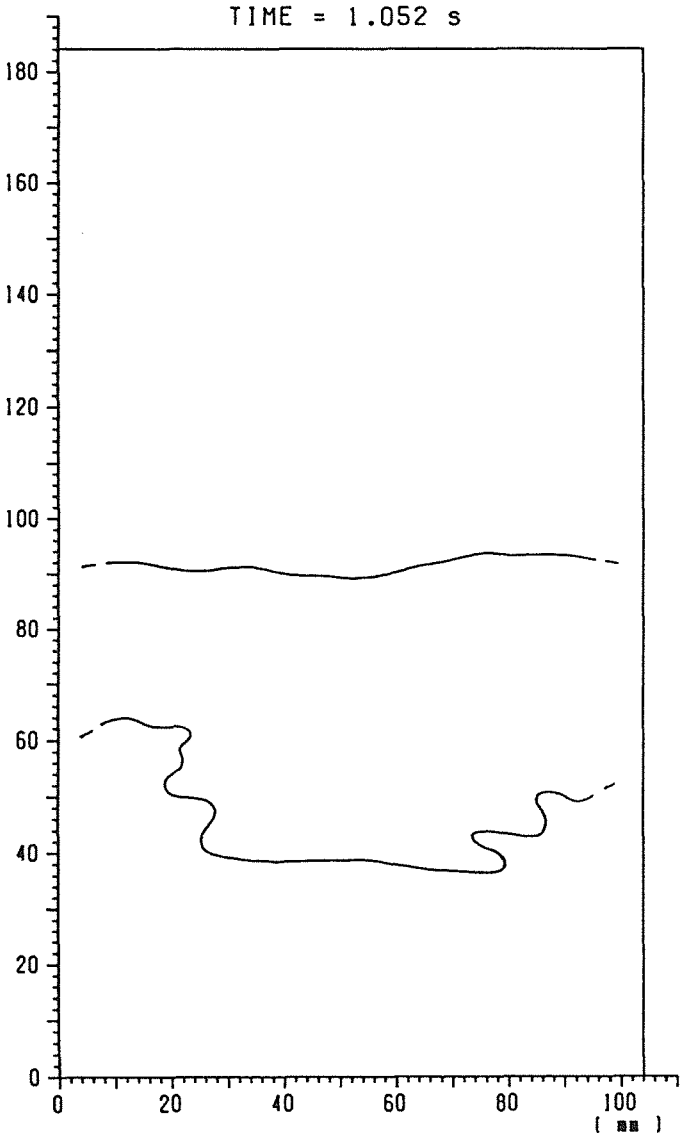

Fig.7i Isothermal Test Interfaces MMB-07

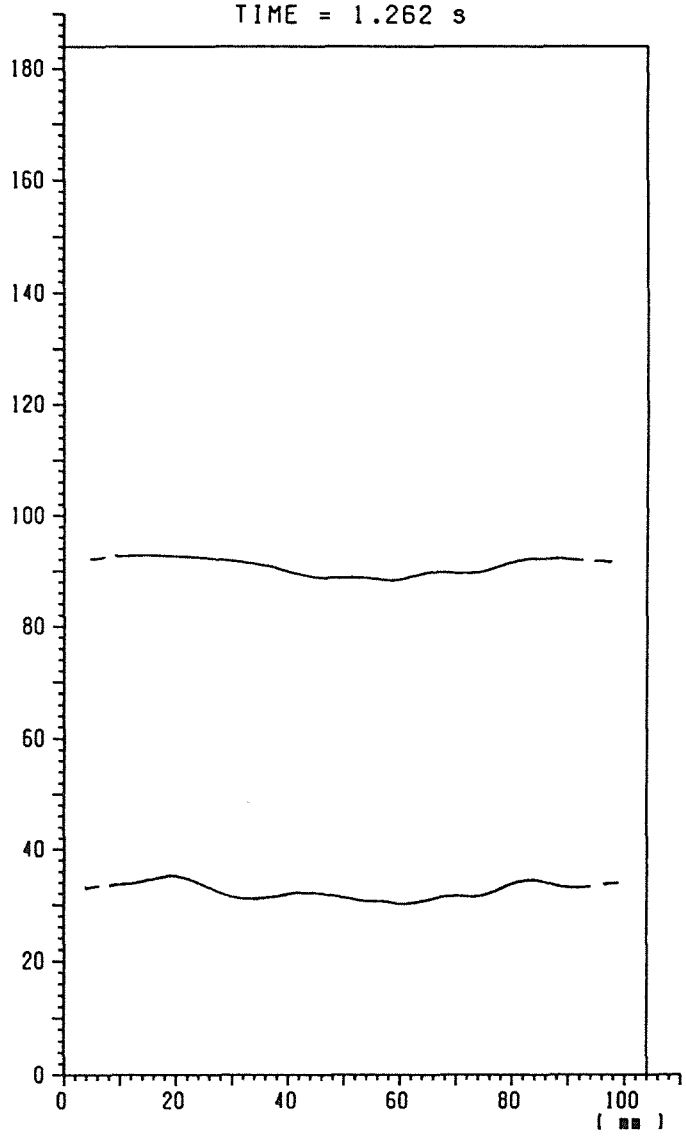

Fig.7j Isothermal Test Interfaces MMB-07

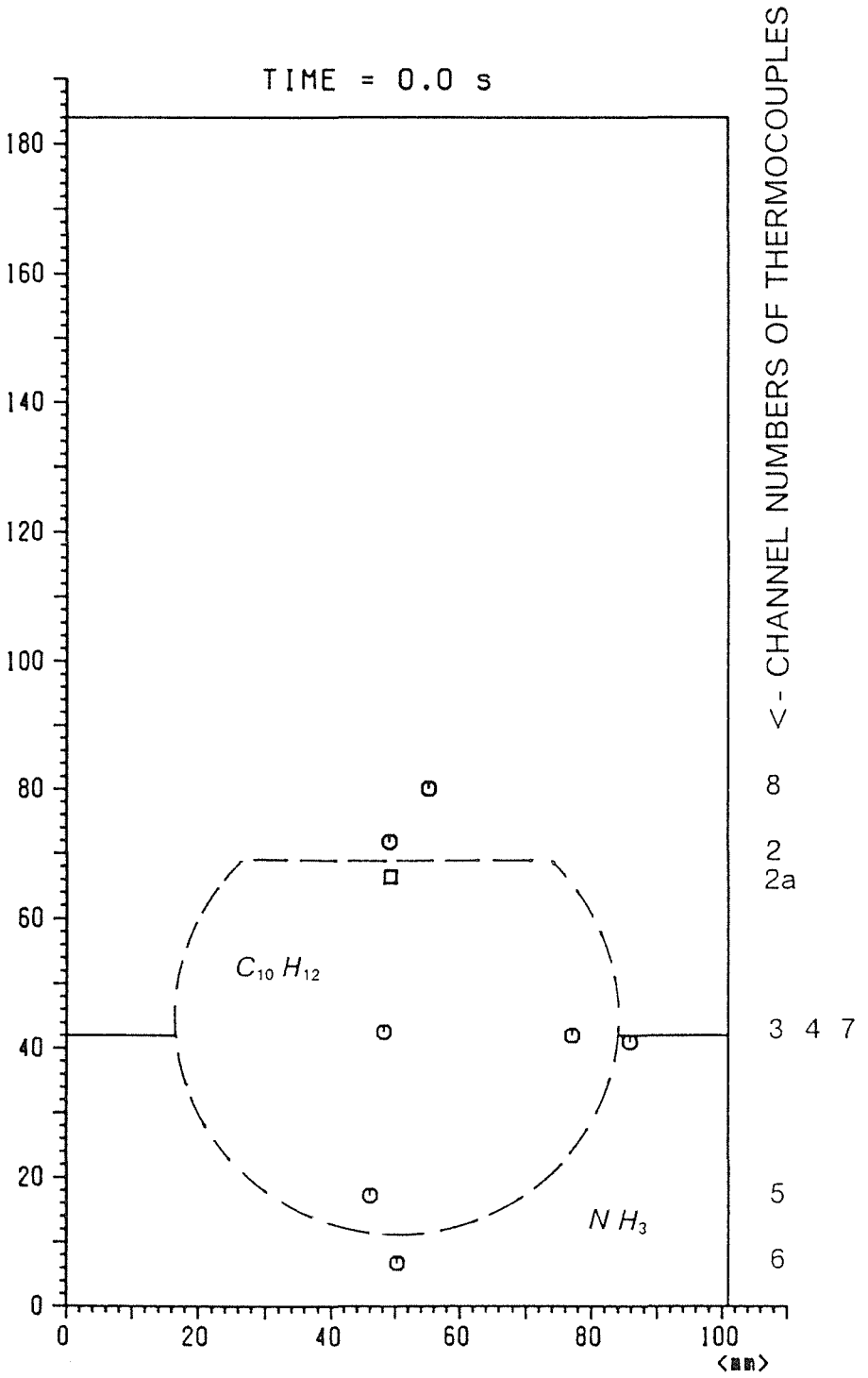

Fig.8 Idealized Initial Configuration MMB-19

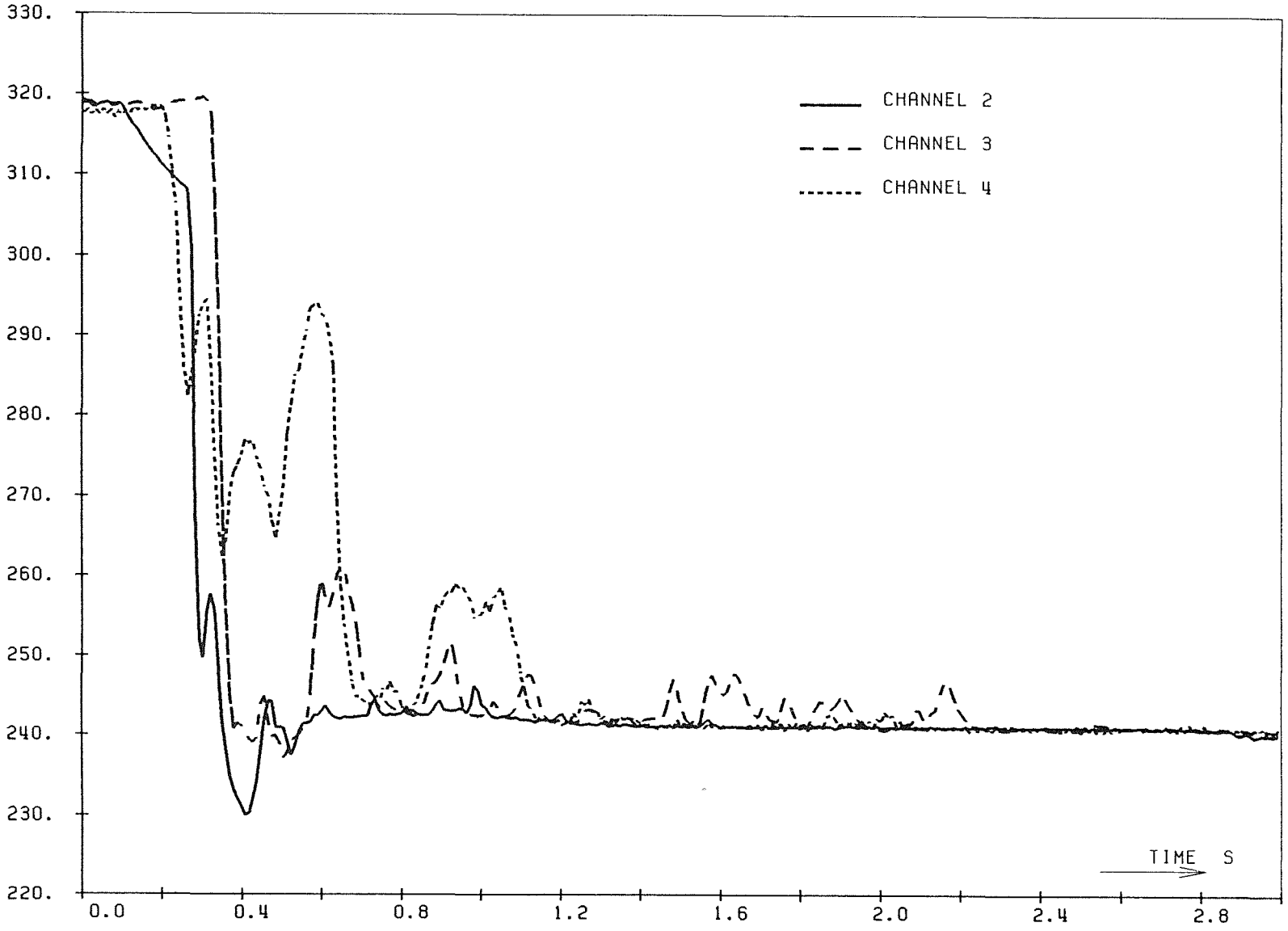

Fig.9 MMB-19 Temperatures (K) Versus Time

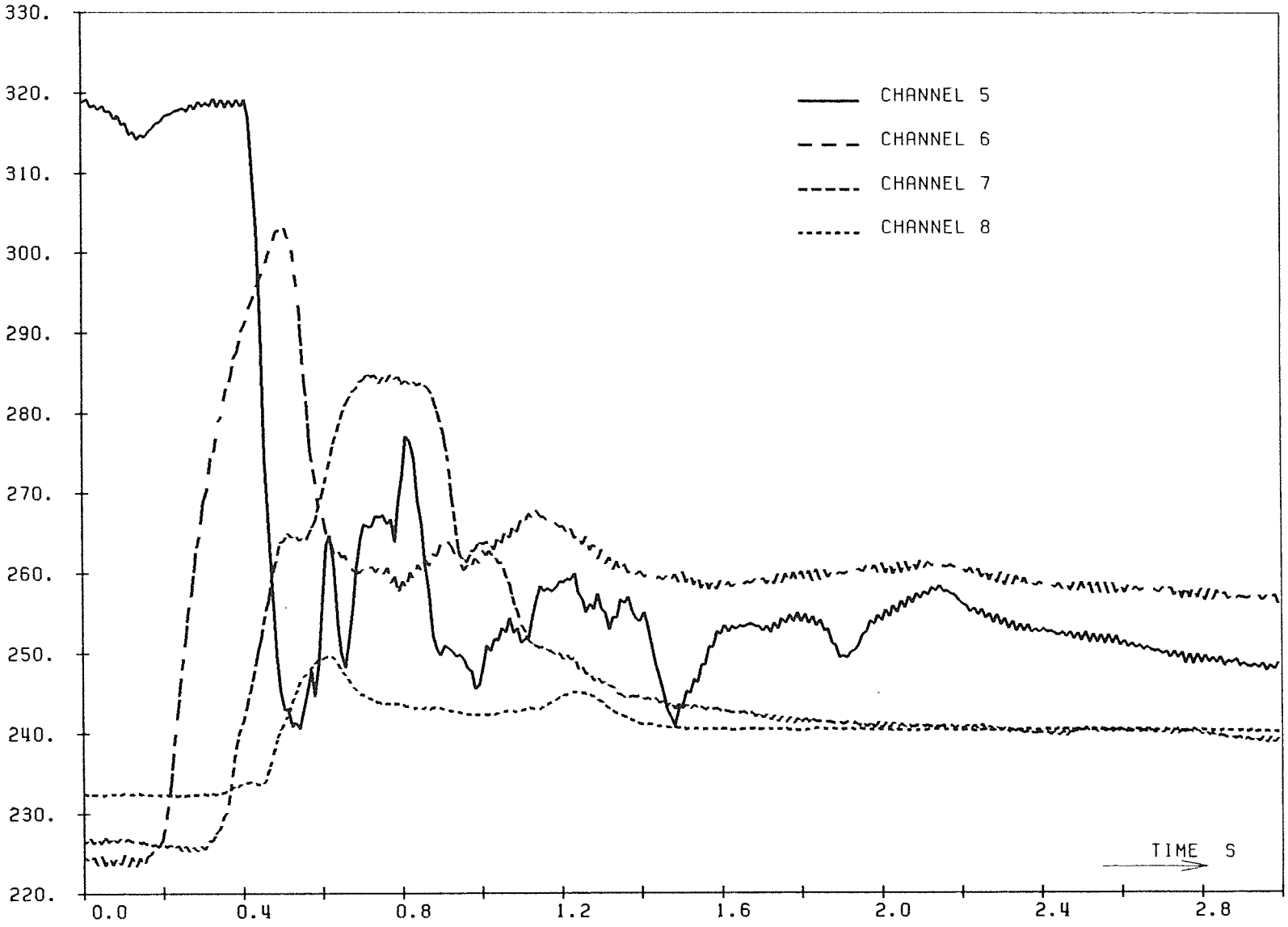

Fig.10 MMB-19 Temperatures (K) Versus Time

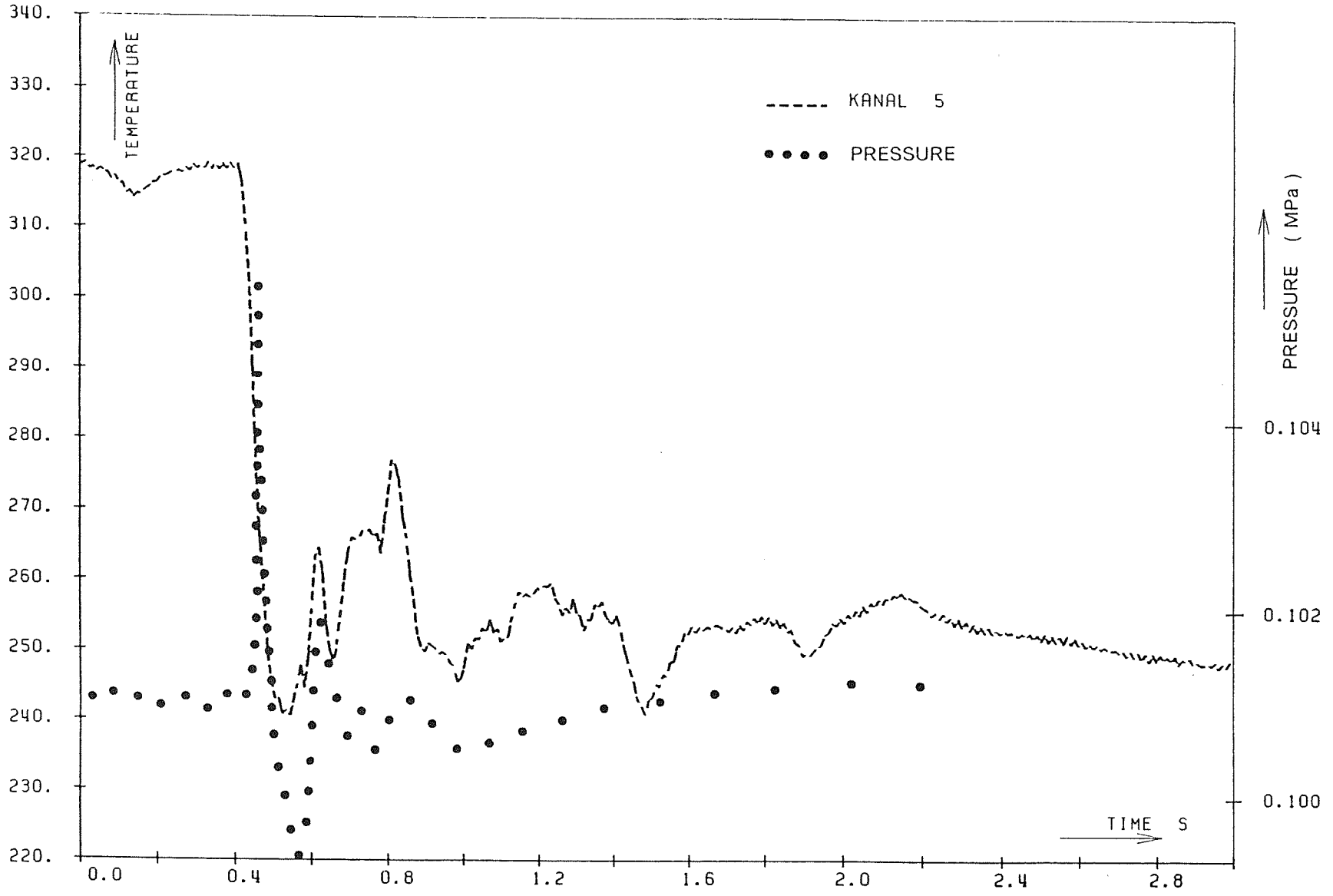

Fig.11 MMB-19 Pressure and Temperature (K) of Channel 5

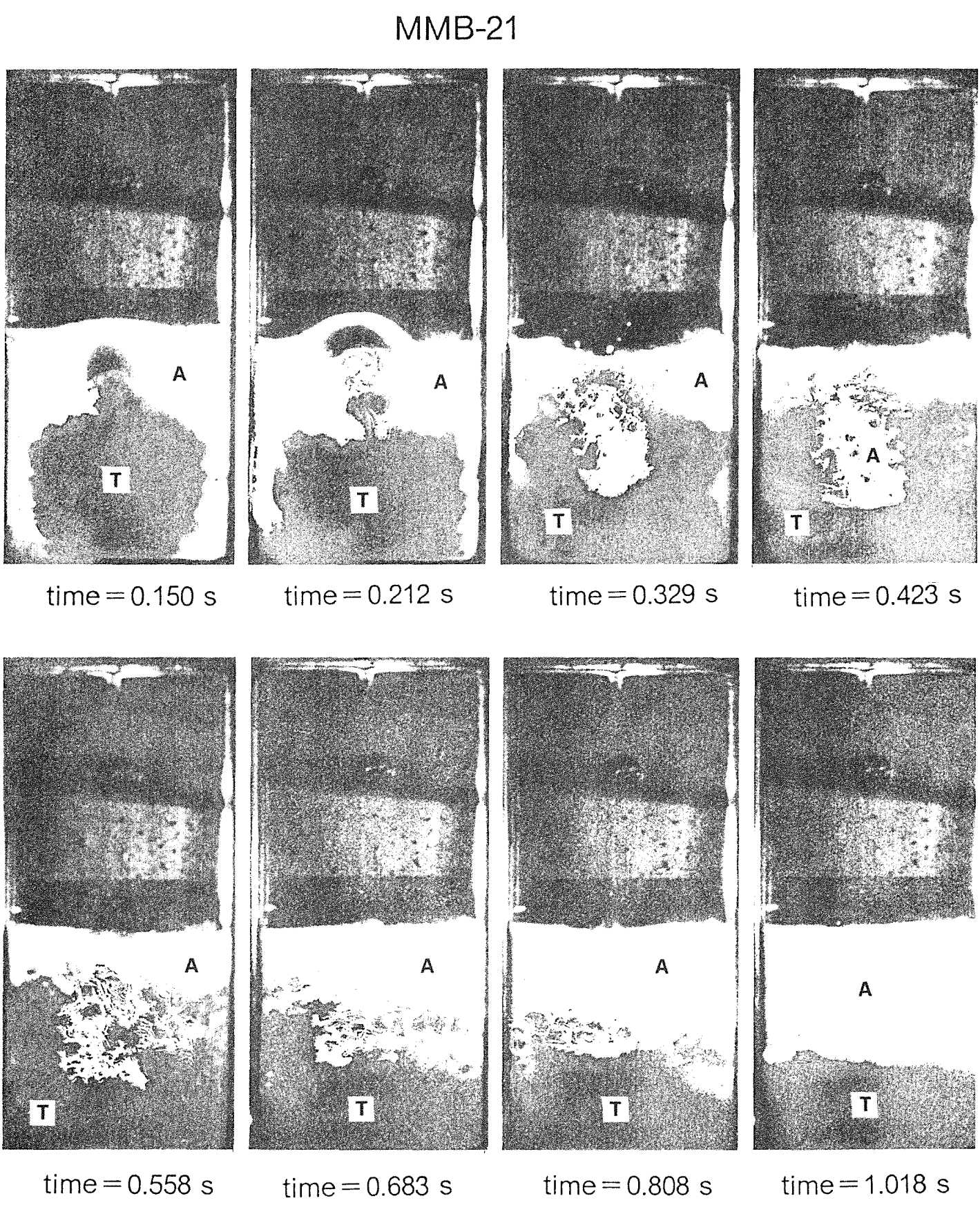

Fig.12 MMB-21 High Speed Movie Frames of Tetralin (T) and Ammonia (A)

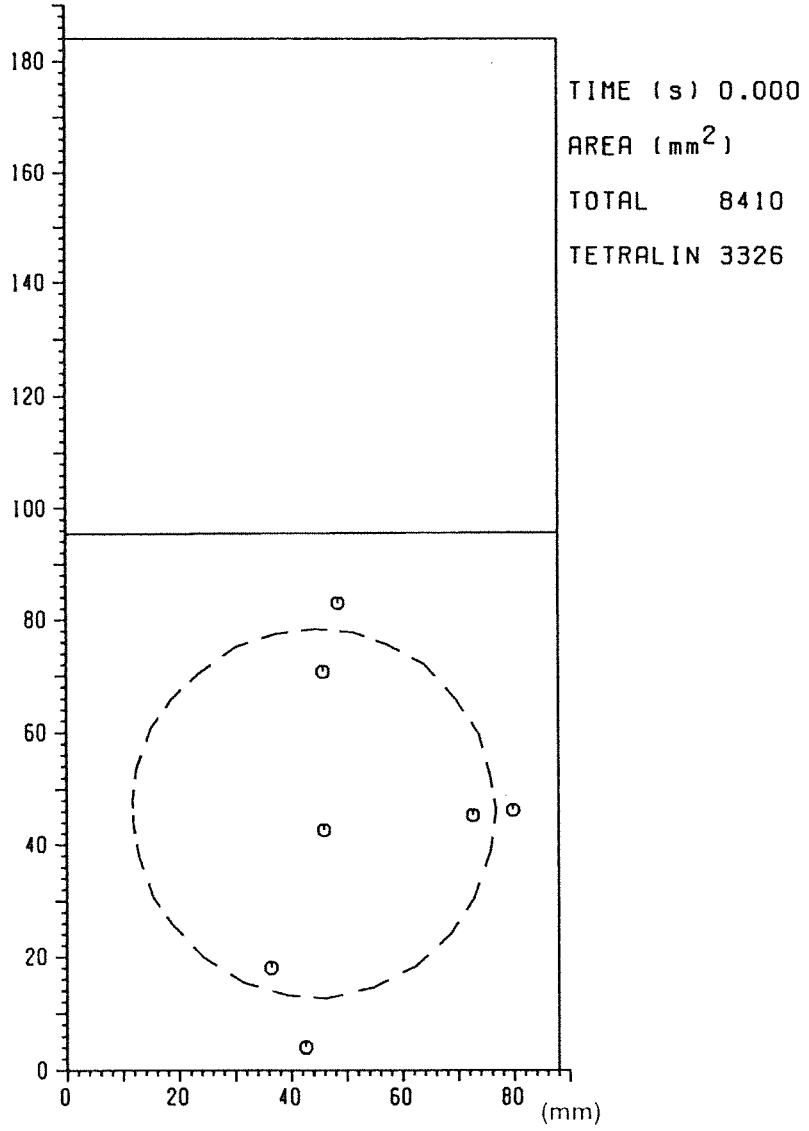

Fig.13a Initial Configuration *MMB-21*

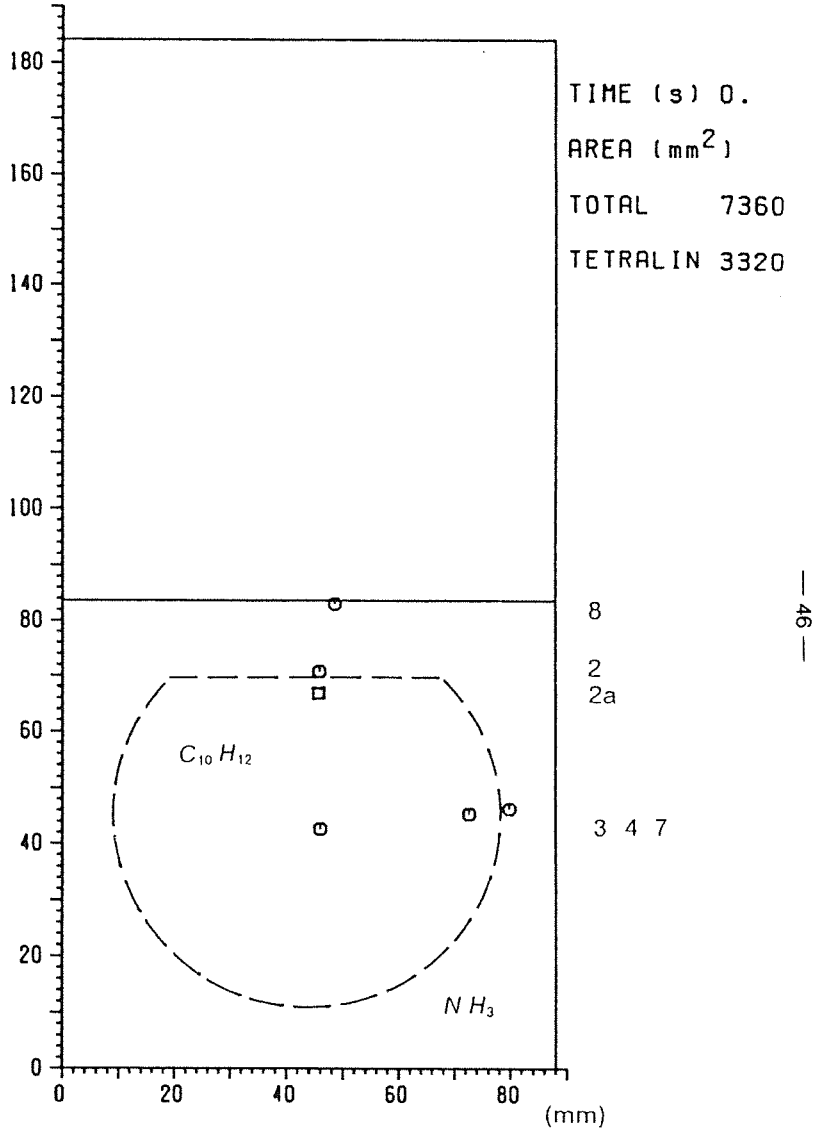

Fig.13b Idealized Initial Configuration *MMB-21*

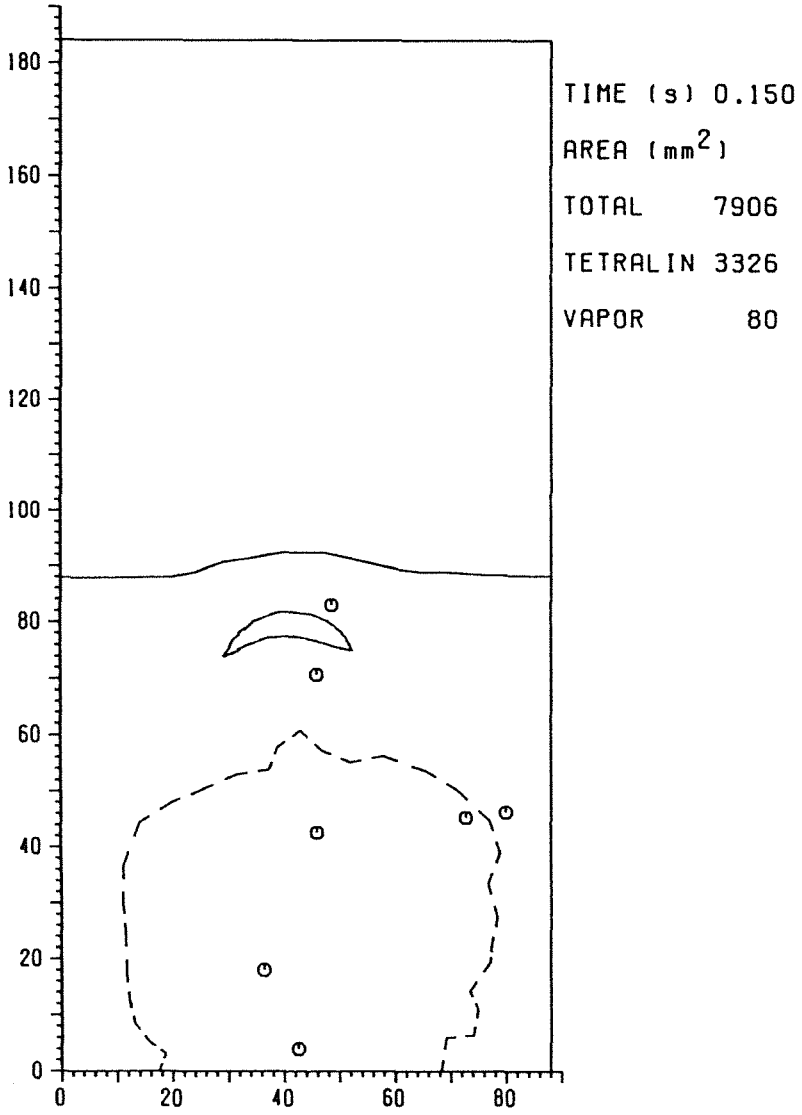

Fig.14a Isothermal Test
Actual Interfaces MMB-21

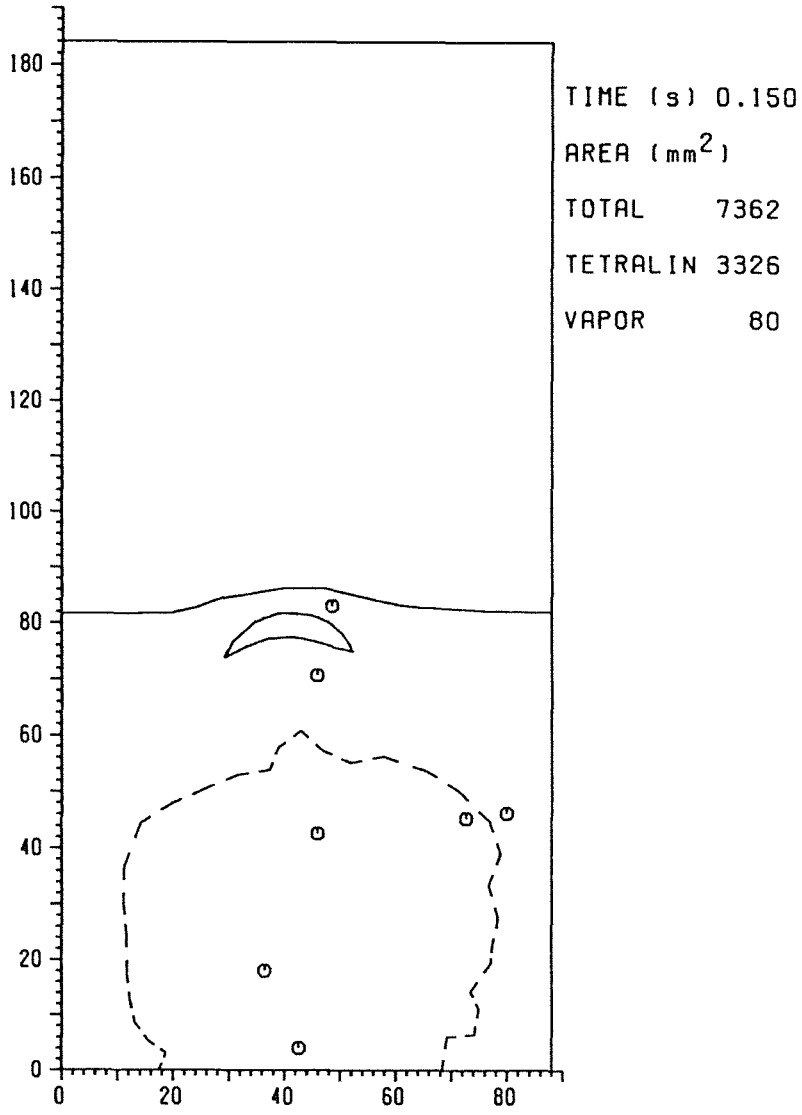

Fig.14b Isothermal Test
Corrected Interfaces MMB-21

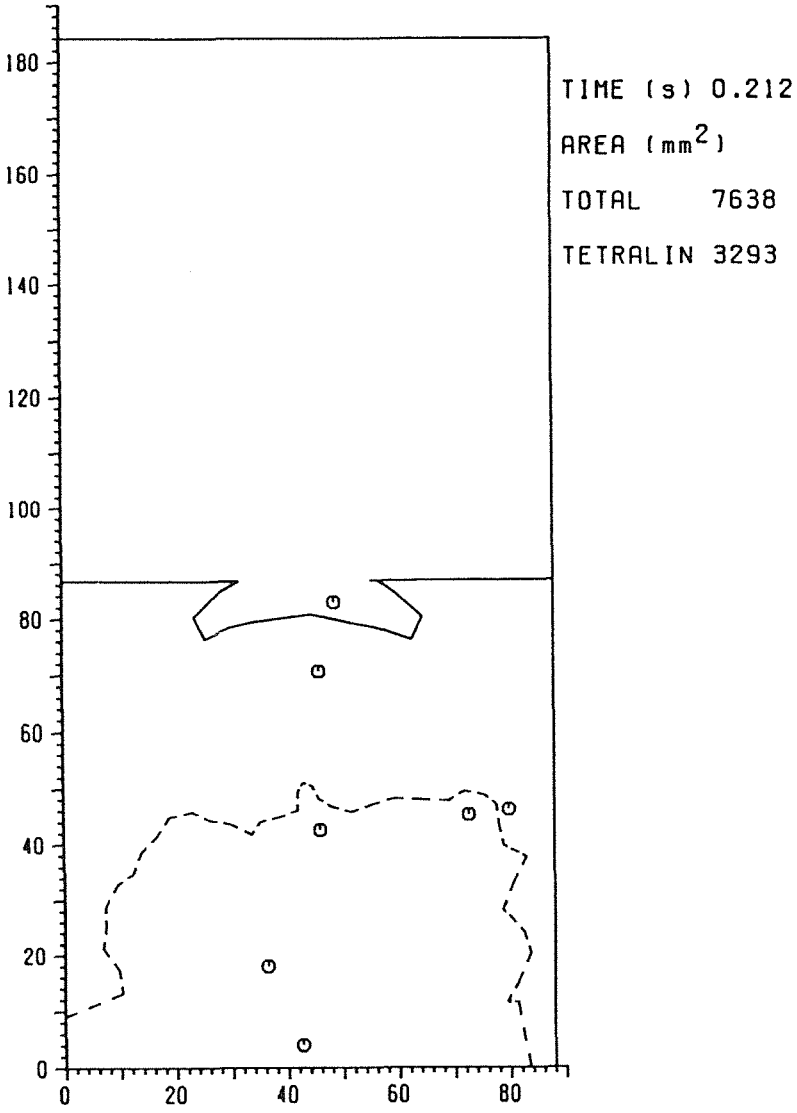

Fig.15a Isothermal Test
Actual Interfaces *MMB-21*

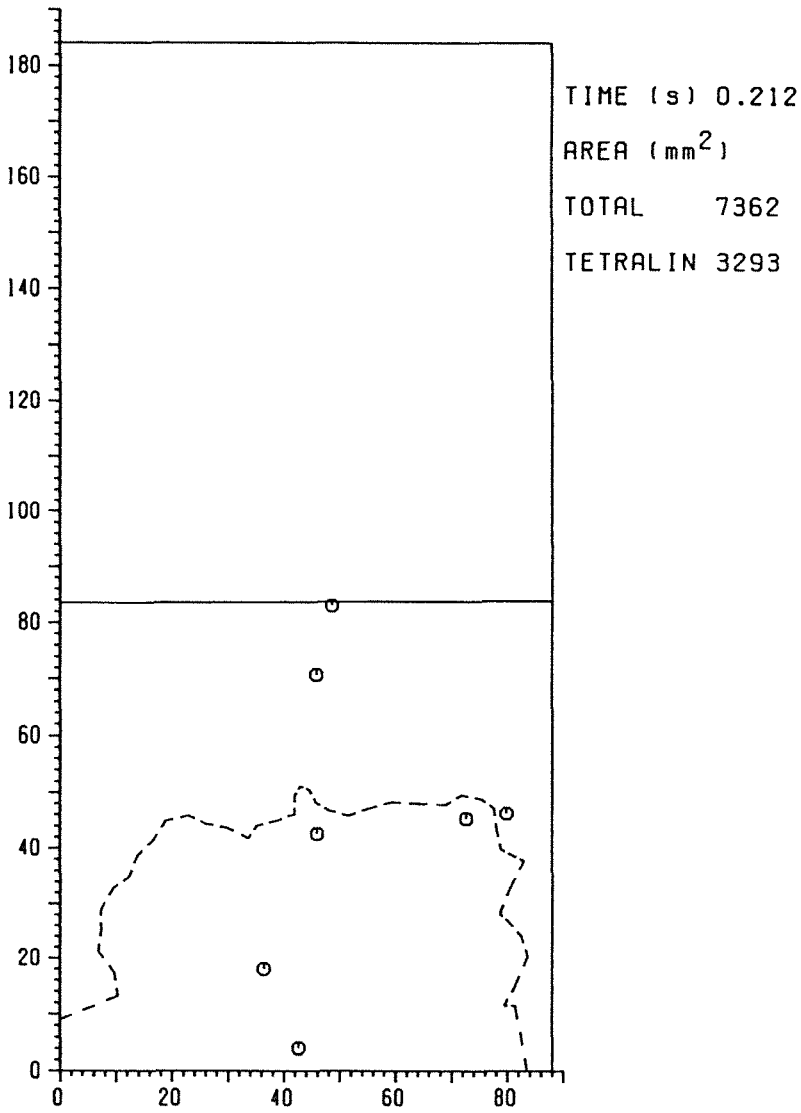

Fig.15b Isothermal Test
Corrected Interfaces *MMB-21*

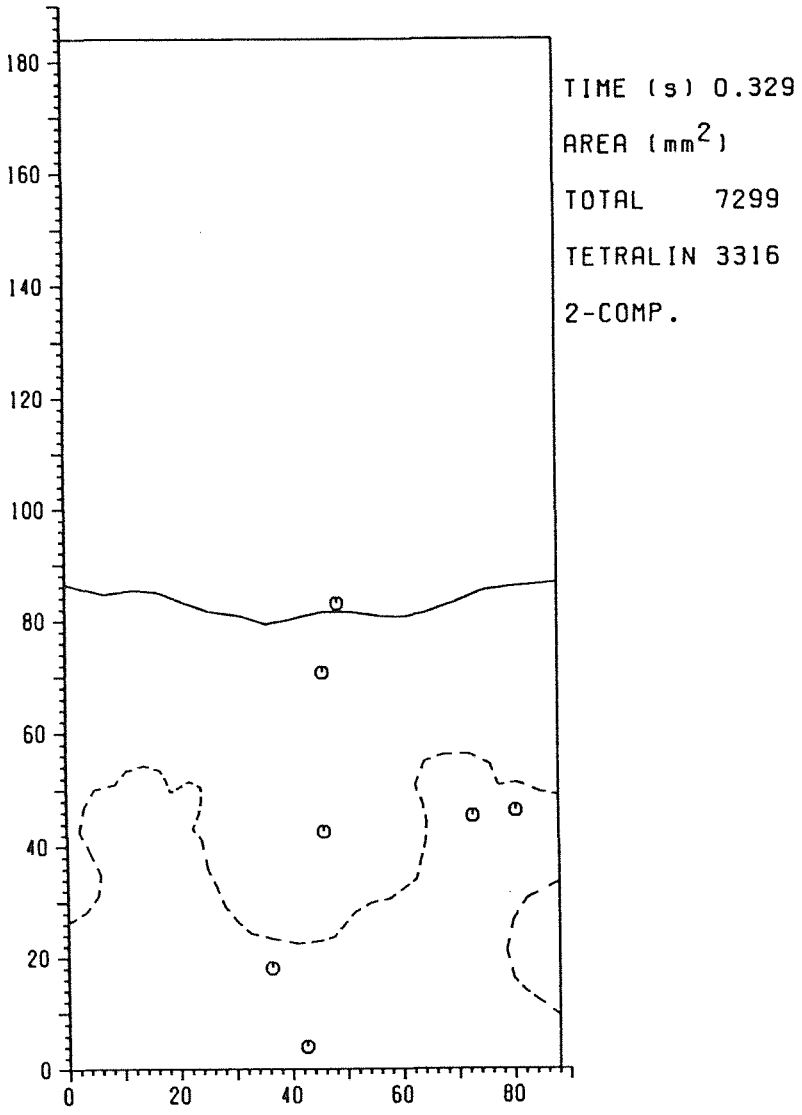

Fig.16 Isothermal Test Interfaces *MMB-21*

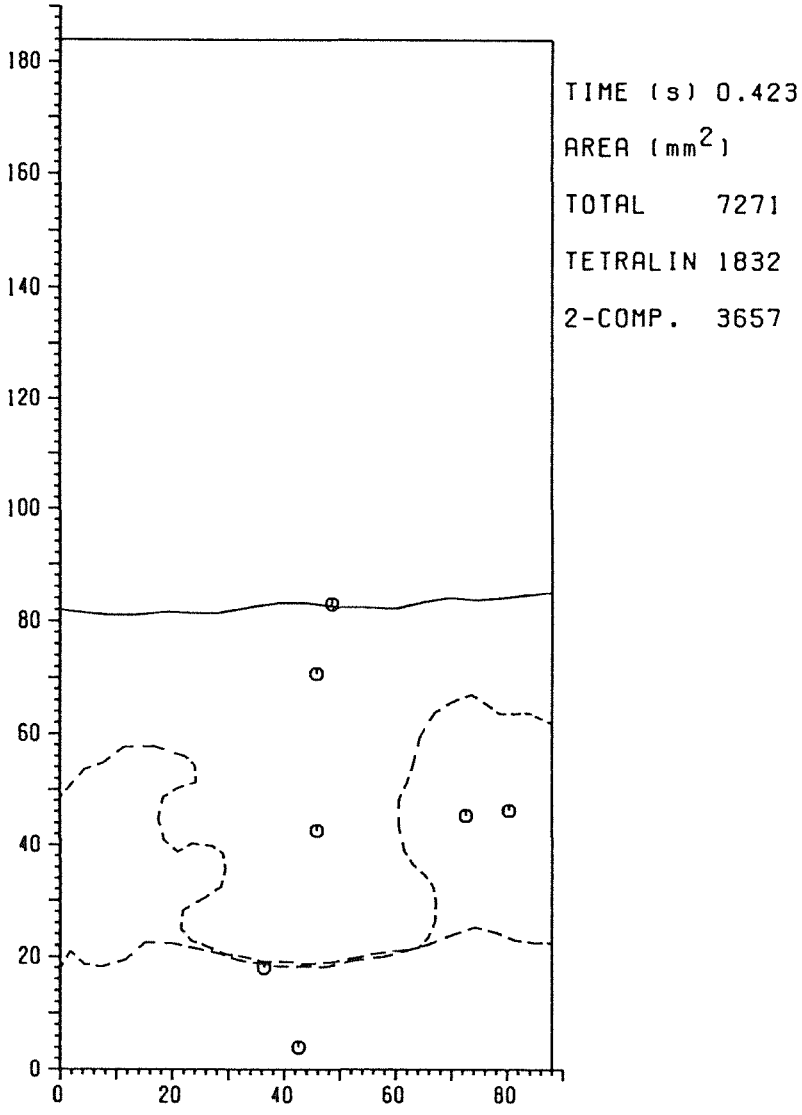

Fig.17 Isothermal Test Interfaces *MMB-21*

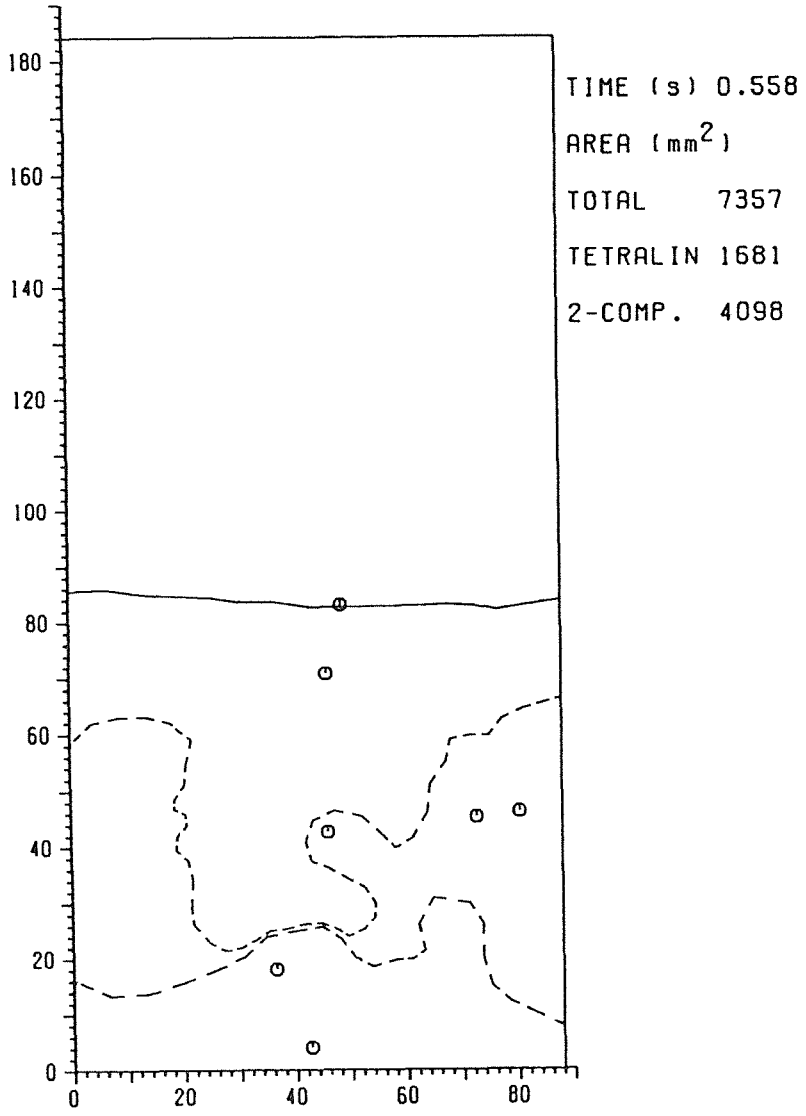

Fig.18 Isothermal Test Interfaces MMB-21

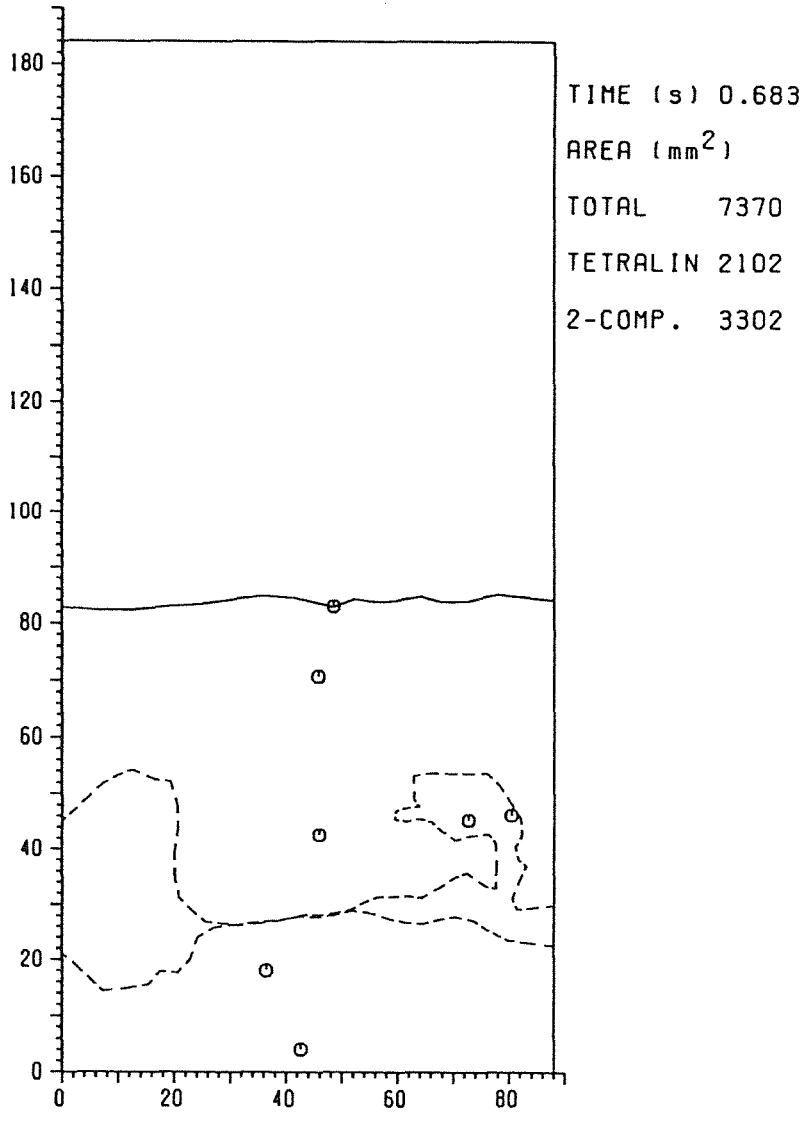

Fig.19 Isothermal Test Interfaces MMB-21

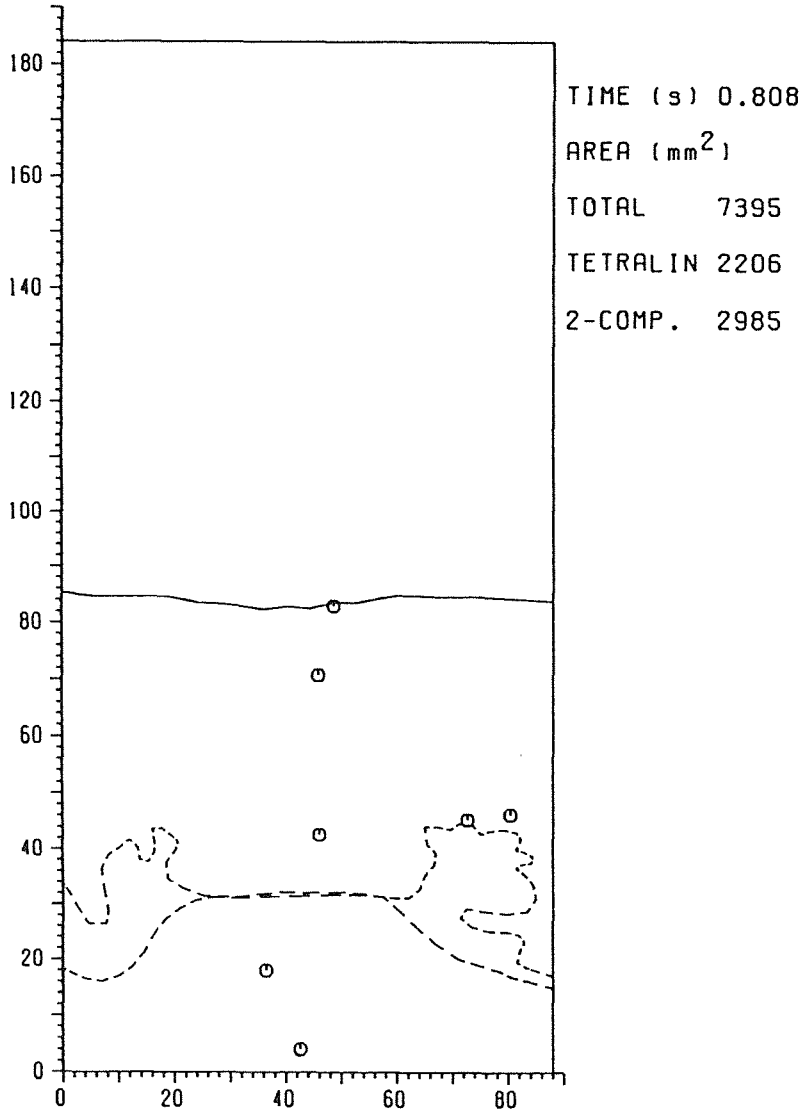

Fig.20 Isothermal Test Interfaces *MMB-21*

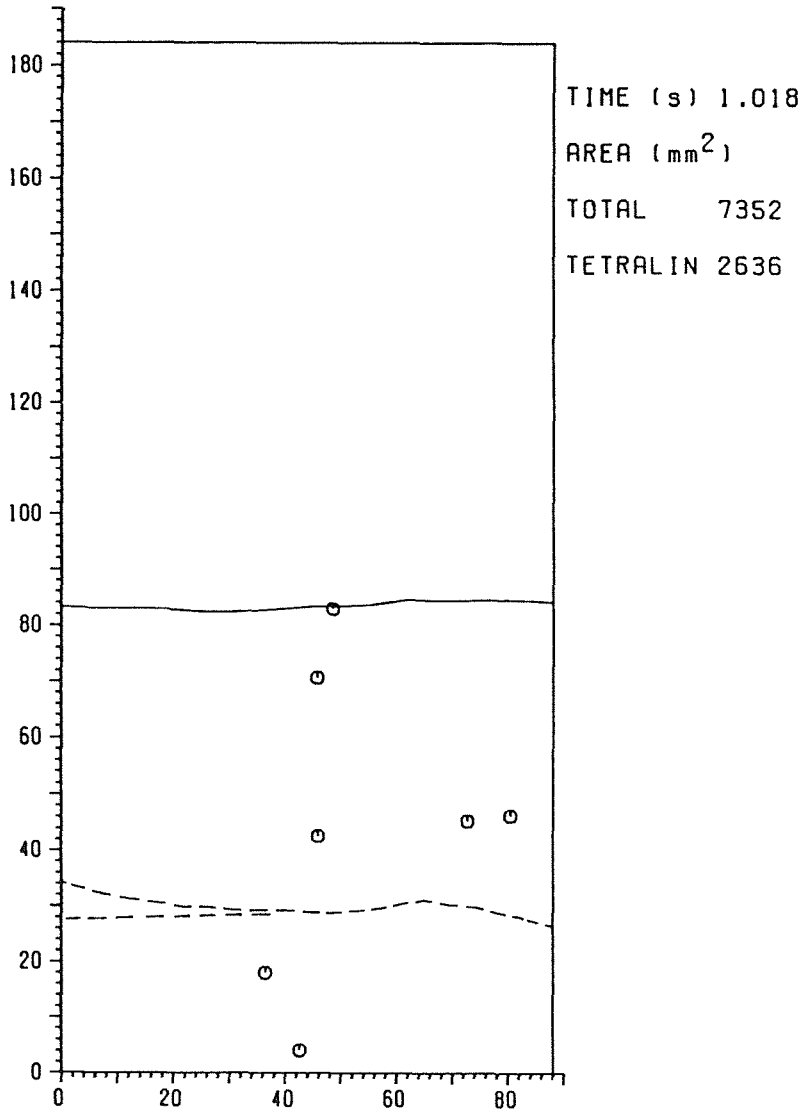

Fig.21 Isothermal Test Interfaces *MMB-21*

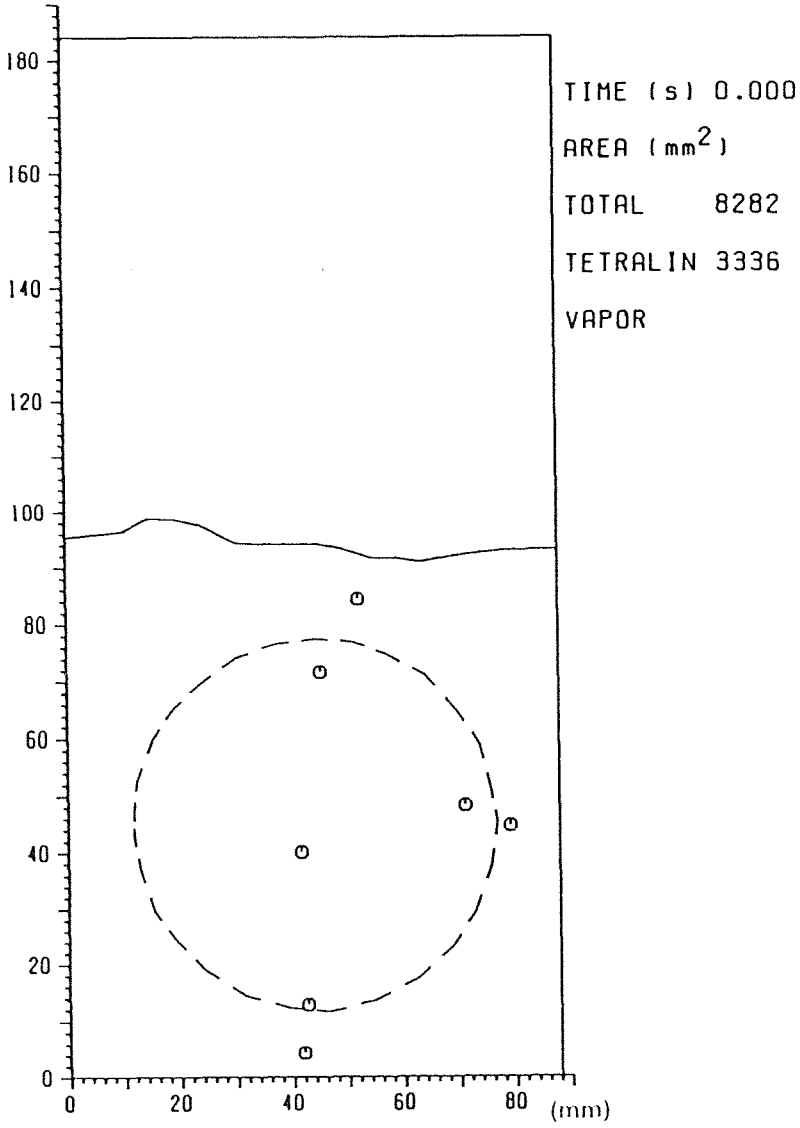

Fig.22a Initial Configuration *MMB-26*

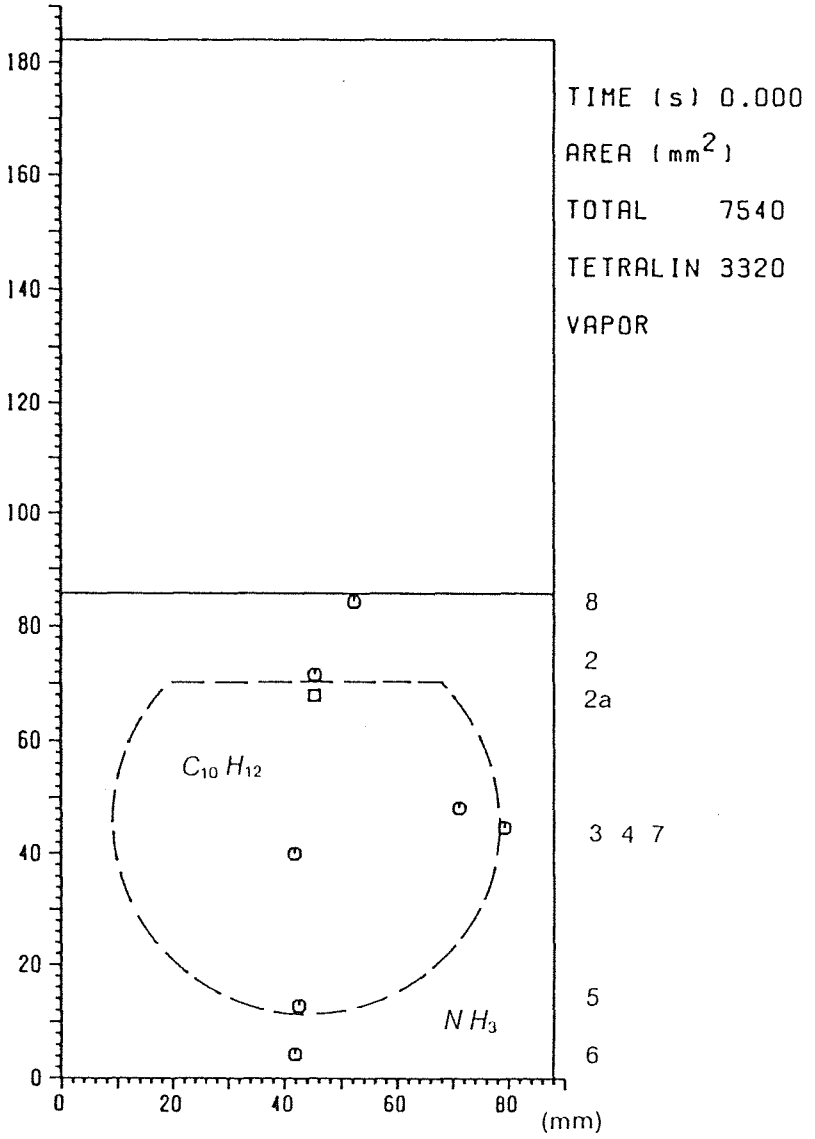

Fig.22b Idealized Initial Configuration *MMB-26*

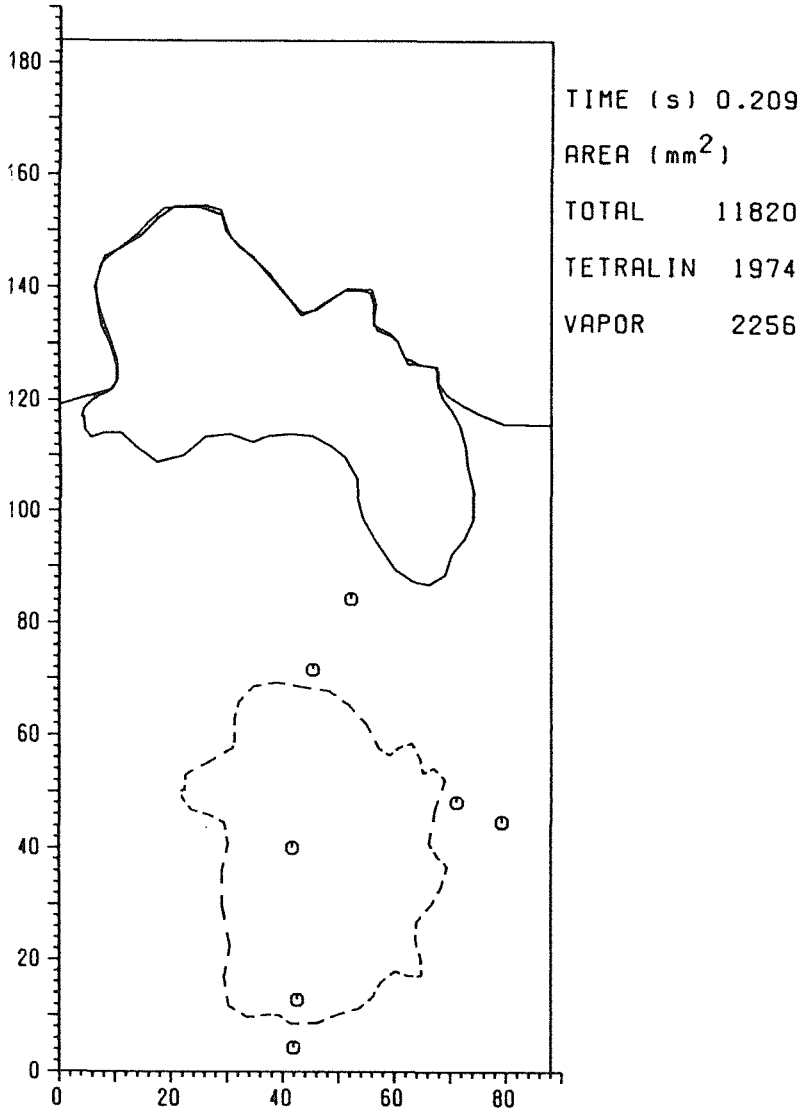

Fig.23 Interfaces *MMB-26*

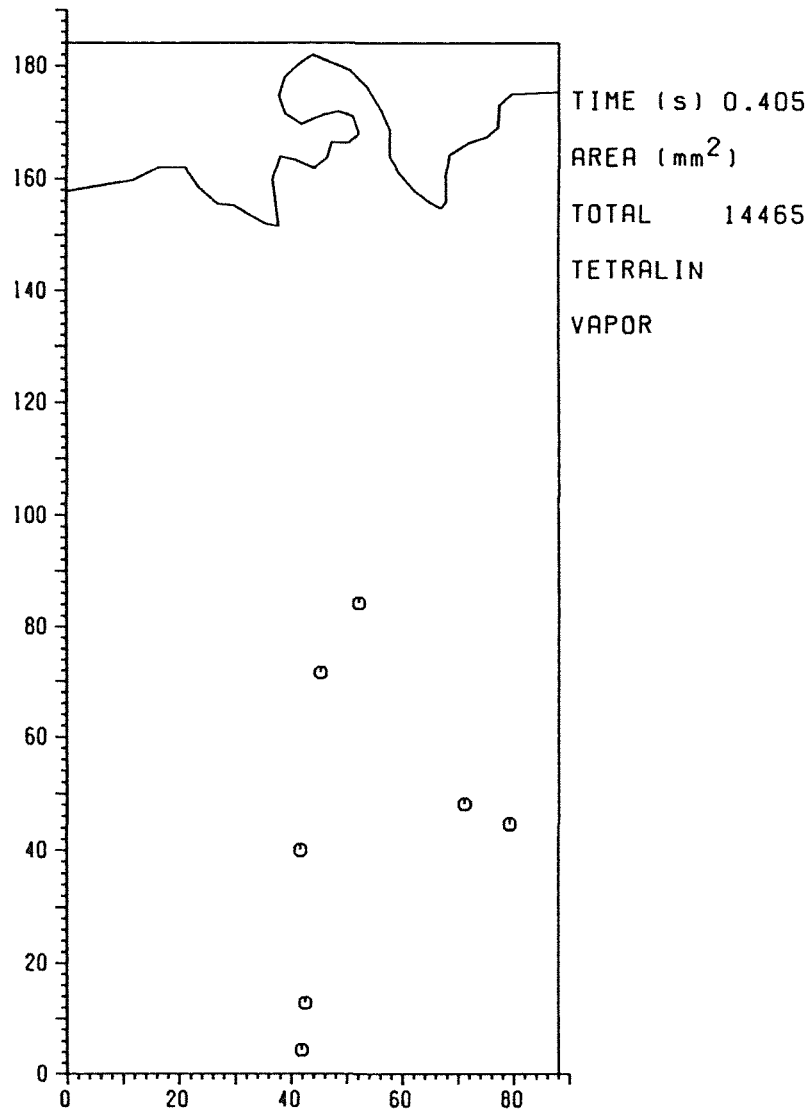

Fig.24 Interfaces *MMB-26*

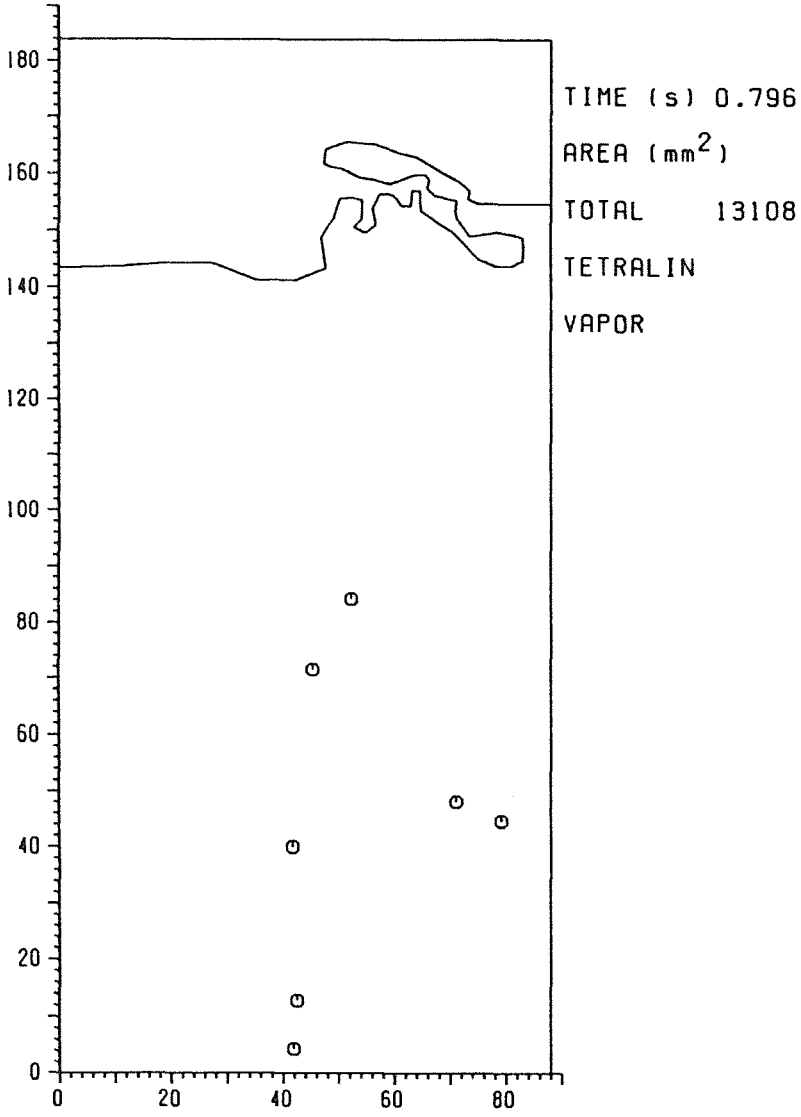

Fig.25 Interfaces *MMB-26*

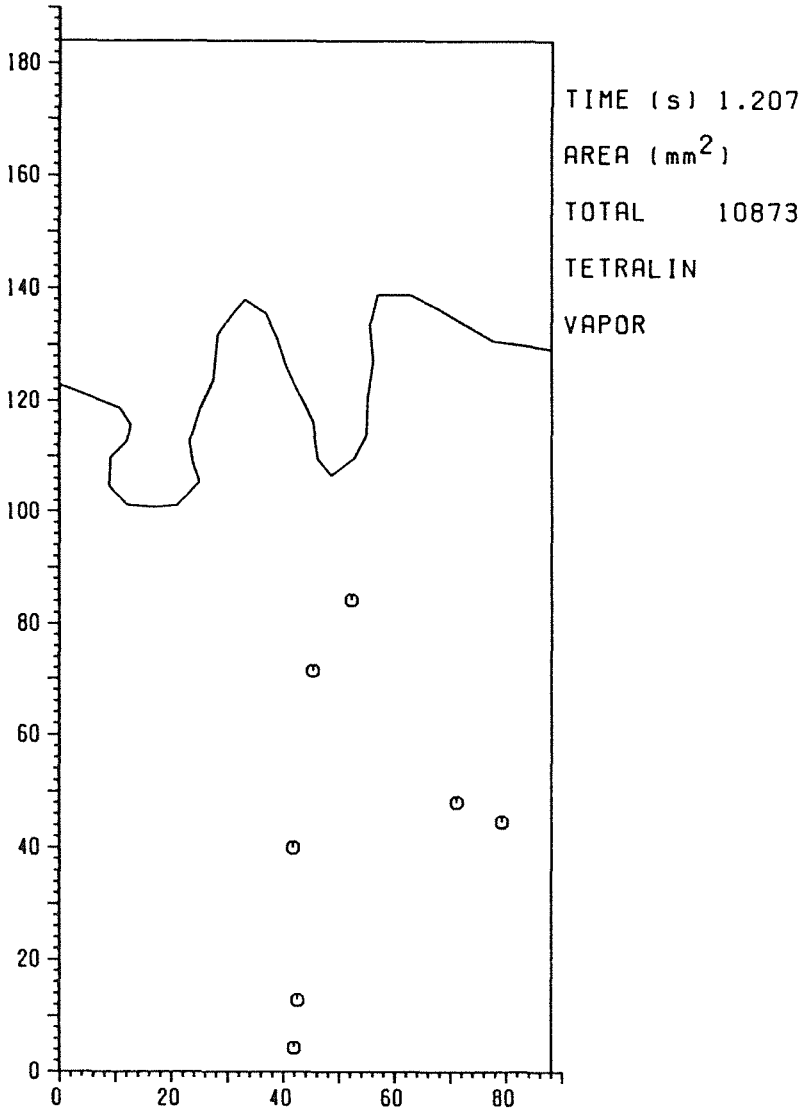

Fig.26 Interfaces *MMB-26*

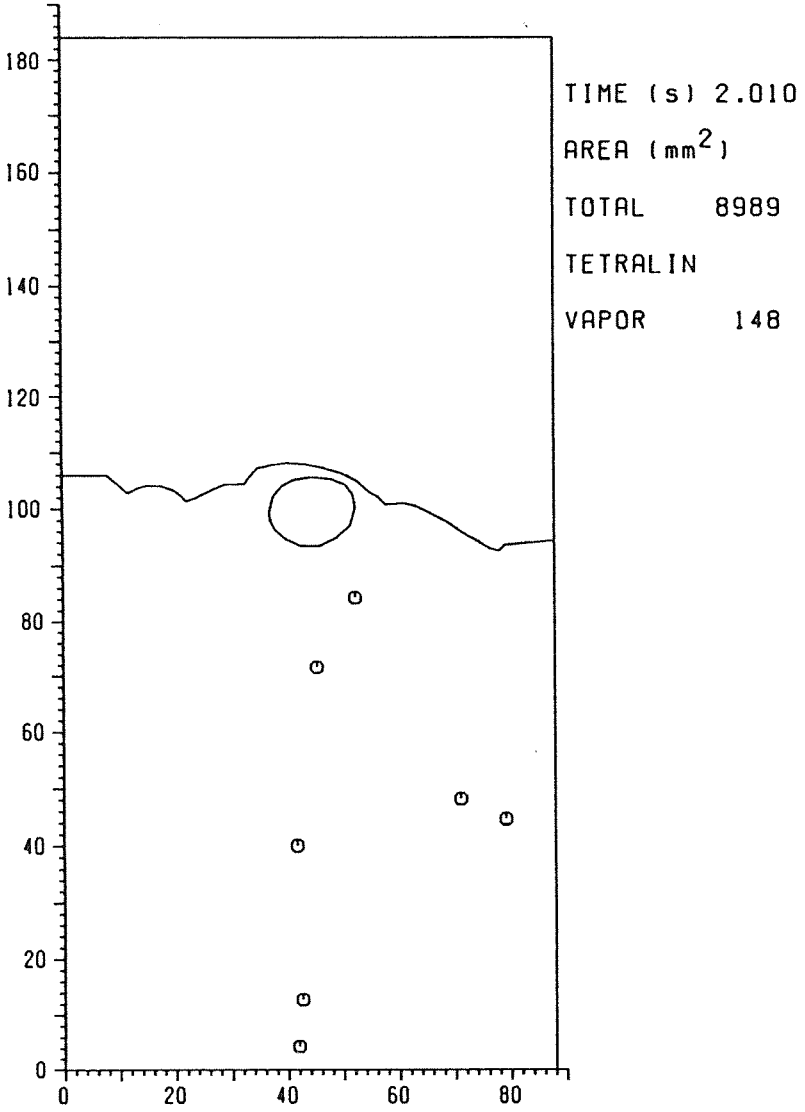

Fig.27 Interfaces MMB-26

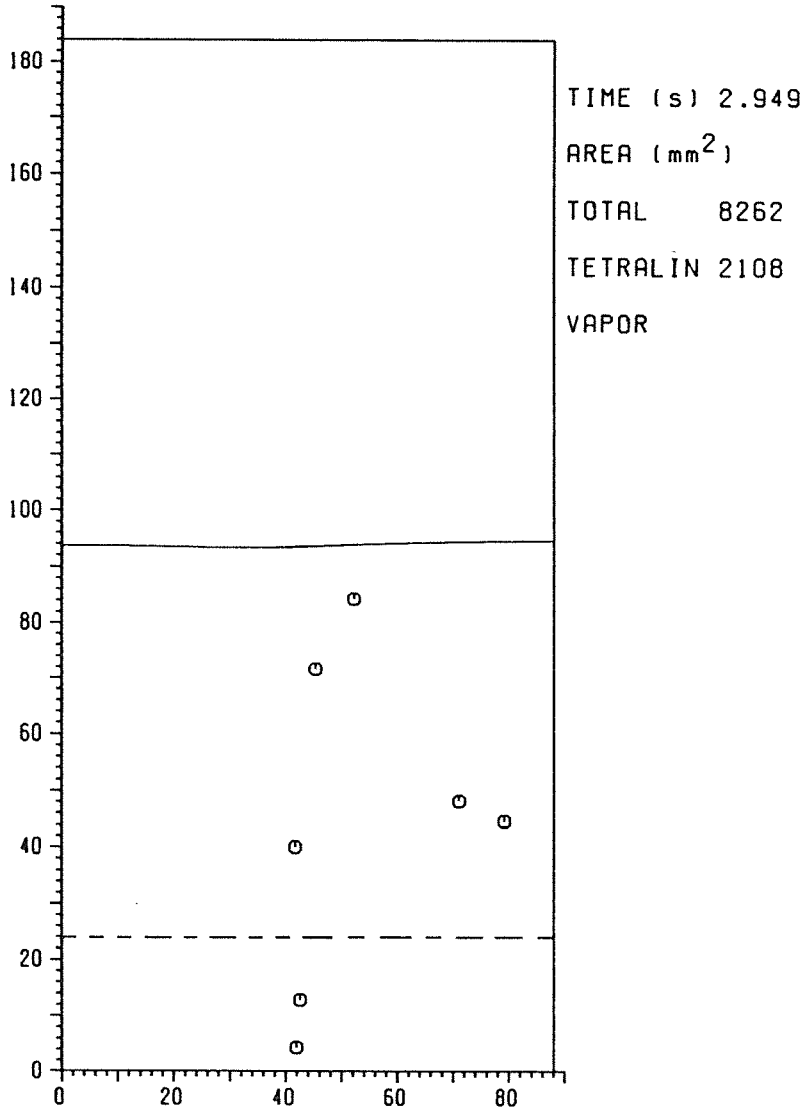

Fig.28 Interfaces MMB-26

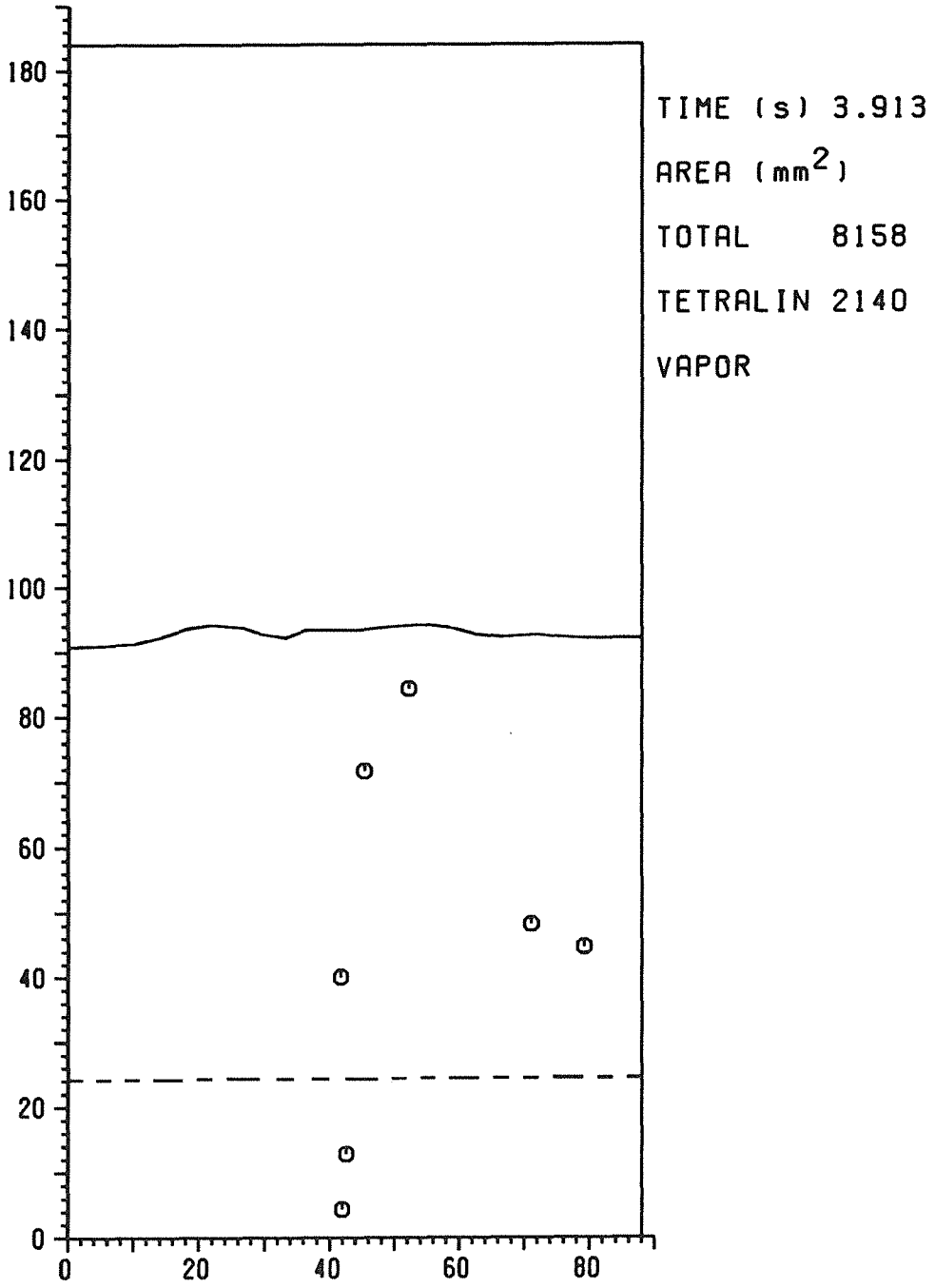

Fig.29 Interfaces

MMB-26

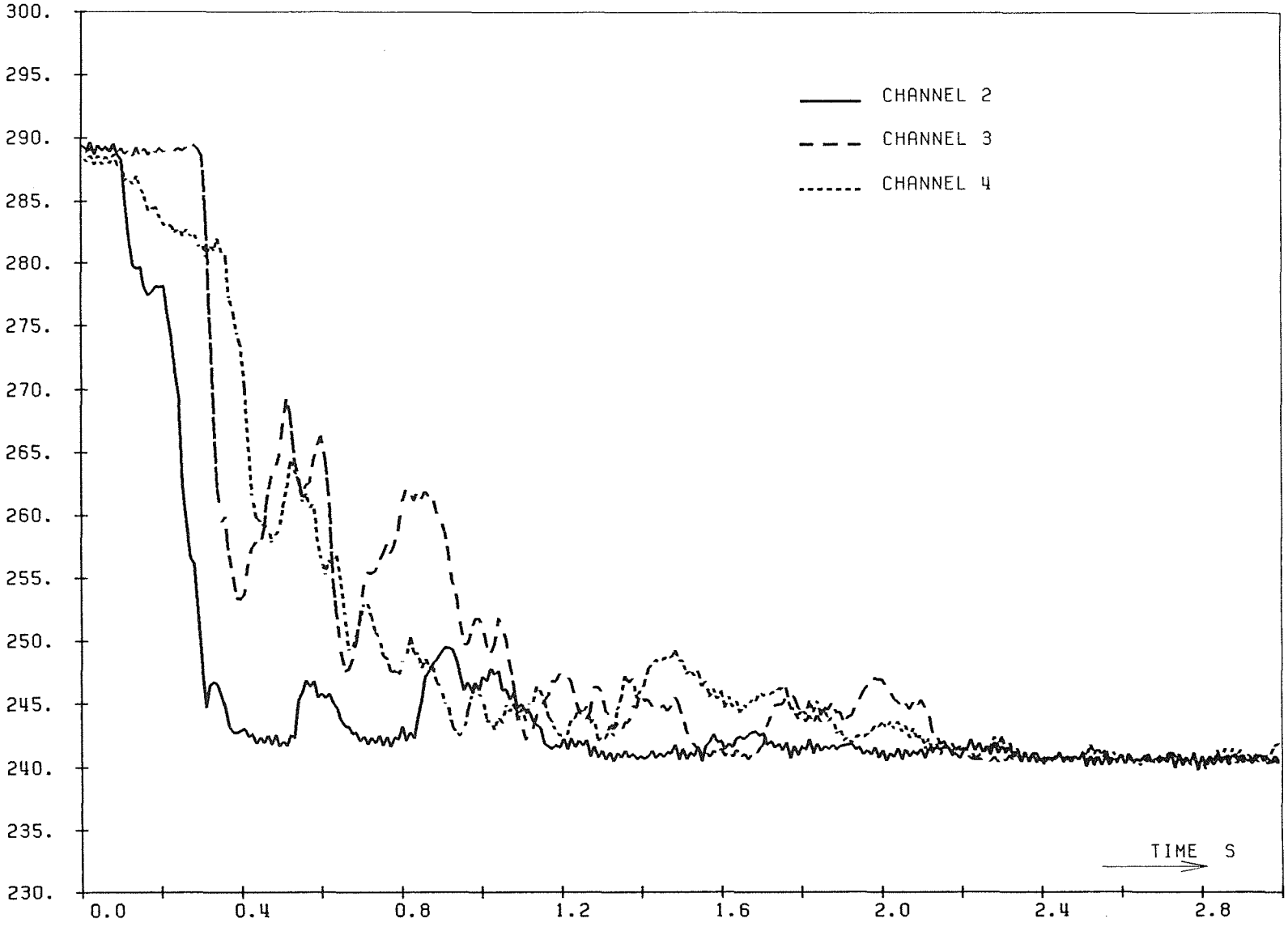

Fig.30 MMB-26 Temperatures (K) Versus Time

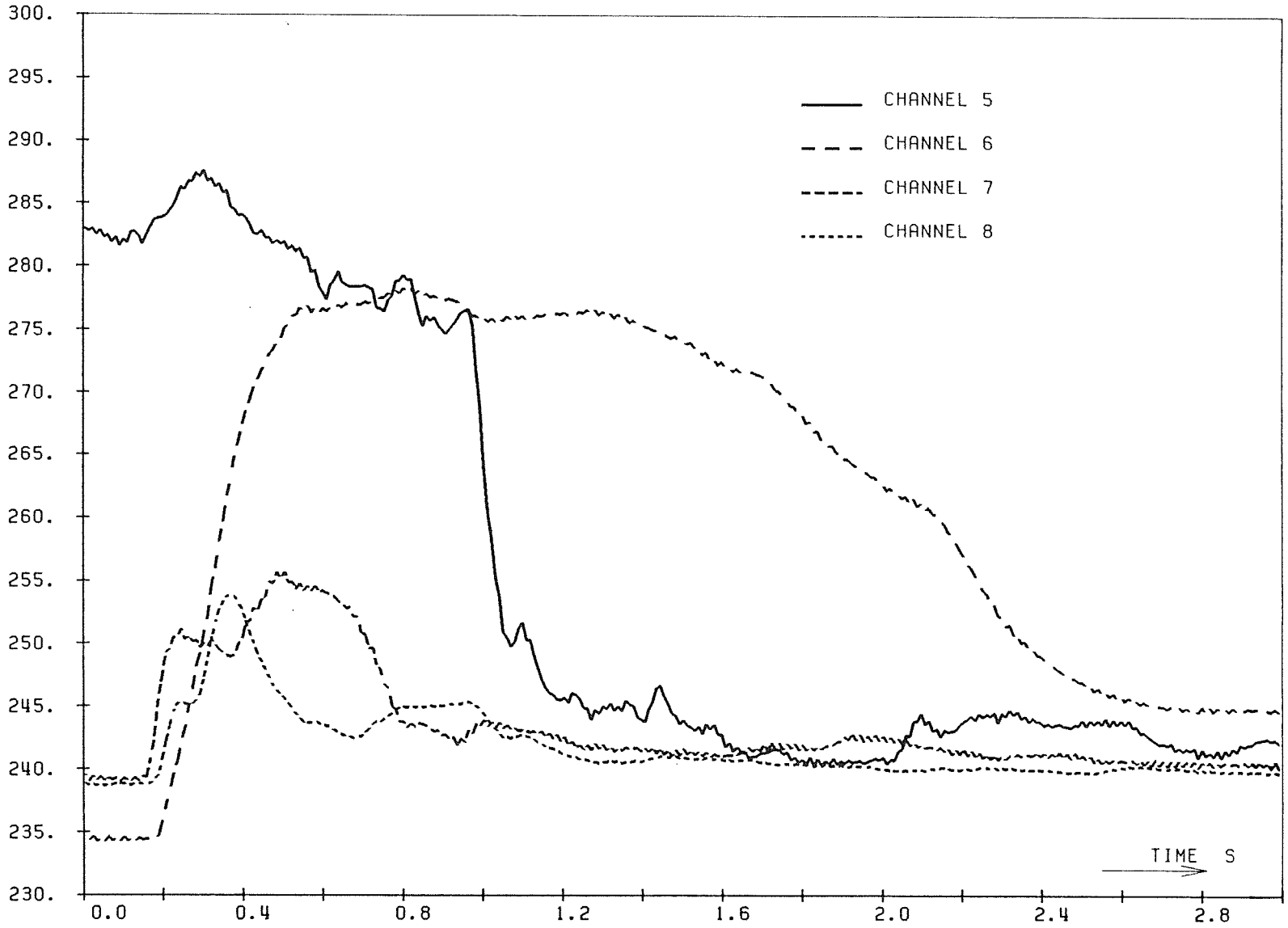

Fig.31 MMB-26 Temperatures (K) Versus Time

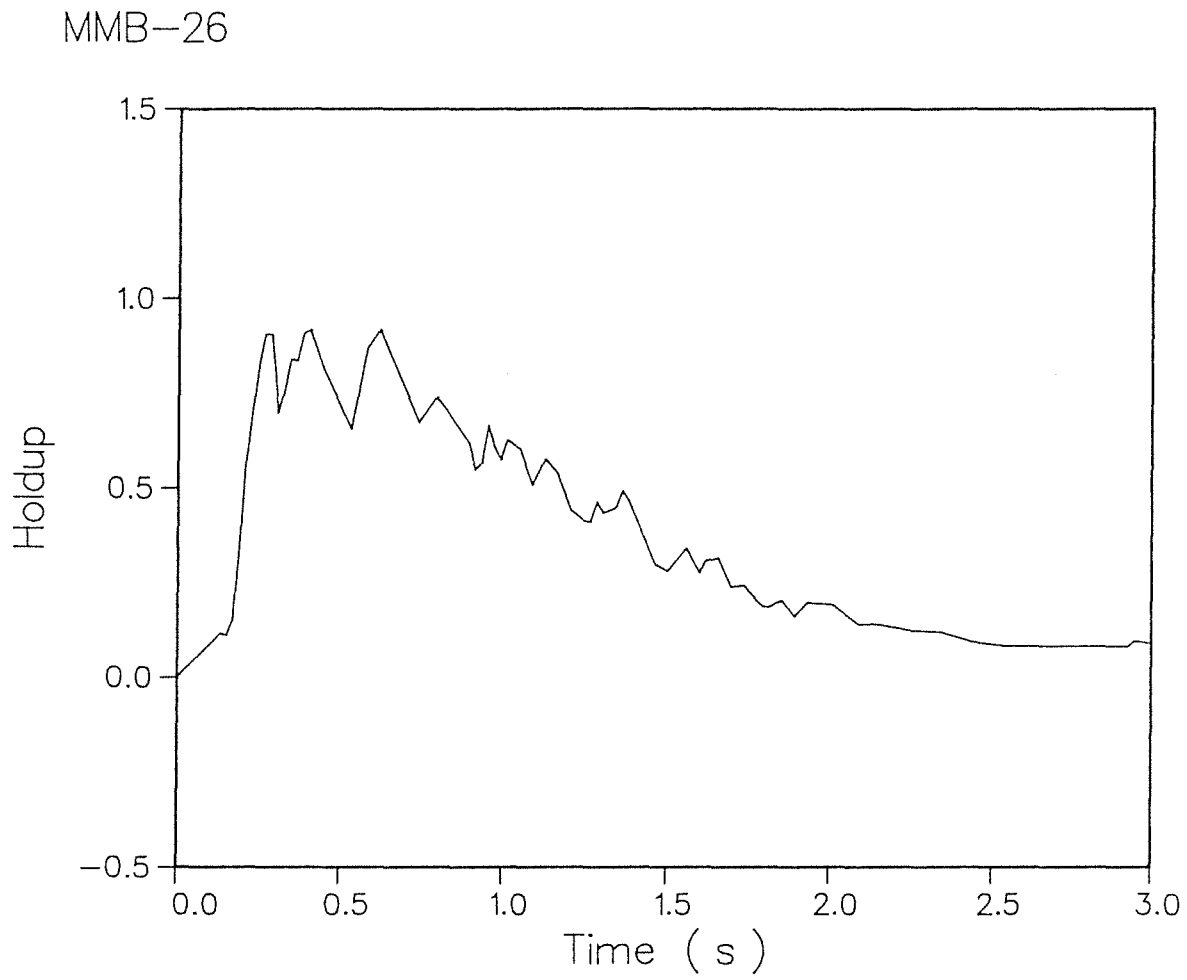

Fig.32 MMB-26 Holdup Versus Time

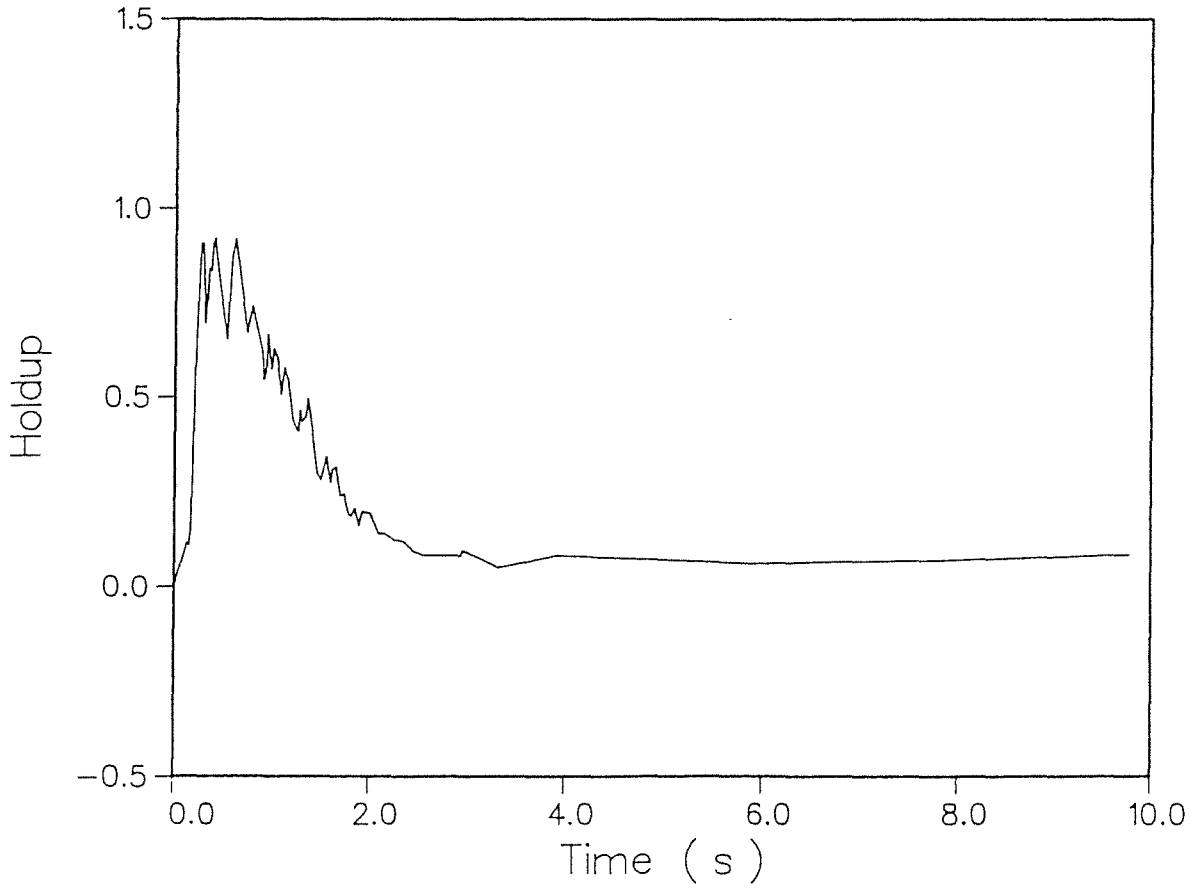

Fig.33 MMB-26 Holdup Versus Time

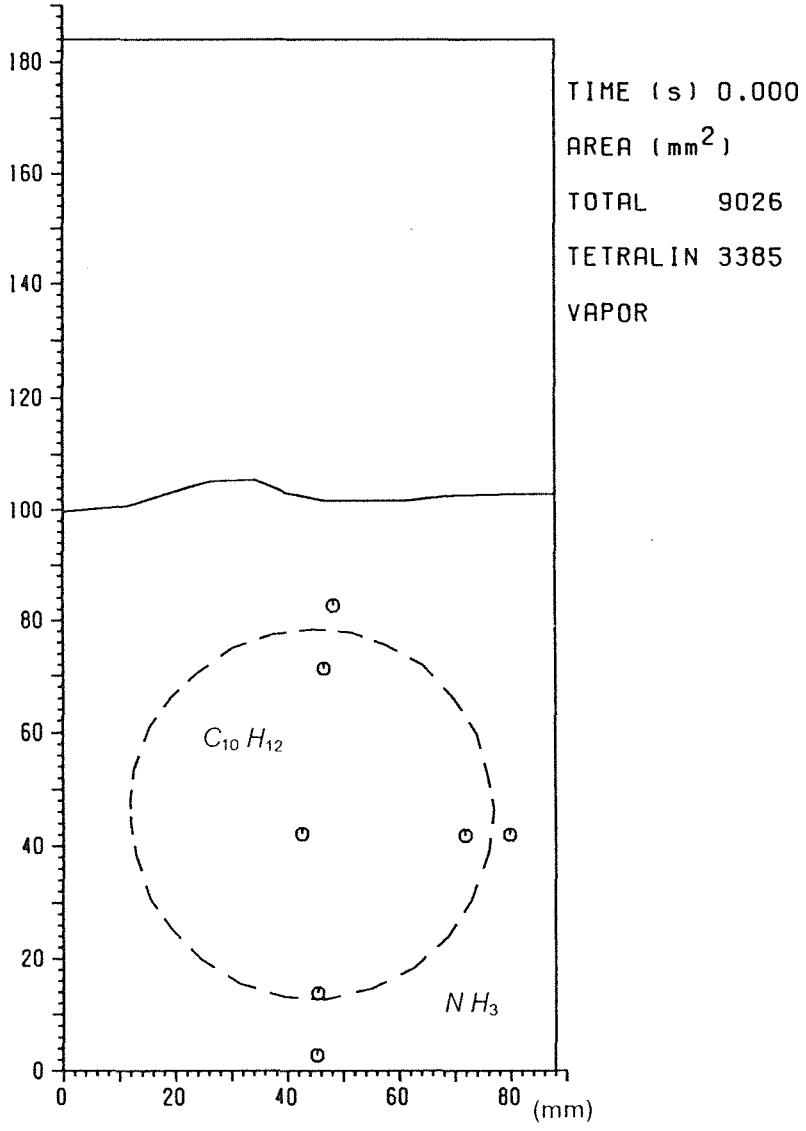

Fig.34a Initial Configuration MMB-27

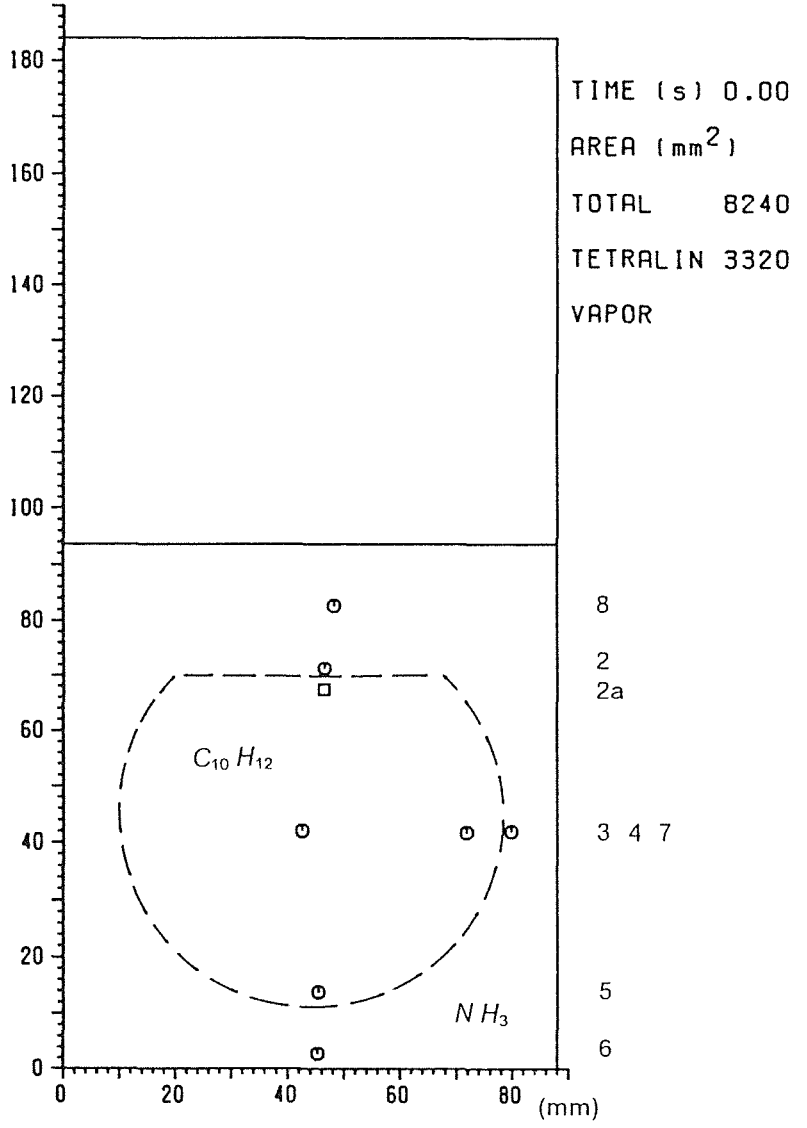

Fig.34b Idealized Initial Configuration MMB-27

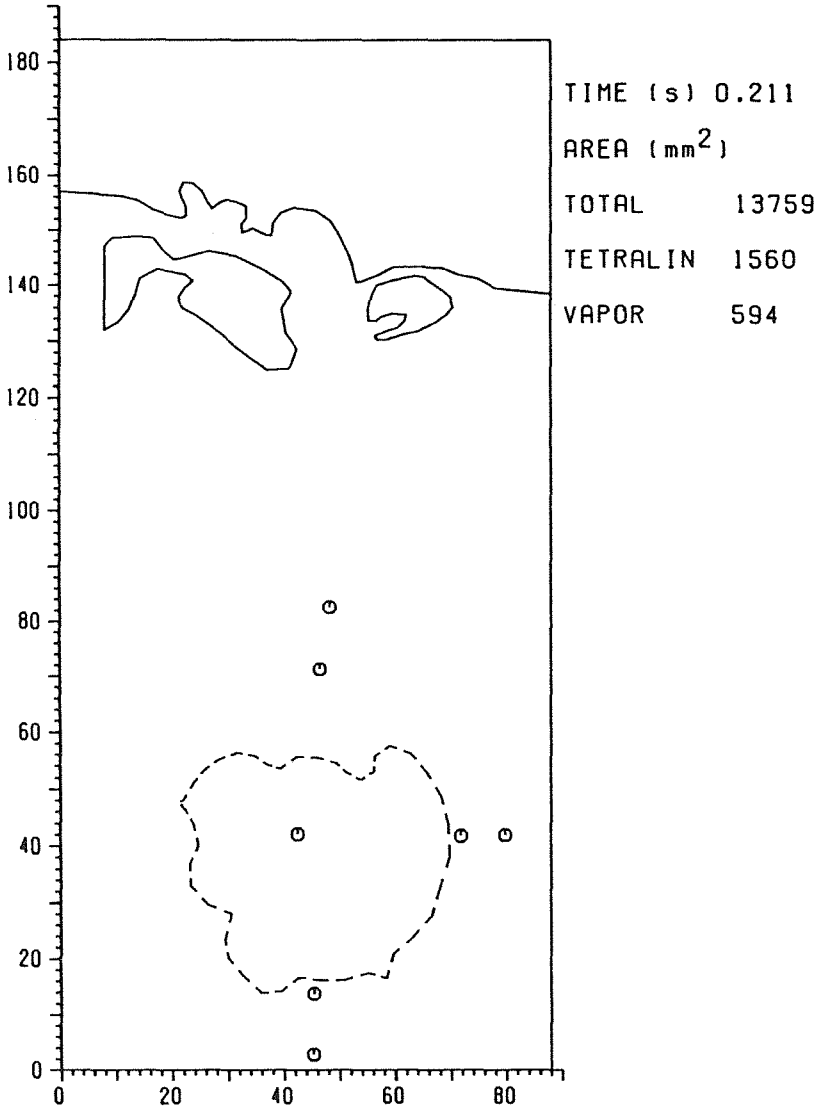

Fig.35 Interfaces MMB-27

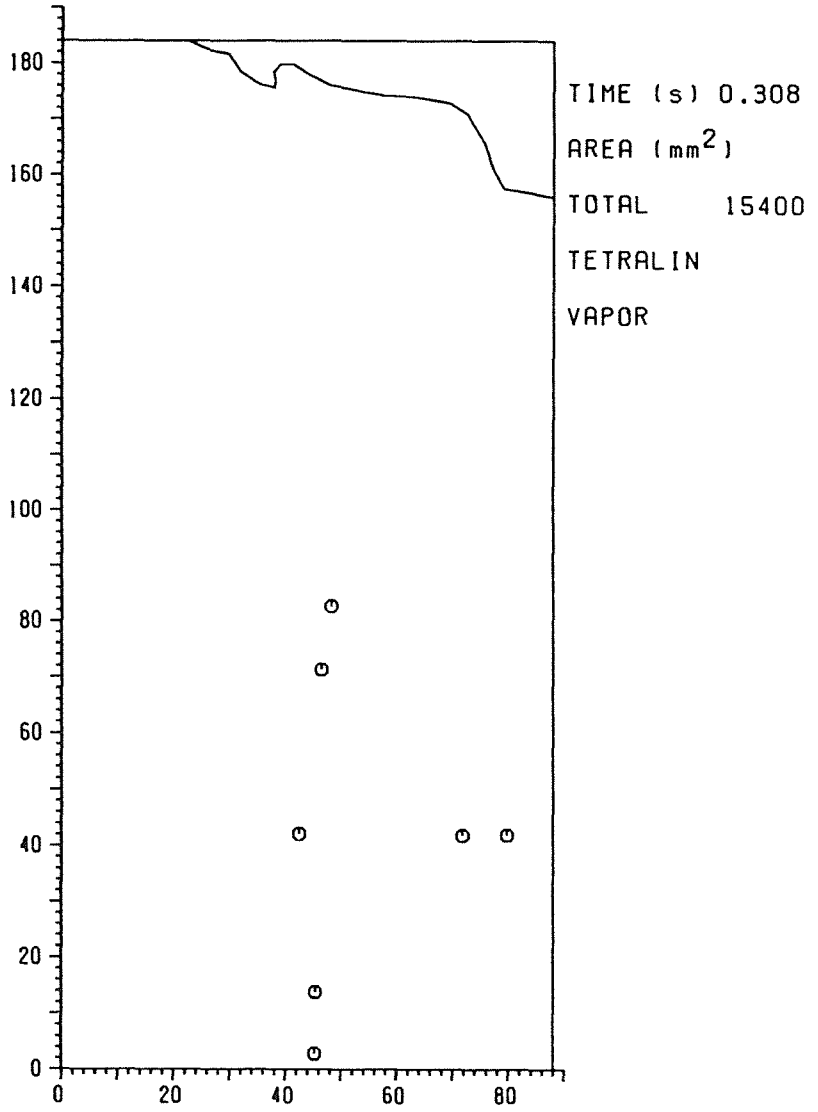

Fig.36 Interfaces MMB-27

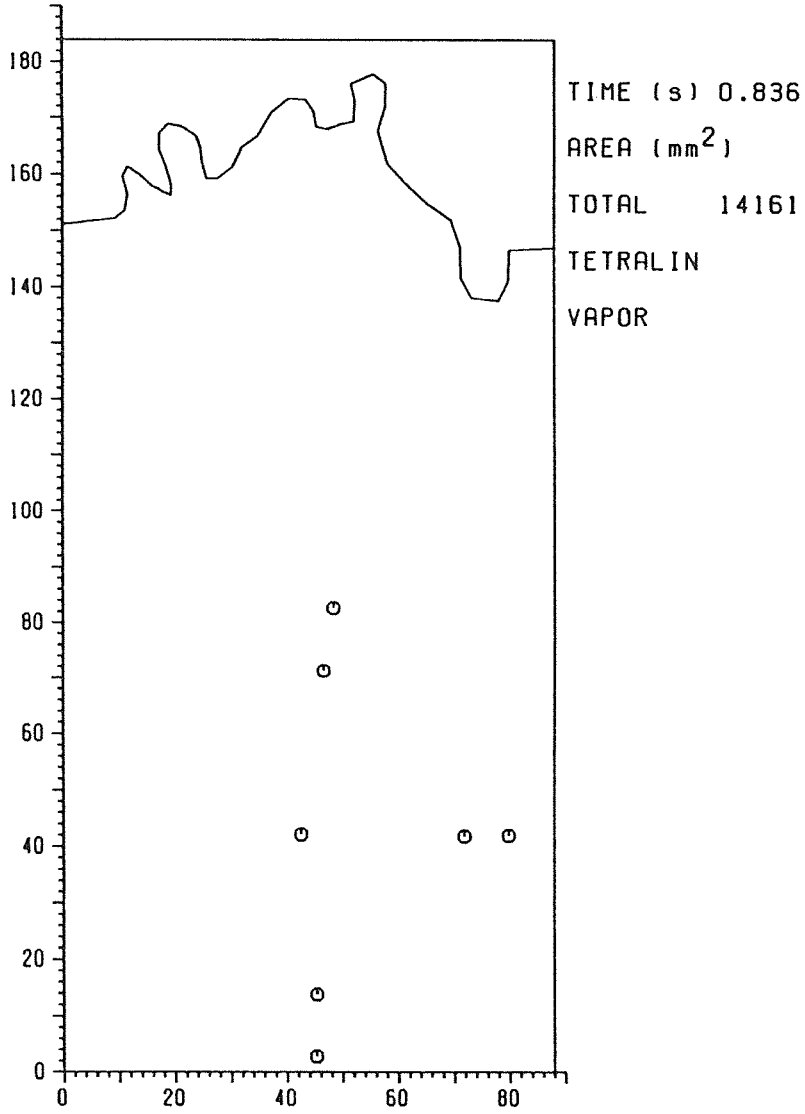

Fig.37 Interfaces MMB-27

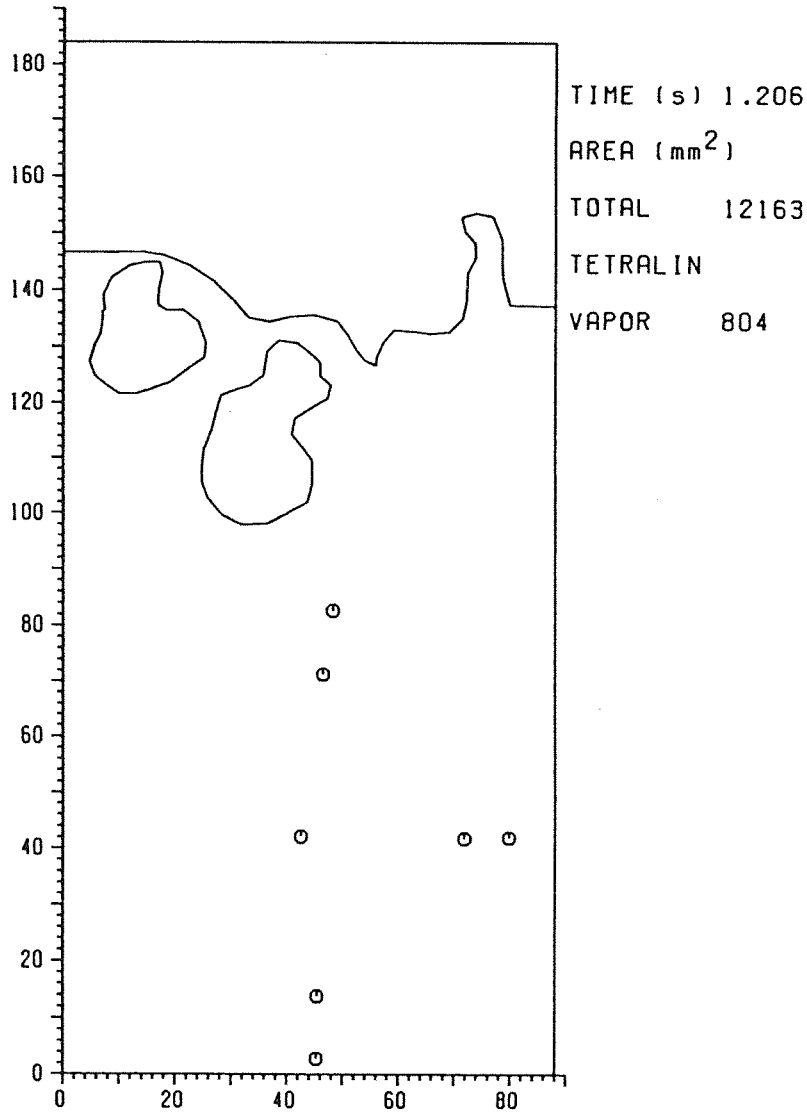

Fig.38 Interfaces MMB-27

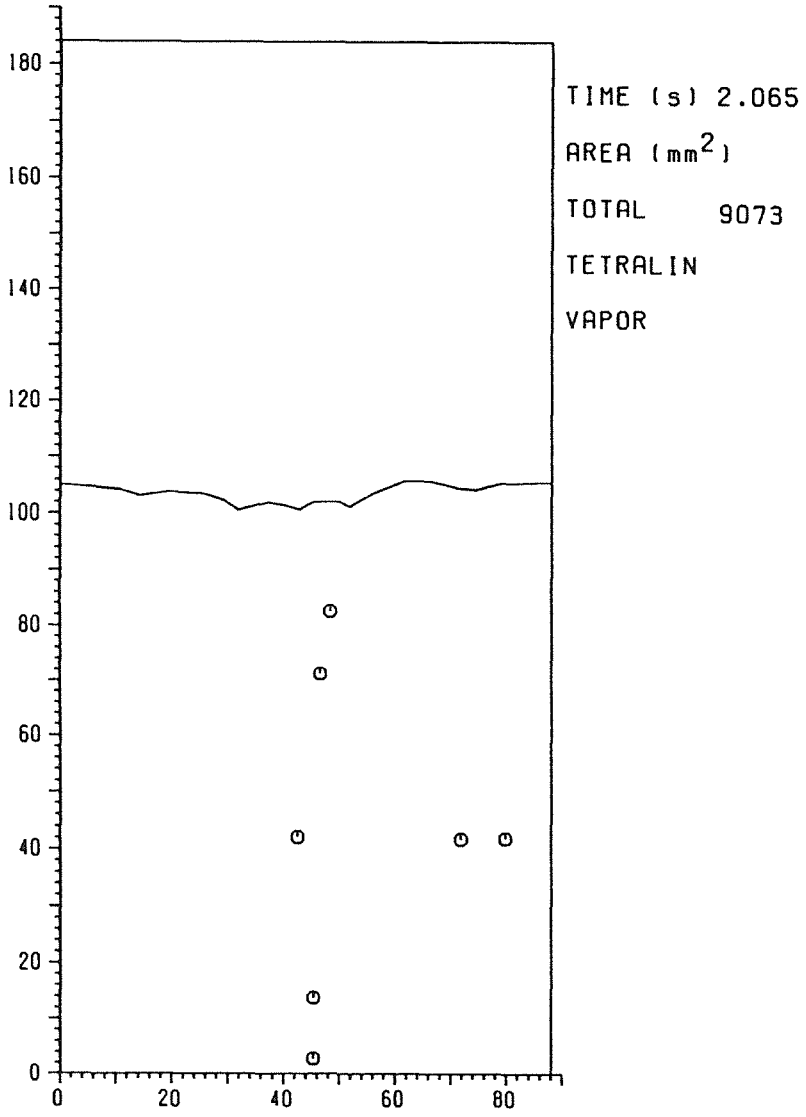

Fig.39 Interfaces MMB-27

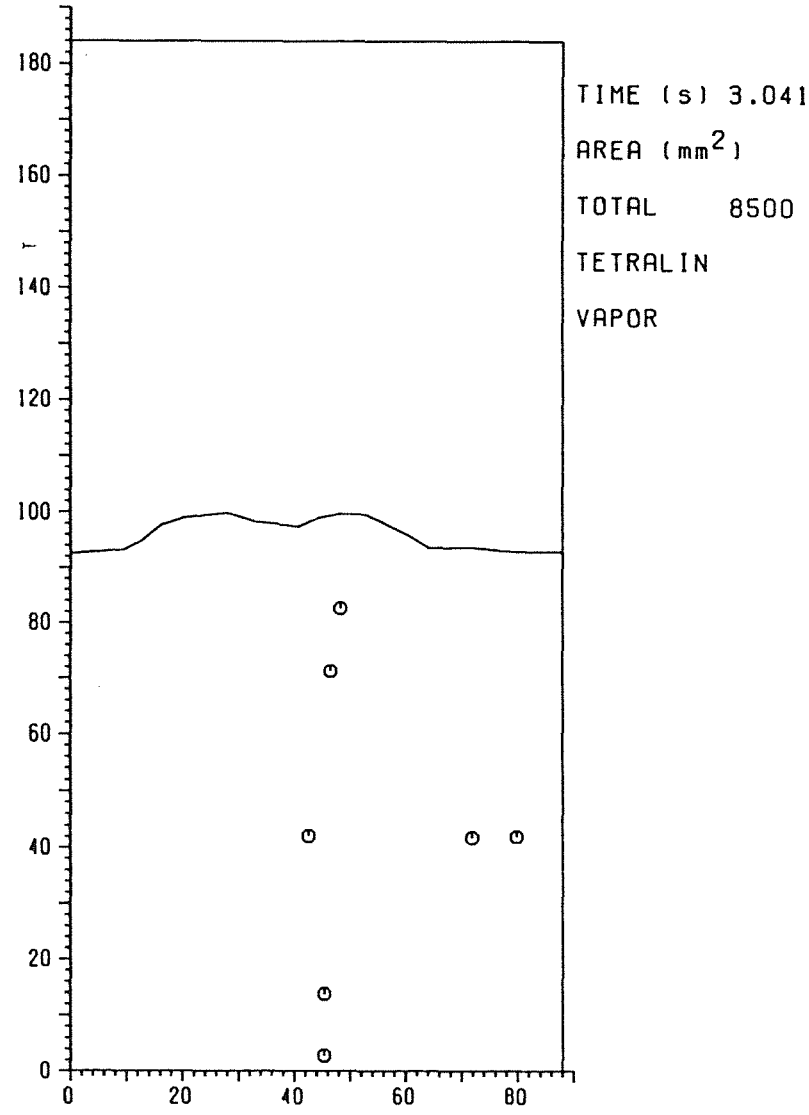

Fig.40 Interfaces MMB-27

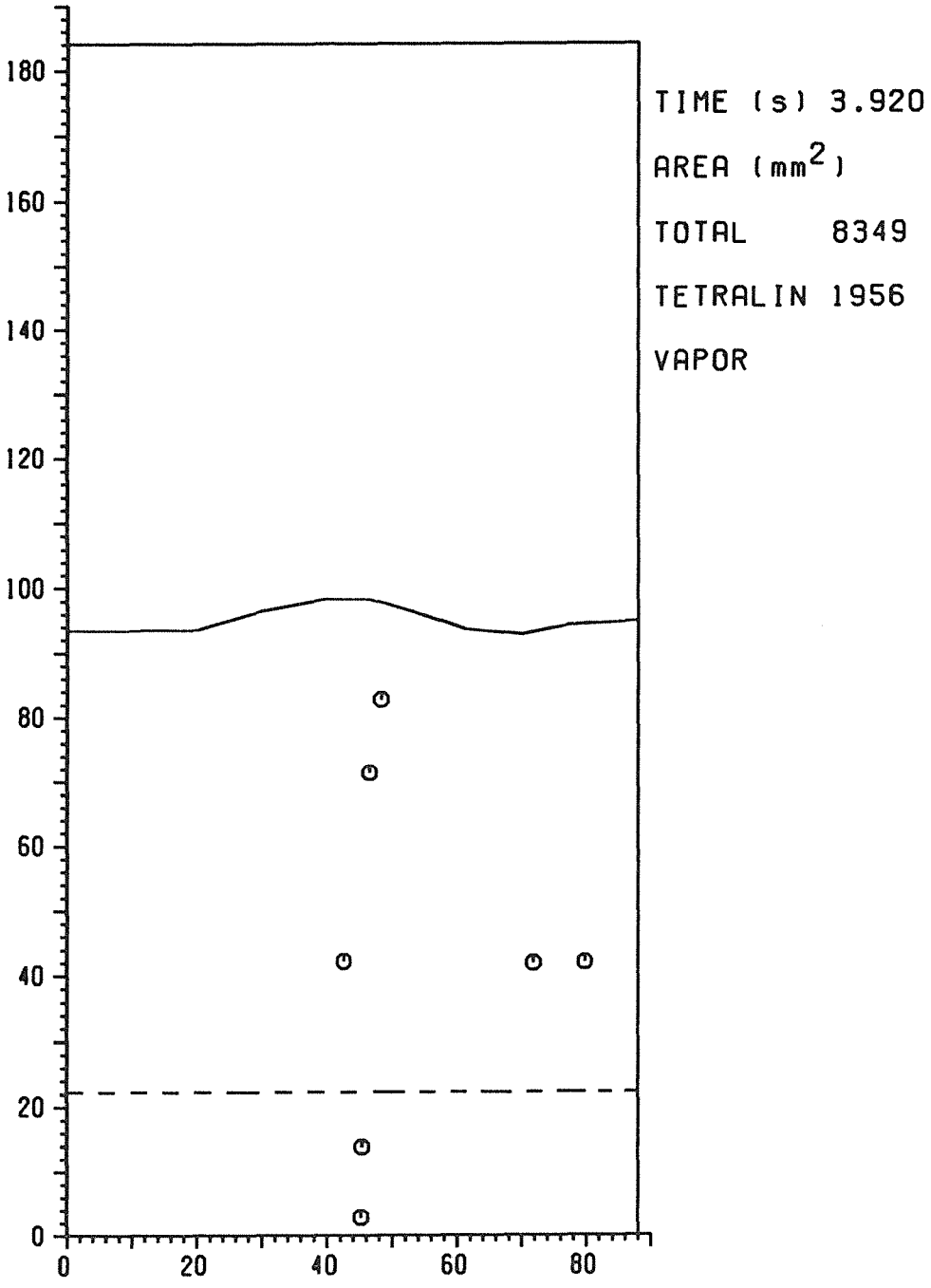

Fig.41 Interfaces

MMB-27

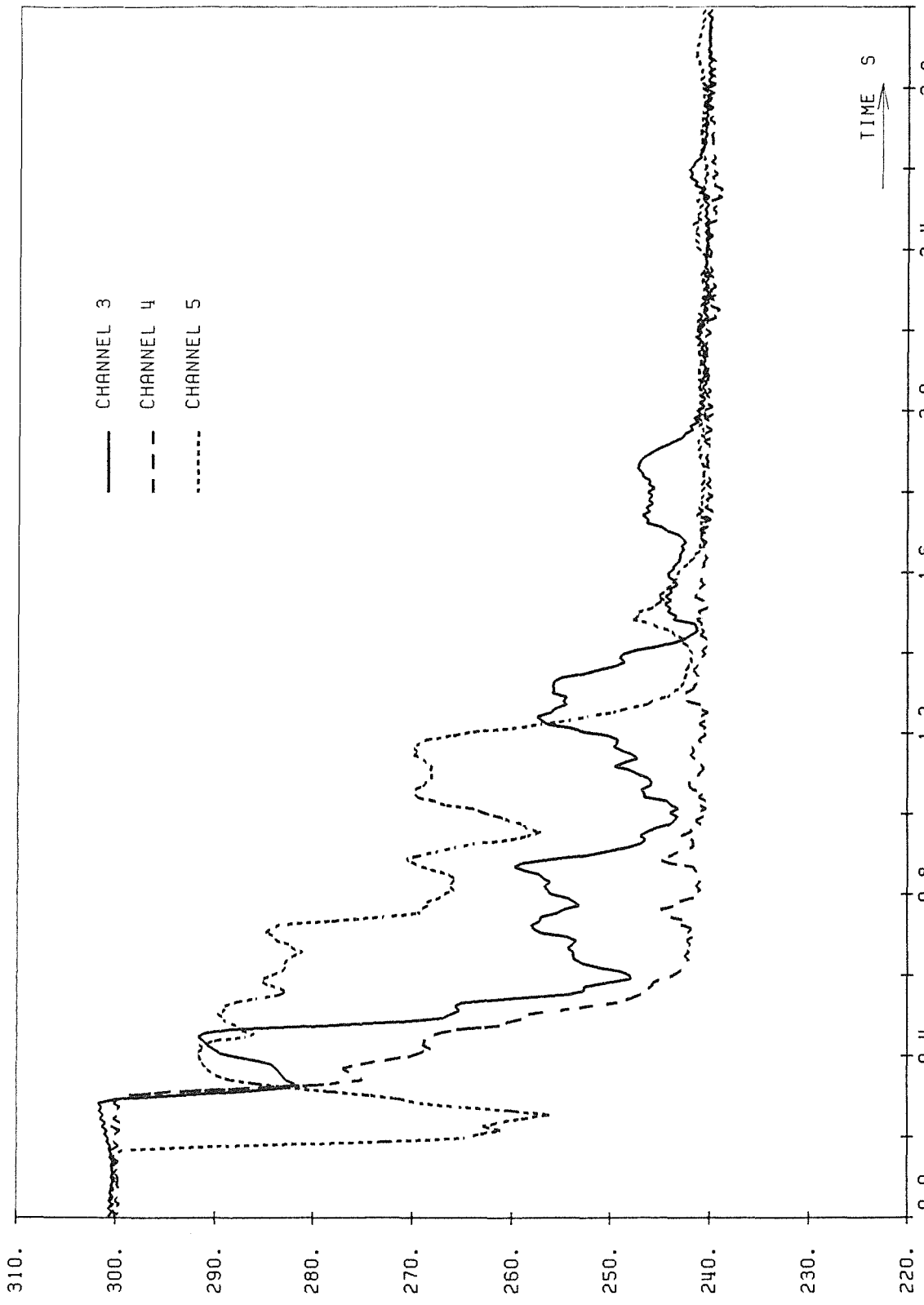

Fig.42 MMB-27 Temperatures (K) Versus Time

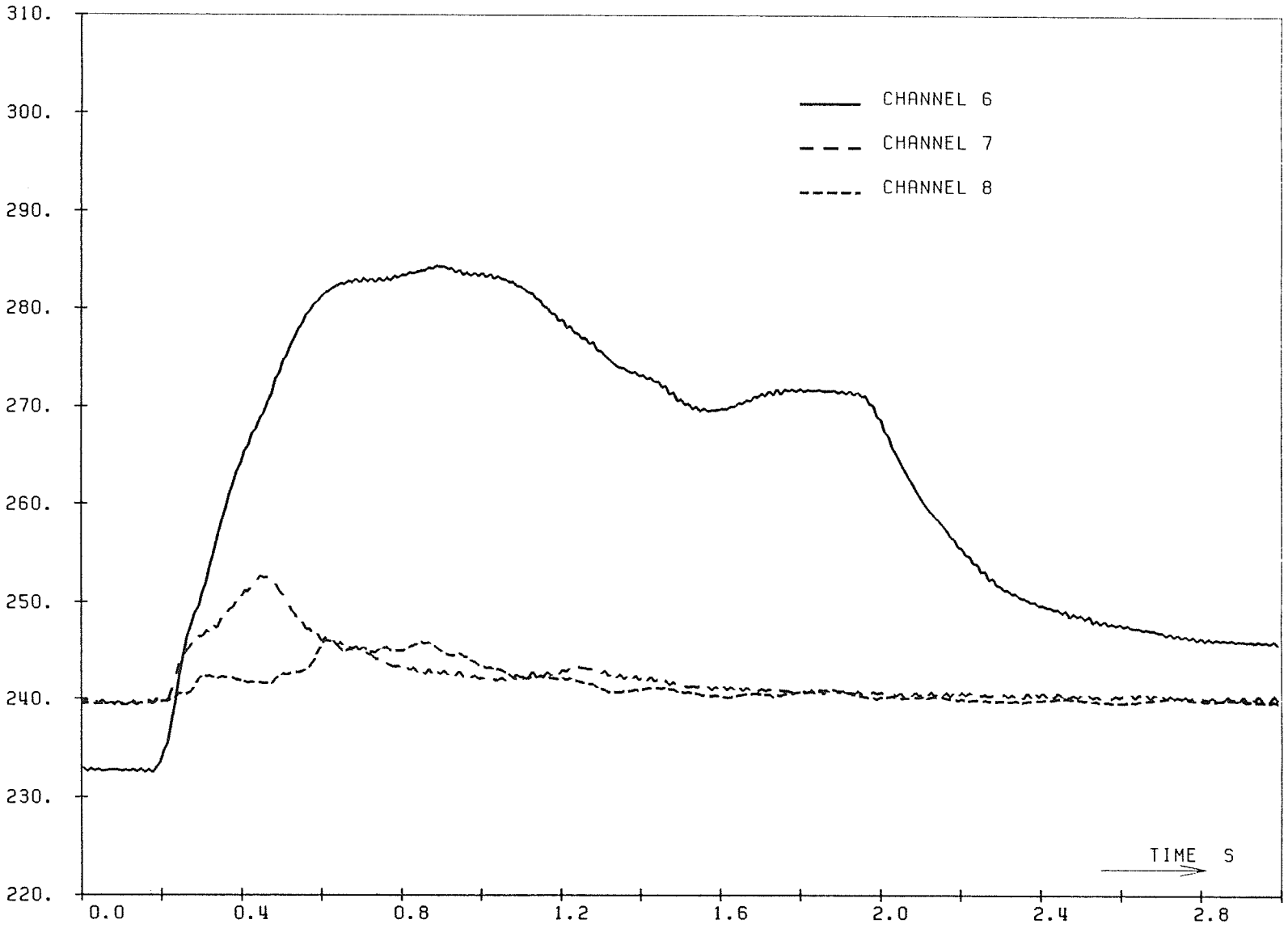

Fig.43 MMB-27 Temperatures (K) Versus Time

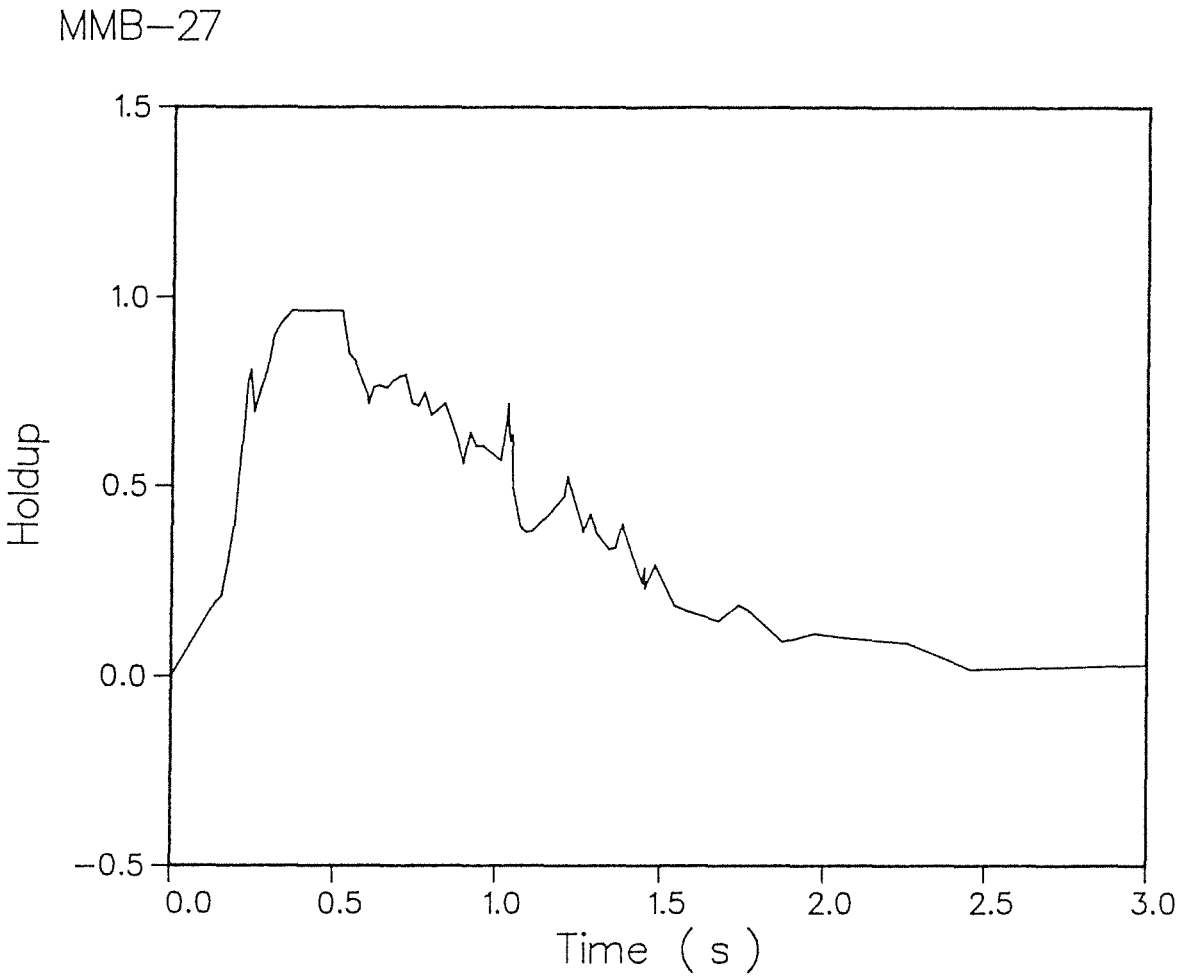

Fig.44 MMB-27 Holdup Versus Time

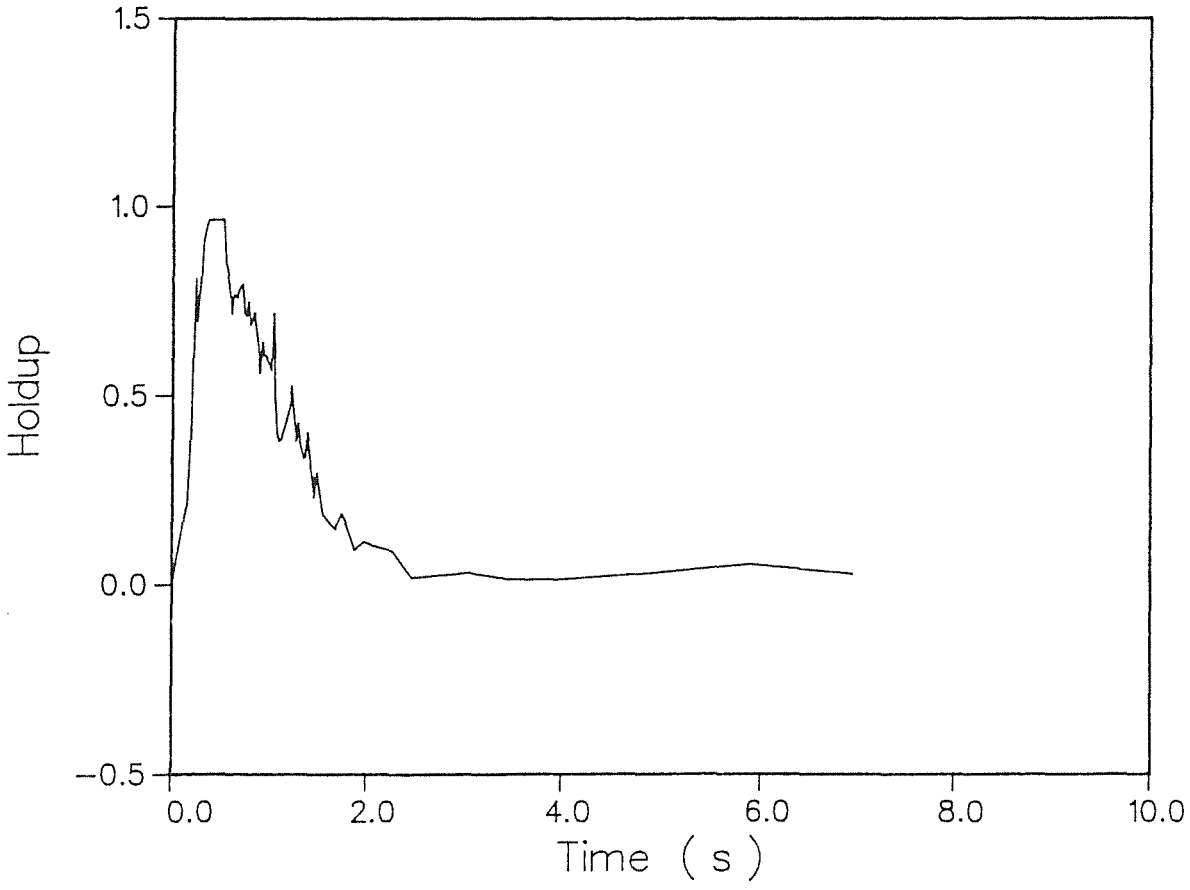

Fig.45 MMB-27 Holdup Versus Time

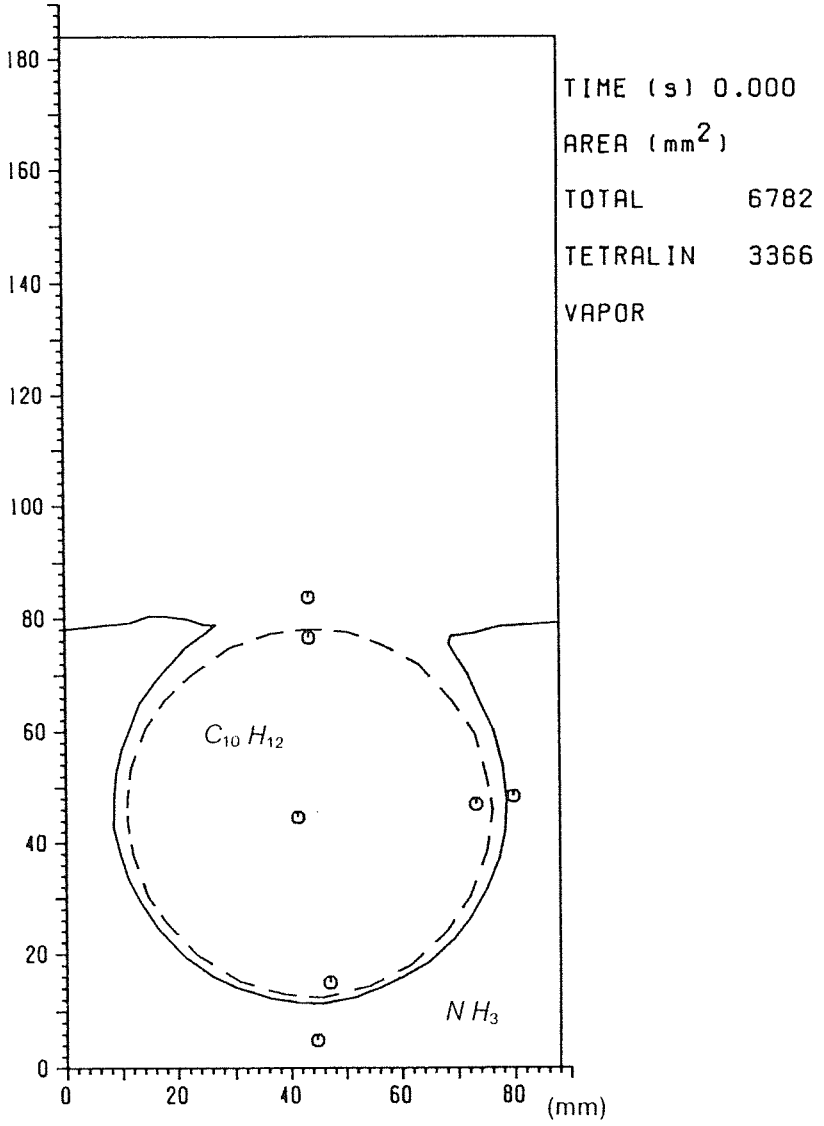

Fig.46a Initial Configuration MMB -28

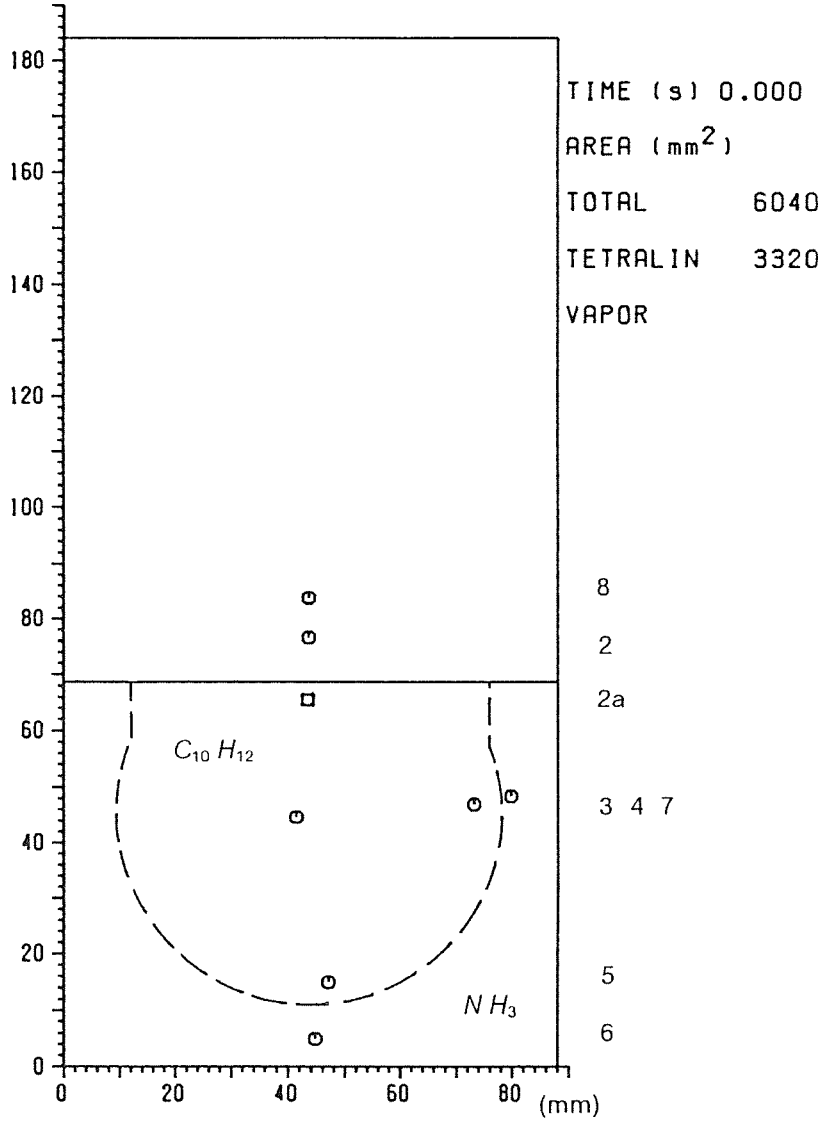

Fig.46b Idealized Initial Configuration MMB -28

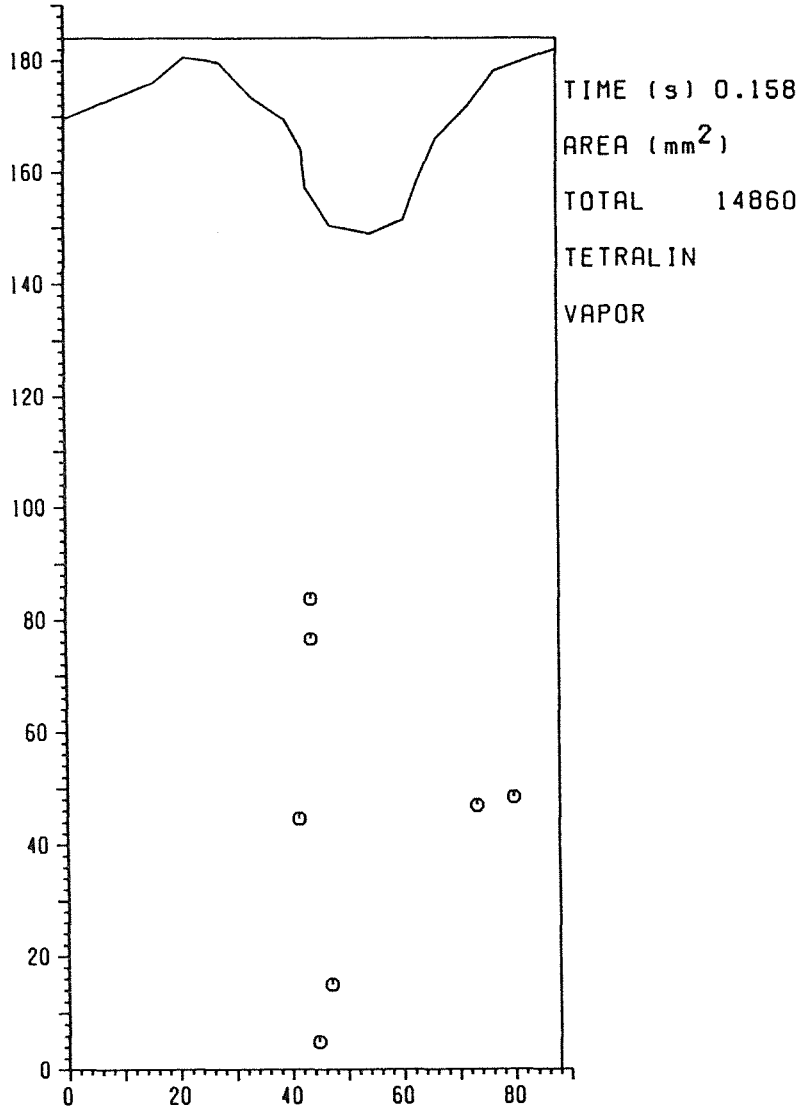

Fig.47 Interfaces MMB-28

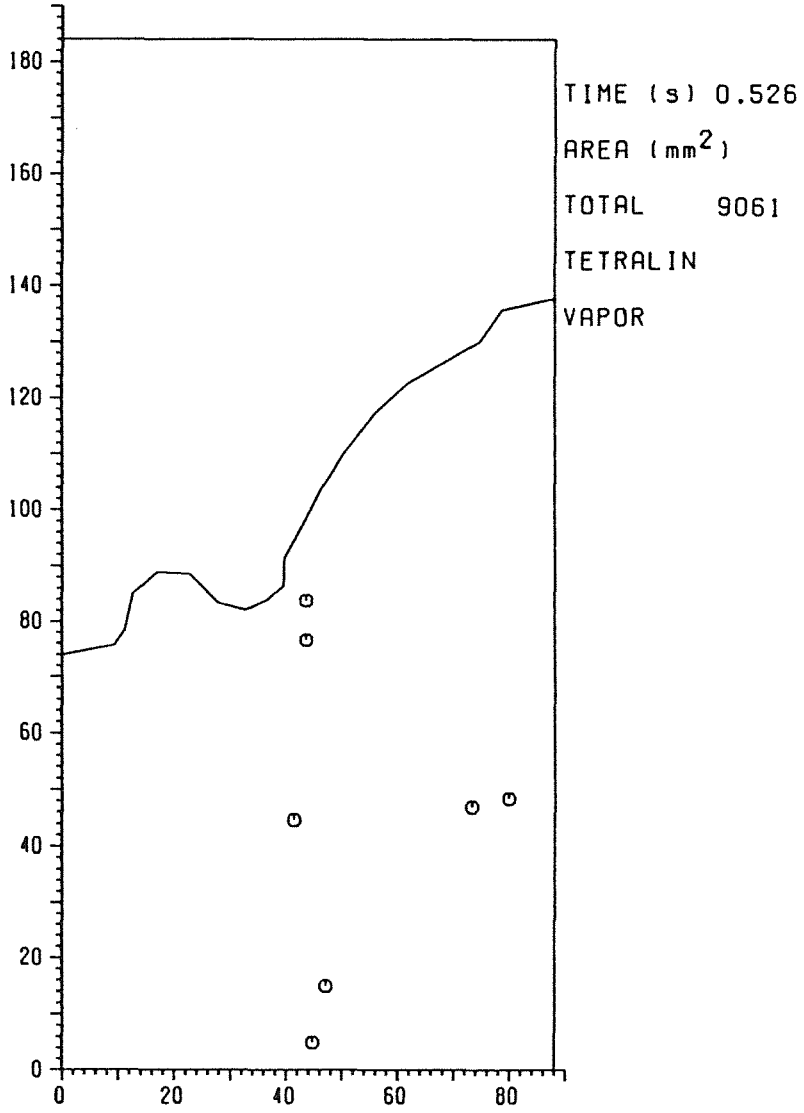

Fig.48 Interfaces MMB-28

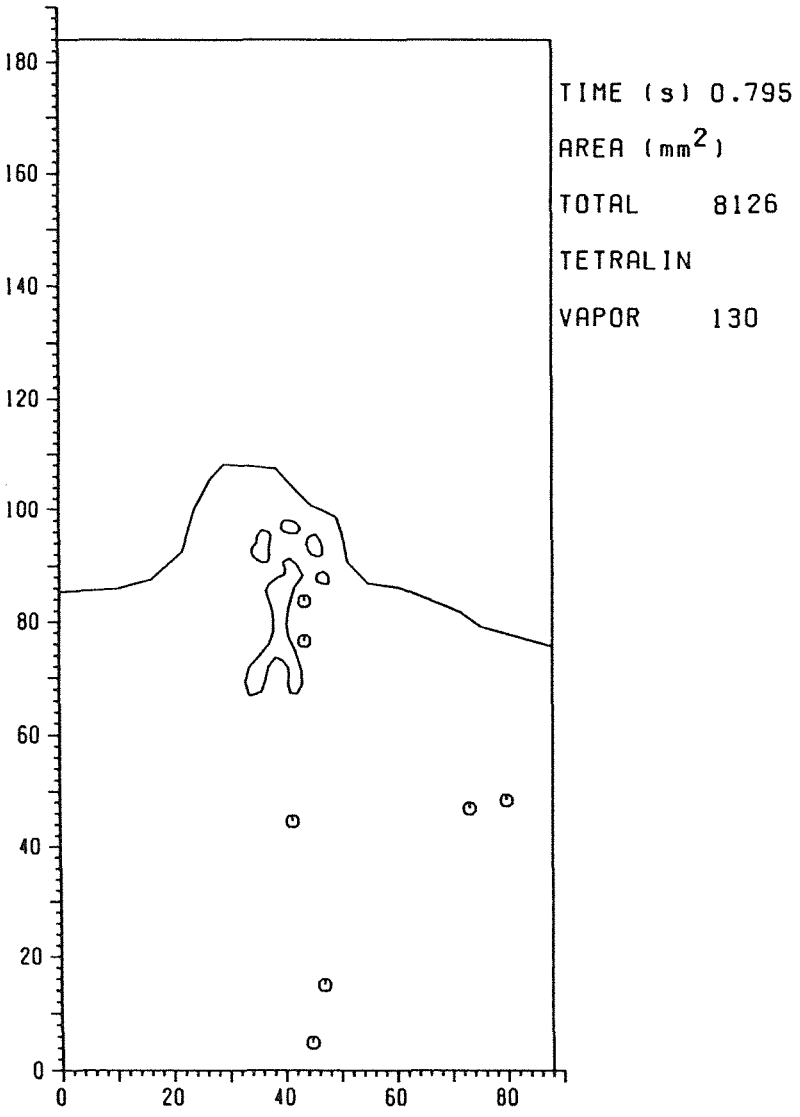

Fig.49 Interfaces MMB-28

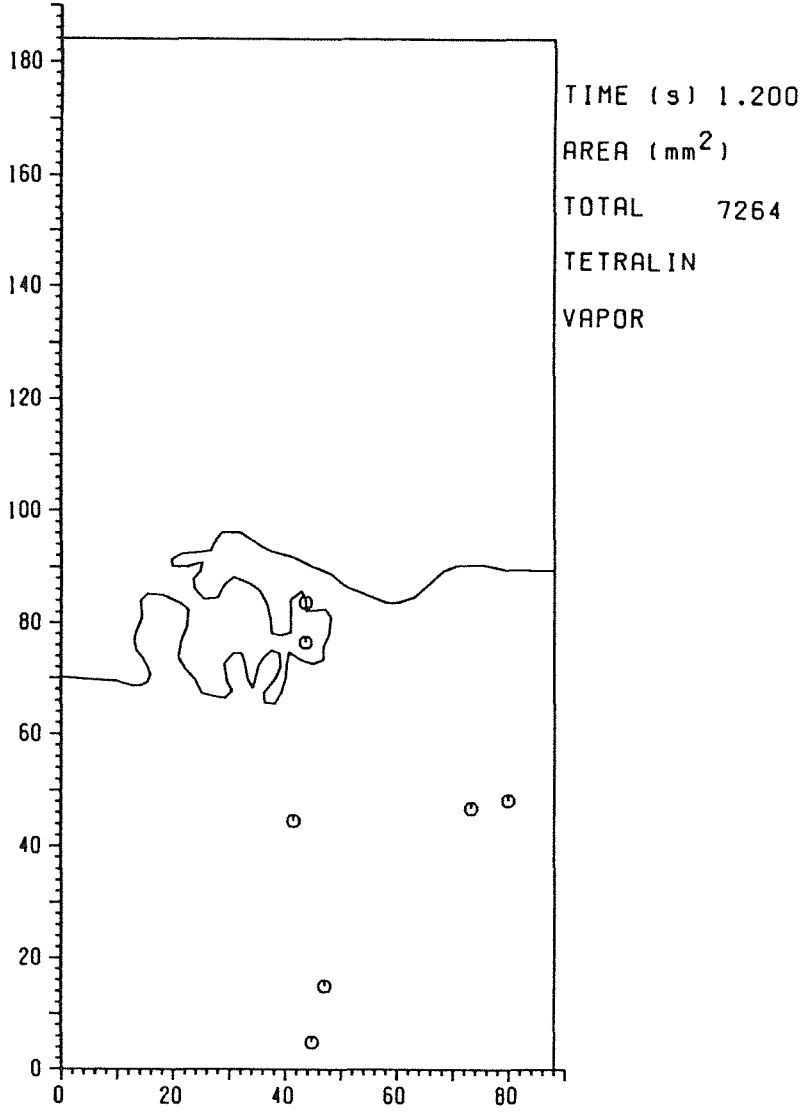

Fig.50 Interfaces MMB-28

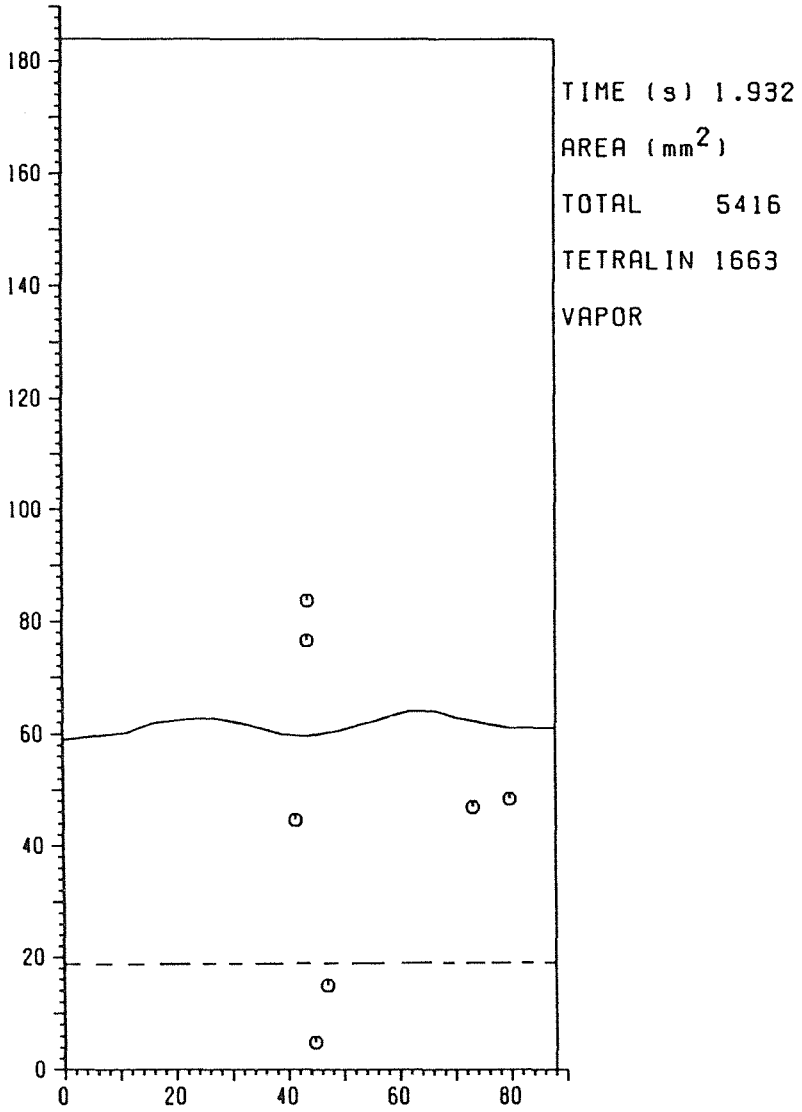

Fig.51 Interfaces MMB-28

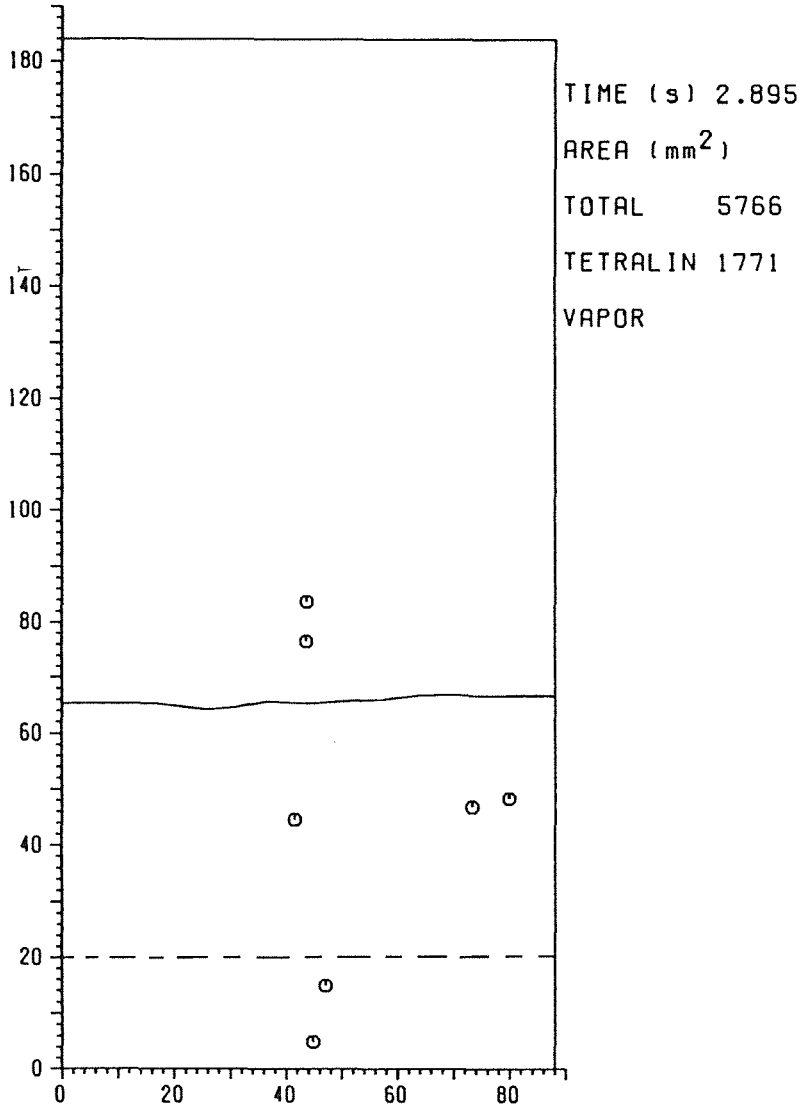

Fig.52 Interfaces MMB-28

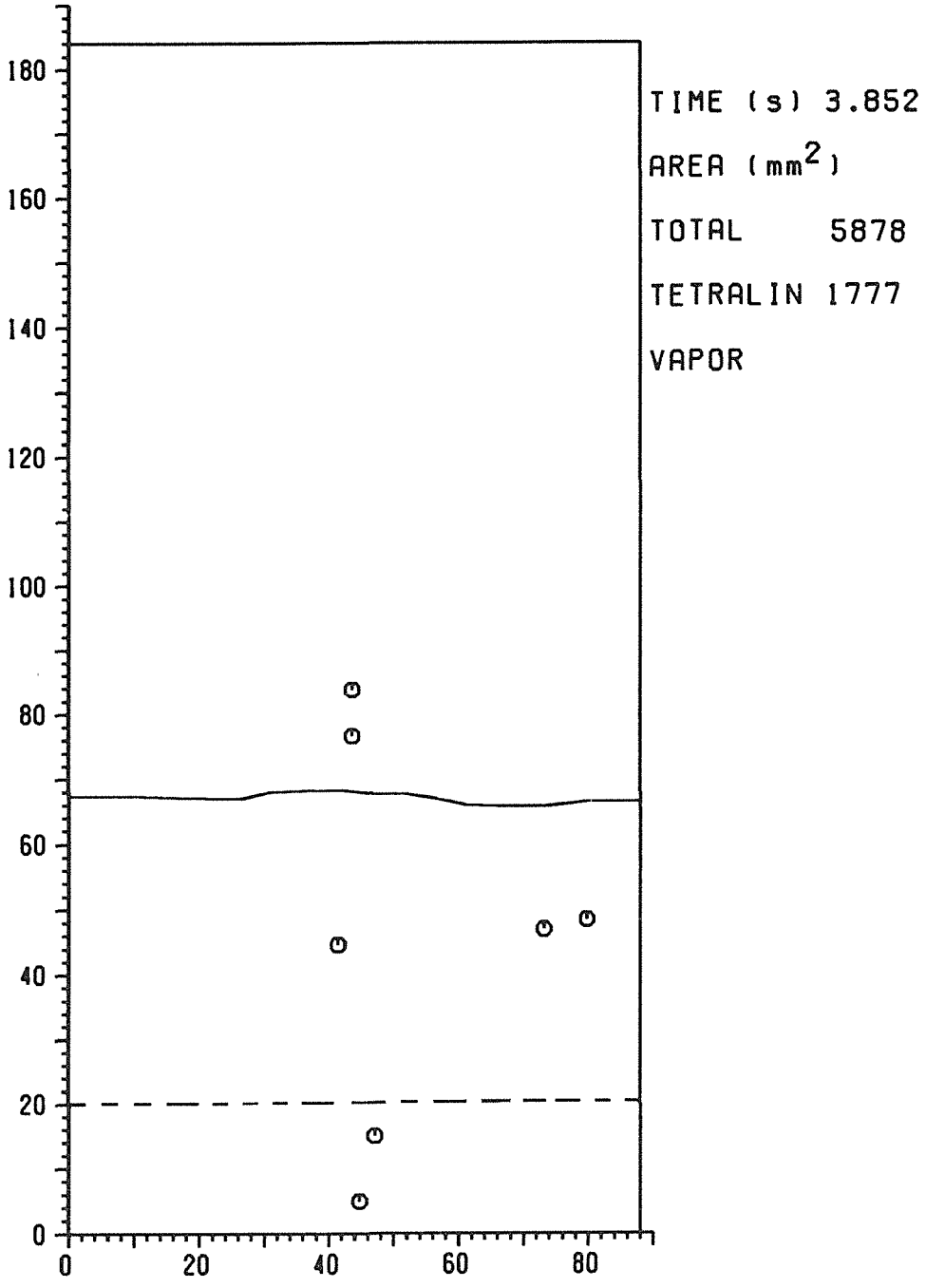

Fig.53 Interfaces

MMB-28

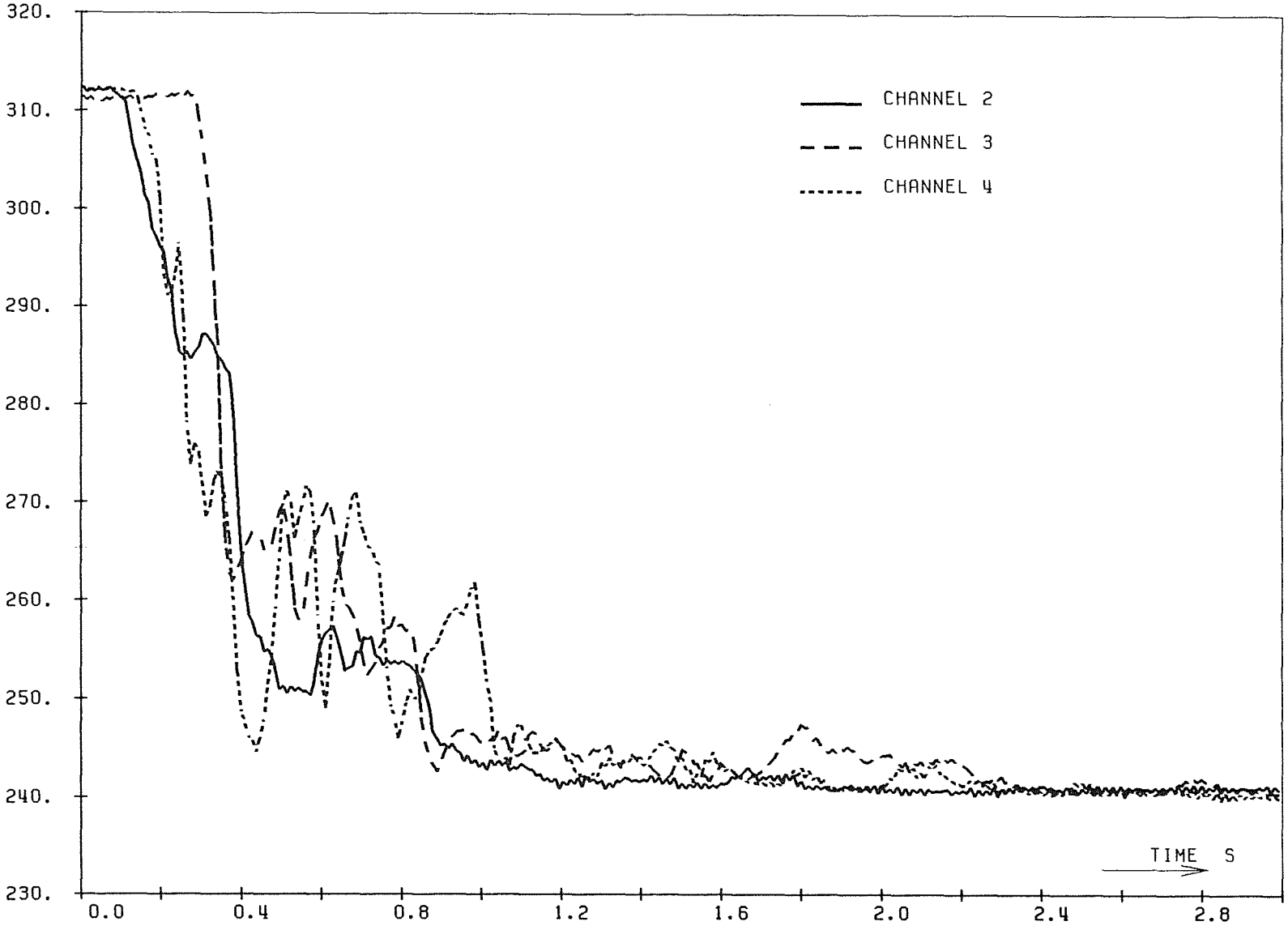

Fig.54 MMB-28 Temperatures (K) Versus Time

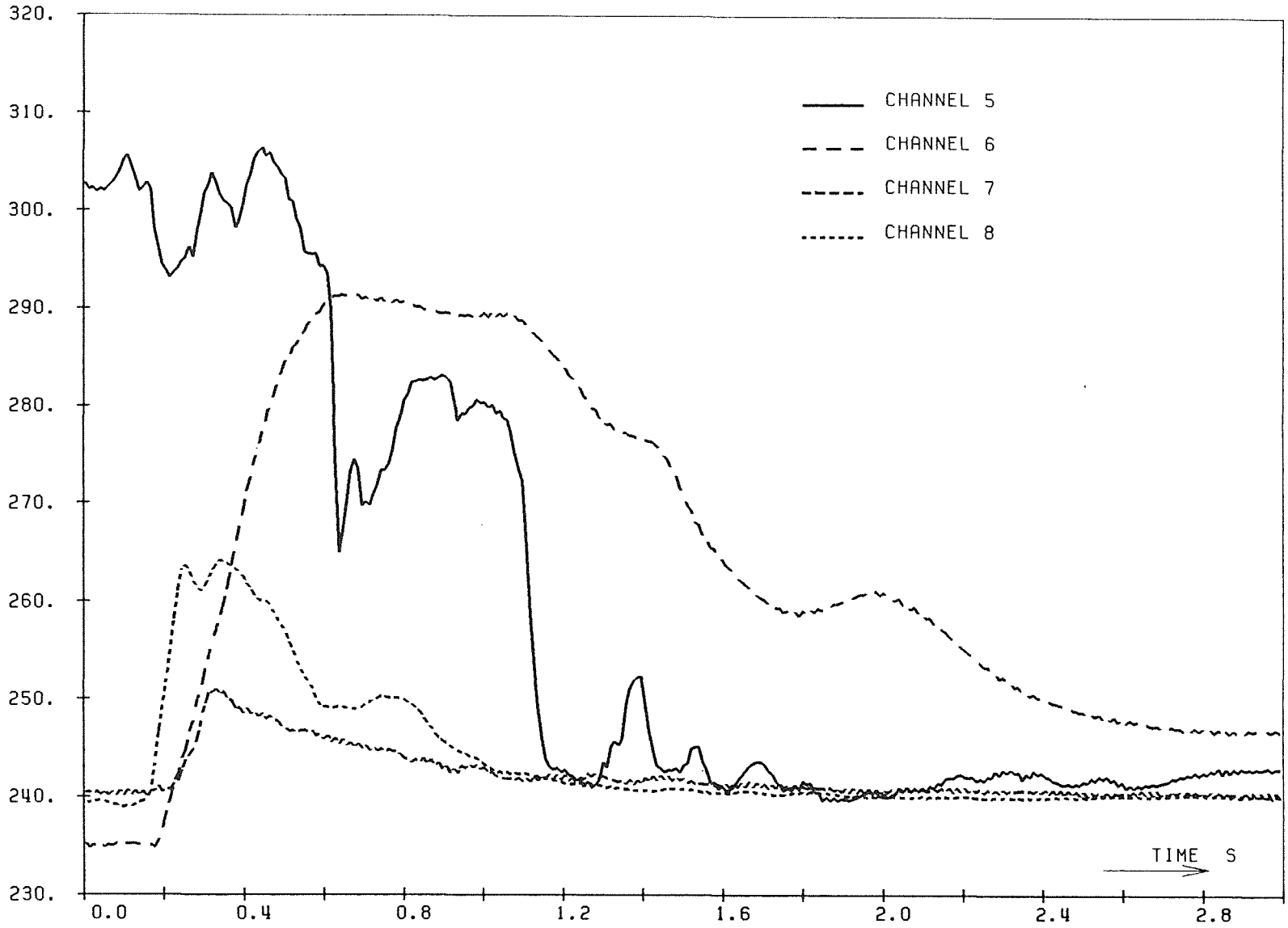

Fig.55 MMB-28 Temperatures (K) Versus Time

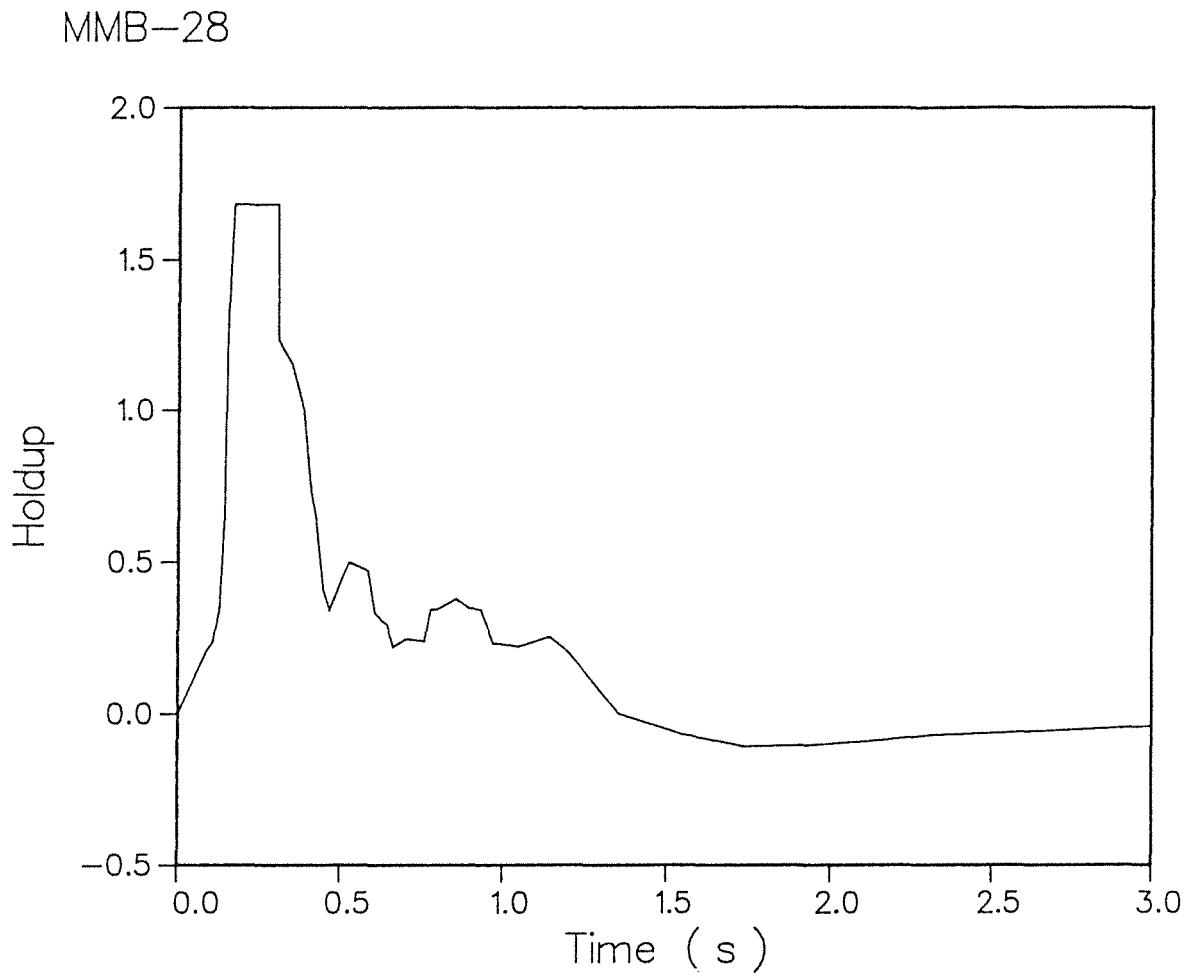

Fig.56 MMB-28 Holdup Versus Time

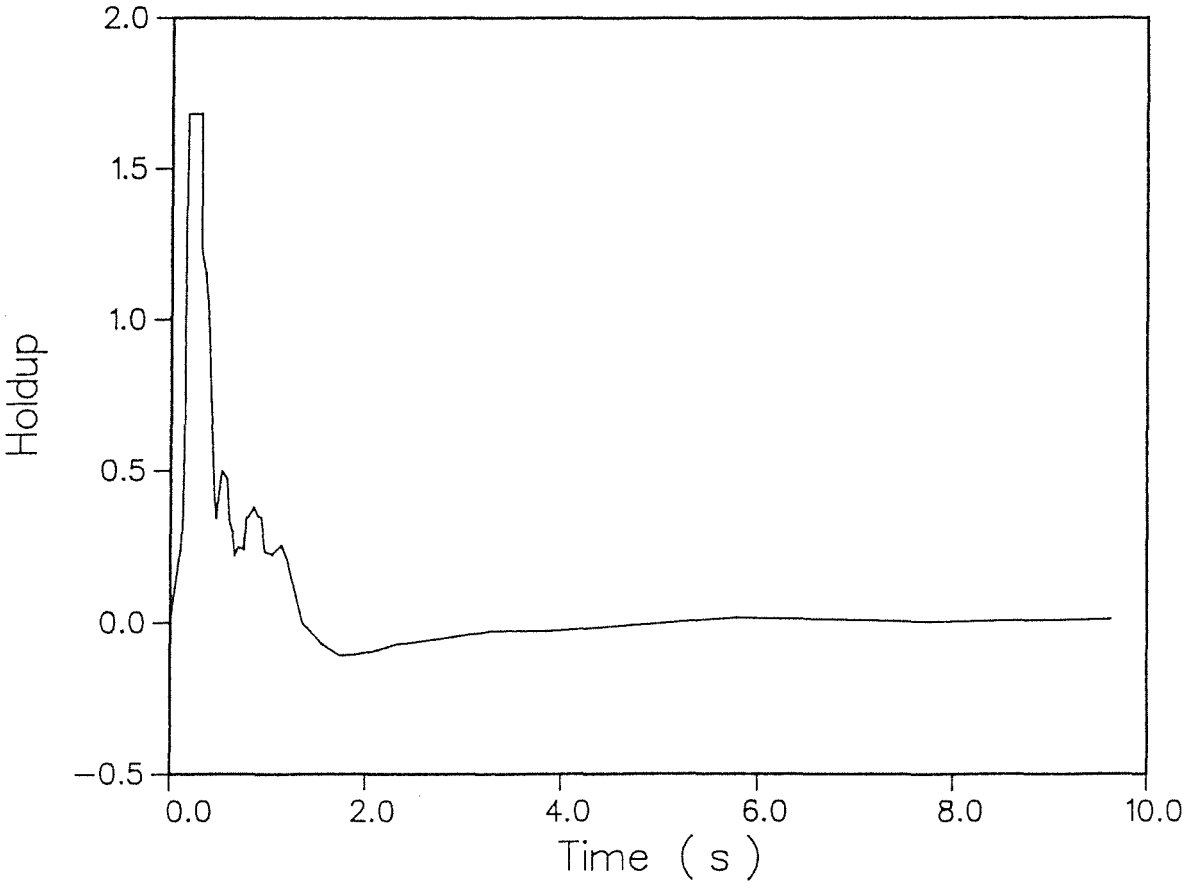

Fig.57 MMB-28 Holdup Versus Time

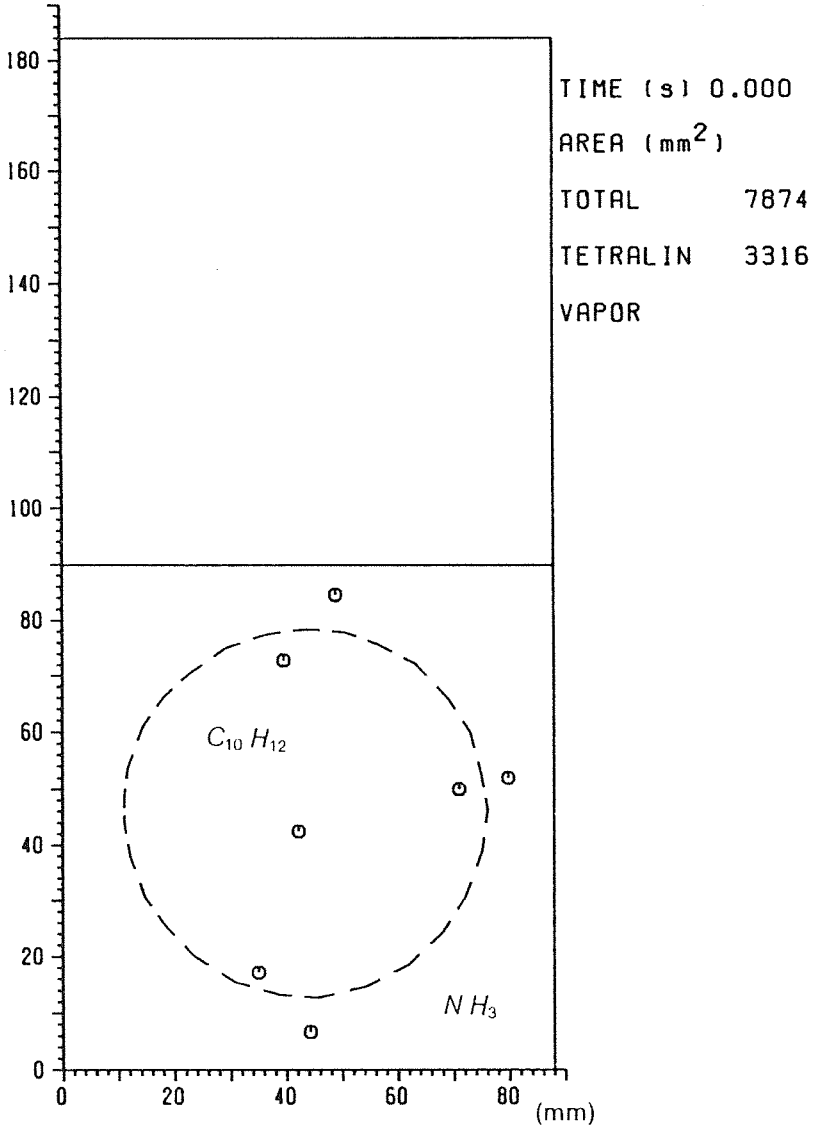

Fig.58a Initial Configuration MMB-34

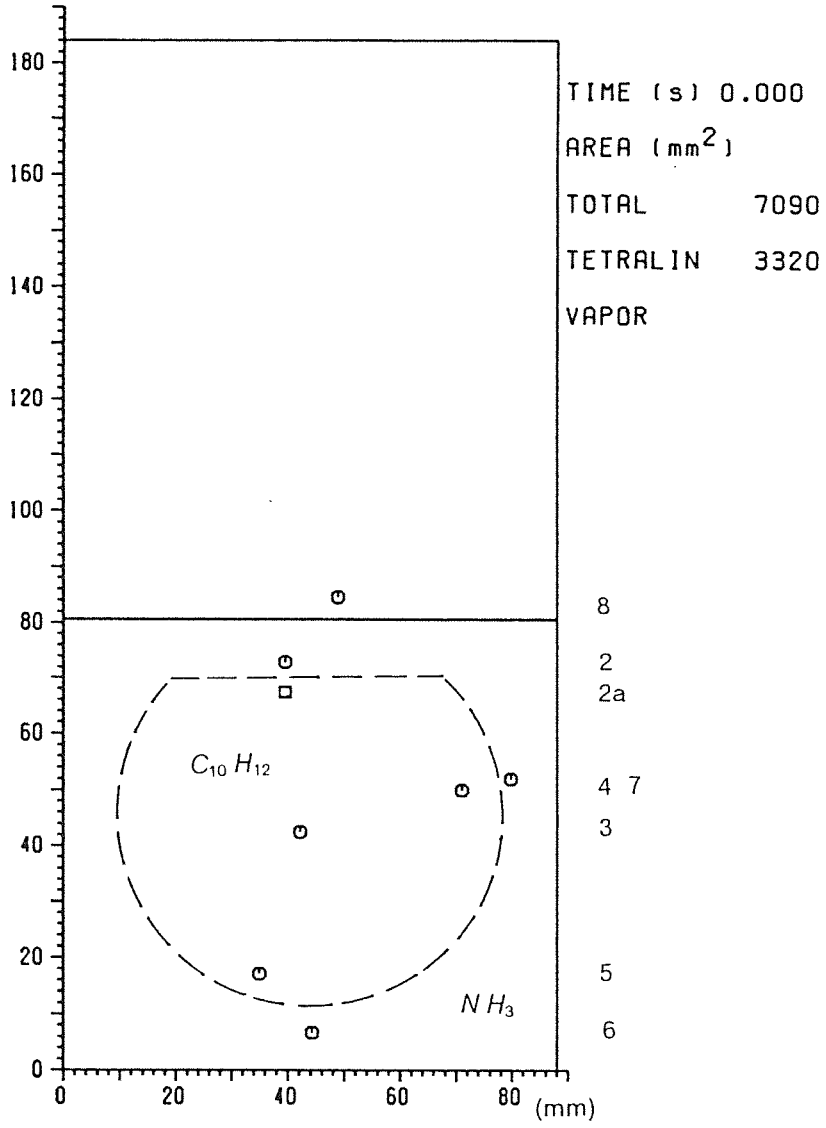

Fig.58b Idealized Initial Configuration MMB-34

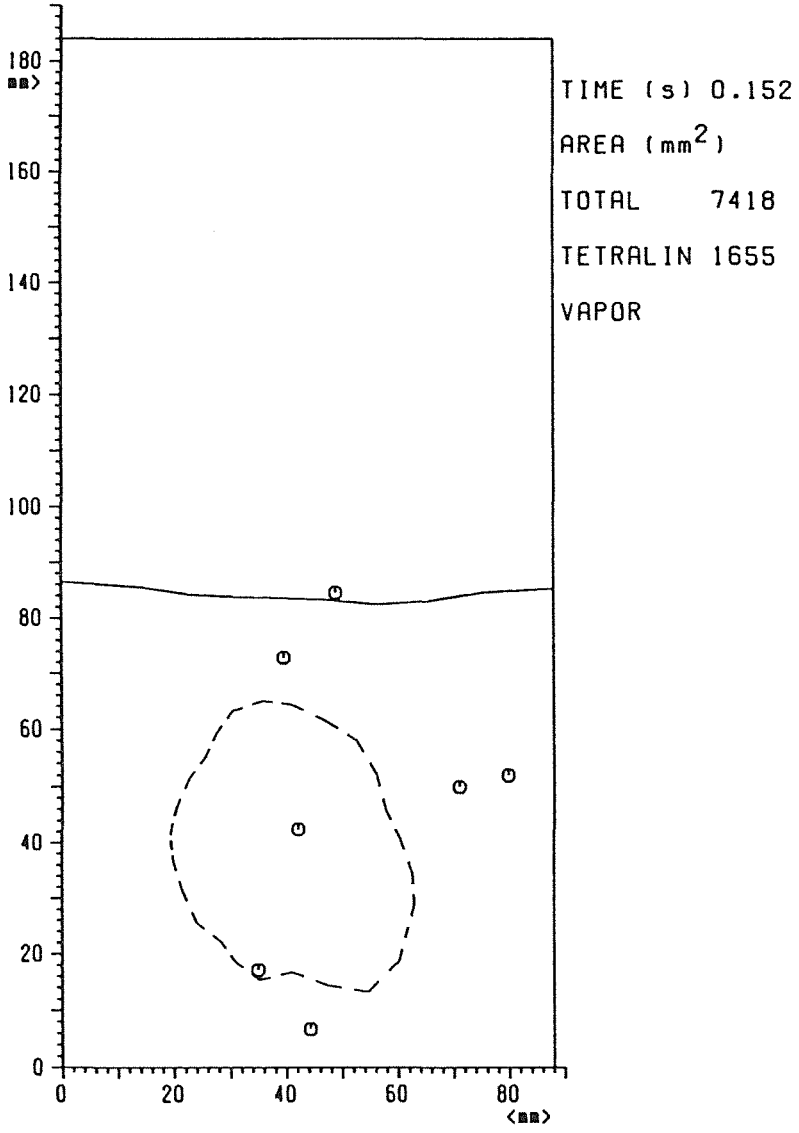

Fig.59 Interfaces MMB-34

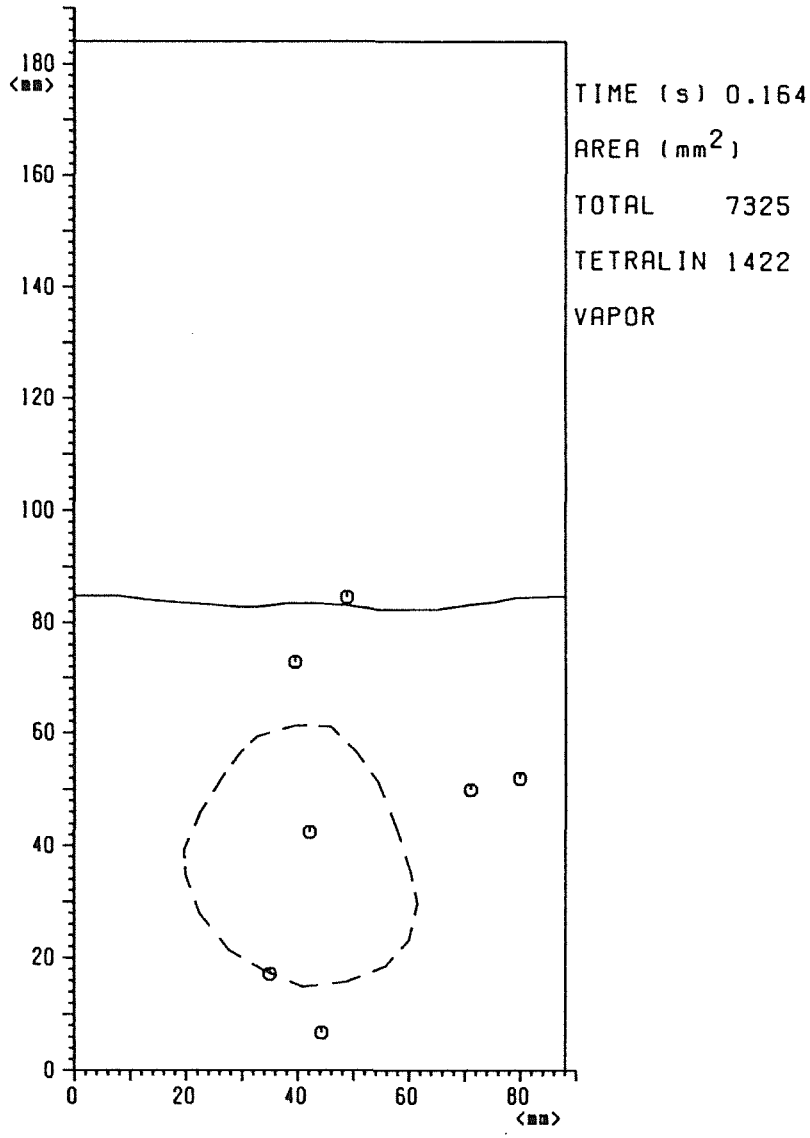

Fig.60 Interfaces MMB-34

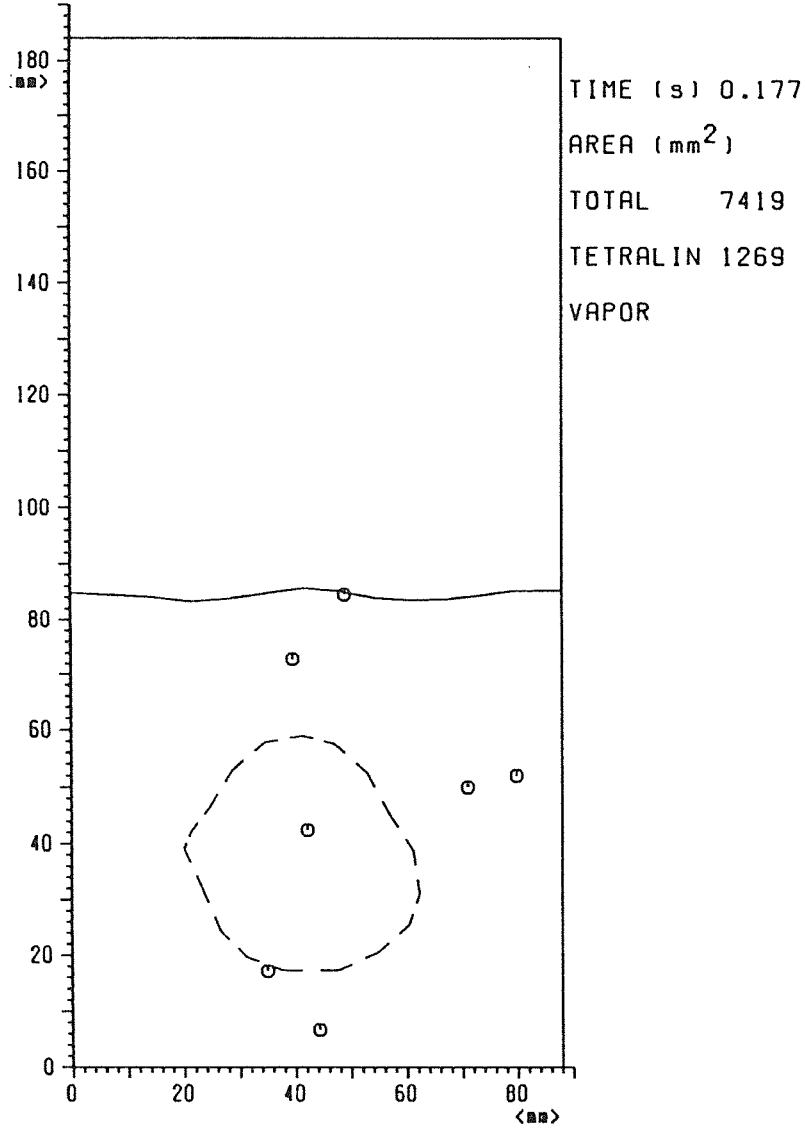

Fig.61 Interfaces MMB-34

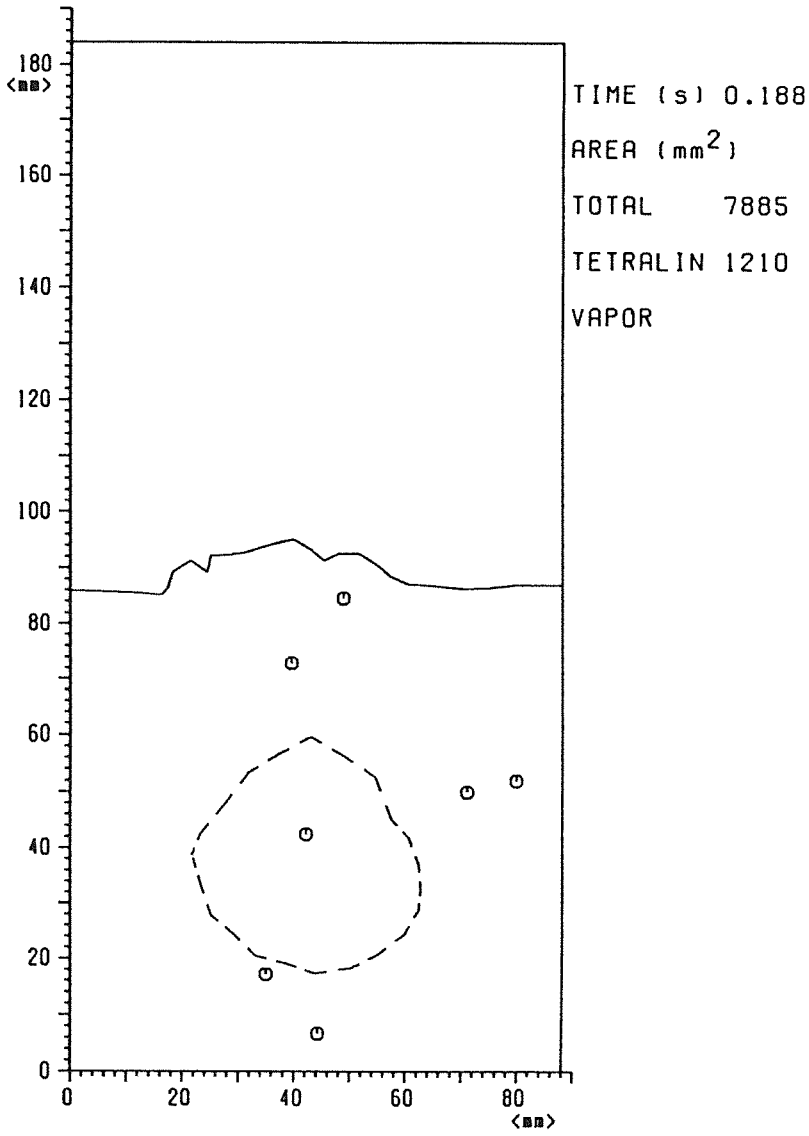

Fig.62 Interfaces MMB-34

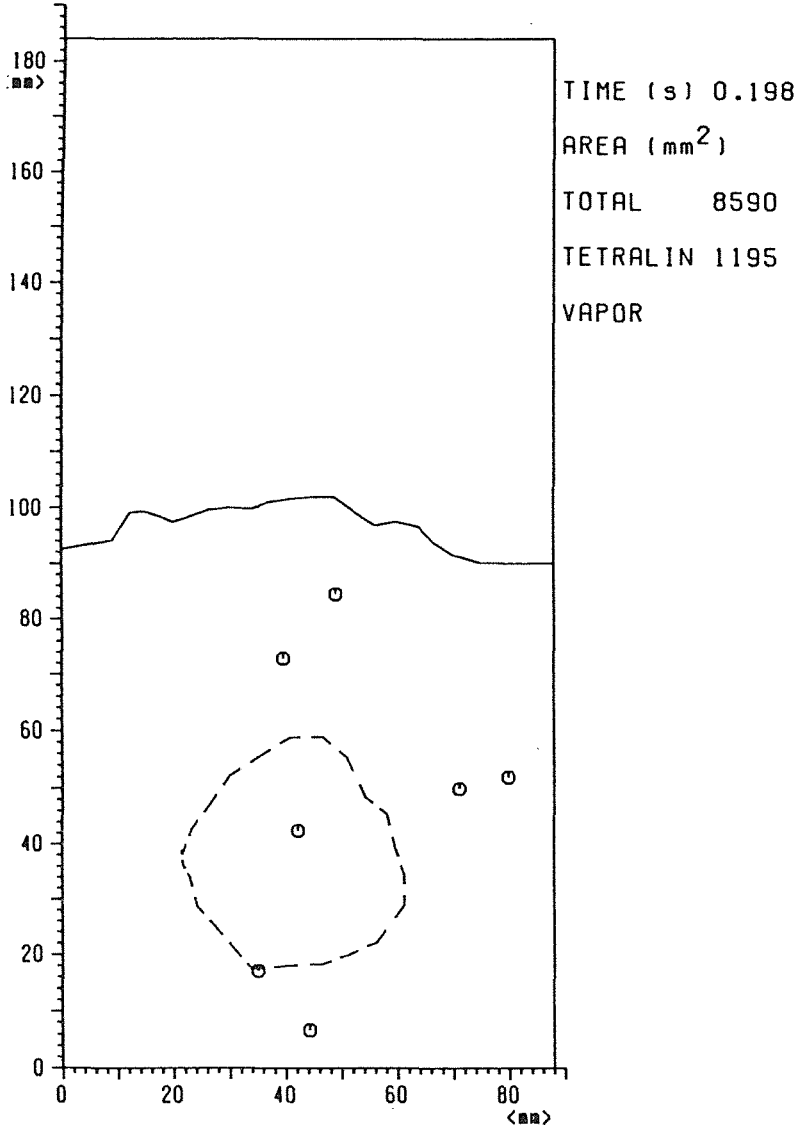

Fig.63 Interfaces MMB-34

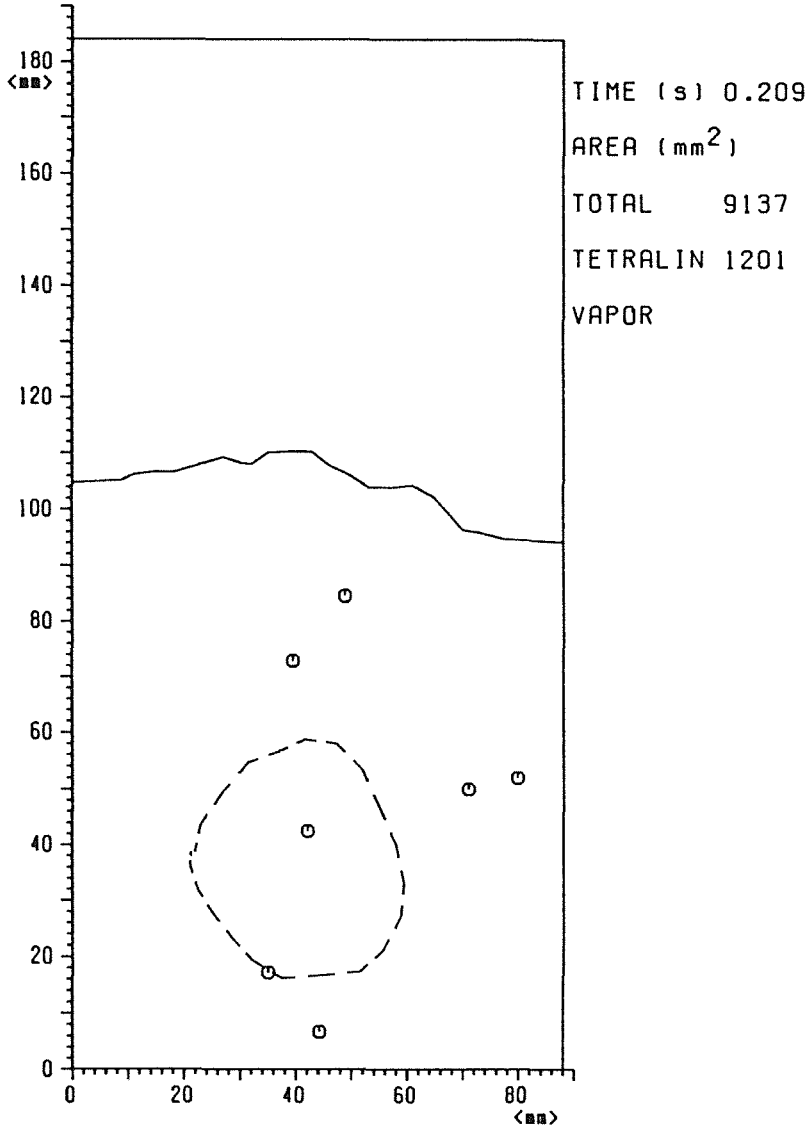

Fig.64 Interfaces MMB-34

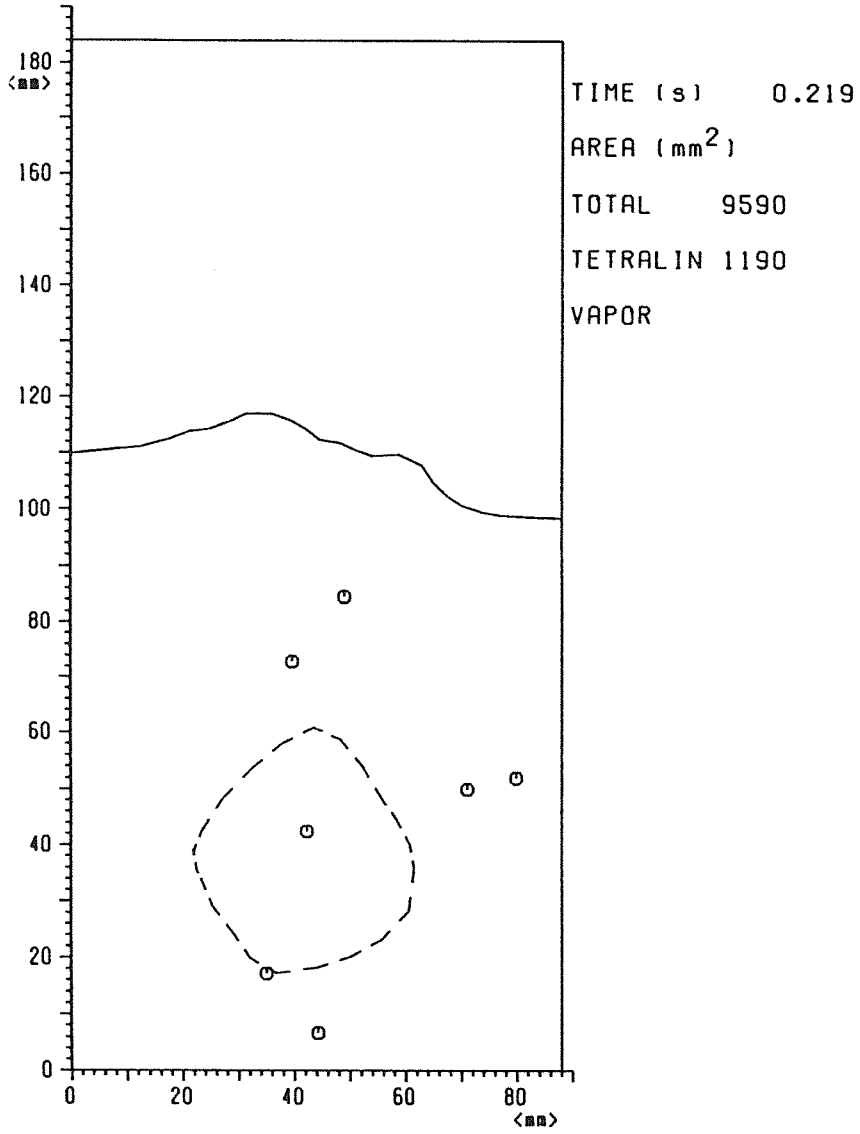

Fig.65 Interfaces MMB-34

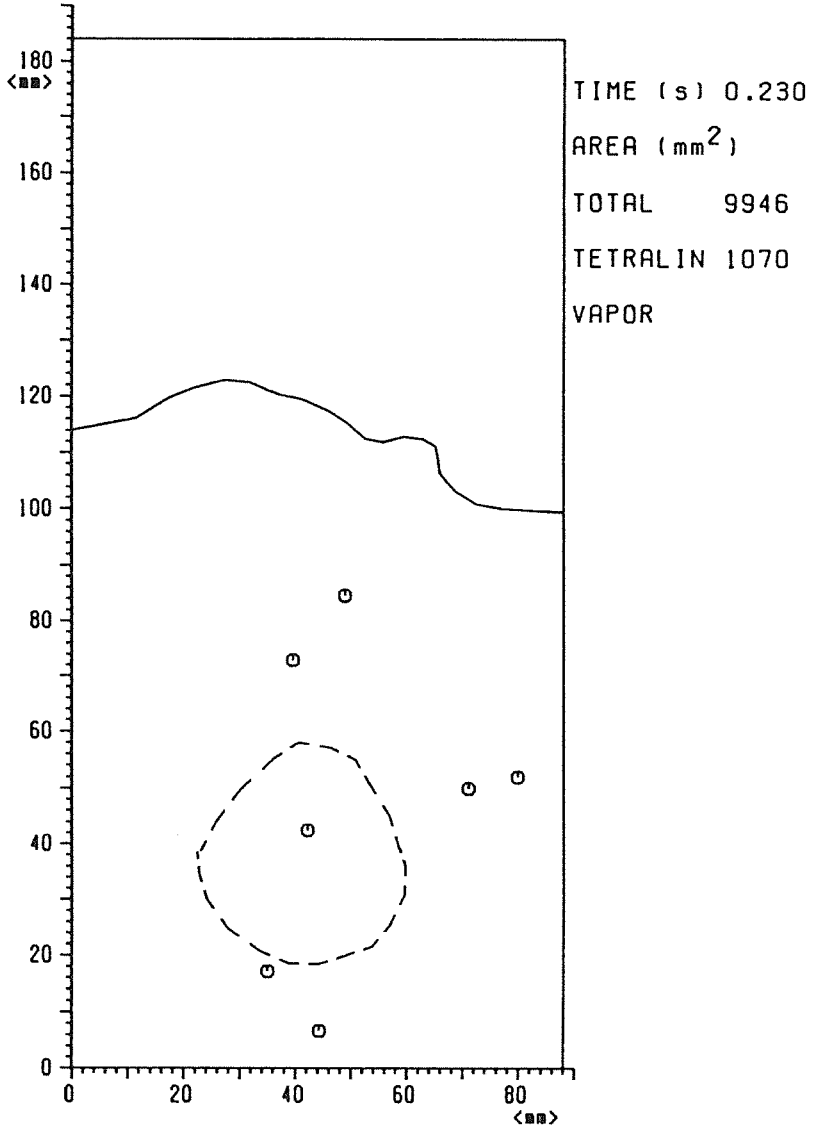

Fig.66 Interfaces MMB-34

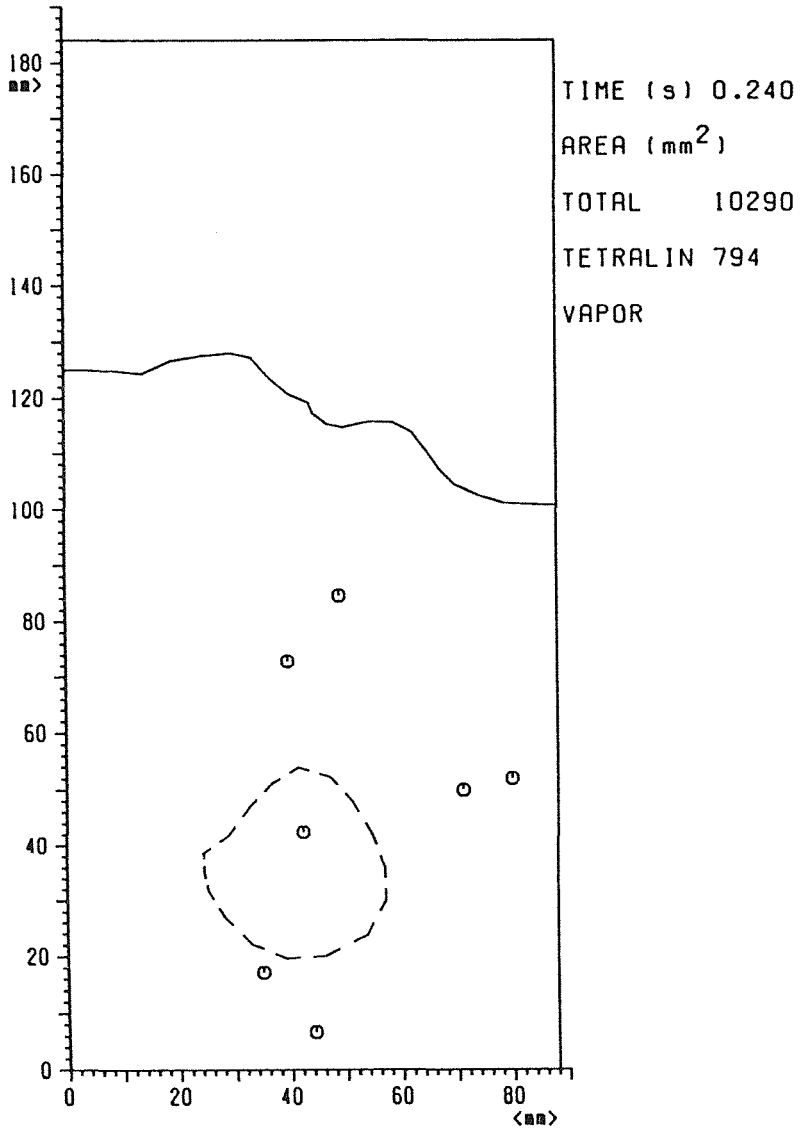

Fig.67 Interfaces MMB-34

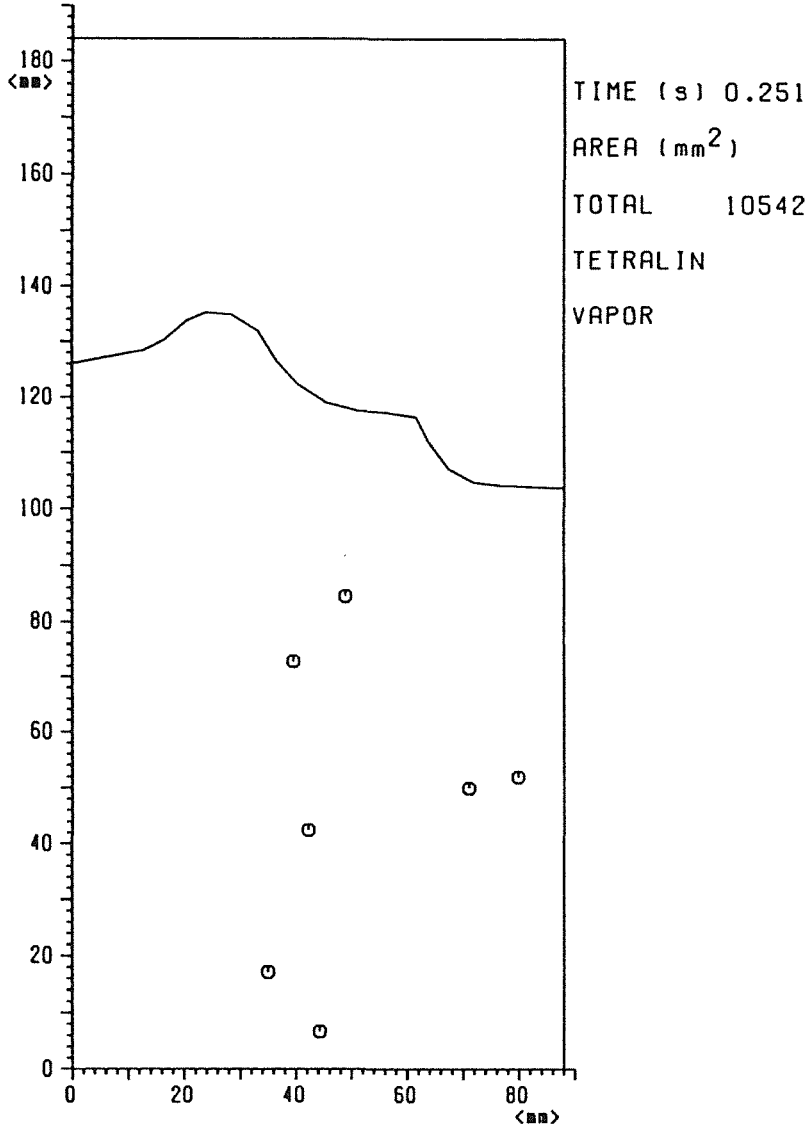

Fig.68 Interfaces MMB-34

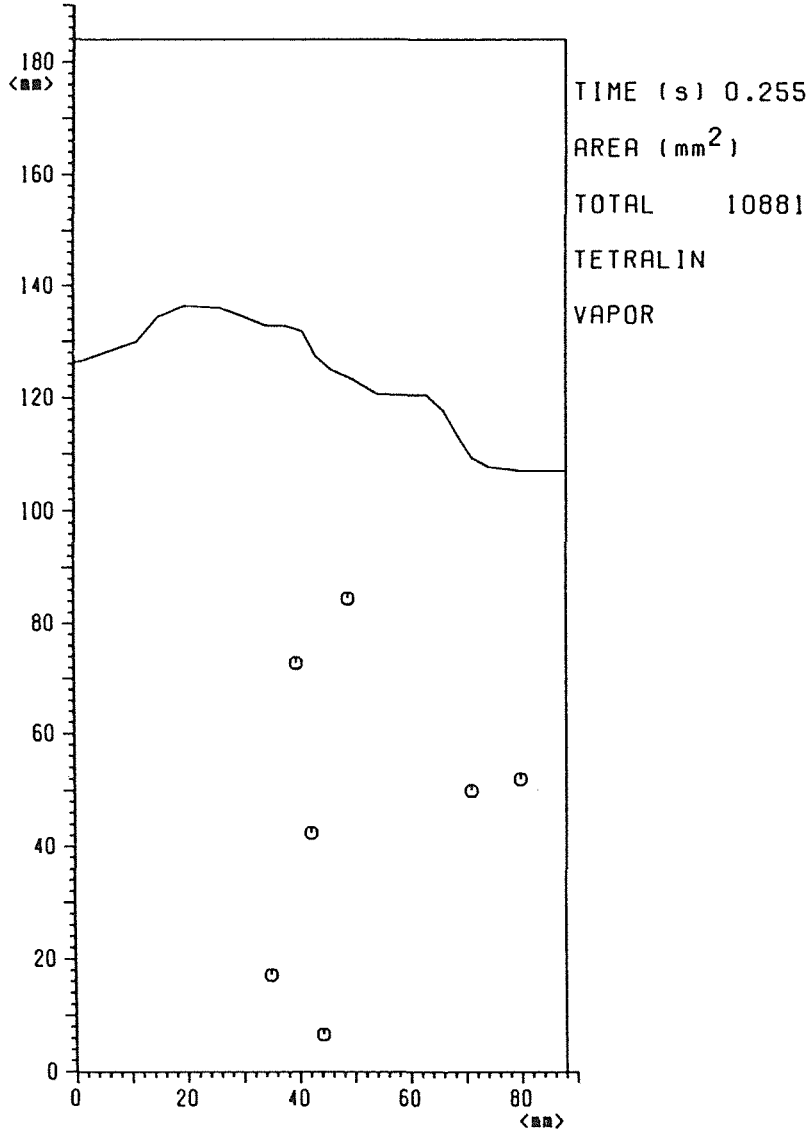

Fig.69 Interfaces MMB-34

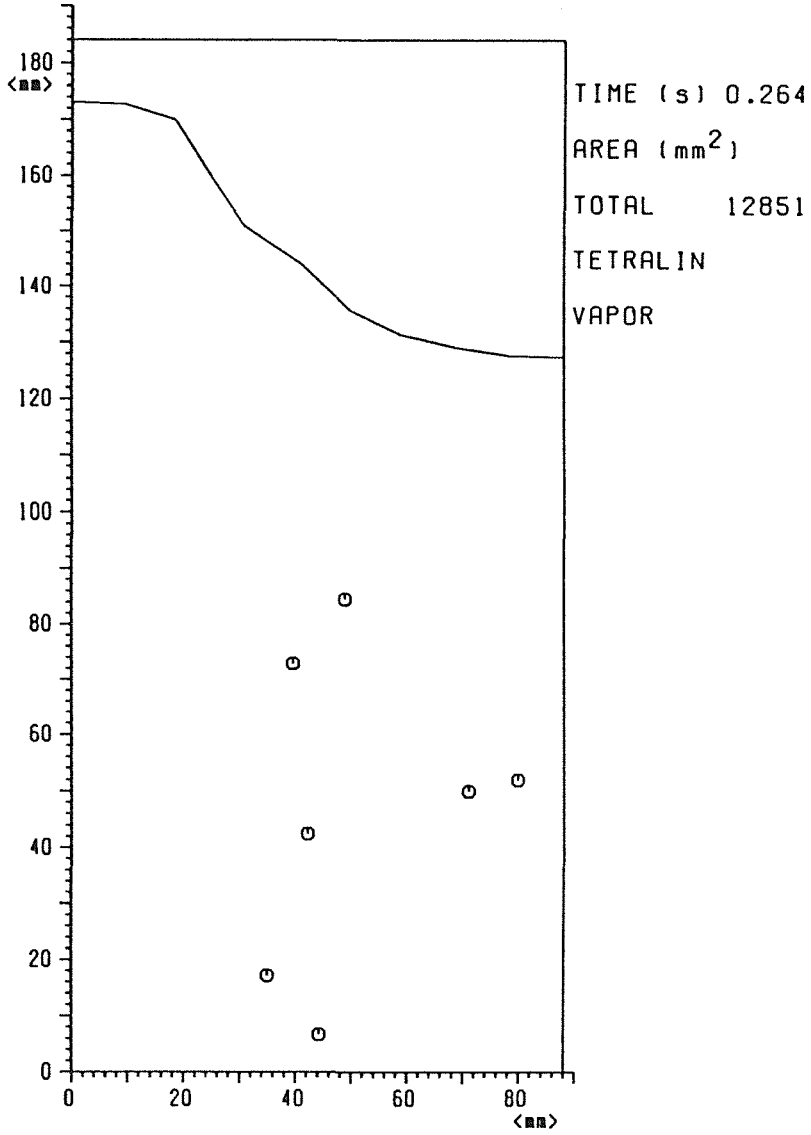

Fig.70 Interfaces MMB-34

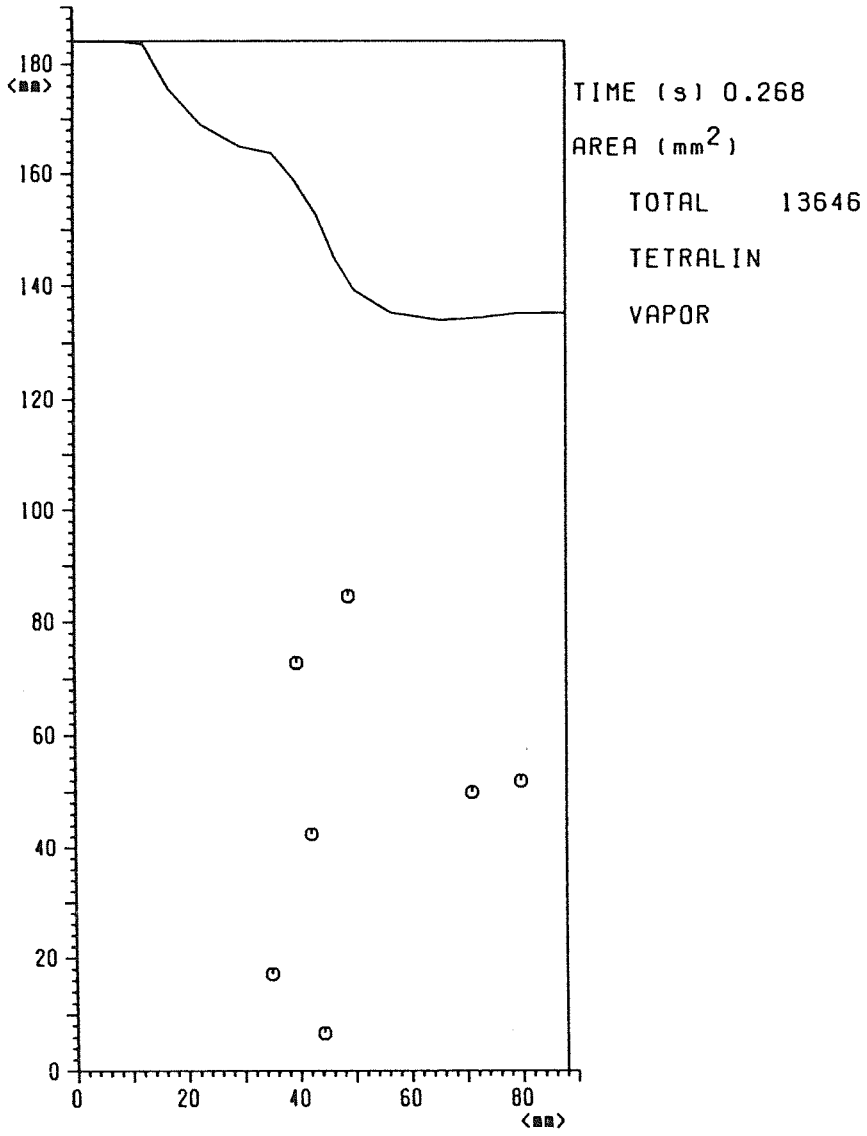

Fig.71 Interfaces MMB-34

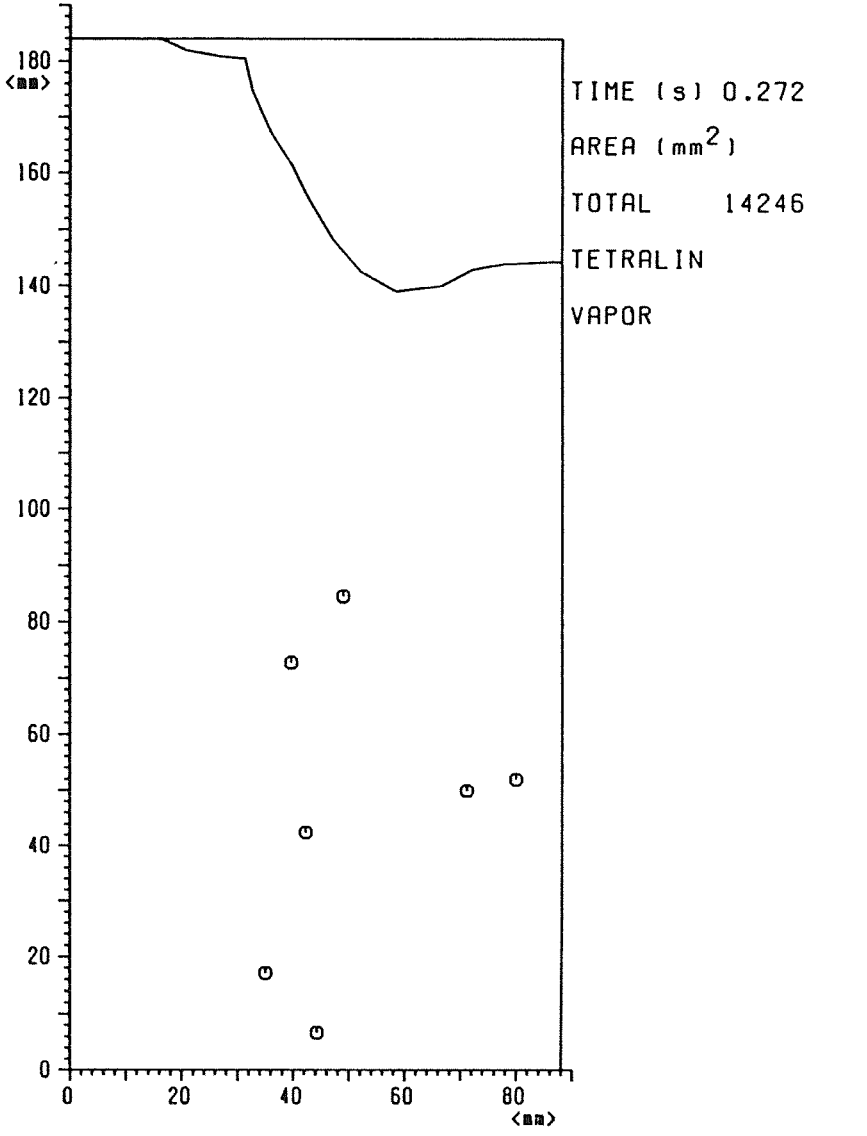

Fig.72 Interfaces MMB-34

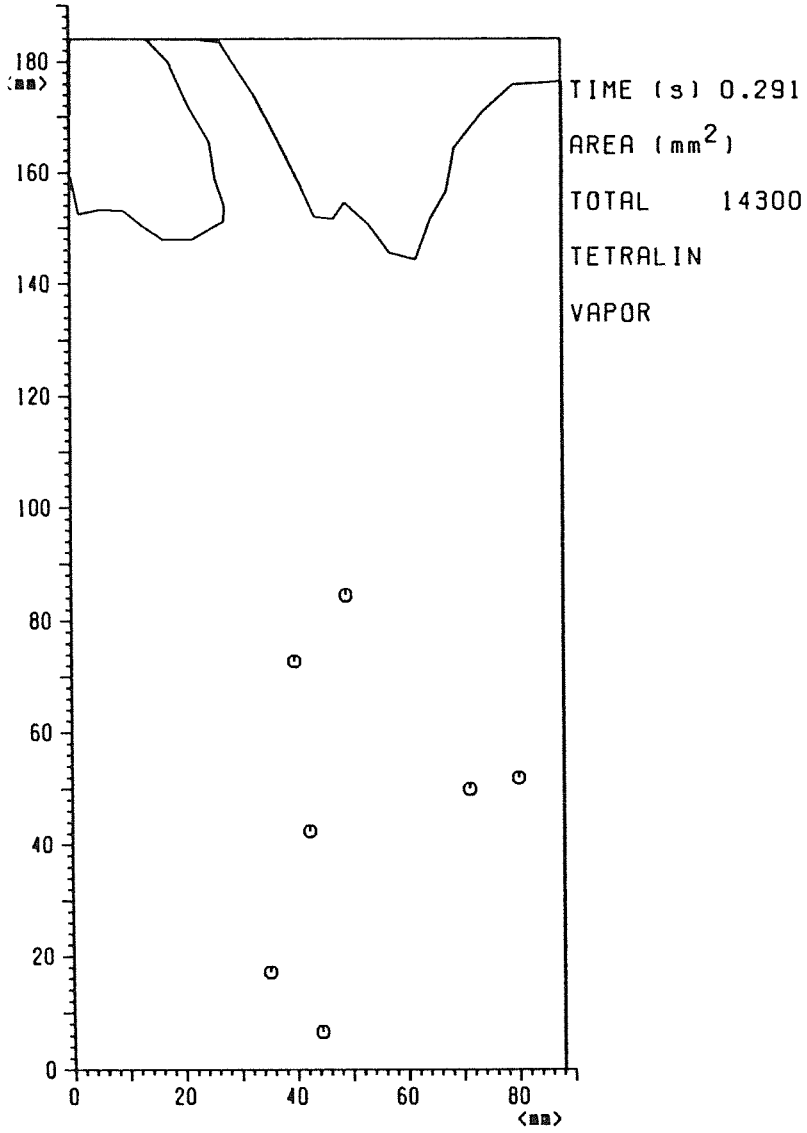

Fig.73 Interfaces MMB-34

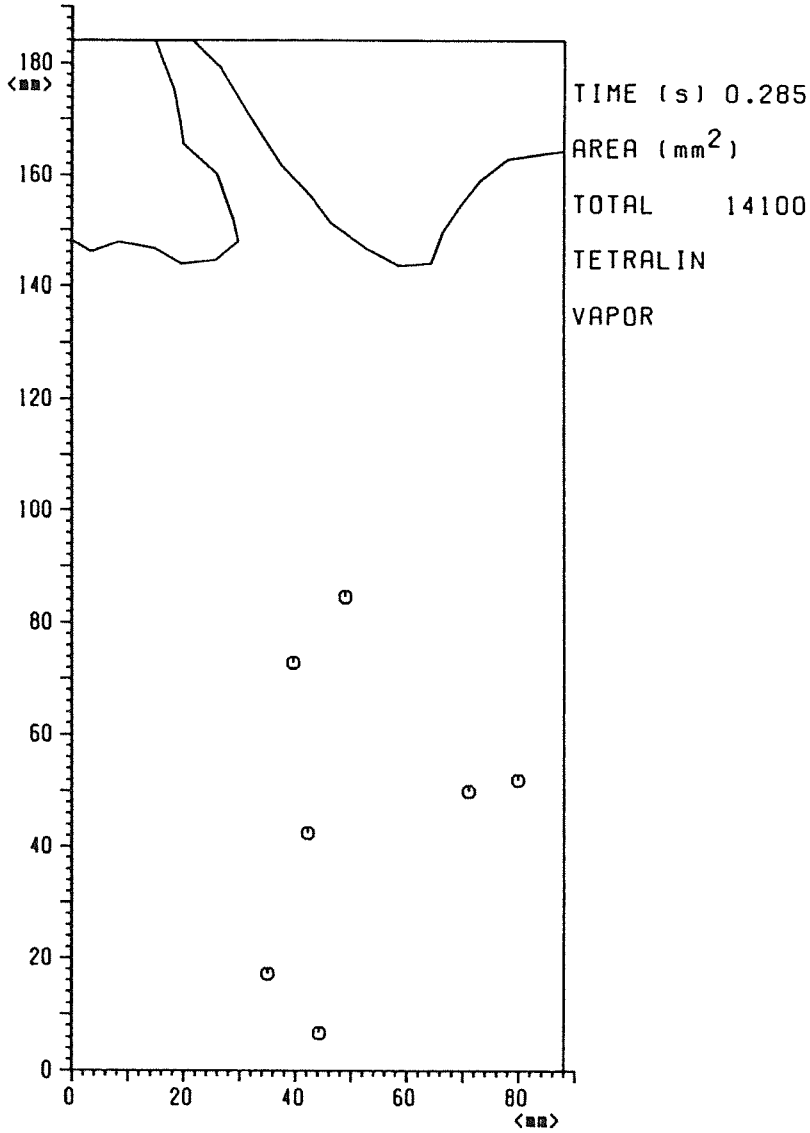

Fig.74 Interfaces MMB-34

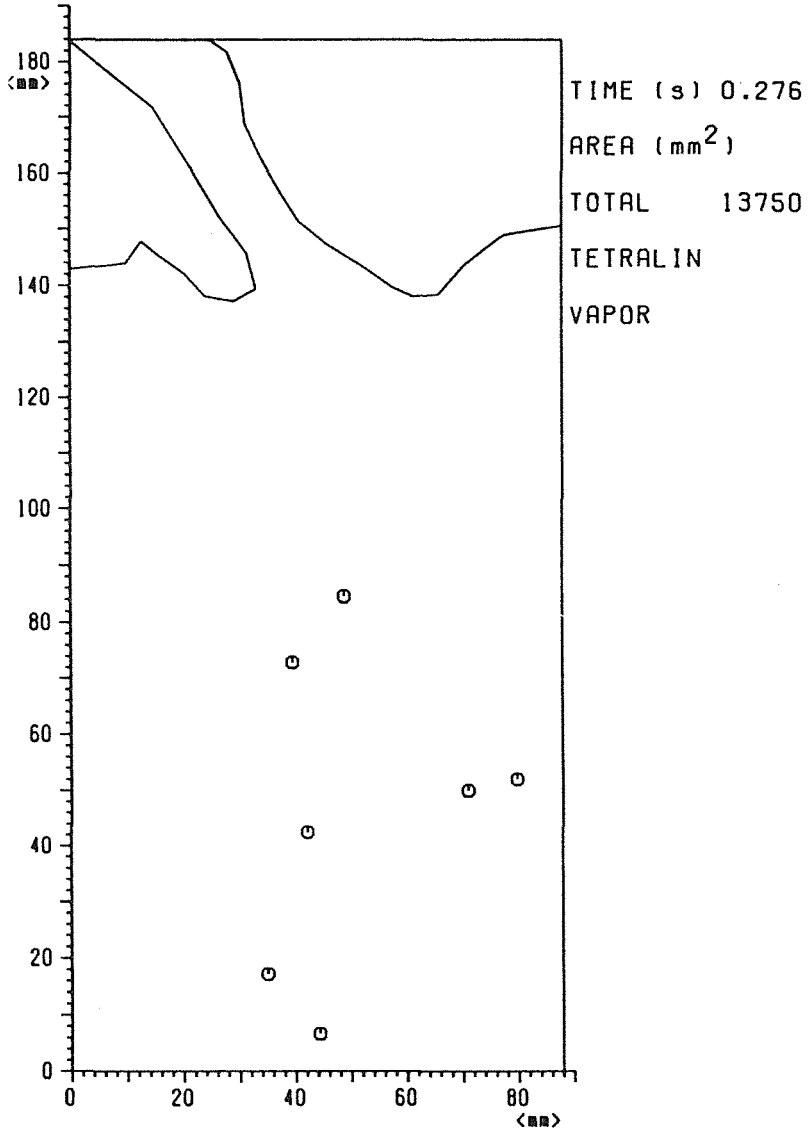

Fig.75 Interfaces MMB-34

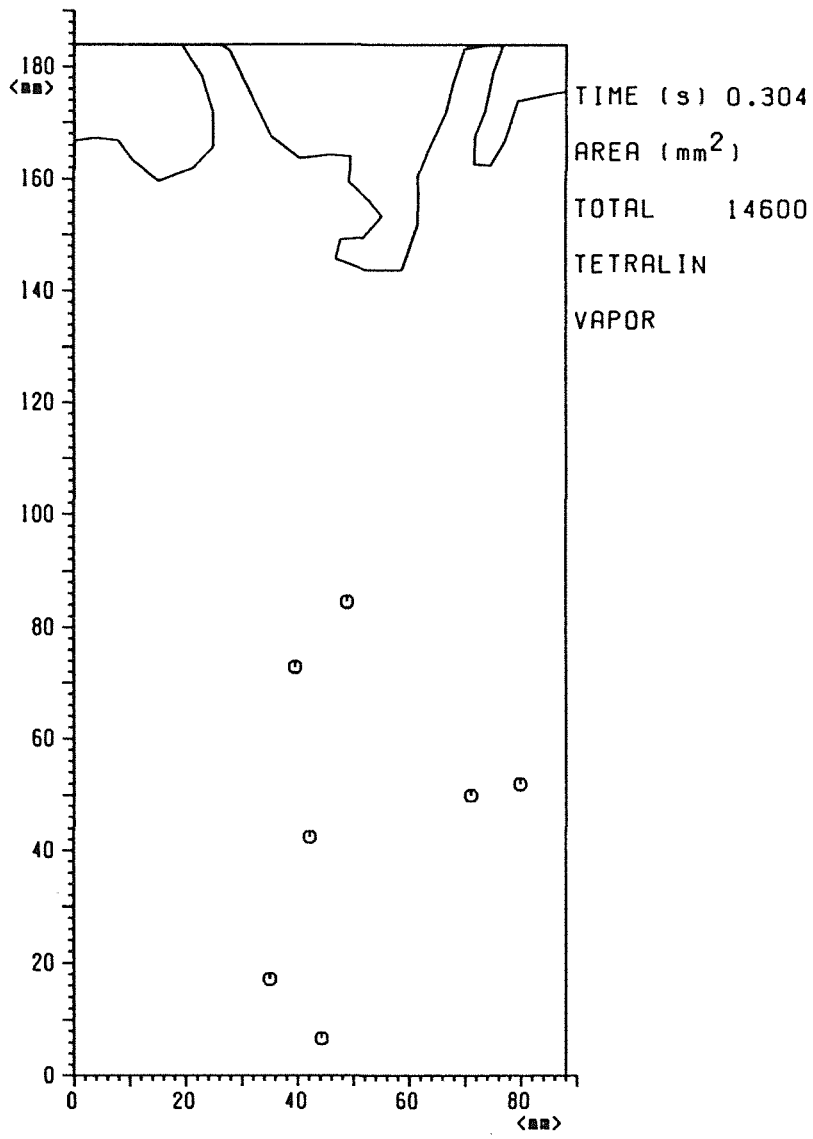

Fig.76 Interfaces MMB-34

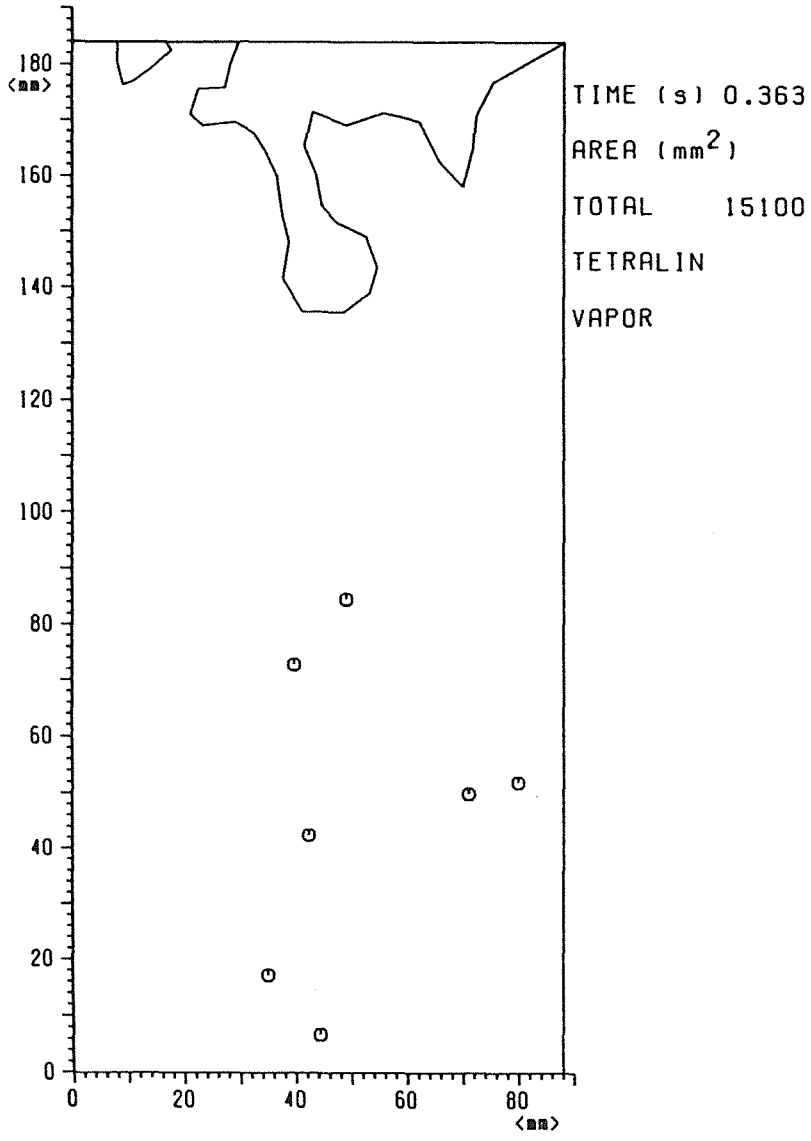

Fig.77 Interfaces MMB-34

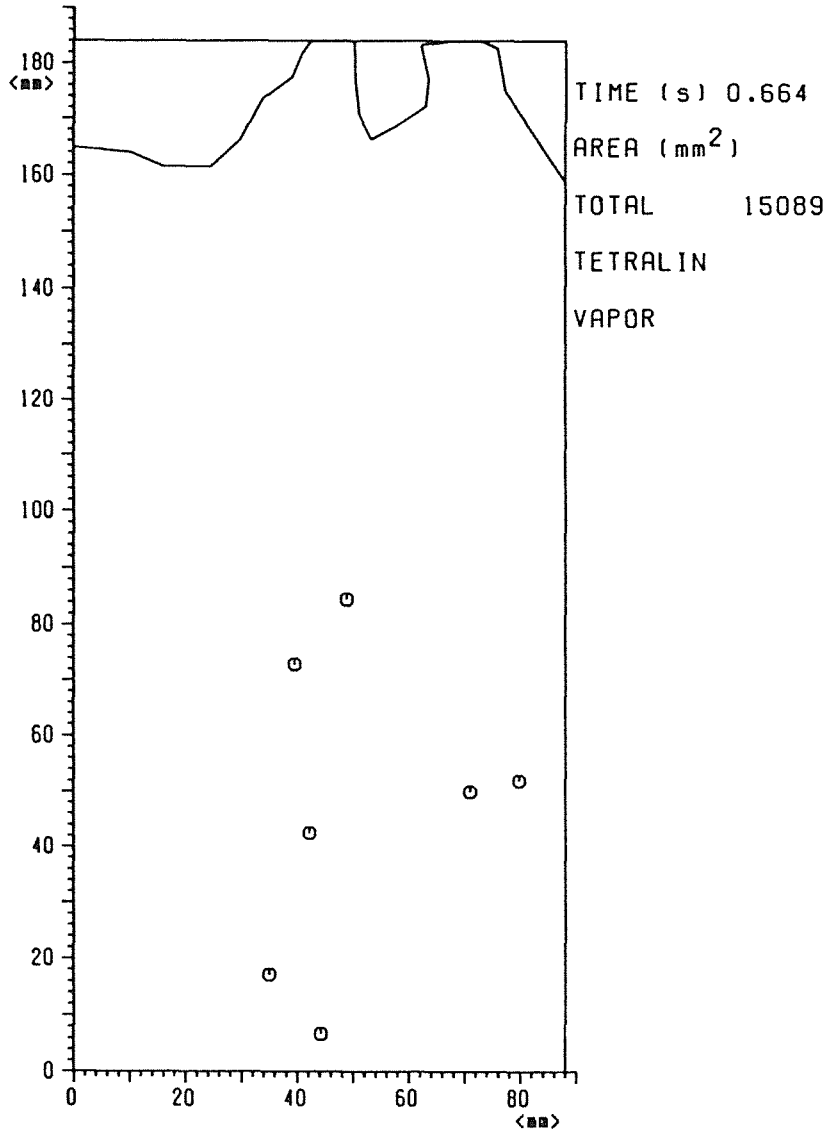

Fig.78 Interfaces MMB-34

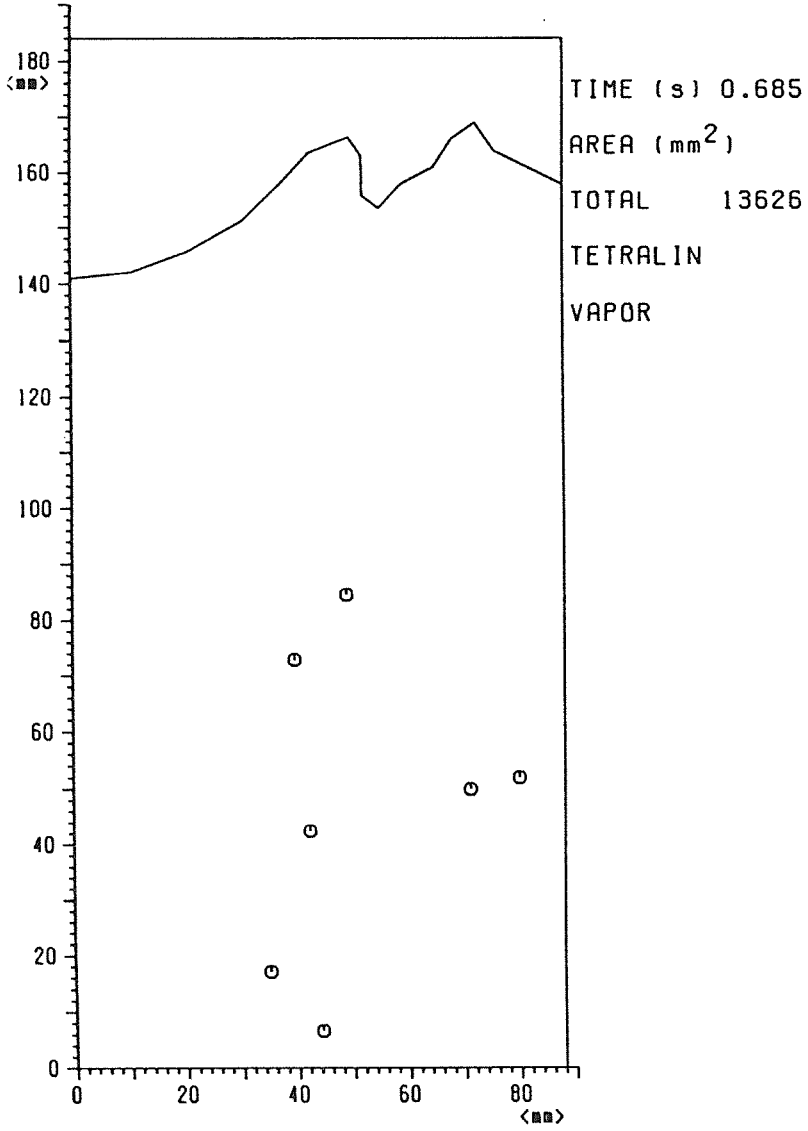

Fig.79 Interfaces MMB-34

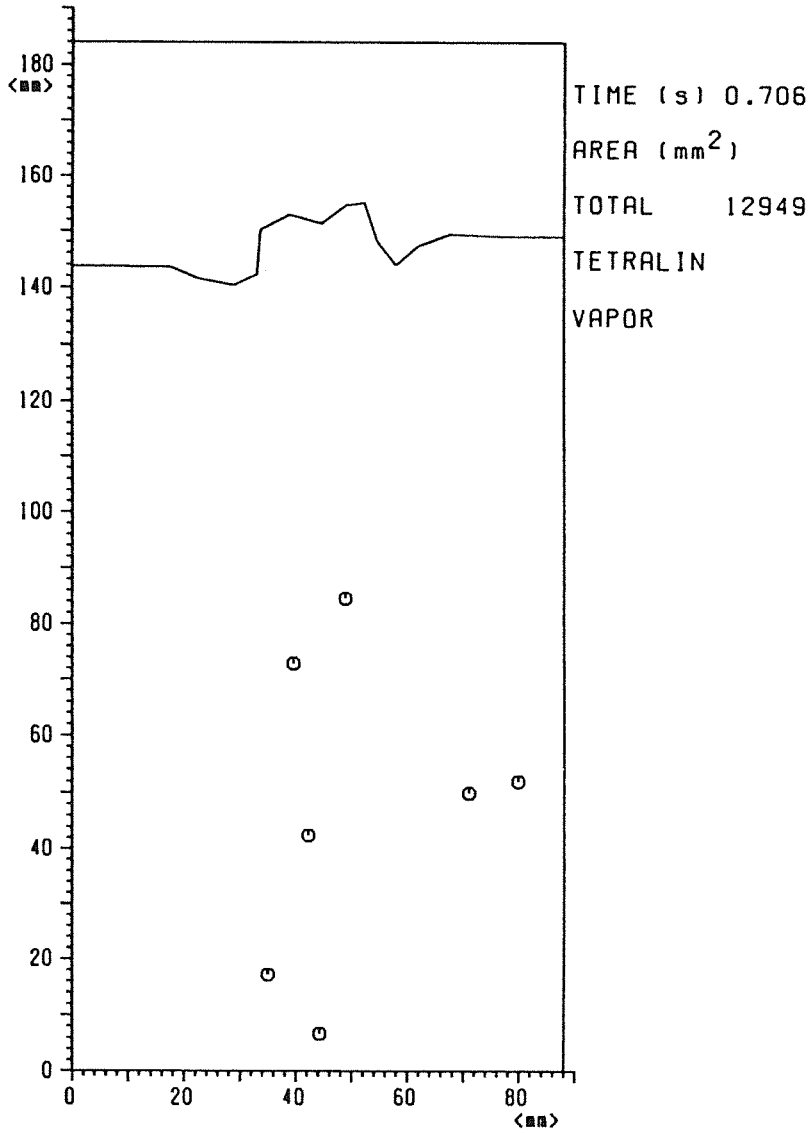

Fig.80 Interfaces MMB-34

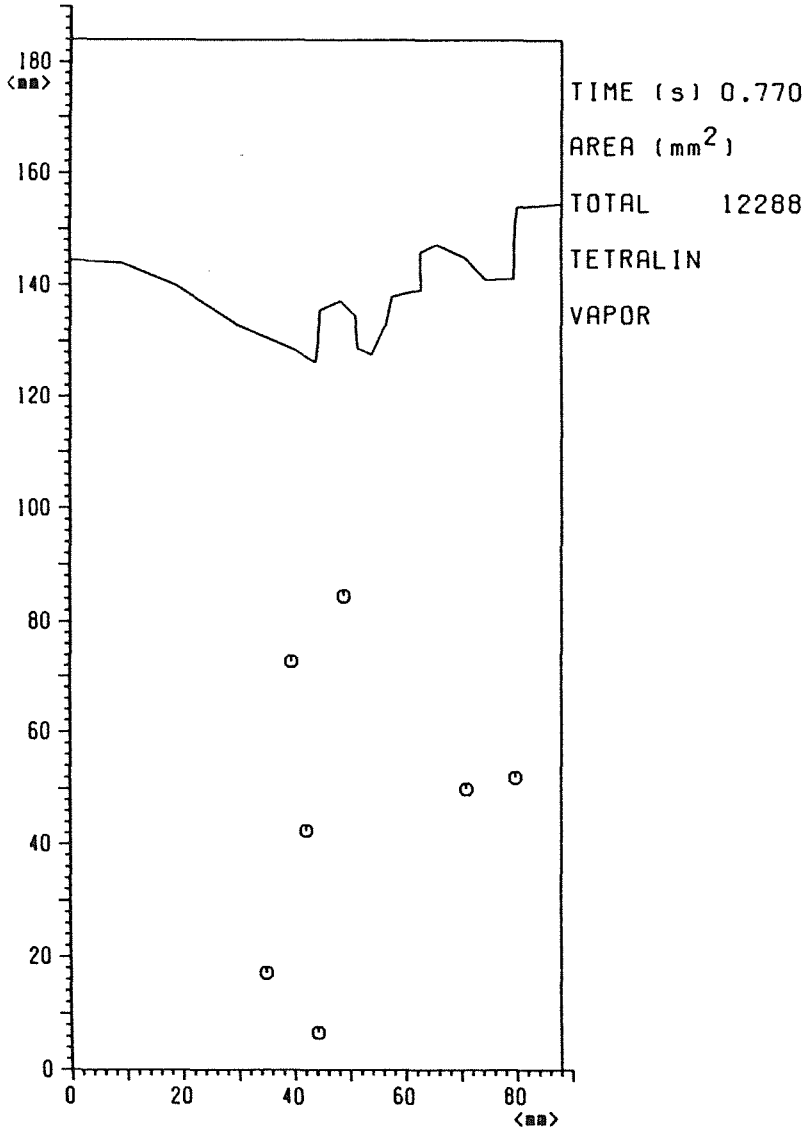

Fig.81 Interfaces MMB-34

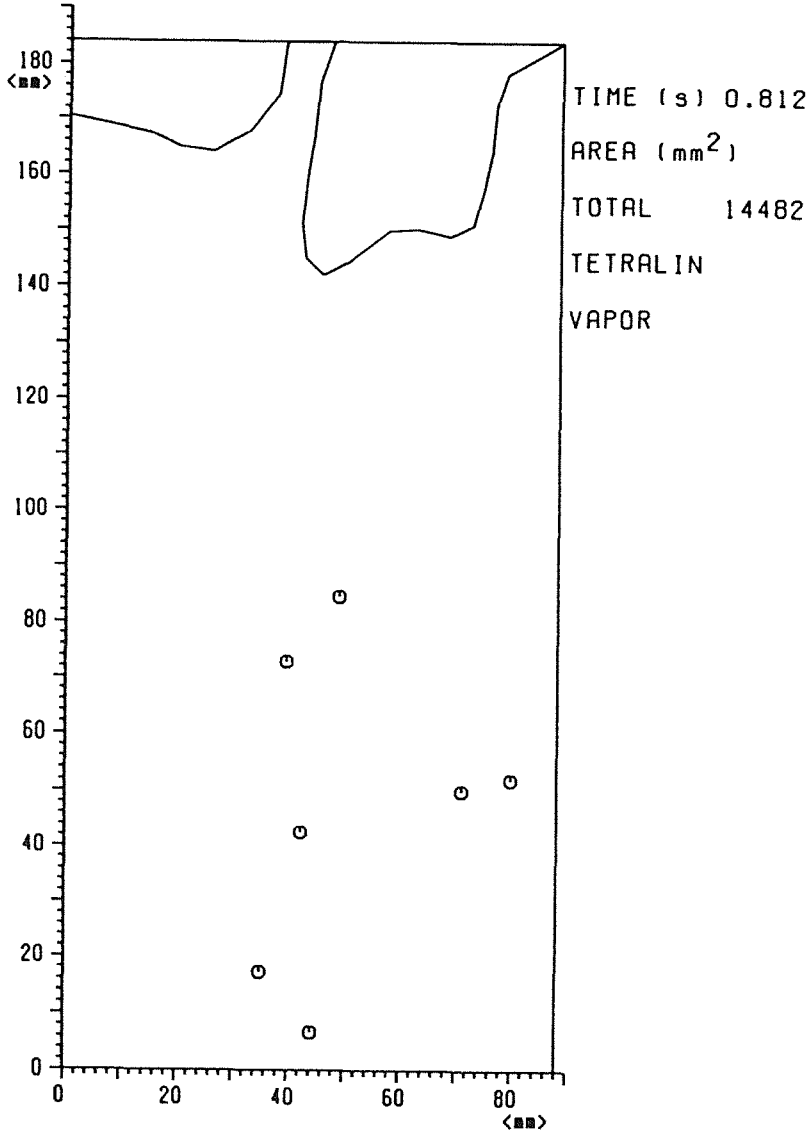

Fig.82 Interfaces MMB-34

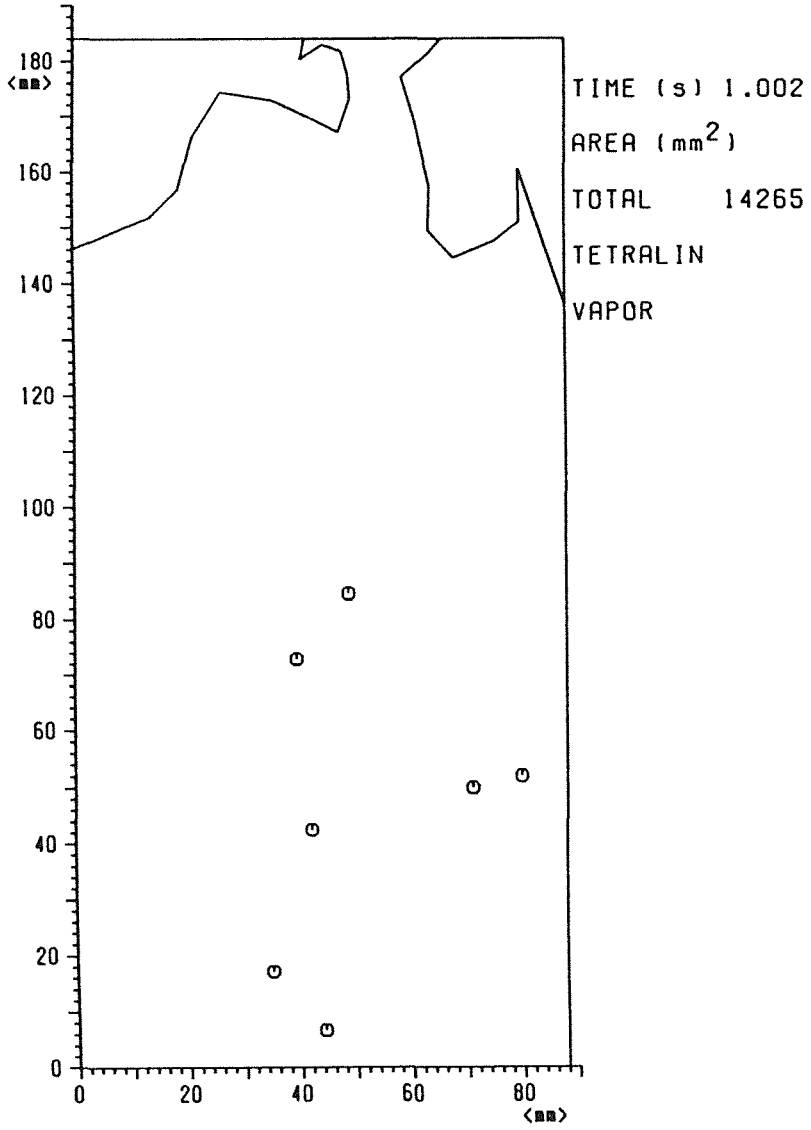

Fig.83 Interfaces MMB-34

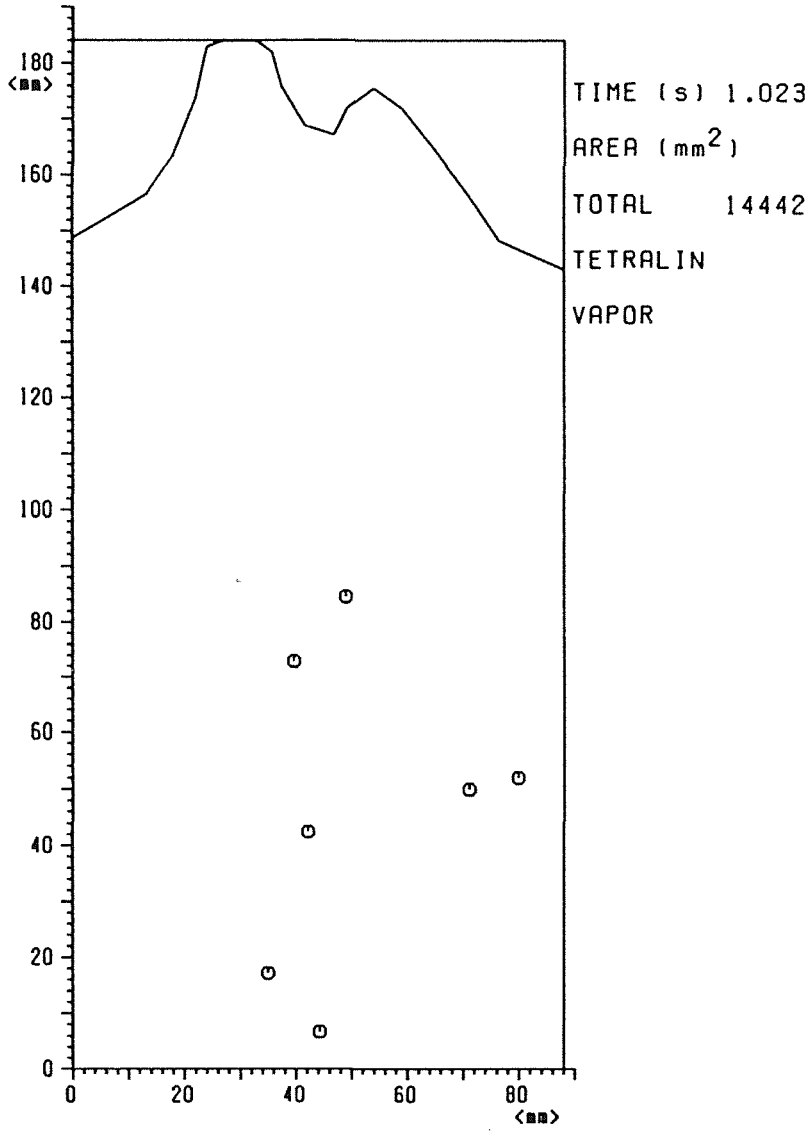

Fig.84 Interfaces MMB-34

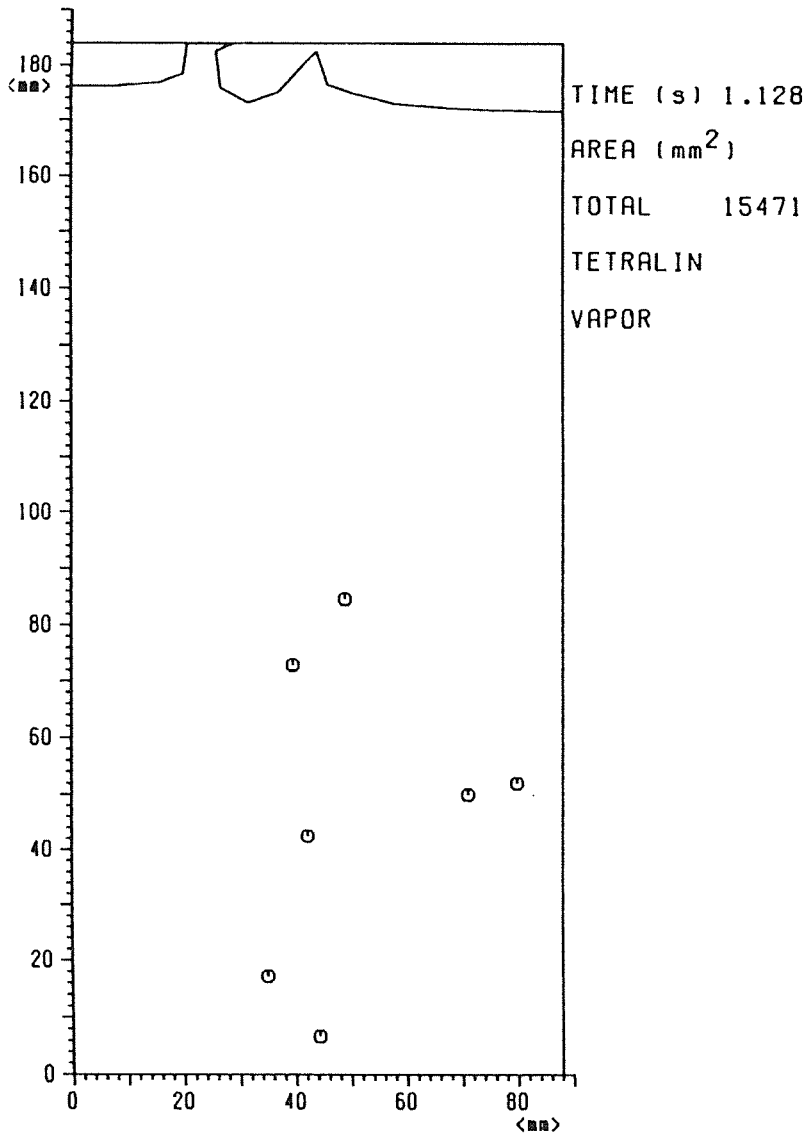

Fig.85 Interfaces MMB-34

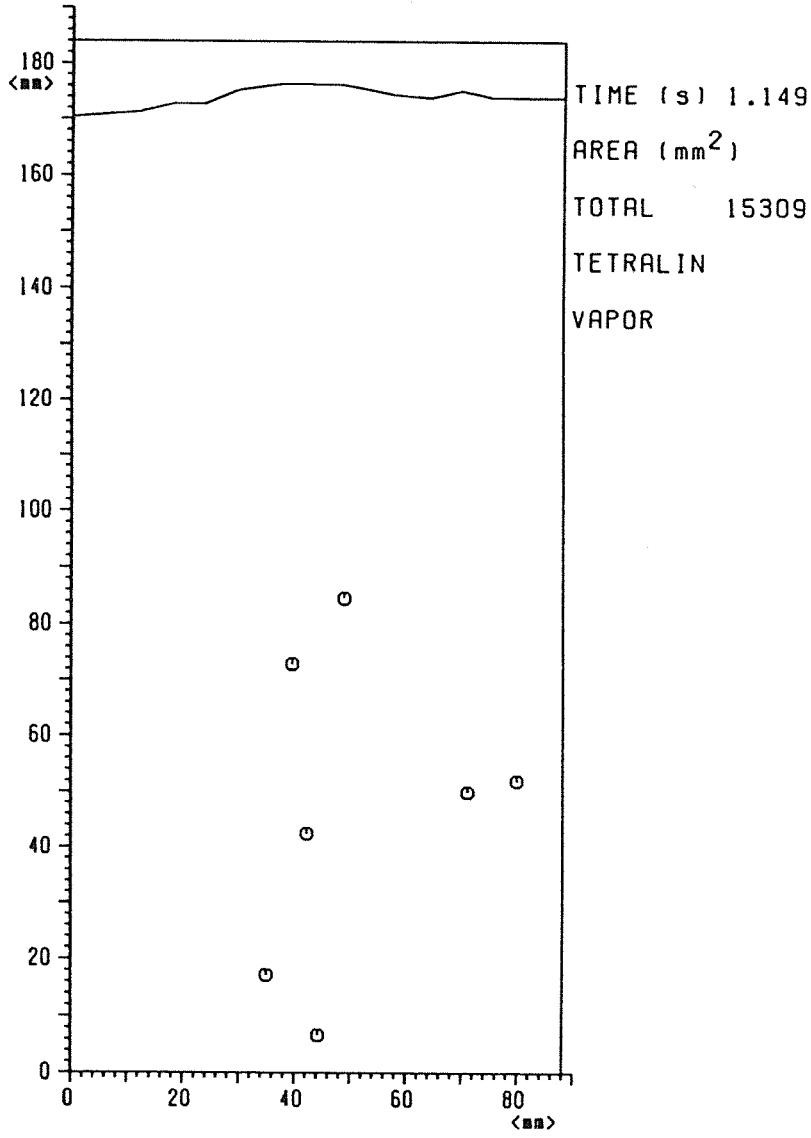

Fig.86 Interfaces MMB-34

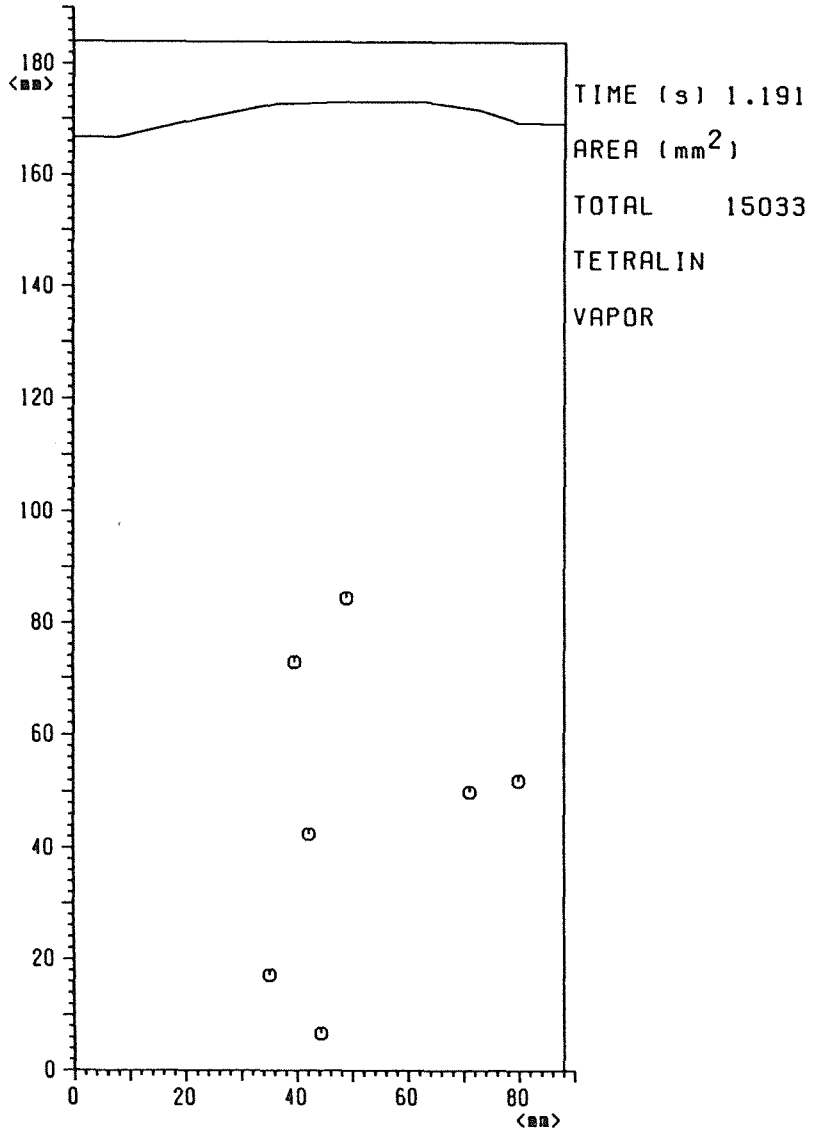

Fig.87 Interfaces MMB-34

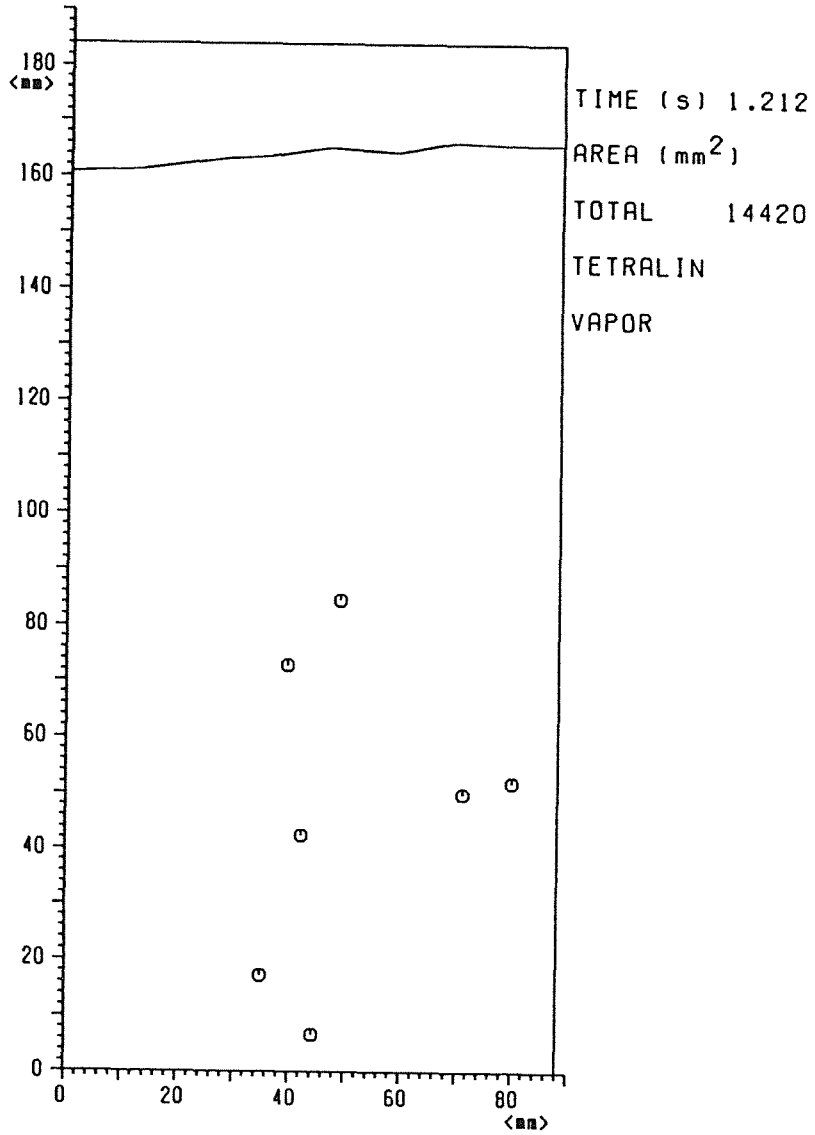

Fig.88 Interfaces MMB-34

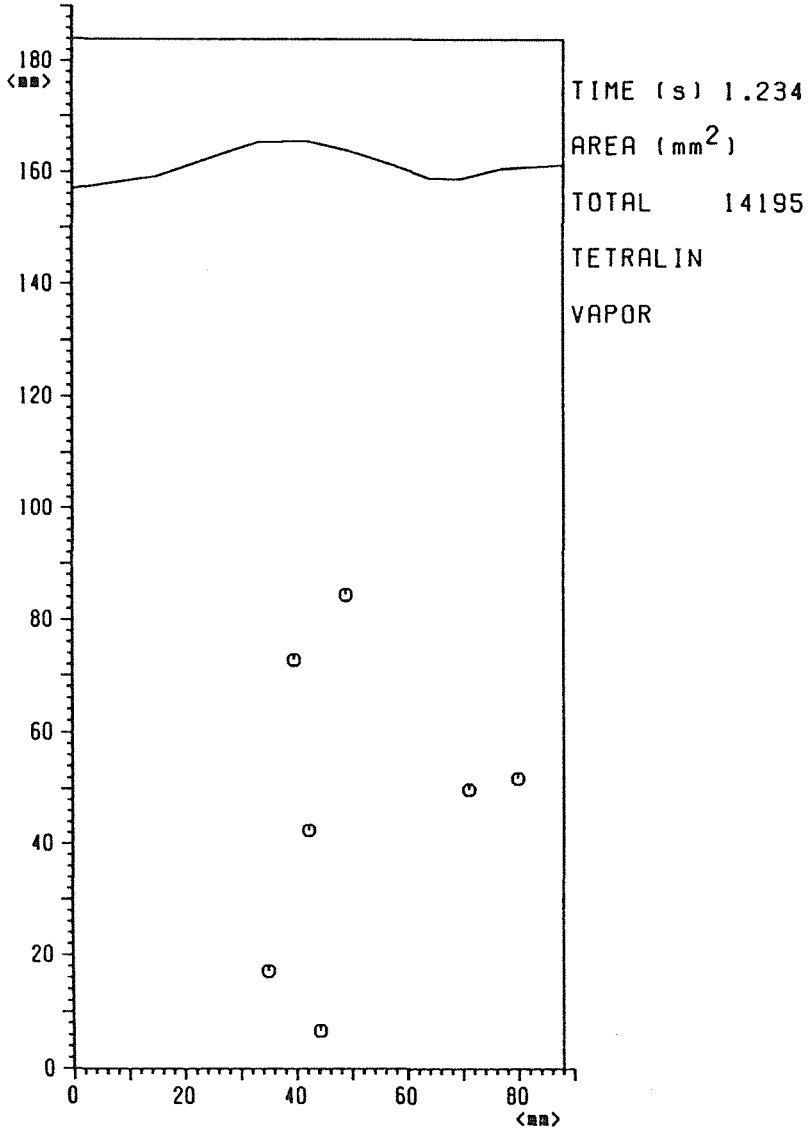

Fig.89 Interfaces MMB-34

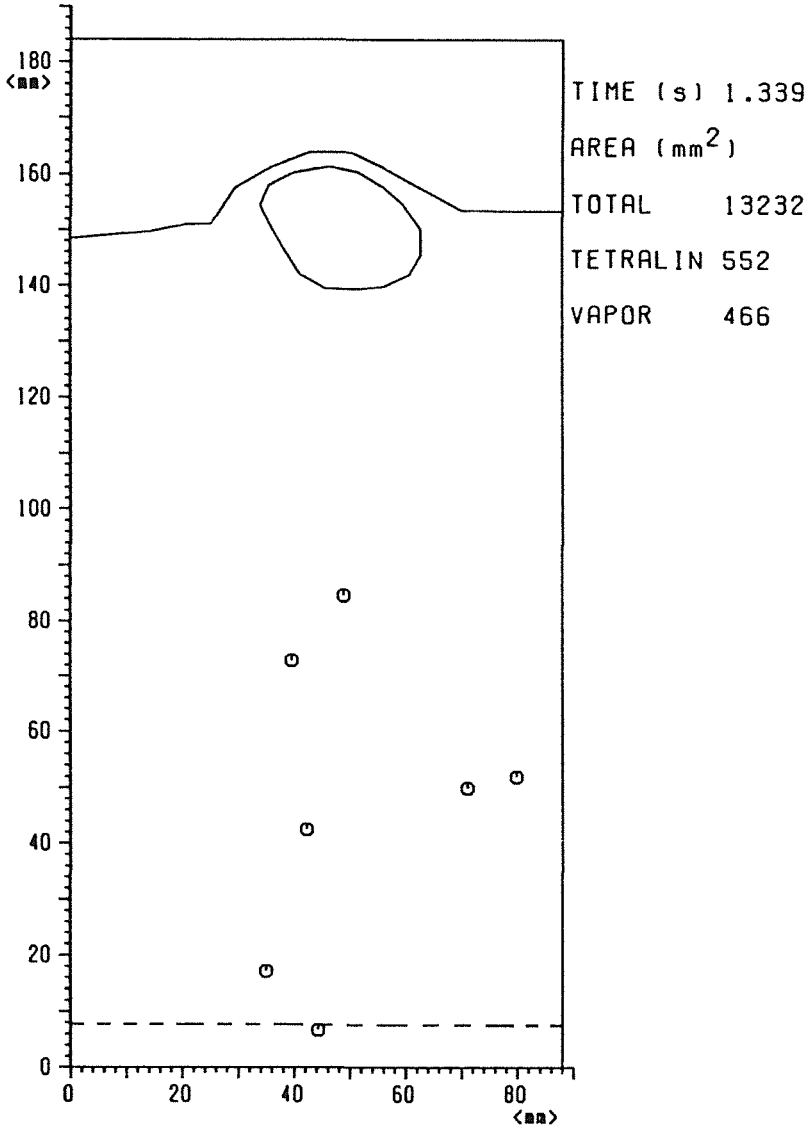

Fig.90 Interfaces MMB-34

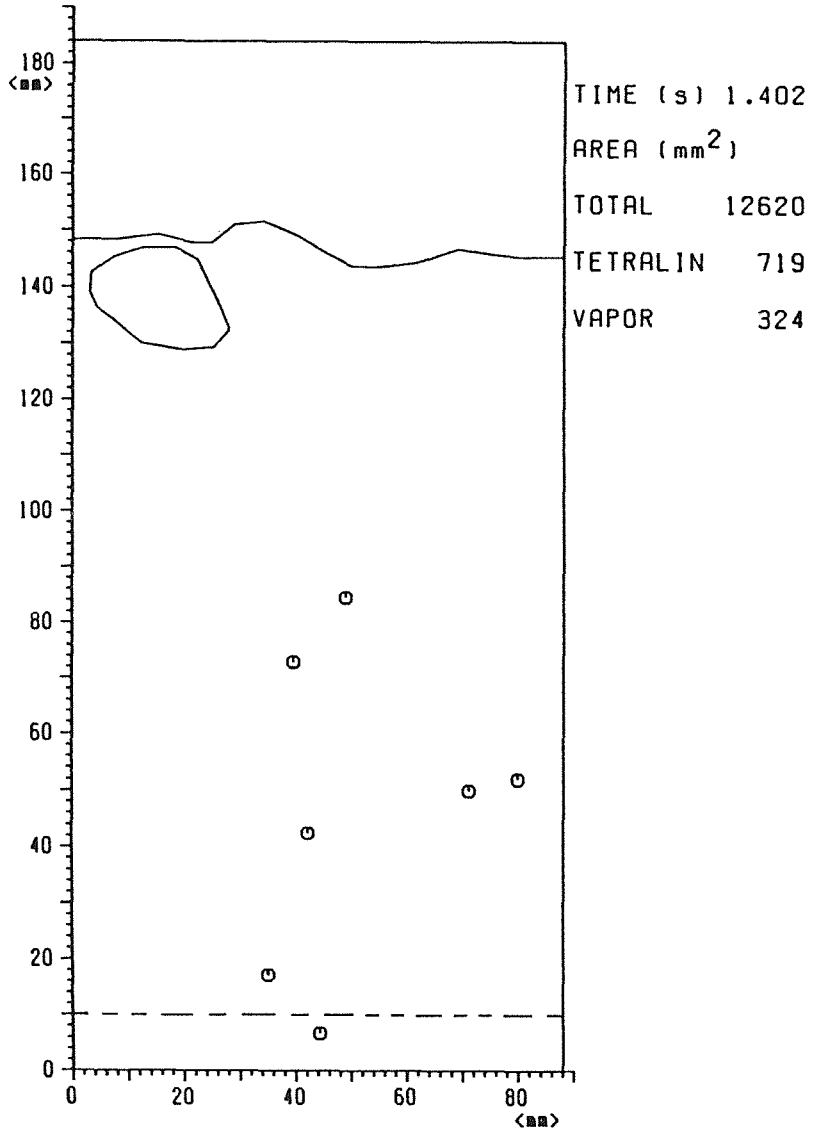

Fig.91 Interfaces MMB-34

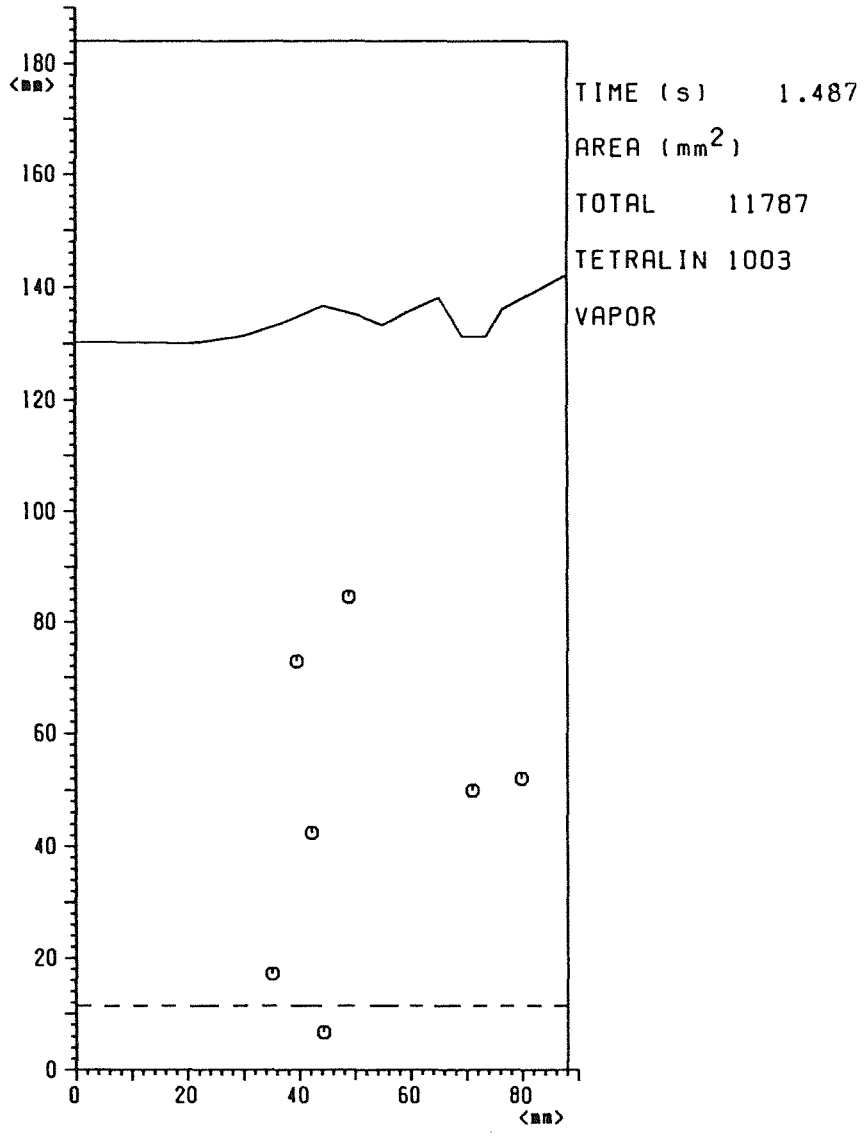

Fig.92 Interfaces MMB-34

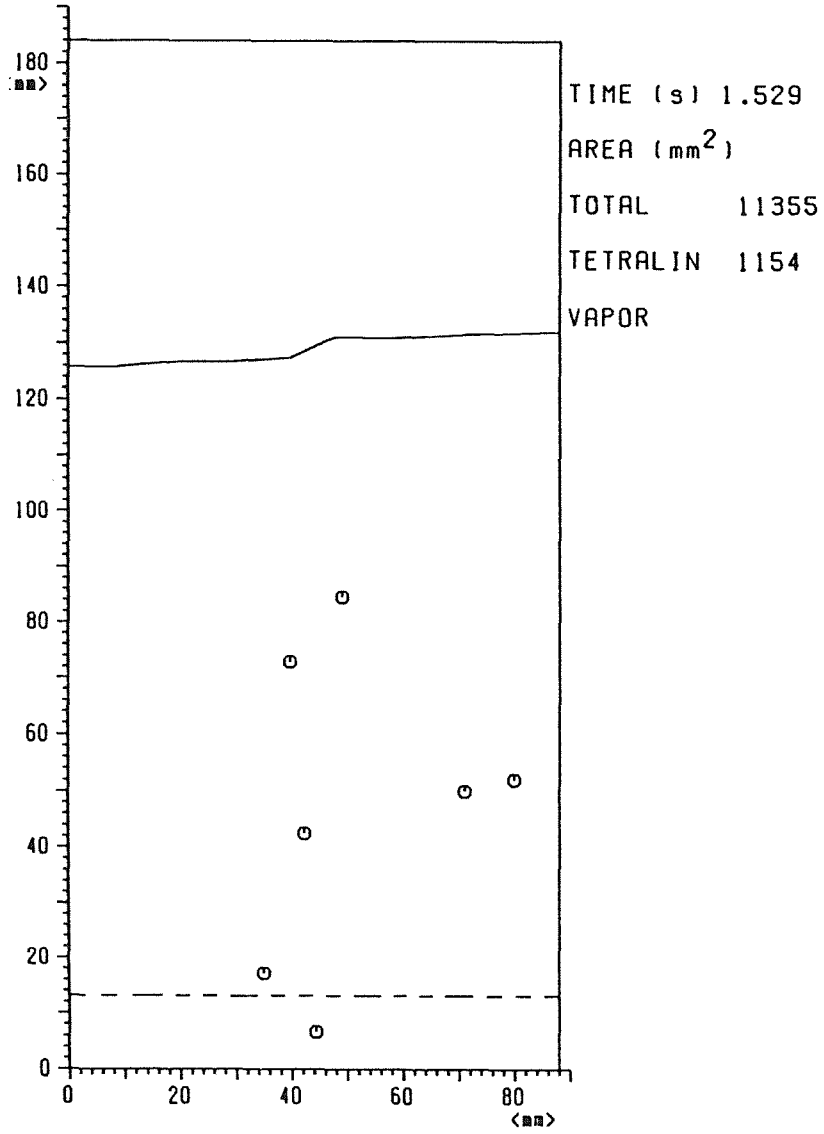

Fig.93 Interfaces MMB-34

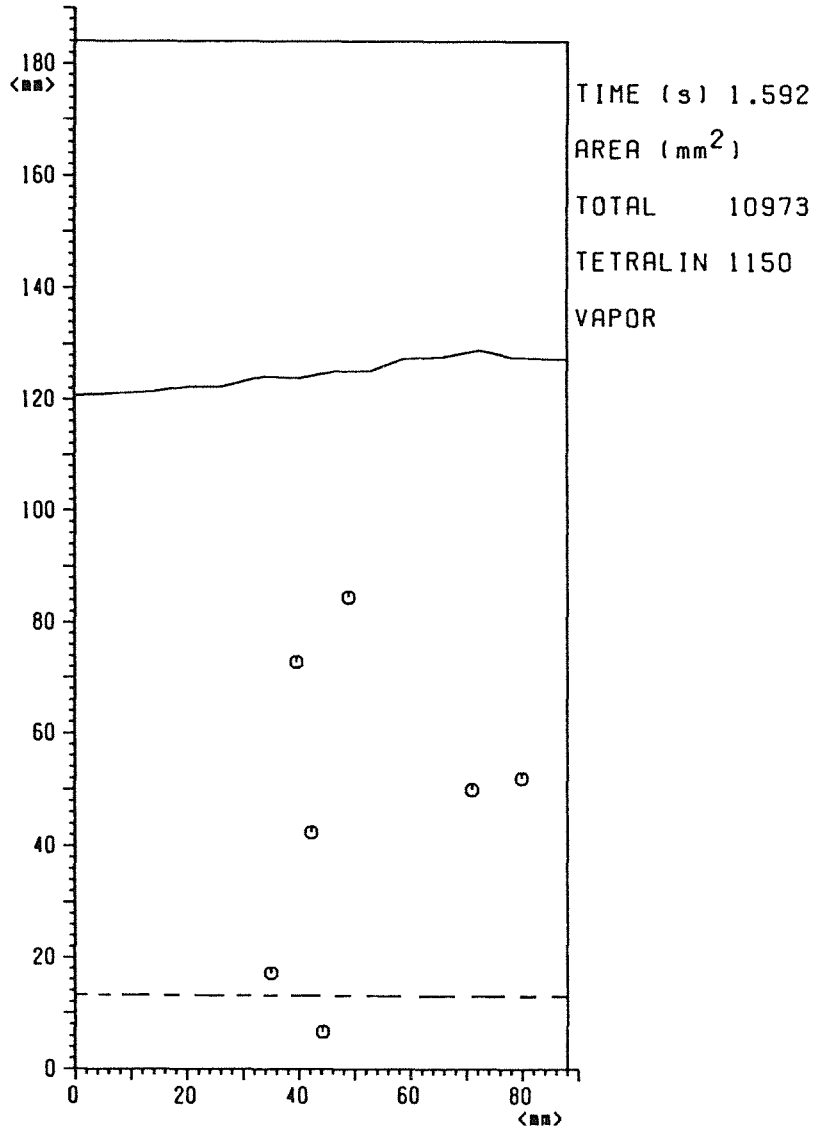

Fig.94 Interfaces MMB-34

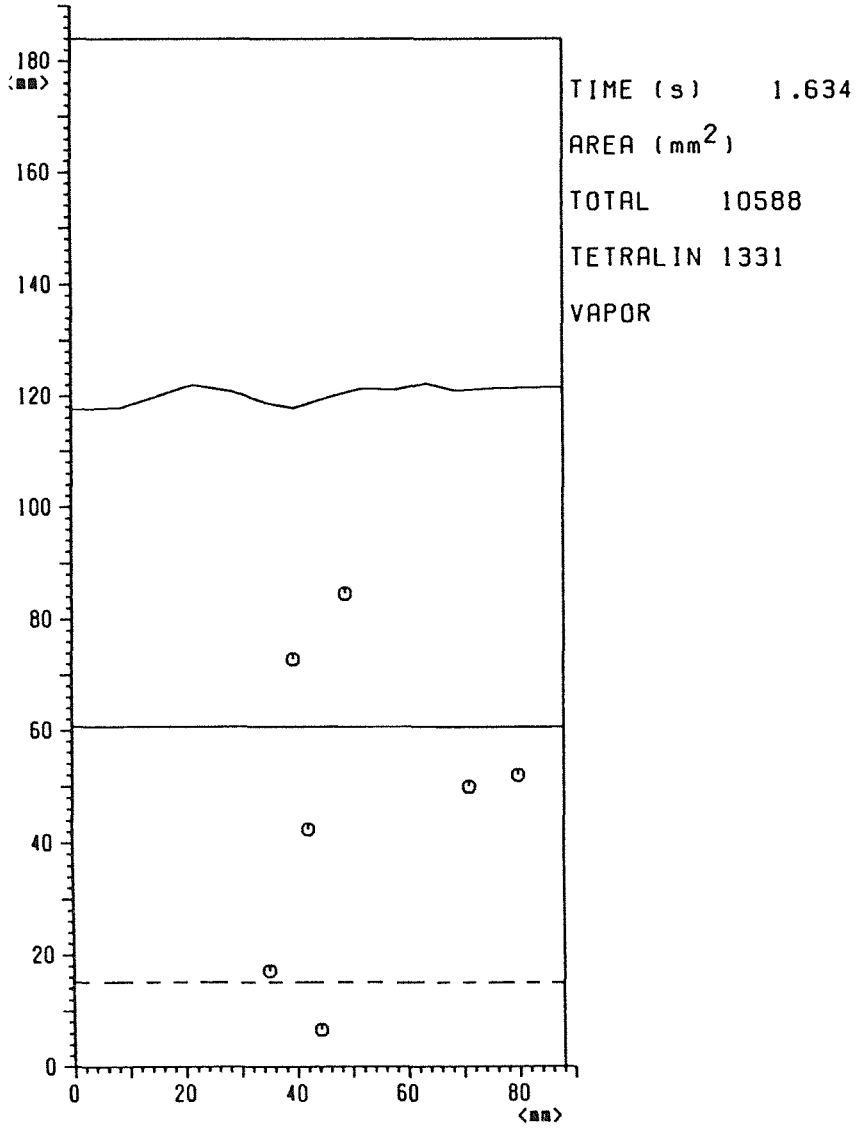

Fig.95 Interfaces MMB-34

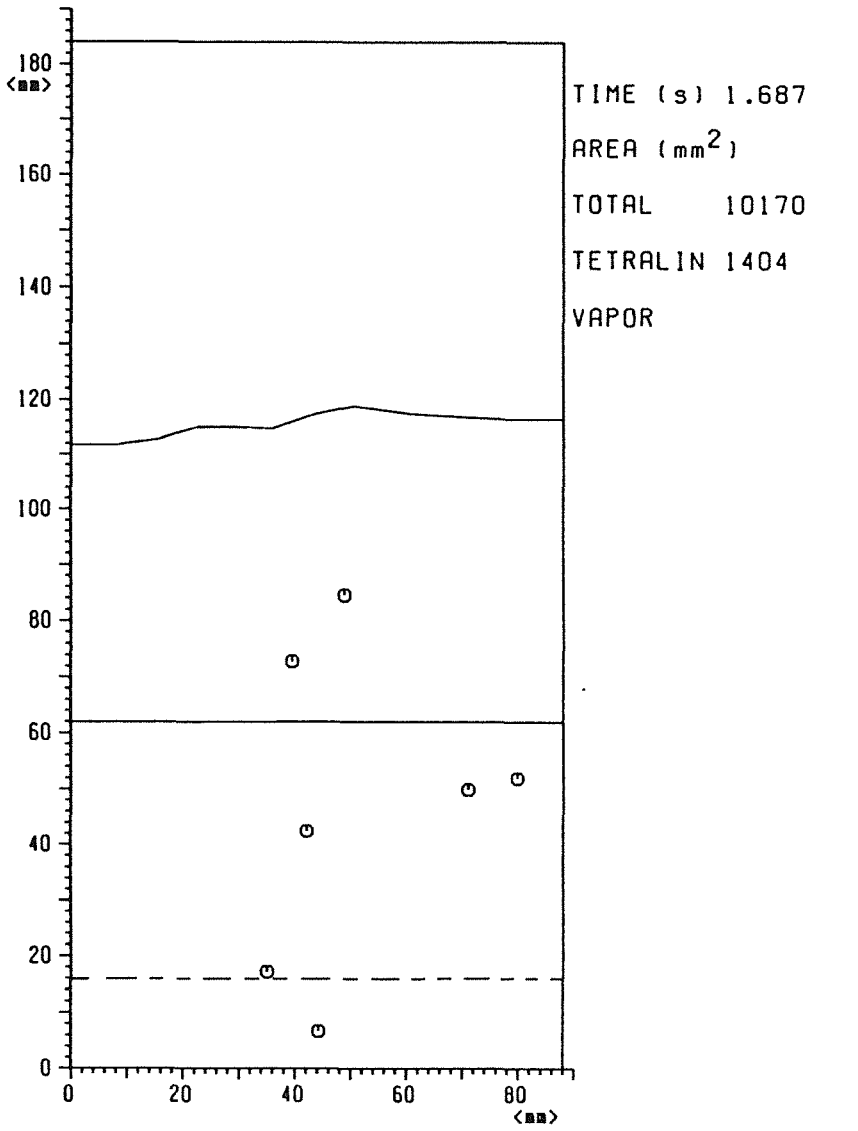

Fig.96 Interfaces MMB-34

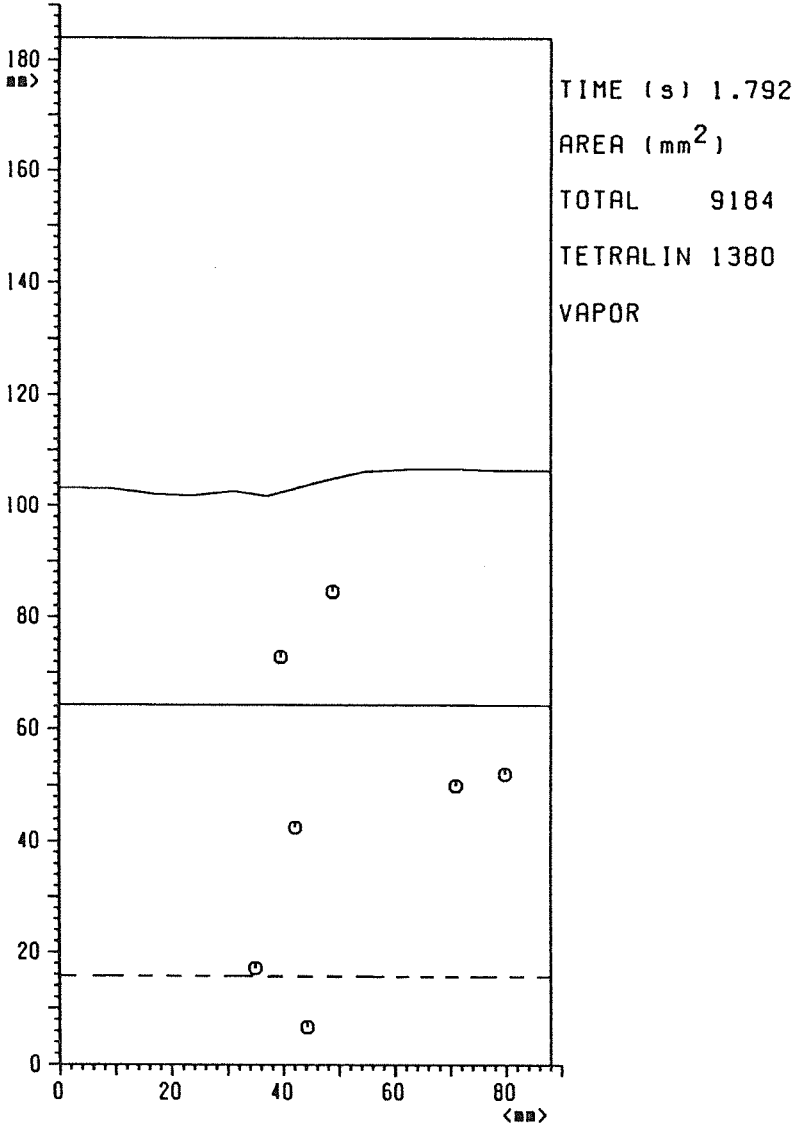

Fig.97 Interfaces MMB-34

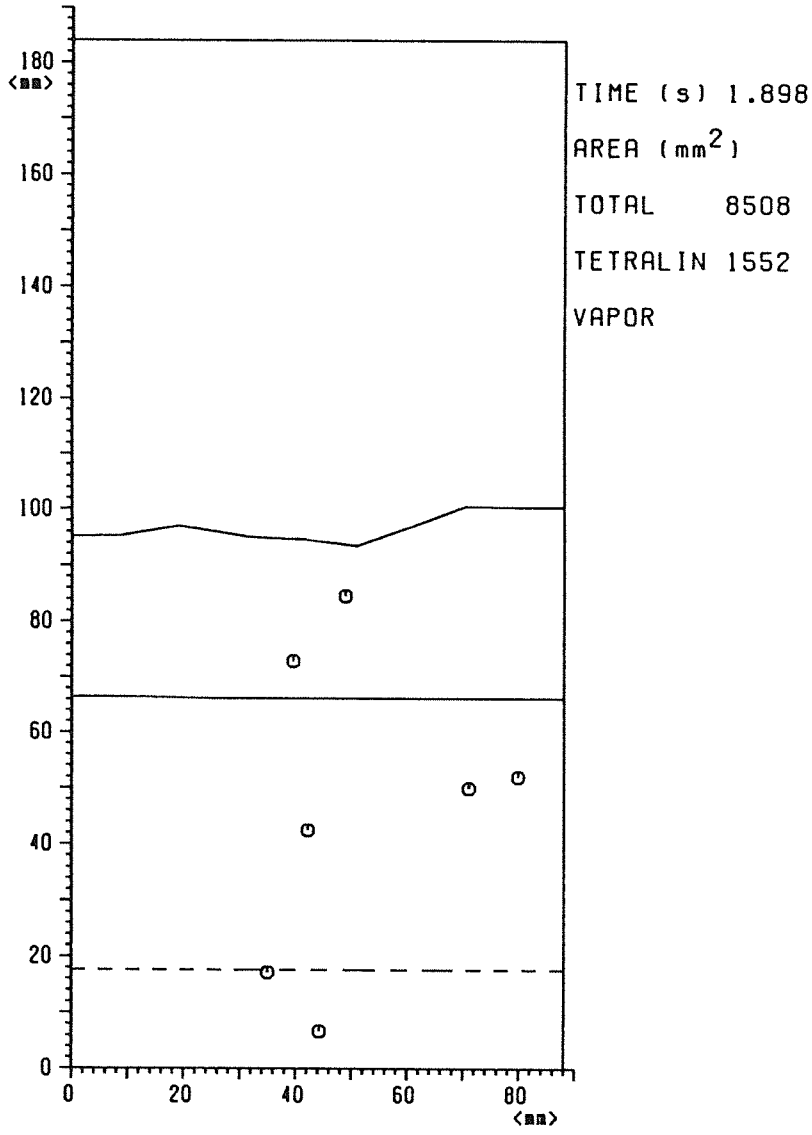

Fig.98 Interfaces MMB-34

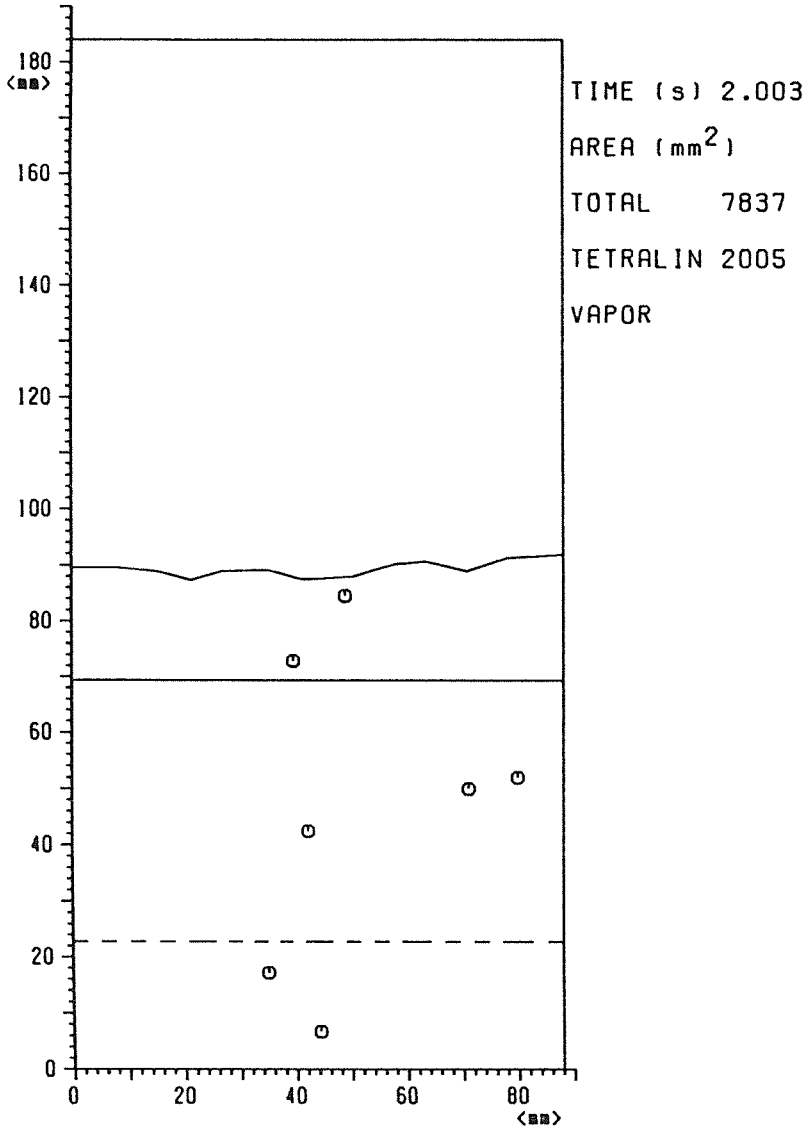

Fig.99 Interfaces MMB-34

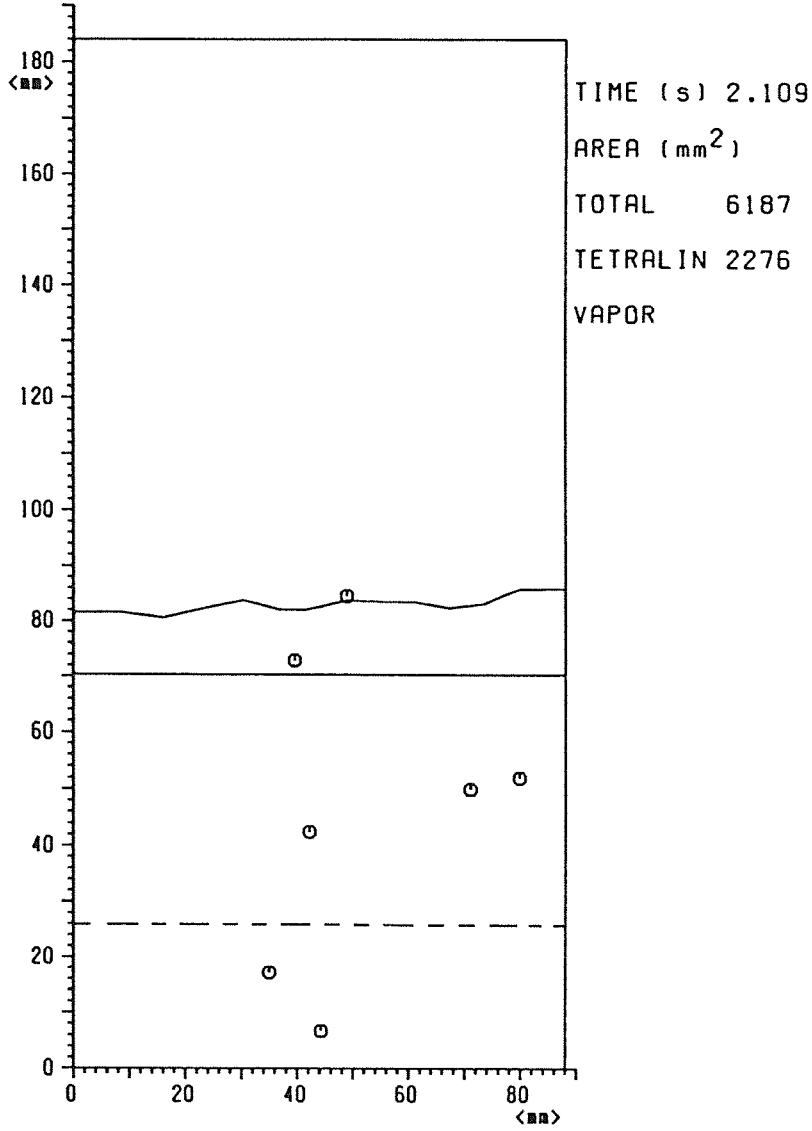

Fig.100 Interfaces MMB-34

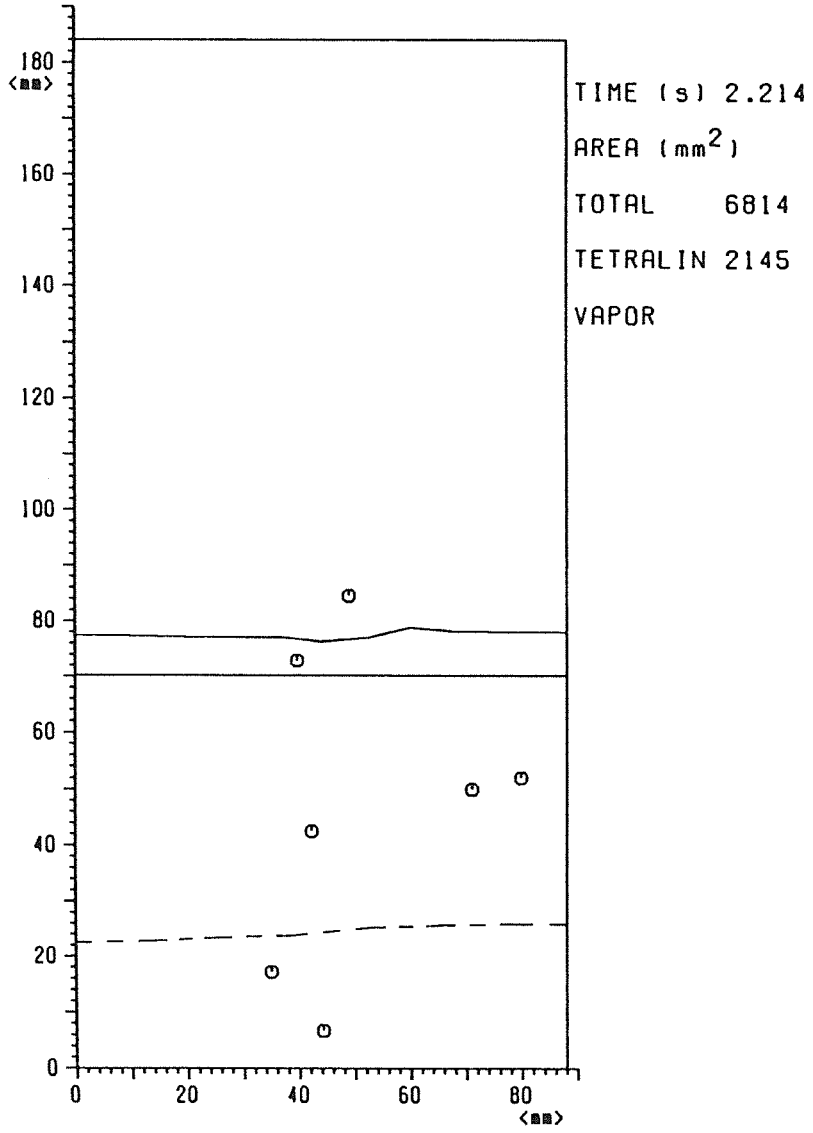

Fig.101 Interfaces MMB-34

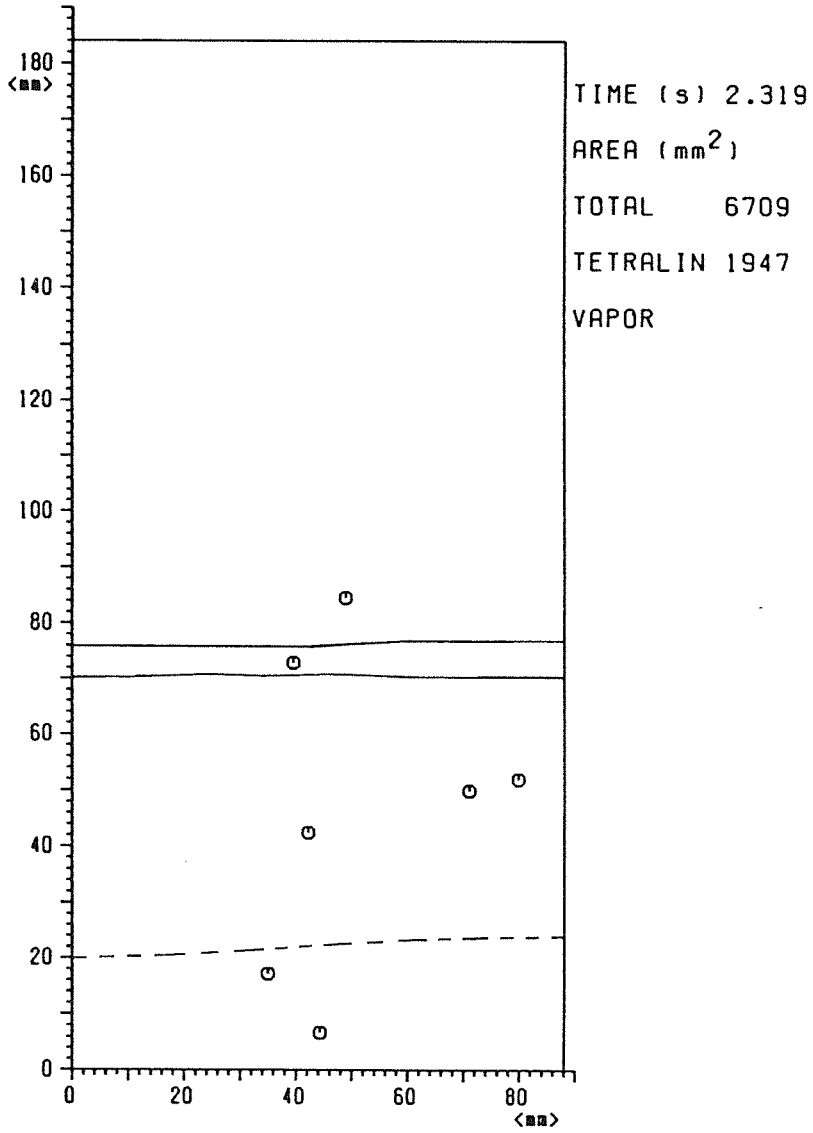

Fig.102 Interfaces MMB-34

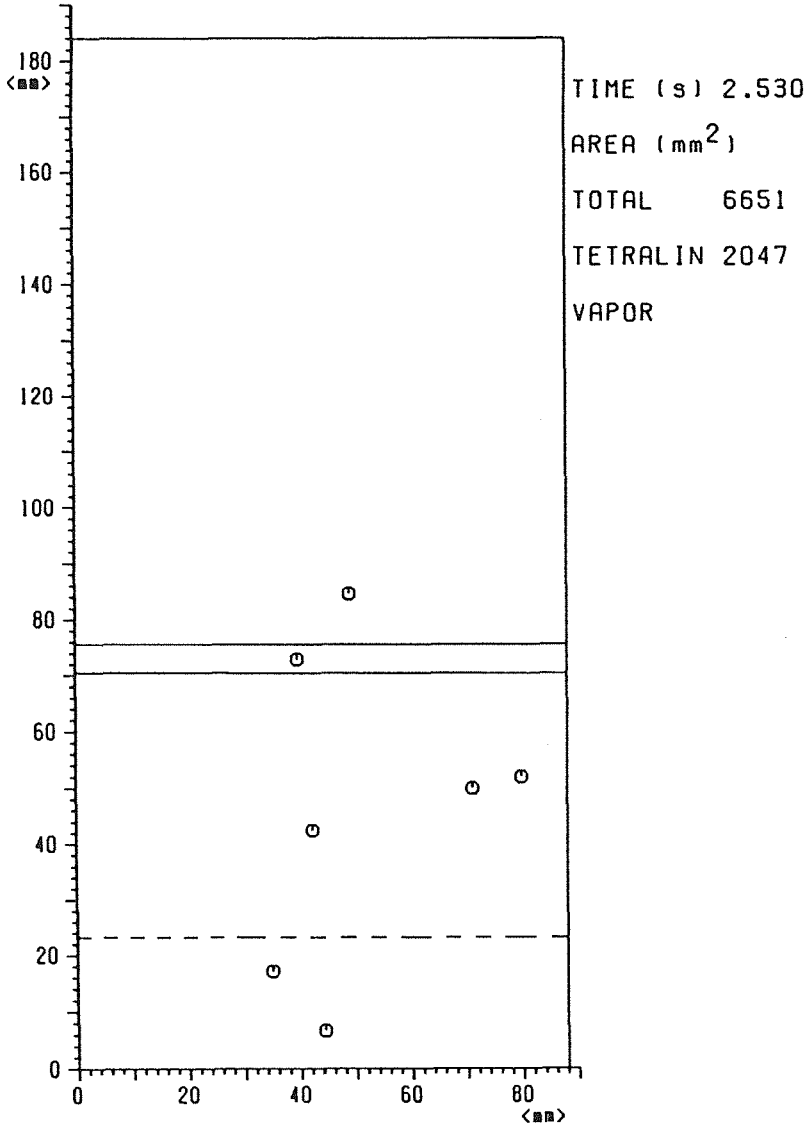

Fig.103 Interfaces MMB-34

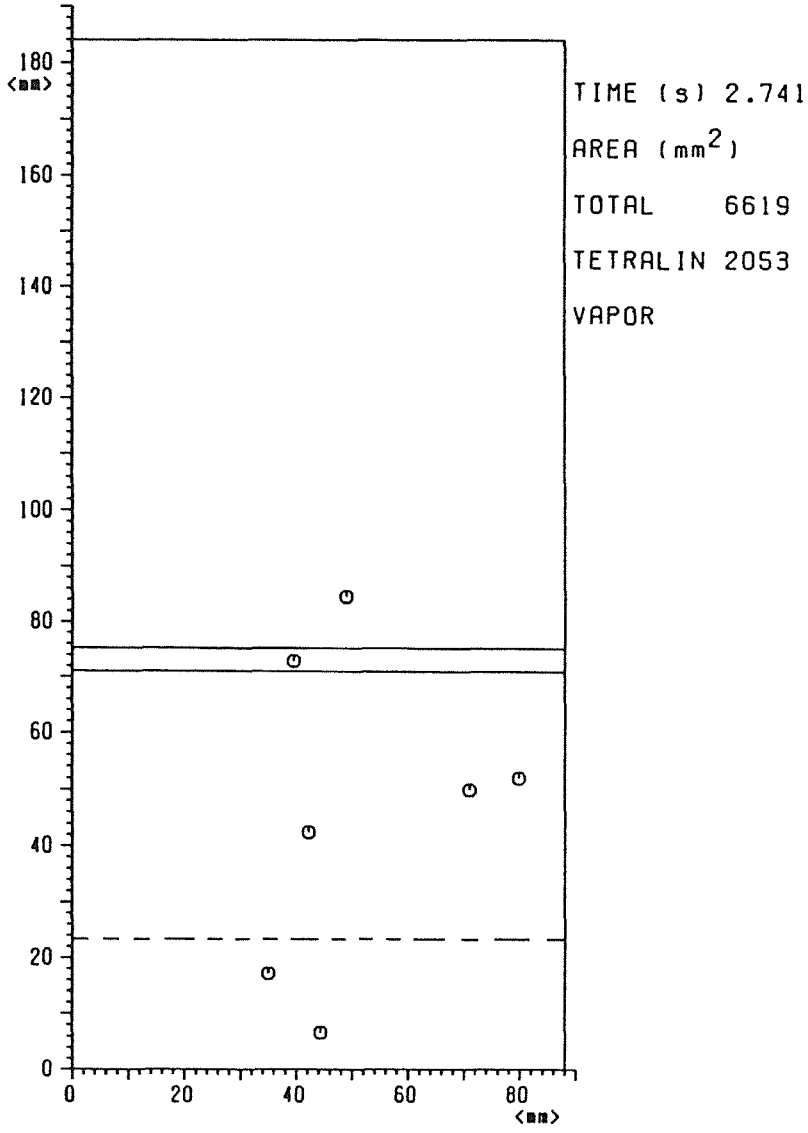

Fig.104 Interfaces MMB-34

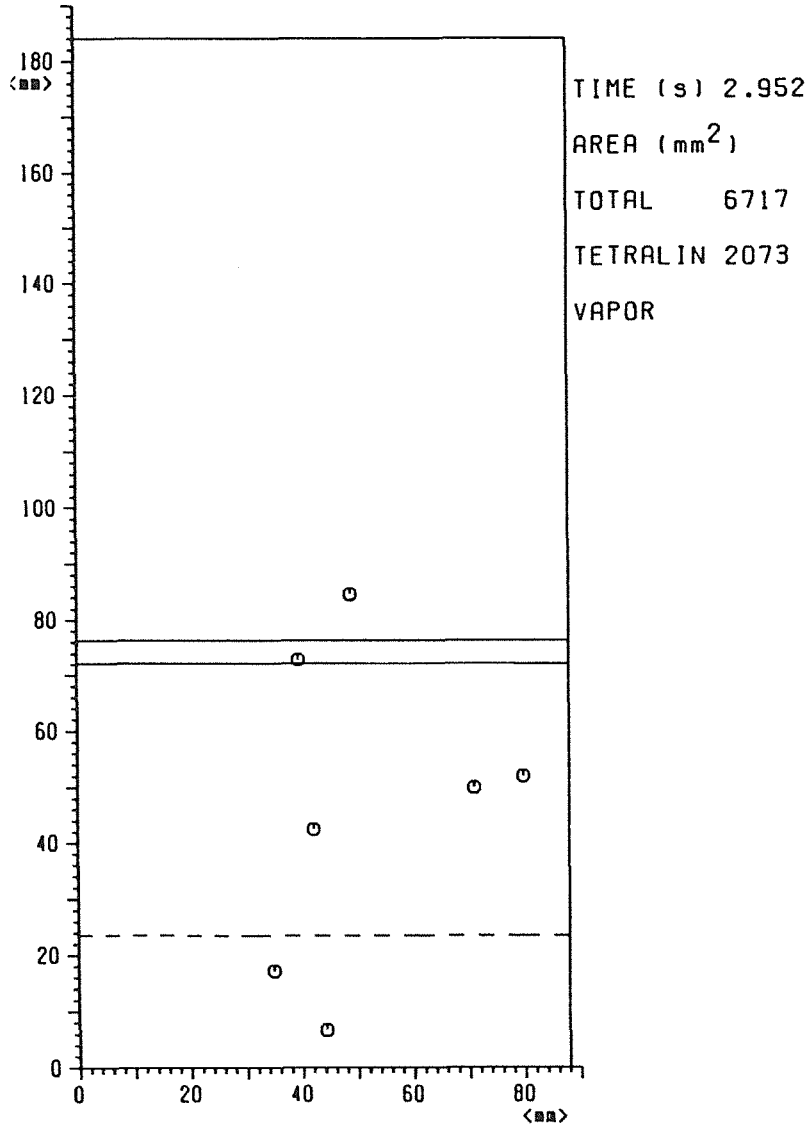

Fig.105 Interfaces MMB-34

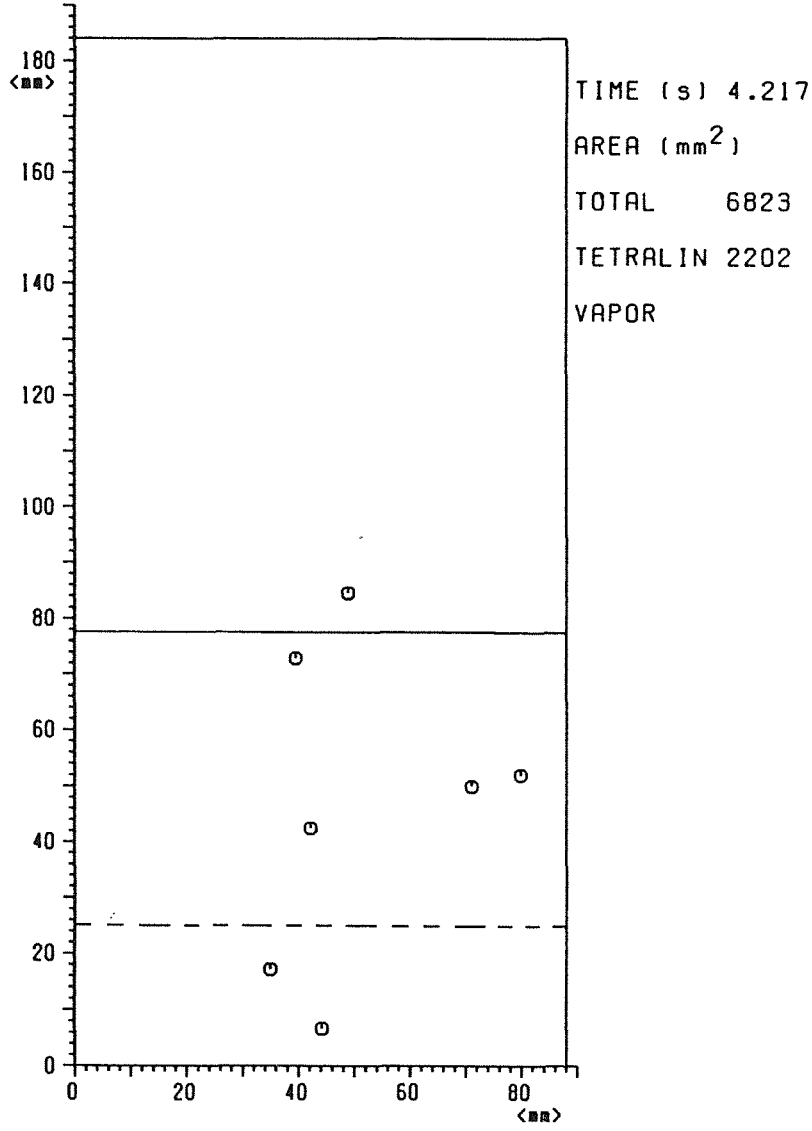

Fig.106 Interfaces MMB-34

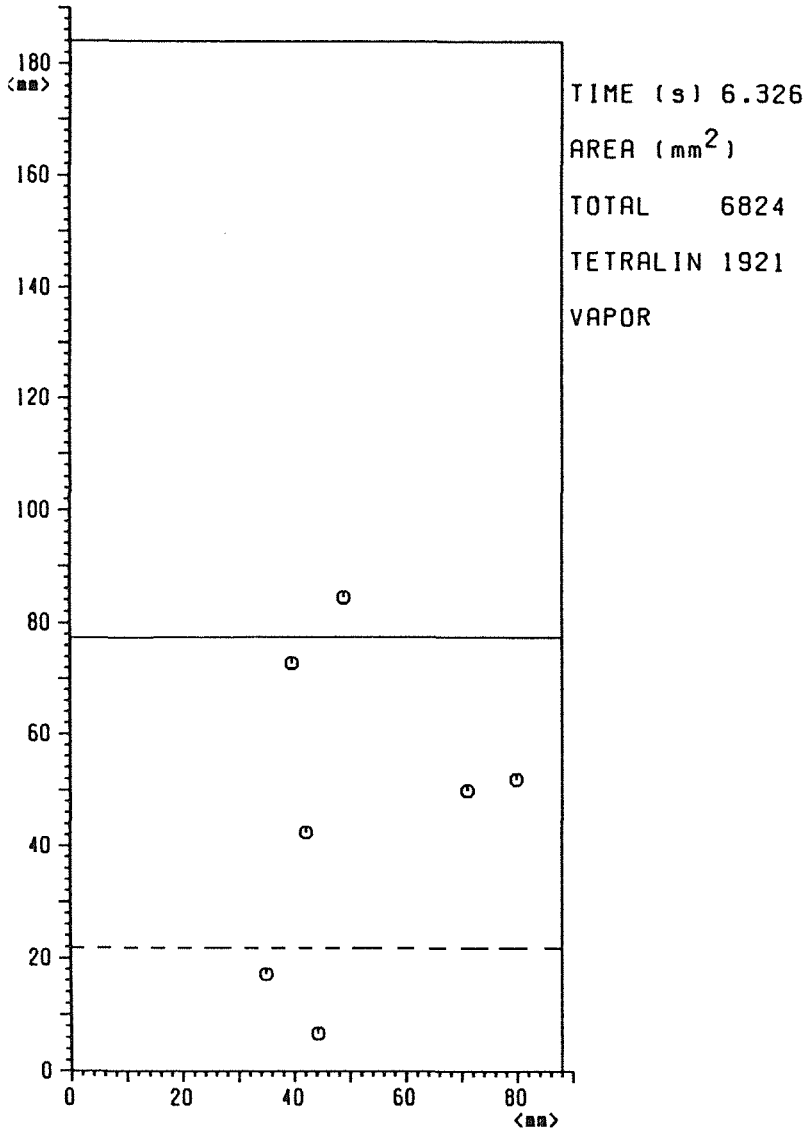

Fig.107 Interfaces MMB-34

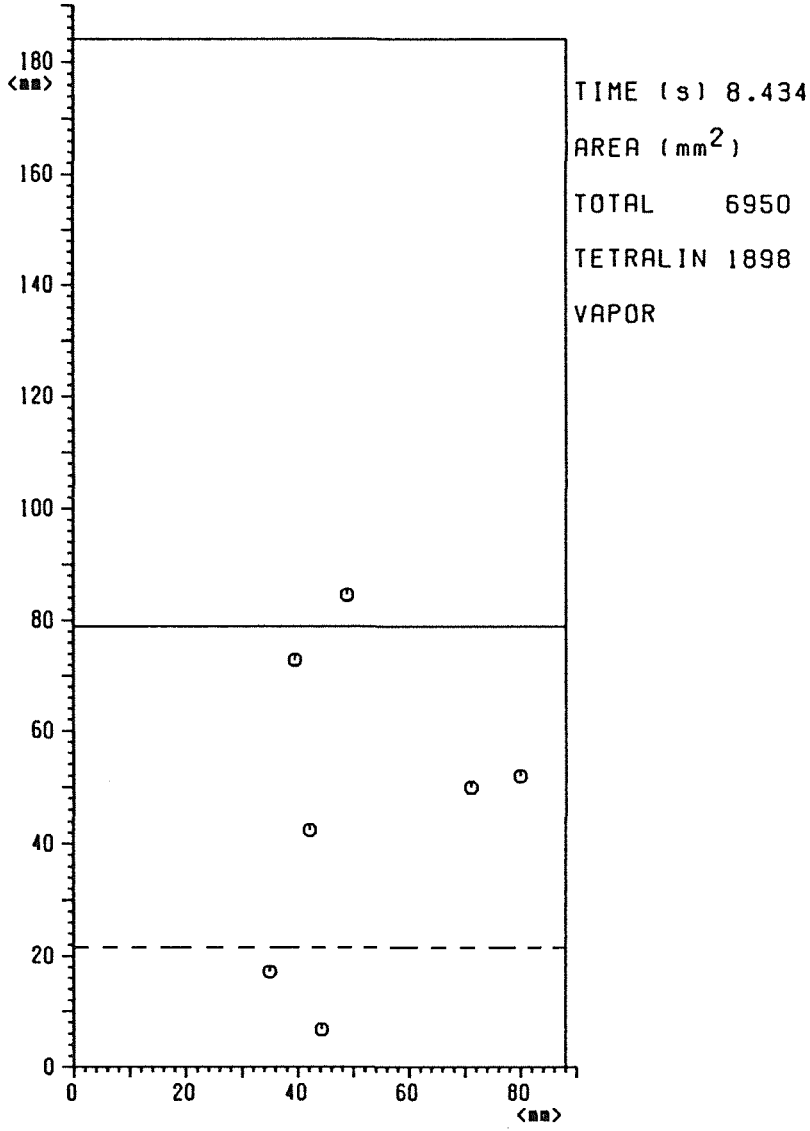

Fig.108 Interfaces MMB-34

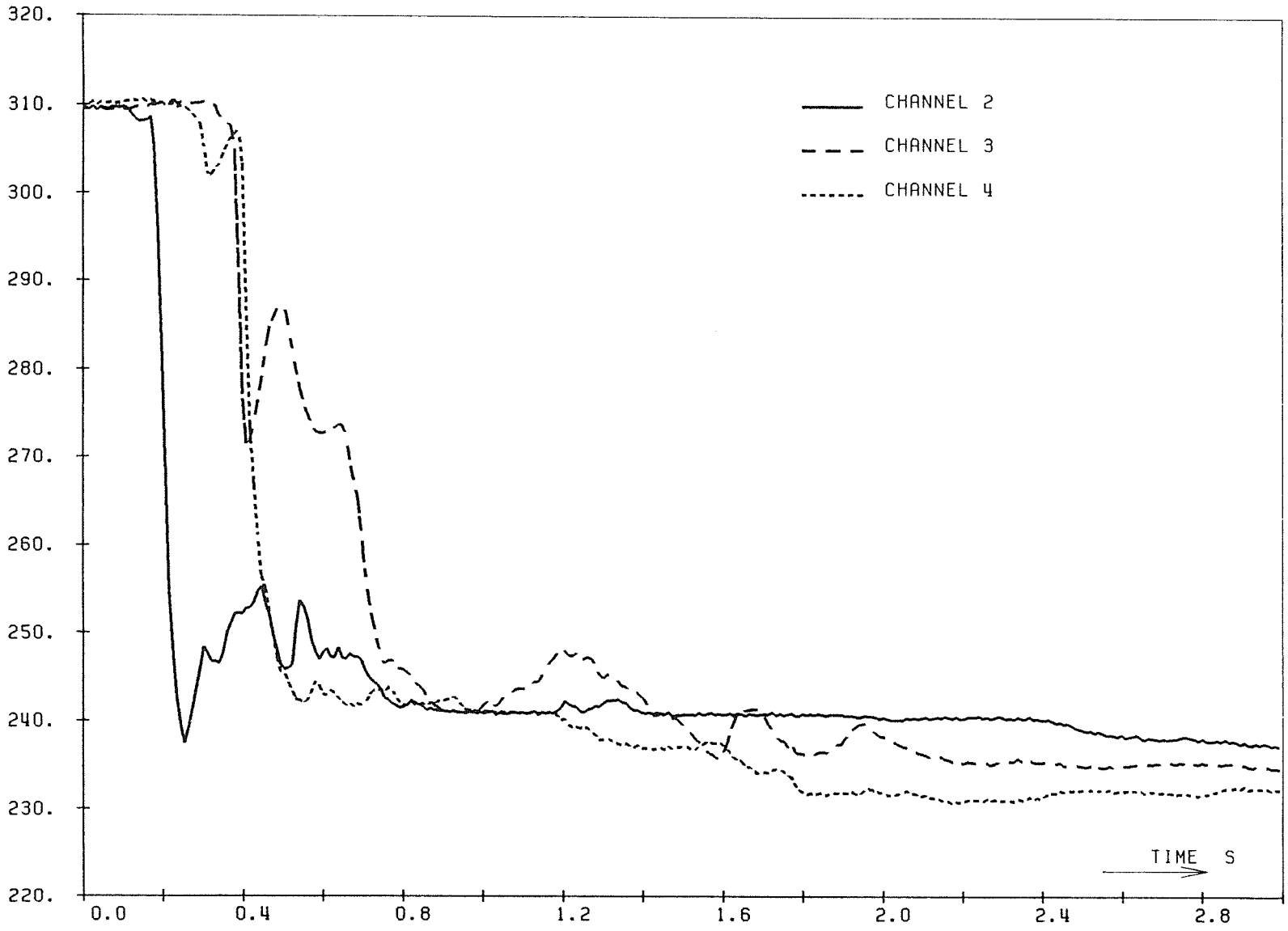

Fig.109 MMB-34 Temperatures (K) Versus Time

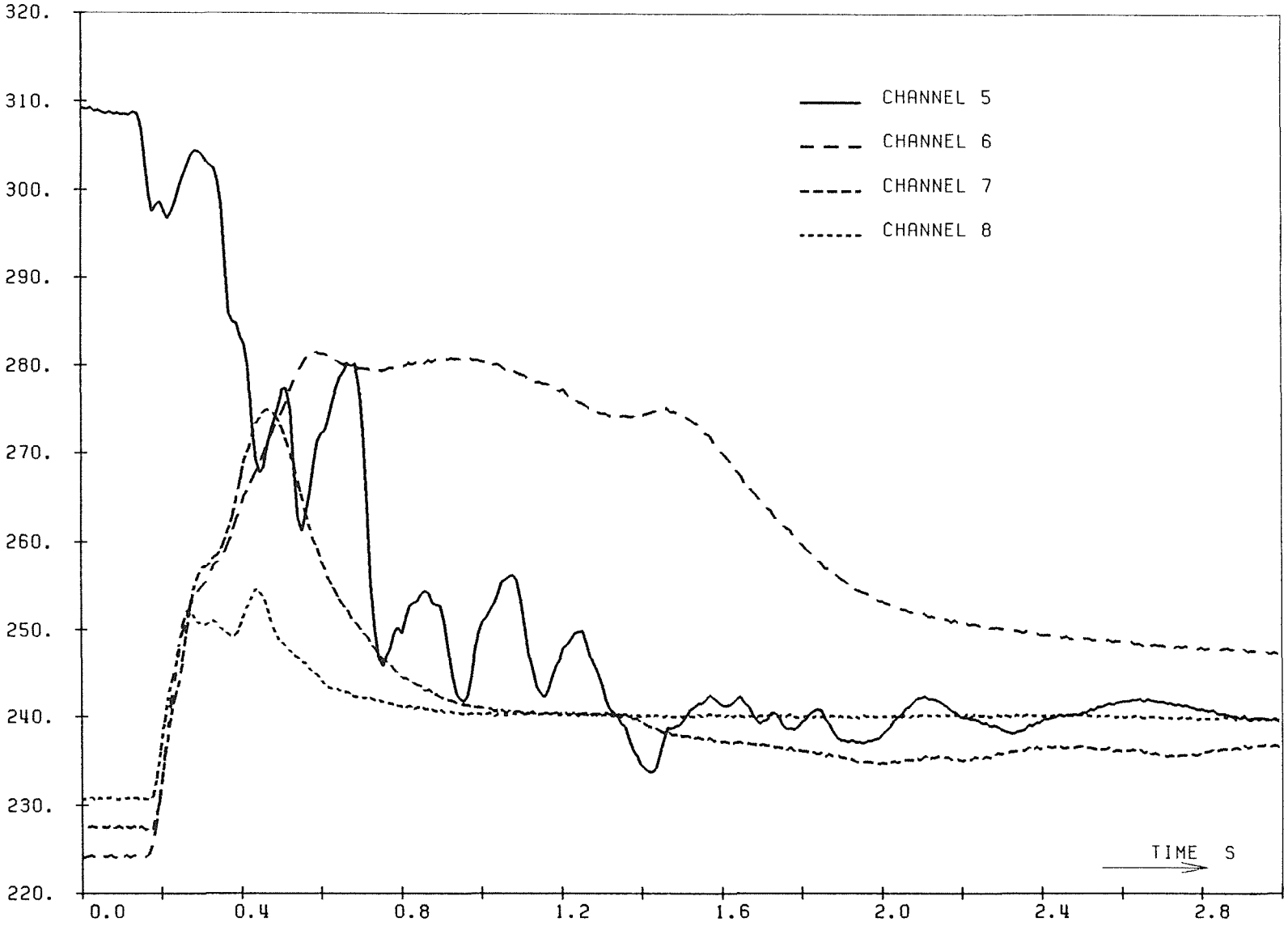

Fig.110 MMB-34 Temperatures (K) Versus Time

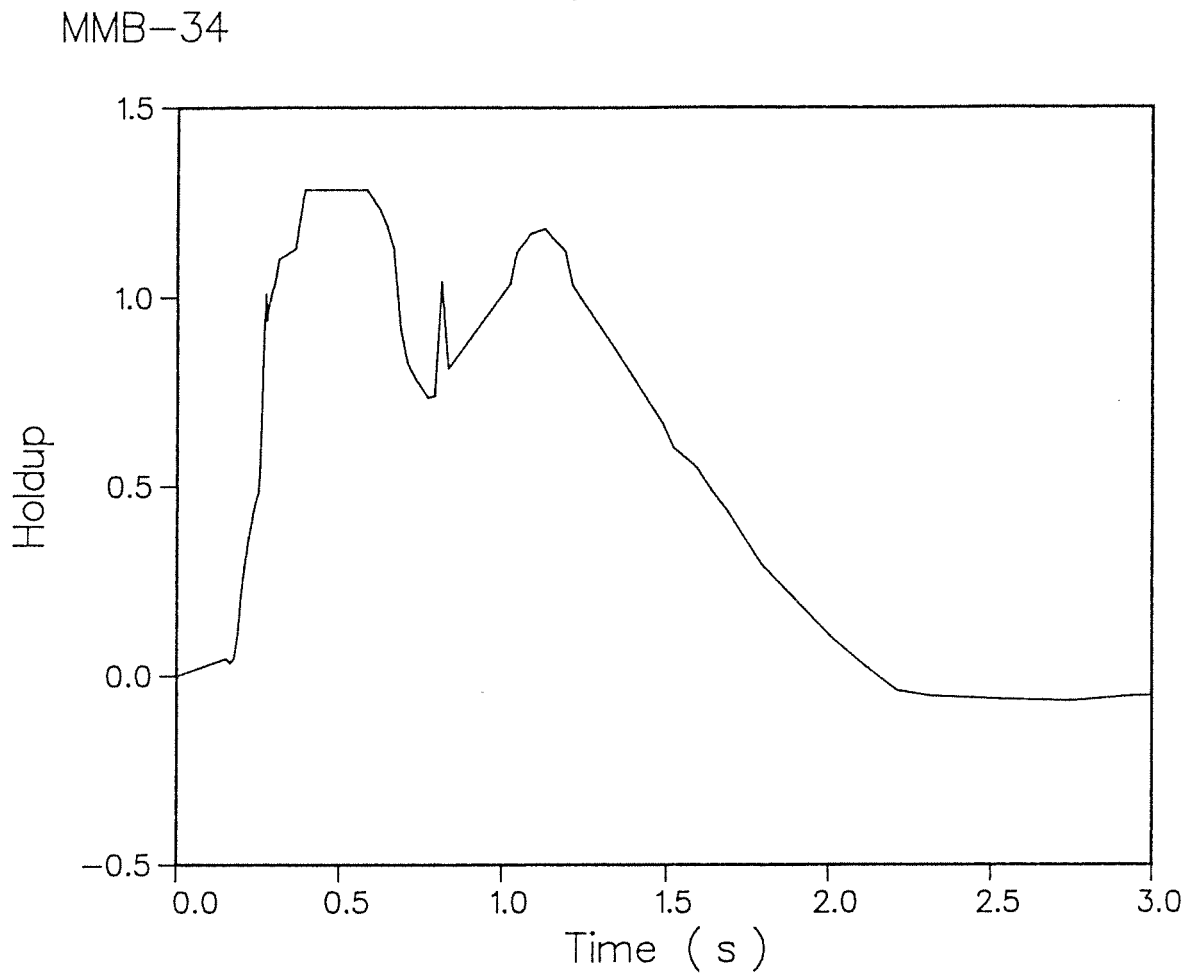

Fig.111 MMB-34 Holdup Versus Time

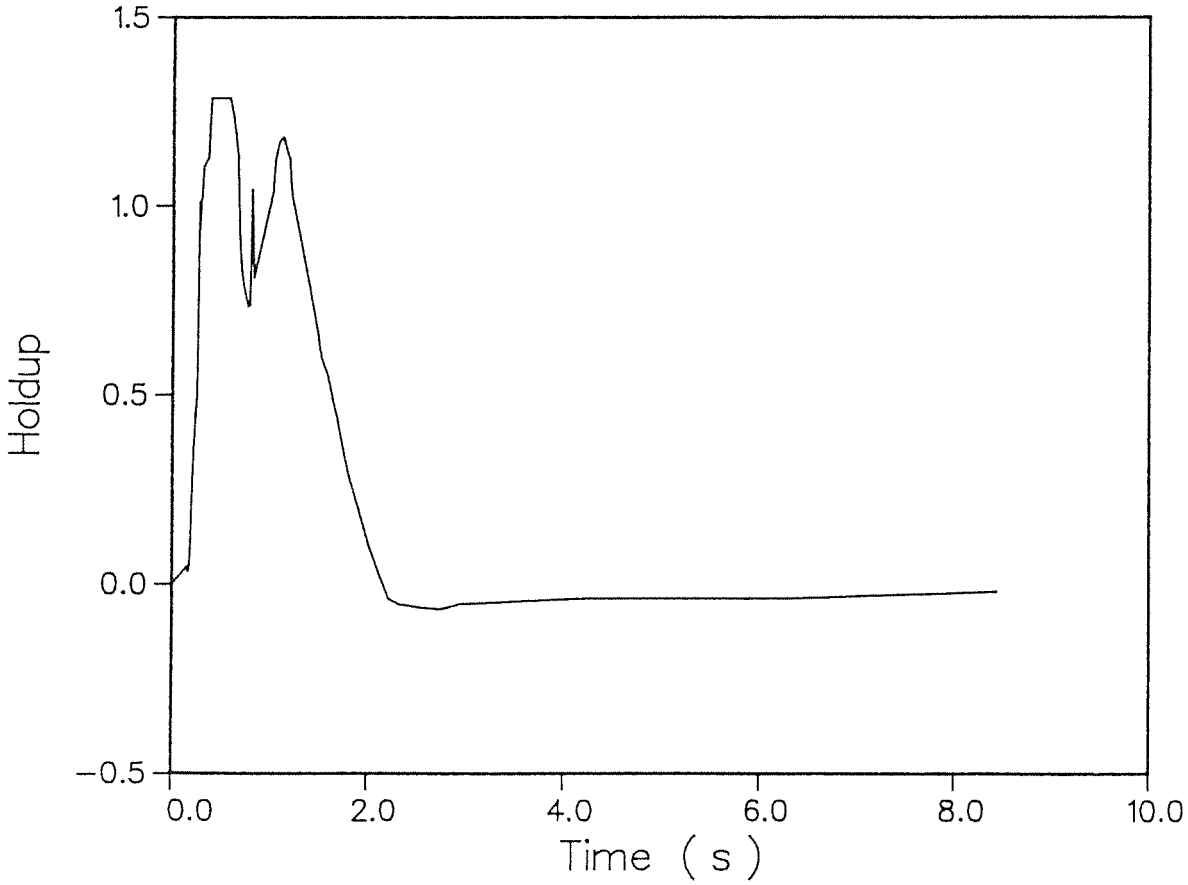

Fig.112 MMB-34 Holdup Versus Time